Modulation of voltage-gated potassium channels by phosphatidylinositol-4,5-bisphosphate

Marina Kasimova

UNIVERSITÉ DE LORRAINE

Collegium Sciences et Technologies — École doctorale SESAMES Lorraine

THÈSE

en cotutelle
entre l'Université de Lorraine et Lomonosov Moscow State University
présentée en vue de l'obtention du titre de

Docteur de l'Université de Lorraine en Chimie

Modulation de canaux potassiques sensibles au voltage par le phosphatidylinositol-4,5-bisphosphate

Modulation of voltage-gated potassium channels by phosphatidylinositol-4,5-bisphosphate

Marina KASIMOVA

soutenue publiquement le 02/12/2014
à l'Université de Lorraine, Nancy, France

Rapporteurs:	**apl. Prof. Bert de Groot**	Max Planck Institute for Biophysical Chemistry, Göttingen, Allemagne
	Prof. Erik Lindahl	KTH Royal Institute of Technology, Stockholm University, Stockholm, Suéde
Examinateurs:	**Dr. Alain Labro**	University of Antwerp, Antwerp, Belgique
	Dr. Olga Sokolova	Lomonosov Moscow State University, Moscou, Russie
	Prof. Xavier Assfeld	UMR SRSMC, Université de Lorraine, Nancy, France
Directeur:	**Dr. Mounir Tarek**	UMR SRSMC, Université de Lorraine, Nancy, France (D.R. CNRS)

Note that the main text of this thesis is in English. The abstract, introduction and conclusion are presented in both languages (French and English) and each chapter starts with a short summary of the content in French.

ACKNOLEDGMENTS

I would like to thank:

apl. Prof. **Bert de Groot** and Prof. **Erik Lindahl** for agreeing to review this work,

Mounir and **Lucie** for everything that I have learnt from you during these three years; for me, you became the *greatest* teachers,

Gildas Loussouarn, **Abderemane-Ali**, **Jianmin Cui**, **Mark Zaydman**, **Vincenzo Carnevalle** and **Mike Klein** for collaboration in the projects, the results of which are present in this work,

Alexey and **Konstantin Shaitan** for co-supervision of this PhD thesis,

Agi, **Antoine**, **Antonio**, **Benjamin**, **Christian**, **Daniel**, **Guillaume**, **Hatice**, **Hugo**, **Ilke**, **Julian**, **Maura**, **Nicola**, **Oleksandr**, **Thibaut V.**, **Thibaud E.** and **Yassine** for beyond-the-lab pastime; all of you have made these three years in Nancy a great time,

Ahcene, **Alessandro**, **Alexandrine**, **Claude**, **Francesca**, **Gerald**, **Manuel**, **Marilia**, **Severine** and **Xavier** for your scientific and personal support,

Anatoly and **Valentina**, my parents, and **Jenya**, my sister, for always being close to me; it is your indispensable support that gives me the strength to move further.

RÉSUMÉ

Les canaux potassiques (Kv) dépendants du voltage sont des protéines transmembranaires qui permettent le flux passif d'ions potassium à travers une membrane plasmique lorsque celle-ci est dépolarisée. Ils sont constitués de quatre domaines périphériques sensibles au voltage et un domaine central, un pore, qui délimite un chemin hydrophile pour le passage d'ions. Les domaines sensibles à la tension (VSD) et le pore sont couplés, ce qui signifie que l'activation des VSD déclenche l'ouverture du pore, et qu'un pore ouvert favorise l'activation des VSD.

Le phosphatidylinositol-4,5-bisphosphate (PIP_2) est un lipide mineur du feuillet interne de la membrane plasmique. Ce lipide fortement chargé négativement module le fonctionnement de plusieurs canaux ioniques, y compris les membres de la famille Kv. En particulier, l'application de ce lipide à Kv1.2 et Kv7.1, deux canaux homologues, augmente leur courant ionique. Cependant, alors que Kv1.2 est capable de s'ouvrir en l'absence de PIP_2, dans le cas de Kv7.1, ce lipide est absolument nécessaire pour l'ouverture du canal. En outre, dans Kv1.2, PIP_2 induit une perte de fonction, qui est manifesté par un mouvement retardé des VSD. Jusqu'à présent, les mécanismes sous-jacents à de telles modulations des canaux Kv par PIP_2 restent inconnus. Dans ce travail, nous tentons de faire la lumière sur ces mécanismes en utilisant des simulations de dynamique moléculaire (DM) combinées avec une approche expérimentale, entreprise par nos collaborateurs.

En utilisant des simulations de DM sans contrainte, nous avons identifié les sites potentiels de liaison du PIP_2 au Kv1.2. Dans l'un de ces sites, PIP_2 interagit avec le canal de sorte à former des ponts salins dépendants de l'état du canal, soit avec le VSD soit avec le pore. Sur la base de ces résultats, nous proposons un modèle pour rationaliser les données expérimentales connues. En outre, nous avons cherché à évaluer quantitativement la perte de fonction induite par la présence de PIP_2 au voisinage du VSD du Kv1.2. En particulier, nous avons calculé l'énergie libre des deux premières transitions le long de l'activation du VSD en présence et en l'absence de ce lipide. Nous avons constaté que PIP_2 affecte à la fois la stabilité relative des états du VSD et les barrières d'énergie libre qui les

séparent. Enfin, nous avons étudié les interactions entre PIP_2 et un autre membre de la famille Kv, le canal Kv7.1 cardiaque. Dans le site de liaison de PIP_2 que nous avons identifié pour ce canal, l'interaction entre les résidus positifs de Kv7.1 et le lipide sont dépendants de l'état du VSD, comme dans le cas de Kv1.2. On montre que cette interaction est importante pour le couplage entre les VSD et le pore, couplage qui est par ailleurs affaibli à cause de la répulsion électrostatique entre quelques résidus positifs. Ces résultats et prédictions ont été vérifiés par les données expérimentales obtenues par nos collaborateurs.

ABSTRACT

Voltage-gated potassium (Kv) channels are transmembrane proteins that enable the passive flow of potassium ions across a plasma membrane when the latter is depolarized. They consist of four peripheral voltage sensor domains, responding to the applied voltage, and a central pore domain that encompasses a hydrophilic path for passing ions. The voltage sensors and the pore are coupled, meaning that the activation of the voltage sensors triggers the pore opening, and the open pore promotes the activation of the voltage sensors.

Phosphatidylinositol-4,5-bisphosphate (PIP_2) is a minor lipid of the inner plasma membrane leaflet. This highly negatively charged lipid was shown to modulate the functioning of several ion channels including members of the Kv family. In particular, application of this lipid to Kv1.2 and Kv7.1, two homologous channels, enhances their ionic current. However, while Kv1.2 is able to open without PIP_2, in the case of Kv7.1, this lipid is absolutely required for opening. Additionally, in Kv1.2, PIP_2 induces a loss of functioning, which is manifested by delayed motions of the voltage sensors. So far, the mechanism underlying the Kv channels modulation by PIP_2 remains unknown. In the present manuscript, we attempt to shed light on this mechanism using molecular dynamics (MD) simulations combined with experiments, which were undertaken by our collaborators.

Using unconstrained MD simulations, we have identified potential PIP_2 binding sites in Kv1.2. In one of these sites, PIP_2 interacts with the channel in a state-dependent manner forming salt bridges either with the voltage sensor or with the pore. Based on these findings, we propose a model rationalizing the known experimental data. Further, we aimed to estimate the loss of functioning effect induced by PIP_2 on the Kv1.2 voltage sensor. In particular, we have calculated the free energy of the first two transitions along the activation path in the presence and absence of this lipid. We found that PIP_2 affects both the relative stability of the voltage sensor's states and the free energy barriers separating them. Finally, we studied the interactions between PIP_2 and another member of the Kv family, the cardiac channel Kv7.1. In the PIP_2 binding site that we have identified for this channel, the interaction between positive residues of Kv7.1 and the lipid was state-

dependent, as in the case of Kv1.2. This state-dependent interaction, however, is prominent for coupling between the voltage sensors and the pore, which is otherwise weakened due to electrostatic repulsion of some positive residues. These findings are in a good agreement with the experimental data obtained by our collaborators.

TABLE OF ABBREVIATIONS

2d	two dimensional
3d	three dimensional
5-HT3	5-hydroxytryptamine type-3 receptor
A/C	activated/closed
A/O	activated/open
ATP	adenosine triphosphate
Cav	voltage-gated calcium channels
CiVSP	*Ciona intestinalis* voltage sensitive phosphatase
CNG	cyclic nucleotide channel
COM	center of mass
CV	collective variable
DHA	docosahexanoic acid
DOGS	1,2-dioleocyl-glycero-3-succinate
DOPE	discrete optimized protein energy
DOTAP	1,2-dioleoyl-3-trimethylammonium-propane
DSMM	discrete states Markov model
FRET	Förster resonance energy transfer
GlucCer	glucocerebrosides
HCN	hyperpolarization-activated cyclic nucleotide channels
K2P	two-P potassium channel
KCa	calcium-activated potassium channel
Kir	inwardly rectifying potassium channel
Kv	voltage-gated potassium channel
LQTS	long QT syndrome
MD	molecular dynamics
Ms	mechanosensitive
Nav	voltage-gated sodium channel
NMR	nuclear magnetic resonance
PBC	periodic boundary conditions
PD	pore domain
pdf	probability density function
PIP_2	phosphatitylinositol-(4,5)-bisphosphate
PME	Particle Mesh Ewald
POPE	1-palmitoyl-2-oleoyl-glycero-3-phospho-ethanolamine
POPG	1-palmitoyl-2-oleoyl-glycero-3-phosphoglycerol
POPC	1-palmitoyl-2-oleoyl-glycero-3-phosphocholine
PSSM	position-specific score matrix
PUFA	polyunsaturated fatty acid
R/C	resting/closed
RESP	restricted electrostatic potential
RMSD	root mean square deviation
R/O	resting/open
SE	standard error
SQTS	short QT syndrome
TEA	tetraethylammonium
TM	transmembrane
TPC	two-pore channel
TRP	transient receptor potassium channel
VCF	voltage-clamp fluorometry
vdW	van der Waals
VSD	voltage sensor domain
WT	wild type

TABLE OF CONTENT

1 INTRODUCTION

Le transport ionique sélectif à travers une membrane plasmique est à la base de processus physiologiques clés qui surviennent dans les cellules excitables : la production et la transmission de l'influx nerveux. Il y a maintenant plus de trente ans, ce transport a été attribué au fonctionnement de protéines transmembranaires hautement spécialisée (TM) ou de canaux ioniques. Etant donné que ces protéines sont activées lors de la modification du voltage (potentiel) membranaire, ils ont été appelés voltage-dépendants. À la fin du XXe siècle, la révolution dans le domaine de la génétique moléculaire a permis d'accéder à la topologie des canaux ioniques voltage-dépendants; une structure de base de six segments transmembranaires putatifs (hélices) de S1 à S6 répété quatre fois a été révélée [1,2]. Le segment de S1 à S4 compose le domaine sensible à la tension (VSD), qui détecte les variations d'un champ électrique externe (voltage) et y répond en effectuant des réarrangements conformationnels. S4 est le segment transmembranaire le plus mobile du VSD. Cette hélice comporte plusieurs résidus chargés positivement qui se déplacent à travers la membrane [3,4] : vers le haut ou vers le bas lorsque la membrane est dépolarisée ou hyperpolarisée respectivement. Le VSD est activée lorsque S4 est "en haut" et se trouve au repos quand S4 est "en bas". Les hélices S5 et S6 de quatre blocs répétitifs forment un pore dans le domaine central (PD) qui délimite un chemin hydrophile pour le passage des ions et constitue la porte (gate) de conduction. Dans les canaux voltage-dépendants, il existe une communication efficace entre le VSD et le PD, appelé couplage, qui initie les réarrangements de conformation de la porte (ouverte ou fermée) en réponse à ceux du VSD (actif ou au repos) et vice-versa [5]. Ainsi, l'activation de la VSD entraîne l'ouverture du gate, et une porte ouverte facilite l'activation du VSD. Ce couplage rend un canal ionique sensible au voltage, bien que composé de deux domaines fonctionnels différents, une seule et unique sous-unité électromécanique. Un autre éclairage sur l'architecture des canaux ioniques voltage-dépendants a été fourni il y a une dizaine d'années lorsque la première structure cristalline du canal potassique voltage-dépendants chez les mammifères Kv1.2 a été résolue [6]. Pour l'histoire de la découverte des canaux ioniques voltage-dépendants et les détails de leur structure, se référer aux Sections **2.1** et **2.2** de ce manuscrit.

Dans une cellule vivante, la régulation du fonctionnement des canaux ioniques voltage-dépendants s'effectue sur plusieurs niveaux. L'un de ces niveaux est la membrane plasmique. Cette dernière est une matrice, dans laquelle les protéines transmembranaires, y compris les canaux ioniques voltage-dépendants sont insérées. Les propriétés physiques de cette matrice (comme l'épaisseur, la courbure intrinsèque, la viscosité, *etc.*) modulent l'énergie libre des transitions conformationnelles des canaux ioniques voltage-dépendants (voir **2.3**). Par exemple, l'étirement de la membrane plasmique (tension latérale) facilite l'ouverture des canaux potassiques voltage-dépendant (Kv) [7], *etc.*

Un autre moyen de régulation utilisé par la membrane est du à l'interaction directe entre les lipides et les acides aminés (résidus) des canaux ioniques voltage-dépendants (voir **2.3**). Le phosphatidylinositol-4,5-bisphosphate (plus connu sous le nom de PIP_2) est un lipide mineur du feuillet interne des membranes plasmiques connu pour moduler le fonctionnement de plusieurs canaux ioniques, y compris ceux dépendants du voltage [8]. Comme la concentration de ce lipide ne dépasse pas 1% de la teneur totale en lipides de la membrane plasmique [9], on peut considérer que PIP_2 ne modifie pas les propriétés physiques de cette dernière et supposer a priori que PIP_2 module le fonctionnement des canaux ioniques grâce à une interaction directs. Ceci a été récemment confirmé par les structures cristallines du Kir2.1 et de GIRK2 qui montrent que PIP_2 interagit avec les résidus positifs de ces canaux exposés à l'interface entre les feuillets internes de la membrane et le cytoplasme [10,11]. Pour les autres canaux [12–23], des expériences de mutagenèse ont révélé des résidus positifs responsables de la sensibilité au PIP_2. Ces résidus constituent potentiellement un site de liaison putatif pour PIP_2. Toutefois, on notera qu'un effet allostérique ne peut pas être écarté. Pour plus de détails de la modulation de canaux ioniques par PIP_2, voir les Sections **2.3.5–2.3.7**.

Dans le travail actuel, nous nous concentrerons sur deux sous-familles de canaux ioniques voltage-dépendants : Kv1 et Kv7. Plusieurs travaux ont montré que ces deux sous-familles sont sensibles au PIP_2 [12,18,24,25]. En présence de PIP_2, par exemple, le Kv1.2 subit un effet dual qui module le courant ionique et le courant de porte : tandis que l'amplitude des courants ioniques augmente en présence de PIP_2 (gain-de-fonction), le courant de porte apparaît à des voltages plus dépolarisés, indiquant une restriction des mouvements du VSD (perte-de-fonction) [18,24]. Pour le canal de la sous-famille Kv7, Kv7.1, l'application de PIP_2 se traduit également par une augmentation du courant ionique. Cependant, alors que Kv1.2 est capable de s'ouvrir en l'absence de ce lipide, PIP_2 est absolument nécessaire pour

l'ouverture du Kv7.1 [25]. Des expériences récentes ont montré par ailleurs l'importance de PIP_2 dans le couplage entre le VSD et le pore dans Kv7.1 : lorsque la membrane plasmatique est appauvrie en PIP_2, l'activation du VSD ne donne pas lieu à l'ouverture des pores [20].

Bien que de nombreux travaux aient été consacrés à l'étude de la modulation du Kv1.2 et du Kv7.1 par PIP_2, de nombreuses questions importantes restent à explorer :

- Quels sont les sites de liaison des Kv1.2 et Kv7.1 et du PIP_2 ?
- Par quel mécanisme l'interaction du PIP_2, entraîne-t-elle d'une part un gain-de-fonction (augmentation du courant ionique) et d'autre part une perte-de-fonction (encombrement du mouvement du VSD) dans le Kv1.2 ?
- Comment PIP_2 contrôle ou facilite-t-il le couplage entre le VSD et le pore dans Kv7.1 ?
- Pourquoi, à l'inverse du Kv1.2, le Kv7.1 nécessite-t-il le PIP_2 pour le couplage entre le VSD et le pore ?
- Les sites de liaison du PIP_2 aux Kv1.2 et Kv7.1 sont-ils homologues ? Le mécanisme moléculaire de modulation du PIP_2 est-il similaire ou complètement différent ?

Afin de faire la lumière sur ces questions en suspens, nous avons mis à profit des simulations de dynamique moléculaire (DM) combinées avec des expériences en électrophysiologie. Les résultats de nos travaux sont présentés dans le Chapitre **4** ; ils sont divisés en trois sections. La Section **4.1** est consacrée à la modulation du canal Kv1.2 par le PIP_2. Ici, en utilisant des simulations de DM sans contrainte, nous avons identifié trois sites potentiels de liaison de PIP_2. Dans l'un de ces sites, PIP_2 interagit avec le canal Kv1.2 d'une manière dépendante de l'état : lorsque le VSD est au repos et le PD est fermé (appelé l'état repos/fermé), ce lipide chargé négativement forme des ponts salins multiples avec le bas de l'hélice S4. Dans l'état activé/ouvert, PIP_2 interagit plutôt avec l'extrémité de S6, qui forme la porte. Partant de ce constat, nous proposons un modèle qui explique l'augmentation du courant ionique et le décalage du courant de porte vers des tensions dépolarisés pour le Kv1.2 en présence de PIP_2 [18,24]. Dans la Section **4.2**, nous continuons l'étude de la modulation des canaux Kv1.2 par PIP_2. Ici, cependant, on se concentre sur les transitions du VSD, en présence et en l'absence de ce lipide chargé négativement. Utilisant des calculs en métadynamique [26,27], nous avons estimé l'énergie libre des deux premières transitions du VSD le long de son chemin d'activation. Nous démontrons que PIP_2 affecte la stabilité relative des états de ce module sensible à la tension. De plus, nos calculs

montrent qu'en présence de PIP_2, les barrières d'énergie libre séparant ces états sont plus élevées par rapport à celles en l'absence de ce lipide. Nos résultats sont en bon accord avec les données expérimentales indiquant que le PIP_2 rend plus difficile le mouvement du VSD dans le canal Kv1.2. La dernière section, **4.3**, est consacrée à la modulation du canal Kv7.1 par PIP_2. Ce canal représente une cible thérapeutique importante : des mutations sélectives dans Kv7.1 ou dans une de ses sous-unités auxiliaires donnent lieu à de graves maladies héréditaires comme le syndrome du QT long. En utilisant un protocole similaire à celui de la Section **4.1**, nous avons identifié le site de liaison du PIP_2 au Kv7.1 responsable de couplage entre le VSD et le pore. Sur la base de nos résultats, nous avons proposé un mécanisme moléculaire pour le couplage entre le VSD et le pore dépendant du PIP_2. Nous avons également exploré la raison pour laquelle le couplage entre la VSD et la PD exige ce lipide. Nous avons trouvé que l'interaction directe entre ces deux domaines est affaiblie en raison d'une répulsion électrostatique. Nous avons montré qu'à l'inverse du canal sauvage, pour un mutant pour lequel cette répulsion est éliminée, on peut détecter une composante du couplage en l'absence du PIP_2.

Les présents résultats ont été obtenus en collaboration avec trois équipes : le groupe de Gildas Loussouarn à l'Institut du thorax (Nantes, France), le groupe de Mike Klein de l'Université Temple (Philadelphie, États Unis) et le groupe de Jianmin Cui à l'Université Washington de Saint-Louis (Saint Louis, États Unis).

Finalement, nous aimerions insister sur le fait que ce travail est le résultat de simulations extensives de DM (à des échelles de temps de l'ordre de la microseconde - DM non biaisée et métadynamique), ce qui n'aurait pu être possible sans la mise à disposition de plusieurs millions d'heures de calcul généreusement allouées par PRACE.

Publications issues de ce travail :

i) F. Abderemane-Ali, Z. Es-Salah-Lamoureux, L. Delemotte, **M.A. Kasimova**, A.J. Labro, D.J. Snyders, D. Fedida, M. Tarek, I. Baró, G. Loussouarn, Dual effect of phosphatidylinositol-(4,5)-bisphosphate PIP_2 on Shaker K+ channels, JBC, 287 (2012) 36158-36167.
ii) **M.A. Kasimova**, M. Tarek, A.K. Shaytan, K.V. Shaitan, L. Delemotte, Voltage-gated ion channel modulation by lipids: insight from molecular dynamics simulations, BBA Biomembranes, 1838 (2014) 1322-1331.

iii) L. Delemotte, **M.A. Kasimova**, M.L. Klein, M. Tarek, V. Carnevale, Free energy landscape of ion-channel voltage-sensor-domain activation, submitted to Proc. Natl. Acad. Sci. USA.

iv) **M.A. Kasimova**, M.A. Zaydman, J. Cui, M. Tarek, PIP_2-dependent coupling is prominent in Kv7.1 due to weakened interactions between S4-S5 and S6, submitted to Scientific Reports.

v) M.A. Zaydman, **M.A. Kasimova**, K. Delaloye, H. Liang, Z. Beller, J. Shi, M. Tarek, J. Cui, KCNE1 modulates KCNQ1 channel gating, permeation and pharmacology through a single mechanism, submitted to eLIFE.

1 INTRODUCTION

Selective ionic transport across a plasma membrane underlies key physiological processes occurring in excitable cells: generation and transmission of a nerve impulse. More than thirty years ago, this transport has been attributed to functioning of highly specialized transmembrane (TM) proteins, or ion channels. As these proteins were activated upon changes in the membrane potential, they were accordingly called voltage-gated. At the end of the XX century, revolution in the molecular genetics field, allowed one to access the membrane topology of voltage-gated ion channels; a basic structure of six putative transmembrane segments from S1 to S6 repeated four times was revealed [1,2]. The bundle from S1 to S4 composes the voltage sensor domain (VSD), which senses variations of the membrane potential and responds to them undergoing conformational rearrangements. S4 is the most mobile TM segment of the VSD. This helix carries several positively charged residues that move across the membrane along the applied electric field [3,4]: upward or downward when the membrane is depolarized or hyperpolarized respectively. The VSD is activated when S4 is "up" and is resting when S4 is "down". The S5 and S6 helices gathered from four repetitive blocks form the central pore domain (PD), which encompasses a hydrophilic path for passing ions and a gate. There is an effective communication between the VSD and the PD, called coupling, which triggers conformational rearrangement of the pore (open or close) as a response to those of the voltage sensor (activated or resting) and vice versa [5]. Hence, the activation of the VSD results in the gate opening, and the open pore facilitates the activation of the VSD. This coupling makes a voltage-gated ion channel, though being composed of two different functional domains, an integral electromechanical subunit. Further insight into the architecture of voltage-gated ion channels was provided ten years ago when the first crystal structure of the mammalian voltage-gated potassium channel Kv1.2 was resolved [6]. For the history of the voltage-gated ion channels' discovery and the details of their structure, see **2.1** and **2.2**.

In a living cell, regulation of voltage-gated ion channels' functioning is carried out on several levels. One of these levels is represented by the plasma membrane. The plasma membrane is a matrix, in which transmembrane proteins including voltage-gated ion channels are embedded. The physical

properties of this matrix (as thickness, intrinsic curvature, viscosity, *etc.*) may modulate the free energy underlying conformational transitions of voltage-gated ion channels (see **2.3**). For instance, stretching of the plasma membrane facilitates opening of voltage-gated potassium (Kv) channels [7], *etc.*

Another way of regulation utilized by the plasma membrane is through a direct interaction between its lipids and residues of voltage-gated ion channels (see **2.3**). Phosphatidylinositol-4,5-bisphosphate (PIP_2) is a minor lipid of the inner plasma membrane leaflet known to modulate functioning of several ion channels including the voltage-gated ones [8]. Since the concentration of this lipid does not exceed 1 % of the overall lipid content of the plasma membrane [9], one may discard the scenario, in which PIP_2 alters the physical properties of the plasma membrane, and assume that PIP_2 modulates functioning of ion channels via a direct interaction. Indeed, the recently resolved crystal structures of Kir2.1 and GIRK2 indicate that PIP_2 interacts with positive residues of these channels exposed to the interface between the lower membrane leaflet and the cytoplasm [10,11]. For other channels [12–23], mutagenesis experiments revealed positive residues responsible for PIP_2 sensitivity. These residues potentially form a putative binding site for PIP_2; however, note that allosteric effect cannot be discarded. For the details of ion channels' modulation by PIP_2, see **2.3.5 – 2.3.7**.

In the current work, we will focus on two subfamilies of voltage-gated ion channels, the voltage-gated potassium channels Kv1 and Kv7. Both of these subfamilies were shown to be sensitive to PIP_2 [12,18,24,25]. In particular, application of this lipid to Kv1.2 results in a dual effect on the ionic and gating currents of this channel: while the amplitude of the ionic current increases in the presence of PIP_2 (gain-of-function), the gating current appears at more depolarized voltages, indicating hindered motions of the VSD (loss-of-function) [18,24]. For the channel of the Kv7 subfamily, Kv7.1, application of PIP_2 also results in an increase of ionic current. However, while Kv1.2 is able to open in the absence of this lipid, in the case of Kv7.1, PIP_2 is absolutely required for opening [25]. Recent experiments indicate importance of PIP_2 for coupling between the voltage sensor and the pore in Kv7.1: when PIP_2 is depleted from the plasma membrane the activation of the voltage sensor does not lead to the pore opening [20].

While an extensive amount of work was devoted to the issue of Kv1.2 and especially of Kv7.1 modulation by PIP_2, important questions remain unexplored:

- Where are the putative PIP_2 binding sites in Kv1.2 and Kv7.1?

- By which mechanism does PIP_2 binding result, on the one hand, in hindered motions of the voltage sensor and, on the other hand, in an increase of ionic current in Kv1.2?
- How does PIP_2 mediate coupling in Kv7.1?
- Why does Kv7.1 require PIP_2 for coupling between the voltage sensor and the pore, while Kv1.2 does not?
- Are the PIP_2 binding sites in Kv1.2 and Kv7.1 homologous and is the molecular mechanism of PIP_2 modulation similar or completely different?

In order to shed light on these outstanding questions we used molecular dynamics (MD) simulations combined with electrophysiological experiments. The results of our work are presented in Chapter **4**; they are subdivided in three sections. Section **4.1** is devoted to the modulation of the Kv1.2 channel by PIP_2. Here, using unconstrained MD simulations, we have identified three potential PIP_2 binding sites. In one of these sites, PIP_2 interacts with Kv1.2 in a state-dependent manner: in the resting/closed state (*i.e.* the VSD is resting, and the PD is closed), this negatively charged lipid forms multiple salt bridges with the bottom of S4; in the activated/open state, PIP_2 anchors the terminus of S6, which forms the gate. Based on these observations, we propose a model rationalizing the increase of the ionic current and the shift of the gating current toward depolarized voltages for Kv1.2 in the presence of PIP_2 [18,24]. In Section **4.2**, we studied another aspect of the Kv1.2 channel modulation by PIP_2. We focused on the transitions of the Kv1.2 voltage sensor in the presence and absence of this negatively charged lipid. Using metadynamics simulations [26,27], we estimated the free energy underlying the two first transitions of the Kv1.2 voltage sensor along the activation pathway. We demonstrate that PIP_2 affects the relative stability of the voltage sensor's states. Moreover, we show that, in the presence of PIP_2, the free energy barriers separating these states are higher compared to those in the absence of this lipid. Our findings are in a good agreement with the experimental data indicating a hindered motion of the Kv1.2 voltage sensor after application of PIP_2. The last section, **4.3**, is devoted to the modulation of the Kv7.1 channel by PIP_2. This channel represents an important therapeutic target as selective mutations in Kv7.1 or in its auxiliary subunits result in a severe inherited disease, the Long QT Syndrome (LQTS). Using similar protocols as in Section **4.1**, we identified the PIP_2 binding site in Kv7.1 responsible for coupling between the voltage sensor and the pore. Based on our findings, we propose a molecular mechanism of PIP_2-dependent coupling in Kv7.1. We also explored why the coupling between the VSD and the PD requires this lipid. We found that direct interaction between these two

domains is weakened due to electrostatic repulsion. Based on our investigations, our collaborators showed that elimination of this repulsion experimentally resulted in a mutant, for which PIP_2-independent component of coupling was detected.

The present results were obtained in collaboration with three teams: the group of Gildas Loussouarn (Thorax Institute, Nante, France), the group of Mike Klein (Temple University, Philadelphia, USA) and the group of Jianmin Cui (Washington University in Saint Louis, Saint Louis, USA).

Finally, we would like to stress that the present work is the result of extensive MD simulations (microsecond timescales of unbiased MD and of metadynamics), which would have never be possible without several millions CPU-hours generously provided by PRACE.

The related publications are:

i) F. Abderemane-Ali, Z. Es-Salah-Lamoureux, L. Delemotte, **M.A. Kasimova**, A.J. Labro, D.J. Snyders, D. Fedida, M. Tarek, I. Baró, G. Loussouarn, Dual effect of phosphatidylinositol-(4,5)-bisphosphate PIP_2 on Shaker K+ channels, JBC, 287 (2012) 36158-36167.
ii) **M.A. Kasimova**, M. Tarek, A.K. Shaytan, K.V. Shaitan, L. Delemotte, Voltage-gated ion channel modulation by lipids: insight from molecular dynamics simulations, BBA Biomembranes, 1838 (2014) 1322-1331.
iii) L. Delemotte, **M.A. Kasimova**, M.L. Klein, M. Tarek, V. Carnevale, Free energy landscape of ion-channel voltage-sensor-domain activation, submitted to Proc. Natl. Acad. Sci. USA.
iv) **M.A. Kasimova**, M.A. Zaydman, J. Cui, M. Tarek, PIP_2-dependent coupling is prominent in Kv7.1 due to weakened interactions between S4-S5 and S6, submitted to Scientific Reports.
v) M.A. Zaydman, **M.A. Kasimova**, K. Delaloye, H. Liang, Z. Beller, J. Shi, M. Tarek, J. Cui, KCNE1 modulates KCNQ1 channel gating, permeation and pharmacology through a single mechanism, submitted to eLIFE.

REFERENCES

[1] M. Noda, S. Shimizu, T. Tanabe, T. Takai, T. Kayano, T. Ikeda, H. Takahashi, H. Nakayama, Y. Kanaoka, N. Minamino, K. Kangawa, H. Matsuo, M.A. Raftery, T. Hirose, S. Inayama, H. Hayashida, T. Miyata, S. Numa, Primary structure of Electrophorus electricus sodium channel deduced from cDNA sequence, Nature, 312 (1984) 121–127.

[2] A. Kamb, J. Tseng-Crank, M.A. Tanouye, Multiple products of the Drosophila Shaker gene may contribute to potassium channel diversity, Neuron, 1 (1988) 421–430.

[3] H.P. Larsson, O.S. Baker, D.S. Dhillon, E.Y. Isacoff, Transmembrane movement of the Shaker K+ channel S4, Neuron, 16 (1996) 387–397.

[4] N. Yang, R. Horn, Evidence for voltage-dependent S4 movement in sodium channels, Neuron, 15 (1995) 213–218.

[5] S.B. Long, E.B. Campbell, R. MacKinnon, Voltage Sensor of Kv1.2: Structural Basis of Electromechanical Coupling, Science, 309 (2005) 903–908.

[6] S.B. Long, E.B. Campbell, R. MacKinnon, Crystal structure of a mammalian voltage-dependent Shaker family K+ channel, Science, 309 (2005) 897–903.

[7] C.X. Gu, P.F. Juranka, C.E. Morris, Stretch-activation and stretch-inactivation of Shaker-IR, a voltage-gated K+ channel, Biophys. J., 80 (2001) 2678–2693.

[8] B.-C. Suh, B. Hille, PIP2 is a necessary cofactor for ion channel function: how and why?, Annu. Rev. Biophys., 37 (2008) 175–195.

[9] L. Stephens, A. McGregor, P. Hawkins, Phosphoinositide-3-kinases: Regulation by cell-surface receptors and function of 3-phosphorylated lipids, in: S. Cockcroft (ed.), Frontiers of Molecular Biology, Biology of Phosphoinositides, Oxford University Press, Oxford, UK, 2000: pp. 32–107.

[10] S.B. Hansen, X. Tao, R. MacKinnon, Structural basis of PIP2 activation of the classical inward rectifier K+ channel Kir2.2, Nature, 477 (2011) 495–498.

[11] M.R. Whorton, R. MacKinnon, Crystal Structure of the Mammalian GIRK2 K+ Channel and Gating Regulation by G Proteins, PIP2, and Sodium, Cell, 147 (2011) 199–208.

[12] H. Zhang, L.C. Craciun, T. Mirshahi, T. Rohacs, C.M.B. Lopes, T. Jin, D.E. Logothetis, PIP(2) activates KCNQ channels, and its hydrolysis underlies receptor-mediated inhibition of M currents, Neuron, 37 (2003) 963–975.

[13] K.-H. Park, J. Piron, S. Dahimène, J. Mérot, I. Baró, D. Escande, G. Loussouarn, Impaired KCNQ1-KCNE1 and phosphatidylinositol-4,5-bisphosphate interaction underlies the long QT syndrome, Circ. Res., 96 (2005) 730–739.

[14] S. Brauchi, G. Orta, C. Mascayano, M. Salazar, N. Raddatz, H. Urbina, E. Rosenmann, F. Gonzalez-Nilo, R. Latorre, Dissection of the components for PIP2 activation and thermosensation in TRP channels, Proc. Natl. Acad. Sci. U. S. A., 104 (2007) 10246–10251.

[15] J.-S. Bian, T.V. McDonald, Phosphatidylinositol-4,5-bisphosphate interactions with the HERG K(+) channel, Pflüg. Arch. Eur. J. Physiol., 455 (2007) 105–113.

[16] G.E. Flynn, W.N. Zagotta, Molecular mechanism underlying phosphatidylinositol-4,5-bisphosphate-induced inhibition of SpIH channels, J. Biol. Chem., 286 (2011) 15535–15542.

[17] A.M. Thomas, S.C. Harmer, T. Khambra, A. Tinker, Characterization of a binding site for anionic phospholipids on KCNQ1, J. Biol. Chem., 286 (2011) 2088–2100.

[18] A.A. Rodriguez-Menchaca, S.K. Adney, Q.-Y. Tang, X.-Y. Meng, A. Rosenhouse-Dantsker, M. Cui, D.E. Logothetis, PIP2 controls voltage-sensor movement and pore opening of Kv channels through the S4-S5 linker, Proc. Natl. Acad. Sci. U. S. A., 109 (2012) E2399–2408.

[19] V. Telezhkin, A.M. Thomas, S.C. Harmer, A. Tinker, D.A. Brown, A basic residue in the proximal C-terminus is necessary for efficient activation of the M-channel subunit Kv7.2 by PI(4,5)P_2, Pflüg. Arch. Eur. J. Physiol., 465 (2013) 945–953.

[20] M.A. Zaydman, J.R. Silva, K. Delaloye, Y. Li, H. Liang, H.P. Larsson, J. Shi, J. Cui, Kv7.1 ion channels require a lipid to couple voltage sensing to pore opening, Proc. Natl. Acad. Sci., 110 (2013) 13180-13185.

[21] Q. Zhang, P. Zhou, Z. Chen, M. Li, H. Jiang, Z. Gao, H. Yang, Dynamic PIP2 interactions with voltage sensor elements contribute to KCNQ2 channel gating, Proc. Natl. Acad. Sci., 110 (2013) 20093-20098.

[22] K. Eckey, E. Wrobel, N. Strutz-Seebohm, L. Pott, N. Schmitt, G. Seebohm, Novel Kv71-phosphatidylinositol 4,5-bisphosphate (PIP2) interaction sites uncovered by charge neutralization scanning, J. Biol. Chem., 289 (2014) 22749-22758.

[23] F.C. Coyan, F. Abderemane-Ali, M.Y. Amarouch, J. Piron, J. Mordel, C.S. Nicolas, M. Steenman, J. Mérot, C. Marionneau, A. Thomas, R. Brasseur, I. Baró, G. Loussouarn, A Long QT Mutation Substitutes Cholesterol for Phosphatidylinositol-4,5-Bisphosphate in KCNQ1 Channel Regulation, PLoS ONE, 9 (2014) e93255.

[24] F. Abderemane-Ali, Z. Es-Salah-Lamoureux, L. Delemotte, M.A. Kasimova, A.J. Labro, D.J. Snyders, D. Fedida, M. Tarek, I. Baró, G. Loussouarn, Dual effect of phosphatidyl (4,5)-bisphosphate PIP2 on Shaker K+ channels, J. Biol. Chem., 287 (2012) 36158–36167.

[25] G. Loussouarn, K.-H. Park, C. Bellocq, I. Baró, F. Charpentier, D. Escande, Phosphatidylinositol-4,5-bisphosphate, PIP2, controls KCNQ1/KCNE1 voltage-gated potassium channels: a functional homology between voltage-gated and inward rectifier K+ channels, EMBO J., 22 (2003) 5412–5421.

[26] A. Laio, M. Parrinello, Escaping free-energy minima, Proc. Natl. Acad. Sci., 99 (2002) 12562–12566.

[27] A. Laio, A. Rodriguez-Fortea, F.L. Gervasio, M. Ceccarelli, M. Parrinello, Assessing the Accuracy of Metadynamics, J. Phys. Chem. B, 109 (2005) 6714–6721.

2 CANAUX IONIQUES

Les membranes biologiques sont principalement constituées par une double couche de lipides amphiphiles appelée bicouche lipidique. Dans celle-ci, les têtes hydrophiles de ces lipides sont exposées au cytoplasme de la cellule et à la solution extracellulaire. Les chaines hydrophobes sont elles rassemblées au milieu de la bicouche et constituent une barrière imperméable aux espèces chargées, y compris aux ions. Si l'on estime la quantité d'énergie nécessaire pour le transport d'un seul ion à partir d'une solution à une couche hydrophobe W en utilisant la formule de Born :

$$W = \frac{z^2 e^2}{2r}\left(\frac{1}{\varepsilon_s} - \frac{1}{\varepsilon_m}\right), \tag{2.1}$$

la valeur obtenue est de l'ordre de centaines de kcal/mol [1]. Dans la formule de Born pour l'énergie d'un champ électrique créé par un ion a été considéré : z est la valence de l'ion, e est la charge élémentaire, r est le rayon ionique, ε_s et ε_m désignent des constantes diélectriques (permittivité) d'une solution et d'une couche hydrophobe respectivement. Il est possible de réduire l'énergie nécessaire pour un transport transmembranaire, en augmentant une taille efficace d'un ion (r) ou en diminuant la permittivité diélectrique de la couche hydrophobe (ε_m). La nature a mis en place des stratégies suivant la seconde voie en utilisant les canaux ioniques.

Les canaux ioniques sont des protéines intégrées dans les membranes biologiques qui créent des pores hydrophiles (faible permittivité électrique) permettant le transport d'ions et d'autres espèces chargées du cytoplasme de la cellule vers une solution extracellulaire, et vice versa. Contrairement aux pompes à ions, qui utilisent l'énergie de l'ATP pour le transport ionique, les canaux ioniques conduisent les ions selon leur gradient électrochimique [2] :

$$\Delta\mu = RTln\left(\frac{[C]_i}{[C]_o}\right) + zF\varphi. \tag{2.2}$$

Ici, le premier terme de la somme représente le gradient de concentration ionique perpendiculairement à une bicouche lipidique, et le deuxième terme représente l'influence du champ électrique externe, si ce dernier est présent. $[C]_i$ et $[C]_o$ sont les concentrations en ions à l'intérieur et à l'extérieur de la cellule, R est la constante des gaz parfaits, T est la température, φ est le potentiel transmembranaire (TM), et F est la constante de Faraday.

Les canaux ioniques sont omniprésents. Présents à la fois dans les organismes procaryotes et eucaryotes, ils participent à un éventail de processus biologiques : la génération et la propagation de l'influx nerveux, la contraction cardiaque, squelettique et des muscles lisses, le transport trans-épithélial des ions et des nutriments, la sécrétion pancréatique d'insuline, l'activation des lymphocytes T, l'acidification des endosomes, *etc.* Le dysfonctionnement des canaux ioniques causés par des mutations dans leurs séquence peut entraîner des pathologies héréditaires graves appelés canalopathies. Jusqu'à présent, plus de 100 canalopathies ont été caractérisées [3]. Elles affectent les systèmes nerveux central et périphérique (*e.g.* l'épilepsie généralisée avec convulsions fébriles, la migraine hémiplégique familiale, l'ataxie épisodique, la paralysie périodique hyperkaliémique et hypokaliémique), le système cardio-vasculaire (*e.g.* les syndromes de QT long et court, le syndrome de Brugada et la tachycardie catécholaminergique ventriculaire polymorphe), le système respiratoire (*e.g.* la mucoviscidose), le système endocrinien (*e.g.* diabete néonatal, hypoglycémie hyperinsulinémique familiale, la paralysie périodique hypokaliémique thyrotoxique et l'hyperaldostéronisme familial), le système urinaire et le système immunitaire. Certains de ces troubles sont très répandus. Par exemple, selon des statistiques récentes, 1 personne sur 2000 présente des symptômes de QT long ou syndromes de Brugada [4–6]. Notez que ces deux syndromes sont caractérisés par des arythmies ventriculaires qui peuvent conduire à la mort subite d'origine cardiaque. L'importance du rôle des canaux ioniques dans les cellules a fait de ces canaux des objets extrêmement attrayants pour la recherche scientifique. L'objectif final dans la compréhension du fonctionnement des canaux ioniques est la conception de médicaments dits "de Silver Bullet" (Paul Ehrlich) capables de cibler et de restaurer un canal ionique et le traitement d'une maladie avec des effets secondaires minimes.

Ce chapitre est consacré à un aperçu de la structure et du fonctionnement des canaux ioniques avec un accent sur les deux principaux objets d'intérêt : Kv1.2 et Kv7.1. Nous commençons par une description générale des canaux ioniques (Section **2.1**). Un rappel de l'histoire de la découverte de canaux ioniques permettra de mieux comprendre l'évolution dans le domaine des canaux ioniques, y compris la représentation contemporaine d'un canal ionique (à partir d'un pore dans la membrane plasmique à un dispositif complexe composé de différents domaines) et le développement de techniques expérimentales telles que le voltage clamp, le patch clamp, *etc.* Nous discutons de même dans les détails la famille des canaux potassiques dépendants du voltage (Kv) (Section **2.2**). Nous montrons comment ces protéines participent à l'un des processus biologiques les plus

importants : la génération du potentiel d'action. Nous discuterons la structure et les processus d'activation du Kv1.2, le canal de type *Shaker* dont la structure cristalline a été résolue, et les comparer à ceux du canal Kv7.1 cardiaque. Enfin, nous décrirons les mécanismes de modulation des canaux ioniques par la membrane plasmique (Section **2.3**). En particulier, nous allons nous concentrer sur l'effet du phosphatidylinositol-4,5-bisphosphate (PIP_2), un lipide mineur du feuillet interne de la membrane plasmique, qui régule le fonctionnement de plusieurs canaux ioniques dont les Kv1.2 et Kv7.1. Cette dernière section sera une introduction logique au Chapitre **4**, résumant les principaux résultats de notre recherche.

2 ION CHANNELS

Biological membranes are formed by a double layer of amphiphilic lipids usually called a lipid bilayer. In the membrane, the hydrophilic headgroups of these lipids are exposed to the cytoplasm of the cell and to the extracellular solution. The hydrophobic tails, gathered in the middle of the bilayer, constitute an impermeable barrier for charged species including ions. If one estimates the amount of energy required for transport of a single ion from a solution to a hydrophobic layer W using the formula of Born:

$$W = \frac{z^2 e^2}{2r}\left(\frac{1}{\varepsilon_s} - \frac{1}{\varepsilon_m}\right), \tag{2.1}$$

the resulting value is in the order of hundreds of kcal/mol [1]. Here, z is valence of the ion, e is the elementary charge, r is the ionic radius, ε_s and ε_m denote the dielectric constants (permittivities) of the solution and of the hydrophobic layer respectively. One is able to reduce the energy required for a transmembrane transport by increasing the effective size of an ion r or decreasing the dielectric permittivity of the hydrophobic layer ε_m. Nature has implemented strategies along the second route by utilizing ion channels.

Ion channels are proteins embedded into biological membranes that create hydrophilic pores (low permittivity) allowing the transport of ions and other charged species from the cytoplasm of the cell to the extracellular solution and vice versa. In contrast to ion pumps, which use ATP energy for the ionic transport, ion channels conduct according to the electrochemical gradient [2]:

$$\Delta\mu = RTln\left(\frac{[C]_i}{[C]_o}\right) + zF\varphi. \tag{2.2}$$

Here, the first term of the sum represents the gradient of ionic concentration perpendicular to a lipid bilayer, and the second term represents the influence of an external electric field if the latter is present. $[C]_i$ and $[C]_o$ are the concentrations of ions inside and outside the cell, R is the gas constant, T is the temperature, φ is the transmembrane (TM) potential, and F is the Faraday constant.

Ion channels are ubiquitous. Found both in prokaryotic and eukaryotic organisms, they are shown to participate in an entire spectrum of biological

processes: generation and propagation of a nerve impulse, cardiac, skeletal and smooth muscles contraction, transepithelial transport of ions and nutrients, pancreatic β-cell insulin secretion, T-lymphocyte activation, acidification of endosomes, *etc.* Malfunctioning of ion channels caused by mutations in their sequences may result in severe inherited pathologies called channelopathies. So far, more than 100 channelopathies have been characterized [3]. They affect the central and peripheral nervous systems (*e.g.* generalized epilepsy with febrile seizures plus, familial hemiplegic migraine, episodic ataxia, hyperkalemic and hypokalemic periodic paralysis), the cardiovascular system (*e.g.* long and short QT syndromes, Brugada syndrome and catecholaminergic polymorphic ventricular tachycardia), the respiratory system (*e.g.* cystic fibrosis), the endocrine system (*e.g.* neonatal diabetis mellitus, familial hyperinsulinemic hypoglycemia, thyrotoxic hypokalemic periodic paralysis and familial hyperaldosteronism), the urinary system and the immune system. Some of these disorders are wide spread. For instance, according to recent statistics, 1 individual out of 2000 has symptoms of long QT or Brugada syndromes [4–6]. Note that both of these syndromes are characterized by the occurrence of ventricular arrhythmias that may lead to sudden cardiac death. The importance of the ion channels' role in cells has made these objects extremely attractive for the scientific research. The final goal in understanding of ion channels' functioning is the design of so-called "silver bullet" drugs (Paul Ehrlich), able to target and restore a malfunctioning part of an ion channel and to treat a disease with minimal side effects.

This chapter is devoted to an overview of the structure and the functioning of ion channels with an accent on the two main objects of interest: Kv1.2 and Kv7.1. We will start with a general description of ion channels (Section **2.1**). Recalling the history of ion channels' discovery will provide a better understanding of the progress made in this field, including contemporary representation of an ion channel (from a pore in the plasma membrane to a complicated device composed of different domains) and the development of experimental techniques such as voltage clamp, patch clamp, *etc.* to study them. Further, we will discuss in detail the family of voltage-gated potassium (Kv) channels (Section **2.2**). We will show how these channels participate in one of the most important biological processes: the generation of the action potential. We will discuss the structure and the gating processes of Kv1.2, the *Shaker* type channel, for which we have a high-resolution 3d structure, and compare them to those of the cardiac channel Kv7.1. Finally, we will describe two mechanisms of the ion channels' modulation by the plasma membrane (Section **2.3**). In particular, we will focus on the effect of phosphatidylinositol-4,5-bisphosphate (PIP_2), a minor

lipid of the inner plasma membrane leaflet, which is known to regulate functioning of several ion channels including Kv1.2 and Kv7.1.

2.1. Short history of ion channels' discovery: from the experiments of Galvani to the first crystal structure

Our encounter with ion channels began in the XVIII century with the first experiments of Galvani on frogs: a frog preparation, consisting of the lower body half with exposed nerves and a metal wire inserted across the vertebral canal, started contracting when Galvani touched its nerves with a lancet, and a spark rose from a distant electric machine [7]. Galvani concluded that the animal tissue contained an innate vital force, which he termed "animal electricity". Since that time, the history of ion channels' discovery remained intimately connected with the study of a nerve impulse's initiation and propagation.

The processes of initiation and propagation of a nerve impulse are mediated by functioning of specific ion channels, called voltage-gated, sensitive to changes in the TM potential. These channels constitute only one class among all the diversity of ion channels characterized so far. Below, we will briefly discuss the modern classification of ion channels and show, which place in it voltage-gated ion channels occupy.

This Section is mostly based on the review of Bezanilla [8] and on the book of Ochs [9].

2.1.1. Classification of ion channels

In the human genome, the ion channel family is larger than the nuclear hormone receptor family, half the size of the kinase and protease families and accounts for approximately 1 % of the estimated 20,000 human protein coding genes [10]. This family is extremely diverse: ion channels differ by their physiological role (generation of transmembrane potential, signal transduction, neurotransmitter release, muscle contraction, hormone

secretion, volume regulation, growth, motility, apoptosis, *etc.*) and by their location (the central and peripheral nervous systems, the heart, the skeletal and smooth muscles, the respiratory system, the urinary system, *etc.*). Some of these channels are rather simple in their architecture. For instance, a voltage-gated proton channel Hv consists of 2 subunits; each of them spans the membrane 4 times [11]. Other ion channels are more complicated. The voltage-gated sodium and calcium channels are composed of a 24 TM α-subunit, extensively extending into the cytoplasm. Additionally, in some organs, an α-subunit may form complexes with a TM β-subunit, modulating the gating [12]. The skeletal muscle ryanodine receptor (RyR1) is another example of a complex ion channel. RyR1 is actually one of the largest ion channels cloned so far. It consists of four subunits; each of them is 5037 amino acids long and has a mass of 595 kDa [13]. For comparison, the molecular weight of an α-subunit of the voltage-gated sodium channels is around 260 kDa [12].

According to the IUPHAR database (the database of G-protein-coupled receptors and ion channels) [14], ion channels can be divided into two superfamilies: the voltage-gated ones, which activate upon changing TM voltage and the ligand-gated ones, which activate upon association with a specific ligand.

Voltage-gated ion channels are especially critical in excitable neuronal and muscle tissues, where they participate in the propagation of an action potential. This superfamily includes 10 families that share a common cation-selective pore-forming module composed of 2 TM segments and an inverted P-loop [14,15] (see Figure 2.1.1.1). The voltage-gated sodium (Nav) and calcium (Cav) channels are the most structurally complex (see above). In addition to their primary regulation by voltage, these channels have slower secondary regulation by numerous signaling pathways. Members of the two-pore channel family (TPC), whose functional properties are unknown, are composed of two separate subunits; each of these subunits has two linked domains with 6 TM segments. Five ion channels families are tetramers of 6 TM subunits. Voltage-gated potassium channels (Kv) are primarily regulated by voltage and secondary by G-proteins and second-messenger signaling pathways. Calcium-activated potassium channels (KCa), transient receptor potential channels (TRP), hyperpolarization-activated cyclic nucleotide-gated channels (HCN) are jointly regulated by voltage, membrane lipids and intracellular ligands. Cyclic nucleotide-gated ion channels (CNG) are primarily regulated by cyclic nucleotides. Finally, the two structurally simplest voltage-gated ion channels have only a pore-forming domain. Inwardly rectifying potassium channels (Kir) are composed of tetramers of 2

TM subunits. Two-P potassium channels (K2P) are composed of dimers of subunits having two linked pore-forming motifs; each is similar to Kir. Kir and K2P are regulated by membrane lipids and intracellular ligands as G-proteins, Mg^{2+}, polyamines and ATP.

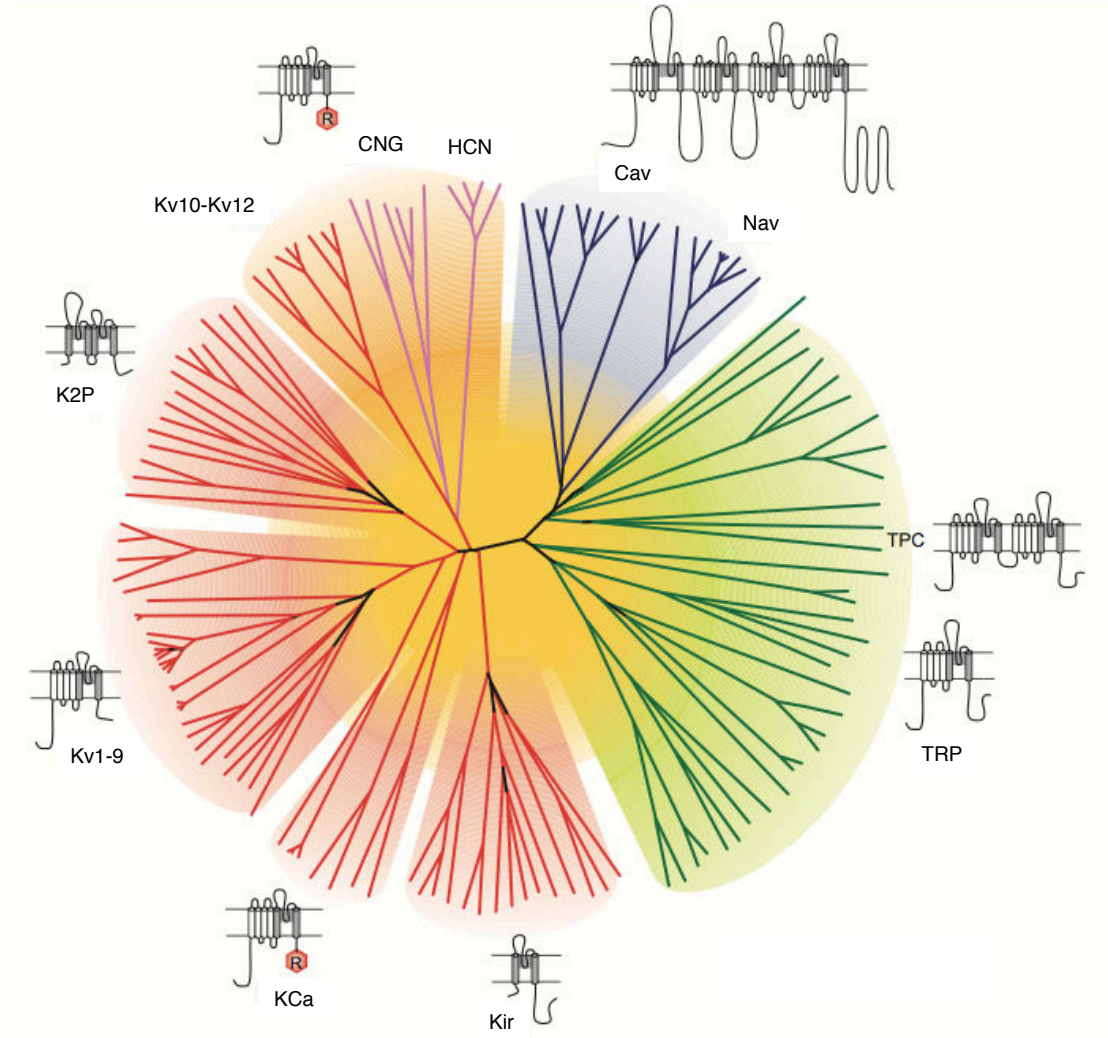

Figure 2.1.1.1. The voltage-gated ion channels superfamily. Four-domain channels (Cav and Nav) are shown as blue branches, potassium-selective channels (Kv, K2P, KCa and Kir) are shown as red branches, cyclic nucleotide-gated channels (CNG and HCN) are shown as magenta branches, transient receptor potential channels (TRP) and the two-pore channel family (TPC) are shown as green branches. The figure is adapted from [16].

Ligand-gated ion channels are usually located at synapses. There, they convert a chemical signal of pre-synaptically released neurotransmitter into a post-synaptic electrical signal. The ligand-gated ion channels form three superfamilies on the basis of homology in their amino acids sequences and topology of their component subunits, namely, the pentameric Cys-loop (tetramers), the cation-selective ionotropic glutamate (trimers) and P2X (trimers) receptors [14]. The Cys-loop receptors comprise the cation-selective nicotinic acetylcholine and 5-hydroxytryptamine type-3 (5-HT3) receptors (with 17 and 5 subunits respectively) and the anion-selective GABAA and

glycine receptors (with 19 and 5 subunits respectively). A cation-selective zinc-activated channel forms an additional member of the Cys-loop superfamily. Ionotropic glutamate receptors comprise the N-methyl-D-aspartate (7 subunits), a-amino-3-hydroxy-5-methyl-4-isoxazolepropionic acid (4 subunits) and kainite (5 subunits) receptor classes. The P2X subunits are from P2X1 to P2X7.

Another stimulus that triggers the activation of ion channels is mechanic. There is a superfamily of ion channels called mechanosensitive (Ms), which are primarily regulated by stretching of the biological membranes, pressure and displacement [17]. The bacterial mechanosensitive ion channels of small (MscS) and large (MscL) conductance represent penta- and heptamers respectively. Each subunit of MscL has 2 TM segments for a total of 10, whereas MscS has 3 TM segments per subunit for a total of 21. In eukaryotes, mechanosensitive ion channels are usually polymodal, *i.e.* they may be activated by several stimuli including the mechanical stress. They are K2P, TRP (see above) and ENaC, the amiloride-sensitive epithelial sodium channels. The latter is a hetero-oligomer of unknown stoichiometry. The secondary structure and membrane topology of ENaC are similar to those of bacterial MscL: each subunit has 2 TM segments.

Finally we note that another classification splits all ion channels in selective and non-selective. The formers can be further divided in ion channels selective to potassium, sodium, calcium, chloride ions and protons.

2.1.2. Toward the work of Hodgkin and Huxley

Since the experiments of Galvani, the next major breakthrough in the ion channels' field, which was made by Nobel laureates Hodjkin and Huxley, had to wait two centuries. During this time, several important concepts were developed that prepared the scientific community for understanding of initiation and propagation of a nerve impulse in terms of ions passing through specialized proteins in the plasma membrane.

- At the end of the XIX century – the beginning of the XX century two of these concepts were formulated. The first one postulates the existence of self-consistent charged species, or ions: acids and bases are substances that dissociate in water, yielding electrically charged atoms or molecules (Arrhenius theory of dissociation). The second concept states for a lipoid

nature of the barrier surrounding living cells: there is a positive correlation between lipid solubility of the compound and its anesthetic potency (Meyer and Overton lipid solubility-anesthetic potency correlation).

- Another important observation was made by Nobili and Matteucci [9]. They found a potential difference in muscle between a site that had been cut or injured and an intact part of the muscle, a phenomenon they termed the "injury potential" or "demarcation potential". The potential difference so produced causes a flow of current, the "injury current", between the two sites of the muscle. This observation led to a hypothesis that, during initiation and propagation of a nerve impulse, the resting potential of the membrane changes to an action one (see **2.2.1**).
- At the beginning of the XX century, Bernstein has postulated that the resting potential is created due to selective permeability of the membrane to different ionic species [9]: while potassium ions diffuse following their electrochemical gradient, others are not able to permeate. The potential so produced φ is given by the Nernst equation (W. Nernst was awarded a Nobel Prize in Chemistry, 1920):

$$\varphi = \frac{RT}{F} ln\left(\frac{P_K[K]_o + P_{Na}[Na]_o + P_{Cl}[Cl]_o}{P_K[K]_i + P_{Na}[Na]_i + P_{Cl}[Cl]_i}\right). \qquad (2.1.2.1)$$

Here, P_X is the relative permeability of an ion X, where the latter substitutes for potassium, sodium or chloride; $[X]_o$ and $[X]_i$ denote concentrations of an ion X inside the cell and at the extracellular solution respectively; R is the gas constant, T is the temperature, and F is the Faraday constant. The action potential was further attributed to a transient increase of ionic current through the membrane.

Along with the evolving concepts of the resting and action membrane potentials, development of a new experimental technique, allowing one to record directly ionic current flowing across the membrane without any resultant change in the membrane potential, played an important role in the work of Hodgkin and Huxley. This technique, called voltage-clamp [2], was first proposed by Cole and was further improved by Hodgkin and Huxley. Briefly, the setup (see Figure 2.1.2.1) uses two electrodes: one to record the membrane voltage (V_2), and the other to apply current to the cell (V_2 or I_2). The command potential is maintained by a negative feedback system. The electrodes are connected to an amplifier (amp), measuring the membrane potential and translating the signal to a feedback amplifier (clamping amp). The latter subtracts the membrane potential from the command one and sends an output signal to the electrode (V_2 or I_2). If the membrane potential deviates from the command one, the appropriate electrode (V_2 or I_2) conducts

a current into the cell, reducing this deviation to zero. The injected current is monitored via a current-to-voltage converter to provide a measure of the total membrane current.

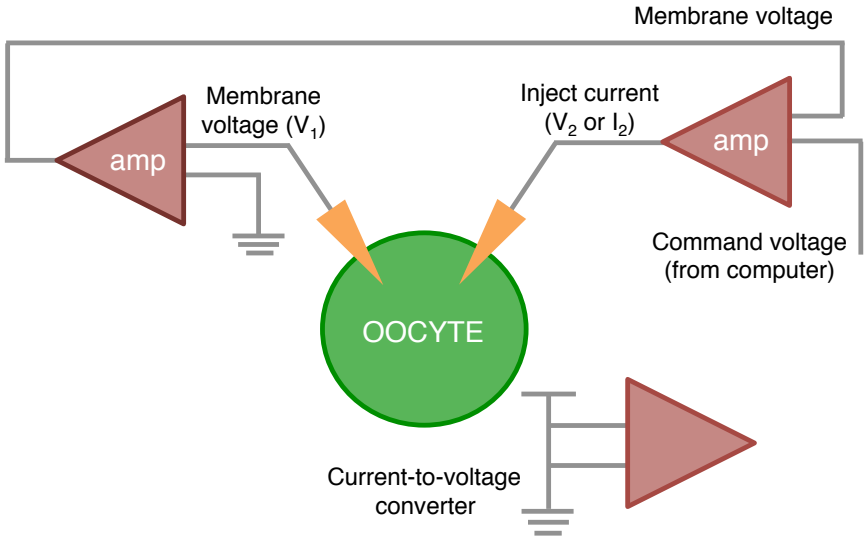

Figure 2.1.2.1. Schematic representation of the voltage clamp setup. V_1 and V_2 (I_2) are electrodes measuring the membrane voltage and passing current into the cell respectively; amp is an amplifier. For details, see the main text.

2.1.3. The Hodgkin and Huxley work

In 1953, Hodgkin and Huxley postulated one of the most important concepts in the ion channels' field that changed the in-mind representation of ionic currents through a biological membrane [18–21]: the latters do not simply represent a diffusive property of the membrane, but occur at discrete sites. Hodgkin and Huxley called these sites "carriers"; later, they were identified as ion channels.

Fitting their experimental data, Hodgkin and Huxley proposed a kinetic model, which was able to quantitatively describe ionic currents. In this model, a carrier conducts all-or-nothing according to the displacement of charged "particles" that are part of or associated with the carrier. Acting as a molecular voltmeter, these relevant charged particles sense changes in the membrane potential and move in response to them. A sodium (transient) carrier has two such particles, the activation particle h and the inactivation particle m. Accordingly, this carrier may have three states: deactivated (h and m did not move), activated (h has moved but m did not) and inactivated (both h and m have moved). A potassium (persistent) carrier has only one particle

n. Accordingly, this carrier may be either activated (n has moved) or deactivated (n did not move). The empirical expressions of sodium (I_{Na}) and potassium (I_K) average currents read:

$$I_{Na} = h^3 m \bar{g}_{Na}(\varphi - \varepsilon_{Na}), \quad (2.1.3.1)$$

$$I_K = n^4 \bar{g}_K(\varphi - \varepsilon_K). \quad (2.1.3.2)$$

Here, $\bar{g}_X$ is a single-pore conductance of a carrier (X stands for sodium or potassium), h, m and n denote respective probabilities of the sodium activation, sodium inactivation and potassium particles being translated in response to changes in the membrane φ, and ε is the electromotive force.

One of the most important outcomes of the work of Hodgkin and Huxley is their hypothesis of moving charged particles as the trigger of the carriers' activation. Hodgkin and Huxley even pointed out that the movement of charged particles within the membrane should be detectable in a voltage clamp as a small electric current that would precede the ionic currents. Indeed, in 1970s, this transient current was detected by several independent experimental groups [22–25]. As this current is responsible for the change in the carrier's (ion channel's) opening probability, it was accordingly called the *gating* current. The overall charge associated with this gating current and being transferred across the membrane is called the *gating charge*.

For their discoveries, Hodgkin and Huxley were awarded a Nobel Prize in Physiology and Medicine in 1963.

2.1.4. Overall architecture of an ion channel captured from the voltage clamp experiments

After the seminal work of Hodgkin and Huxley, it became widely accepted that ions pass across the membrane through discrete sites, namely, ion channels. However, the nature of these channels was still debated: whether they are holes in the membrane or highly specialized proteins embedded into it. Rojas and Luxoro provided the first evidence advocating for the proteic nature of ion channels [26]. They demonstrated that a specific protease (pronase) is able to destroy inactivation of sodium current completely, though leaving potassium current unaltered. Another piece of evidence came from Agnew and colleagues [27]. They extracted a 230 kDa protein from an eel electric organ; embedded into liposomes or bilayers, this protein was shown to produce sodium current [28,29].

The first insight into the architecture of ion channels came from the experiments with toxins that temporary block ionic currents. Hence, applying tetraethylammonium (TEA) and its derivatives to a giant axon, Armstrong found that the block of potassium current occurred *after* the channel opening [30]. This observation led to the concept of a discrete gate. This gate was further attributed to the intracellular region of the channel, while the extracellular region was proposed to be responsible of ionic selectivity [31]. In 1959, Mullins wrote that ions entering the channel loose their hydration shell at least partially, thus allowing the channel to distinguish between different types of ions [32]. Before his work, selectivity of the membrane was assumed to stem from the difference in radius of hydrated potassium and sodium ions. However, Mullins noticed that rubidium and cesium ions have hydrated radii very close to that of potassium, but they behave quite differently with respect to their ability to depolarize the membrane or to penetrate though it. "… This difficulty can be avoided by assuming that ions move though pores that fit them rather closely; these pores serve to replace the hydration that the ion would have in an aqueous solution …".

2.1.5. Patch clamp, an advanced technique for measuring ionic currents

While the voltage clamp was a widely used technique for measuring ionic currents, it could only be applied to rather big cells, as sharp microelectrodes were needed to penetrate the membrane. In the late 1970s, Sakmann and Neher suggested an alternative technique, which they called patch clamp [33,34]. Applying the latter to a frog skeletal muscle, they resolved for the first time single channel currents flowing across the membrane. For their invention, Sakmann and Neher received the Nobel Prize in Physiology and Medicine in 1991.

In the patch clamp technique [2,35], a tip of a pipette is pressed onto the cell surface, isolating a small patch of the membrane. Then, suction is applied, establishing a high resistance seal. The latter allows ionic current to flow only into the pipette. As the seal resistance increases with decreased surface area, electrical isolation of the small patch reduces leakage sufficiently so that even small ionic currents flowing through a single ion channel could be detected.

Several configurations of patch clamp are known [2,35] (see Figure 2.1.5.1): cell-attached, whole-cell, inside-out and outside-out. In the cell-attached patch clamp (see Figure 2.1.5.1A), the pipette is sealed to the membrane patch, leaving the cell intact. Ionic current of channels residing within the patch is monitored. The solution inside the pipette is controlled, which makes this configuration appropriate for investigating ion channels' modulation by various compounds. In the whole-cell patch clamp (see Figure 2.1.5.1B), a pulse of suction or voltage ruptures the patch. Hence, in contrast to the cell-attached patch clamp, ionic current of the entire membrane is monitored. Additionally, the membrane voltage can be controlled via the voltage clamp. Withdrawing the pipette from the rest of the cell results in a cell-excised configuration (see Figure 2.1.5.1C, D), allowing one to control both the intracellular and extracellular environments of the patch. Pulling the pipette from the cell-attached or whole-cell configurations establishes the inside-out or outside-out configurations, respectively. In the inside-out patch clamp (see Figure 2.1.5.1C), the cytosolic side of the patch is exposed to the bath solution. This configuration is applied for studying ion channels regulated by intracellular ligands. In the outside-out patch clamp (see Figure 2.1.5.1D), outside of the membrane faces the bath solution. This configuration is used to study ion channels regulated by extracellular ligands.

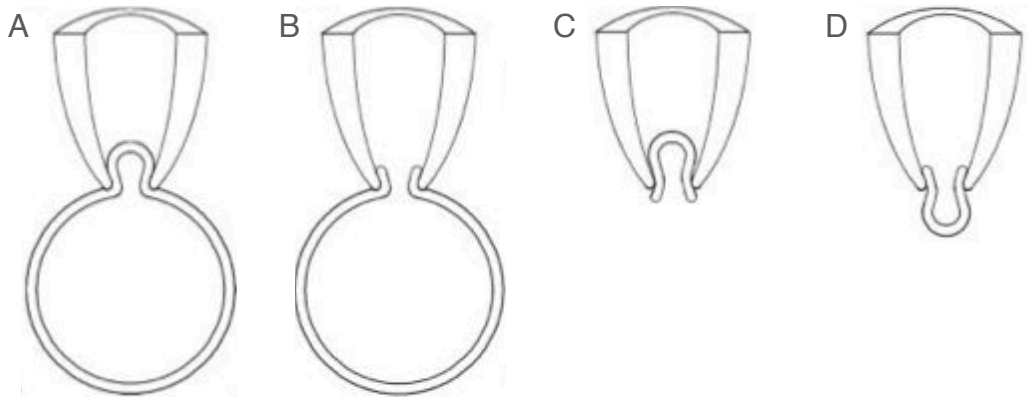

Figure 2.1.5.1. Different configurations of the patch clamp. A. Cell-attached patch clamp. B. Whole-cell patch clamp. C. Inside-out patch clamp. D. Outside-out patch clamp. For details, see the main text. The figure is adapted from [35].

2.1.6. Accessing the primary structure of ion channels

A revolution in the molecular genetics field, initiated by the invention of the molecular cloning method, played an important role in the history of ion channels' research: one was finally able to access the primary structure or the

amino acid sequence of an ion channel. Knowing this, the membrane topology of a channel could be captured by estimating a hydrophobicity plot. In particular, for voltage-gated sodium and calcium channels, the molecular cloning revealed a basic structure of 6 putative TM segments repeated 4 times in the same polypeptide [36] (see Figure 2.1.6.1A, B). Voltage-gated potassium channels were shown to have 6 TM segments per subunit [37] (see Figure 2.1.6.1C); the stoichiometry of four subunits in these channels was demonstrated later and required several biophysical tricks [38–40].

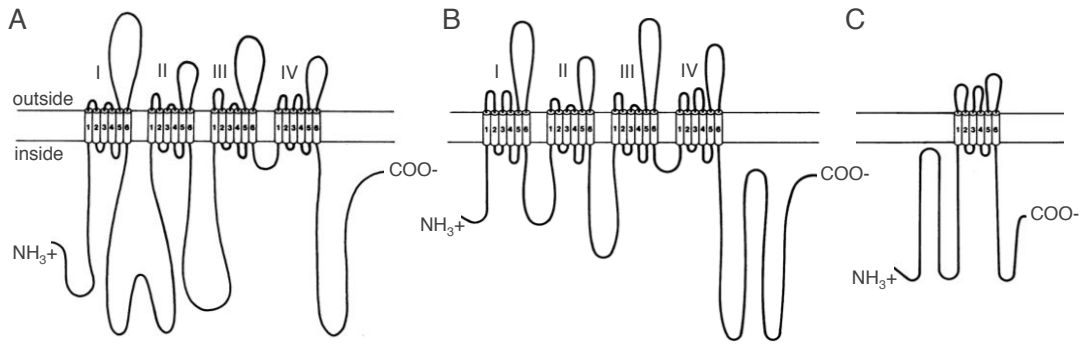

Figure 2.1.6.1. Schematic representation of subunits of voltage-gated sodium (A), calcium (B) and potassium (C) channels. In potassium channels, one subunit has 6 TM segments. The channel is formed by four identical subunits (homotetramer). In sodium and calcium channels, one subunit constitutes an entire channel and spans the membrane 24 times. The figure is adapted from [41].

The molecular cloning method opened an opportunity for site-directed mutagenesis experiments. The latters resulted in the identification of the voltage sensing segment, the highly positively charge helix S4, in voltage-gated ion channels [42,43]. Cysteine scanning of this segment revealed that some of its residues are accessible only at more depolarized voltages, while at more hyperpolarized voltages they cannot be modified by membrane-impermeant reagents [44,45]. This was a direct evidence advocating for S4 movement during application of an electric field (recall the movement of gating charges predicted by Hodgkin and Huxley, see **2.1.3**). Performing mutagenesis of the *Shaker* voltage-gated potassium channel, residues composing the intercellular gate and a putative signature sequence GYGD responsible for selectivity were revealed [46,47].

2.1.7. The first crystal structure of an ion channel

Though experimental methods such as site-directed mutagenesis provided an extremely valuable insight into the architecture of ion channels, the latter remained rather obscure until the end of the XX century, when the first crystal

structure of an ion channel was resolved. MacKinnon and colleagues succeeded to crystallize the transmembrane domain of a bacterial pH-dependent potassium channel KcsA from *Streptomyces lividans* and to resolve its atomistic structure [48,49]. For this breakthrough, MacKinnon was further awarded the Nobel Prize in Chemistry in 2003. Revealing the atomistic structure of KcsA initiated a new revolution in the general understanding of structure and functioning of ion channels and, additionally, brought more scientists using molecular modeling methods such as molecular dynamics (MD) simulations into the ion channels' field.

The structure of KcsA closely resembles the pore domain of mammalian voltage-gated potassium (Kv) channels [50] and, therefore, may be a good model for studying their mechanisms of gating and selectivity ([51–54], rev. [55,56]). KcsA is a tetramer; each subunit has 2 α-helical TM segments called M1 and M2 (see Figure 2.1.7.1). The M1 helices gathered from the four subunits encompass the conductive pore. There is also a small pore helix (P-helix) shifted to the extracellular site of the channel and following this helix loop, forming the selectivity filter [48,49].

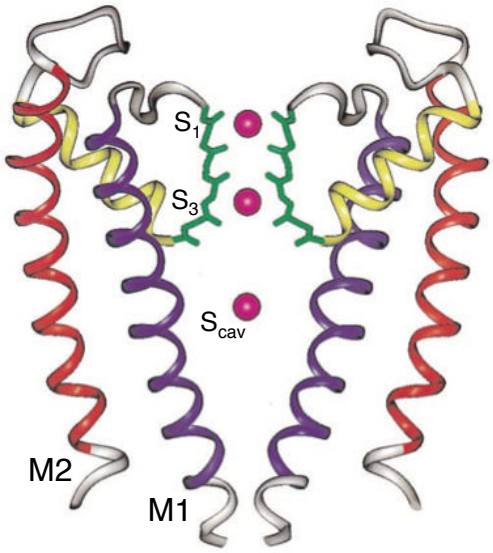

Figure 2.1.7.1. The crystal structure of the bacterial pH-dependent potassium channel KcsA. The extracellular side is at the top and the intracellular side is at the bottom. The main structural elements are the outer helix M2 (in red), the pore helix (in yellow), the selectivity filter (in green) and the inner helix M1 (in purple). Three potassium ions located at the outer and inner sites of the selectivity filter (S_1 and S_3) and at the center of the aqueous cavity (S_{cav}) are shown in magenta. The figure is adapted from [57].

The gate composed of the M1 segments faces the intracellular side. In the crystal structure of KcsA, in particular, this gate is closed [54,58]. Basically, due to a constriction of the pore below 2.0 Å at the level of the gate, a fully hydrated potassium ion, for which the average distance between K and

O (of a water molecule within its hydration shell) atoms is 2.8 Å [59], is not able to permeate. The central part of the channel constitutes an aqueous cavity. Here, the pore radius is larger than at the level of the gate and is about 5 Å, which allows a potassium ion to reside inside the channel retaining its hydration shell. The latter reduces the electric permittivity of the ion's environment and represents one of the mechanisms of ionic transport through the membrane (see **2**).

In the aqueous cavity of KcsA, a single potassium ion coordinated by 8 water molecules (S_{cav}) was resolved (see Figure 2.1.7.1). The selectivity filter, composed of the GYGD signature sequence, faces the extracellular side. This part of the channel is the most constricted one: its radius is 1.4 Å. Hence, a potassium ion entering the selectivity filter has to dehydrate at least partially in order to pass through. Four consecutive sites occupied either by potassium ions or by water molecules were identified: S_1, S_2, S_3 and S_4. There are two possible configurations: when potassium ions occupy the S_1 and S_3 sites (1010) or the S_2 and S_4 sites (0101). Water molecules occupy the resting sites. The process of ionic transport through the selectivity filter represents the alternation of configurations 0101 and 1010 [52]. A potassium ion leaving the selectivity filter gets back its hydration shell in the extracellular solution.

2.2. Voltage-gated potassium (Kv) channels

Voltage-gated potassium (Kv) channels mediate potassium transport across the membrane in response to changes in the TM voltage. Among potassium-selective ion channels, this family is the largest: around 40 different genes of Kv channels were cloned so far [60]. The Kv family can be further divided into twelve subfamilies. Subunits of Kv1 (*Shaker*), Kv2 (*Shab*), Kv3 (*Shal*), Kv4 (*Shaw*), Kv7 (*KCNQ*), Kv10 (*Eak*), Kv11 (*Erg*) and Kv12 (*Elk*) compose functional homotetrameric channels. Subunits of other subfamilies (Kv5, Kv6, Kv8 and Kv9) usually associate with Kv2 to form functional heterotetramers. The phylogenetic tree of the Kv family is present in Figure 2.2.1. Kv10, Kv11 and Kv12 stand aside from the other subfamilies. These ion channels are more closely related to CNG and HCN (see Figure 2.1.1.1), as they also have a cyclic nucleotide binding domain.

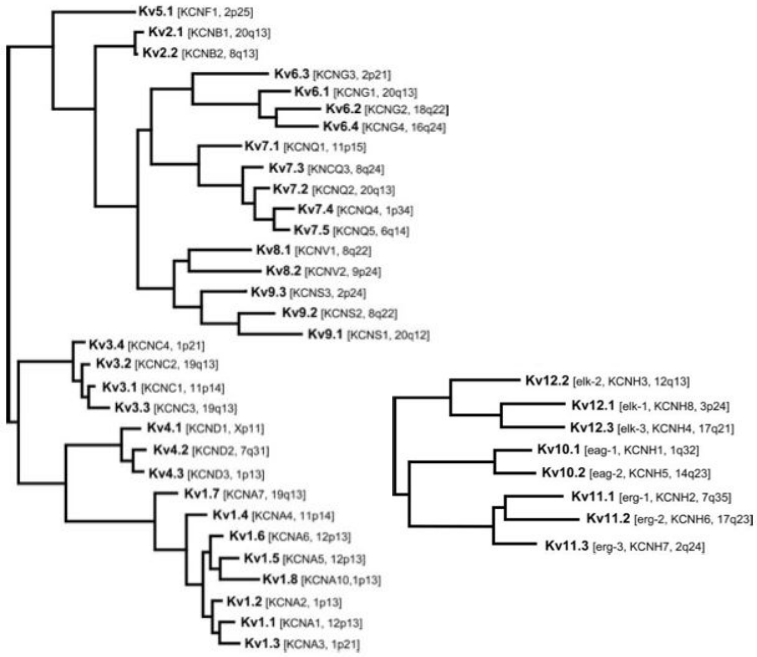

Figure 2.2.1. The phylogenetic tree of the Kv family. Subfamilies from Kv10 to Kv12 stand aside from the others (from Kv1 to Kv9). The figure is adapted from [60].

Voltage-gated potassium channels are expressed in the central and peripheral nervous systems, the heart, the skeletal and smooth muscles, the digestive and urinary systems, *etc.* (see Appendix **2.1**, Table A2.2.1), where they are involved in diverse physiological processes ranging from repolarization of neuronal and cardiac action potentials, regulating calcium signaling and cell volume, to driving cellular proliferation and migration.

2.2.1. Action potentials from a neuron and from a cardiomyocyte

Perhaps, one of the most prominent physiological processes underlined by functioning of Kv channels is repolarization of an action potential. The latter involves different voltage-gated potassium channels in neurons and cardiomyocytes. For instance, Kv1.2, one of the main objects of our interest, participates in the neuronal action potential; while the other voltage-gated potassium channel studied here, Kv7.1, is involved in the cardiac action potential. Below, we will briefly discuss the main phases of both the neuronal and cardiac action potentials.

Neuronal action potential

The schematic representation of the neuronal action potential is shown in Figure 2.2.1.1. A stimulus received by an excitable cell through a chain of events involving calcium, chloride, potassium and sodium channels cause voltage-gated sodium (Nav) channels to open. A resulting inward flow of sodium ions shifts the membrane potential from its resting values (-70 mV) to less depolarized ones. When the membrane potential reaches the gate threshold (-55 mV), more voltage-gated sodium channels open. The latter depolarizes the membrane up to +30 mV. This corresponds to the first phase of the neuronal action potential called depolarization. After a short delay, depolarization triggers activation of voltage-gated potassium channels. An outward potassium flow shifts the membrane potential toward more hyperpolarized values, resulting in repolarization, *i.e.* the second phase of the neuronal action potential. Meanwhile, voltage-gated sodium channels undergo inactivation, which prevents further flow of sodium ions inside the cell. The membrane potential drops down to -90 mV. This is the third phase of the neuronal action potential called hyperpolarization. After a few milliseconds, the membrane potential returns to its resting values, and the neuron can fire again [61].

The described action potential is typical for many neurons. Its shape may further vary from one neuron to another due to expression of different voltage-gated ion channels with their specific current amplitudes, probability of opening and kinetics of gating. For instance, in neurons of the mammalian brain, there are at least 4 or 5 different components of potassium current (Kv1.1, Kv1.2 and Kv1.4 are the most abundant in the brain, Kv7.2/Kv7.3 underlie the M-current, which is activated at sub-threshold membrane potentials, *etc.*), at least 2 or 3 components of sodium current (Nav1.2, Nav1.6 are the principal sodium channels of the axon initial segment and the nodes of Ranvier, *etc.*), and others [62,63].

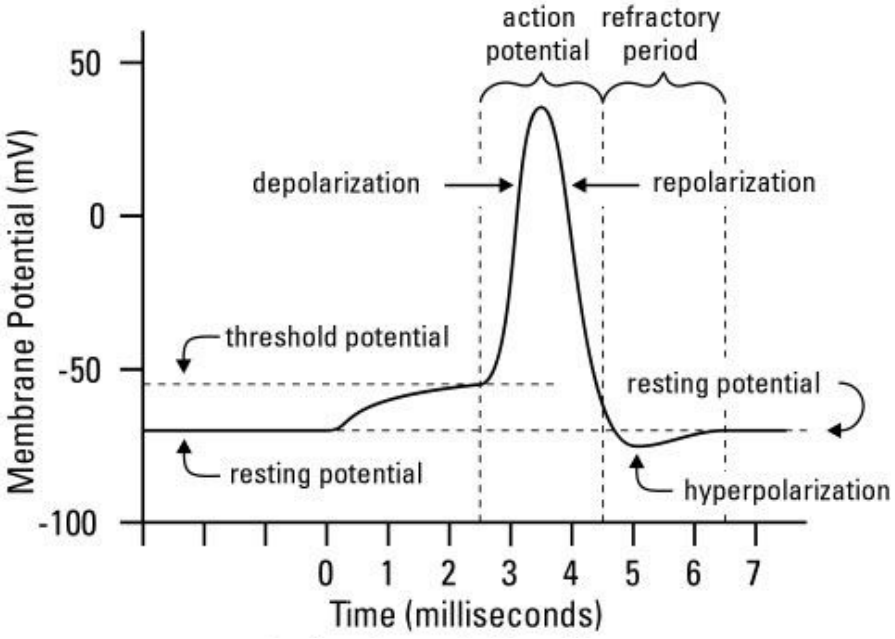

Figure 2.2.1.1. Neuronal action potential. The three phases, namely, depolarization, repolarization and hyperpolarization are shown. During depolarization, the membrane potential changes from -70 mV to +30 mV. Then, due to activation of voltage-gated potassium channels and a corresponding increase of potassium flow inside the cell, the membrane potential drops down to –90 mV (consequently, repolarization and hyperpolarization). Finally, after a few milliseconds, the membrane potential retains its resting values.

Cardiac action potential

The cardiac action potential differs from the neuronal one by:

- the duration: while in a neuron, the action potential lasts for about 1 ms, in a cardiomyocyte, it lasts from 200 to 400 ms;
- the role of calcium ions during depolarization: while in a neuron, depolarization is caused by opening of voltage-gated sodium channels, in a cardiomyocyte, in addition to this, opening of voltage-gated calcium

(Cav) channels prolongs the action potential and produces a characteristic plateau phase;

- the voltage-gated ion channels involved: in a cardiomyocyte, sodium and calcium currents are mediated by Nav1.5 and Cav1.2 respectively; the subfamilies of voltage-gated potassium channels generating outward current include Kv1, Kv2, Kv3, Kv4, Kv7 (Kv7.1) and Kv11 (Kv11.1) [64].

The schematic representation of the cardiac action potential is shown in Figure 2.2.1.2. It consists of five phases: 4) the resting potential (-90 mV); 0) the rapid depolarization of the membrane (voltage-gated sodium and calcium channels are active); 1) the rapid repolarization, which sets the membrane potential for the next phase of the action potential (sodium, calcium and potassium channels are active); 2) the plateau phase (calcium and potassium channels are active); and 3) the rapid repolarization that restores the membrane potential to its resting values (potassium channels are active).

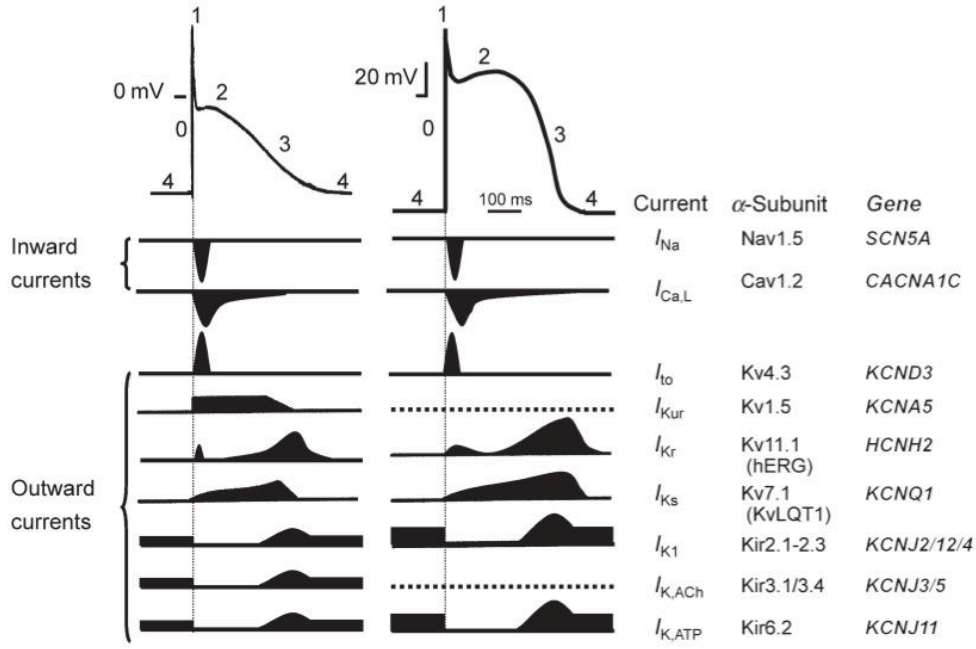

Figure 2.2.1.2. Cardiac action potential: atrial (top left panel) and ventricular (top right panel). The three other panels specify the current name, the ion channel responsible for it and the gene, encoding the ion channel, respectively. The figure is adapted from [65].

2.2.2. Typical structure of a voltage-gated potassium channel

The structures of two representatives of the Kv family, namely, Kv1.2 and the Kv1.2/Kv2.1 paddle chimera, have been resolved [66,67]. The latters provide

an insight into the basic mechanisms of gating, selectivity, activation, interaction with ligands, *etc.* in Kv1.2 and Kv1.2/Kv2.1 specifically and, moreover, in the entire Kv family. In this subsection, we will describe the structure of a typical voltage-gated potassium channel, considering Kv1.2 as an example [66].

Kv1.2 is a homotetramer; each of its four subunits has 6 TM segments. The two TM helices, S5 and S6, gathered from the four subunits constitute the central pore domain (PD) (see Figure 2.2.2.1). The overall architecture of the Kv1.2 pore domain resembles that of KcsA: there is a gate facing the cell cytoplasm, the water cavity and the selectivity filter. In contrast to KcsA, the Kv1.2 structure was resolved in the open state. The pore radius estimated at the level of the gate is about 5 Å, allowing a hydrated potassium ion to pass. There is a conserved PVP region on each of the S6 helices. This region creates a kink in the α-helical structure of S6 resulting in a wide opening of the gate.

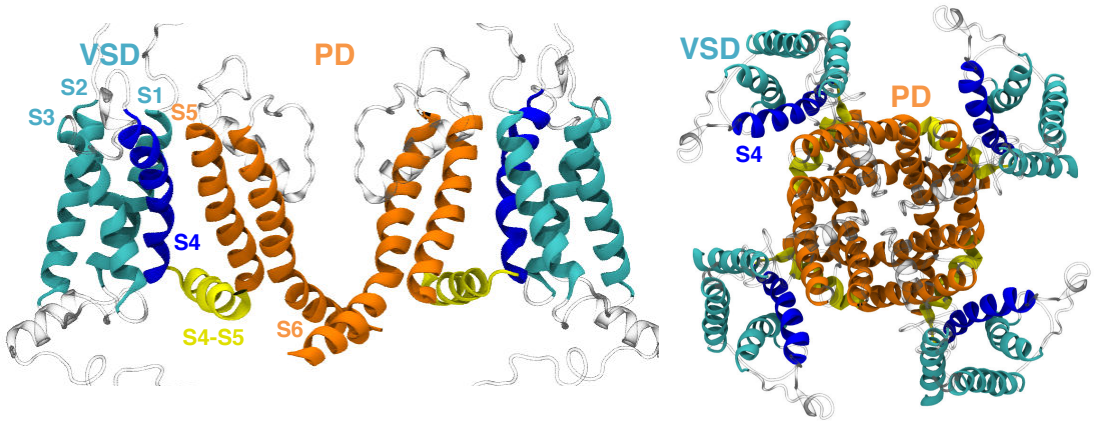

Figure 2.2.2.1. The crystal structure of the TM domain of the voltage-gated potassium channel Kv1.2 (PDB code 3LUT [66]), the side (left) and top (right) views. The Kv1.2 TM part (only two subunits are shown for clarity). The pore domain (PD, shown in orange) is composed of S5 and S6. The voltage sensor domain (VSD) is composed of S1, S2, S3 (shown in cyan) and S4 (shown in blue). The interfacial helix connecting the VSD to the PD, the S4-S5 linker, is shown in yellow.

S1 to S4 form the voltage sensor domain (VSD) of the channel (see Figure 2.2.2.2). The VSD is sensitive to the applied voltage: depending on the direction and the magnitude of the resulting electric field, this domain accordingly changes its conformation. Among the four helices, S4 is the most dynamic one. It carries several positively charged residues; in the case of Kv1.2, they are six: R294, R297, R300, R303, K306 and R309 (further called R1, R2, R3, R4, K5 and R6 respectively). This number varies among the Kv subfamilies: six in Kv1, Kv3, Kv7.2-Kv7.5, Kv10, Kv11 and Kv12, five in Kv2, Kv4, Kv5, Kv8 and Kv9 and four in Kv7.1. The positive residues of S4 sense the electric field and move in response to it: upward when the membrane is depolarized or downward when the membrane is hyperpolarized. The

stability of S4 within the hydrophobic bilayer core is enabled by several countercharges: in the case of Kv1.2, these are one glutamate on S1 (E183, further called E0), two on S2 (E226 and E236, further called E1 and E2 respectively) and one aspartate on S3 (D259, further called D). When S4 is displaced in response to an electric field, its positive residues consequently change their counterparts, with which they form salt bridges. Due to the presence of charged and polar residues in the voltage sensor, water molecules penetrate inside this domain from both the intracellular and extracellular solutions [68]. A conserved phenylalanine (F233) located on the S2 helix along with several other hydrophobic residues surrounding it serves as a plug, which separates the intracellular and extracellular water cavities of the VSD [67,69–71].

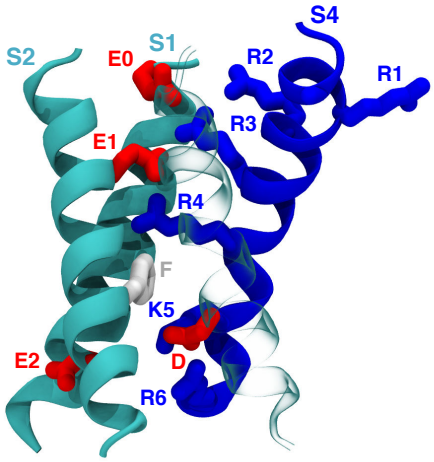

Figure 2.2.2.2. The voltage sensor domain (PDB code 3LUT [66]). R1, R2, R3, R4, K5 and R6 correspond to R294, R297, R300, R303, K306 and R309; E0, E1, D and E2 correspond to E183, E226, D259 and E236; F corresponds to F233. The S3 helix is transparent.

The short interfacial helical segment between S4 and S5, called the S4-S5 linker, links the VSD to the PD (see Figure 2.2.2.1).

2.2.3. Working cycle of Kv1.2, a typical voltage-gated potassium channel: the voltage sensor transitions

In this subsection and the following one, we will discuss the working cycle of a typical voltage-gated potassium channel, referring to the MD simulations of Kv1.2 and to the experimental data obtained for its very close homologue, *Shaker* (the voltage-gated potassium channel isolated from *Drosophila melanogaster*).

From early physiological experiments, it was already known that any ion channel has at least two states: conductive and non-conductive. These states respectively correspond to open and closed conformations of the PD. In voltage-gated ion channels, a minimum of two conformations of the VSD (activated and resting) should be additionally considered when defining a state. Hence, for any voltage-gated ion channel, one can distinguish four states: activated/open (A/O), activated/closed (A/C), resting/open (R/O) and resting/closed (R/C) (see Figure 2.2.3.1); here, the first letter refers to the state of the voltage sensor, and the second one refers to that of the pore. In the activated/open and resting/closed states, the voltage sensor and the pore are effectively coupled, meaning that the activation of the voltage sensor triggers the pore opening, and the open pore facilitates the activation of the voltage sensor. In the other states (activated/closed and resting/open), these two domains operate independently. The probability of an ion channel being in one of these four states depends on external factors (the electric field or the TM voltage applied, the lipid content of the plasma membrane, the presence of small molecules, *etc.*) and internal ones (the conformational free energies of the VSD and the PD, and the energy of interaction between the VSD and the PD). Some of these states were captured by the X-ray method (their crystal structures were resolved): Kv1.2 and the Kv1.2/Kv2.1 chimera – in the A/O state [66,67], NavAB and NavRh, the bacterial voltage-gated sodium channels, – in the A/C state [72,73]. The existence of the other states is indirectly confirmed by simultaneous tracking the conformational rearrangements of the voltage sensor and the pore (for instance, using the voltage/patch clamp fluorometry [74–77]).

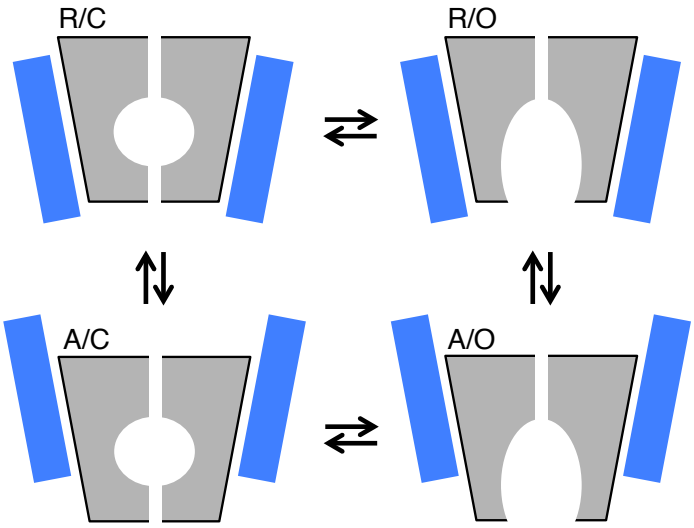

Figure 2.2.3.1. The four states of a typical voltage-gated ion channel: resting/closed (R/C), resting/open (R/O), activated/closed (A/C) and activated/open (A/O). The pore and the voltage sensors are shown in grey and blue respectively.

In the *Shaker* channel, the pore is strongly coupled to the voltage sensor, and the states where these two domains operate independently are scarcely populated. Hence, all the electrophysiological data related to this channel may be fitted with a two-state kinetic model, in which the voltage sensor activation/deactivation plays a role of a driving domain, and the pore domain adapts accordingly (see Figure 2.2.3.2).

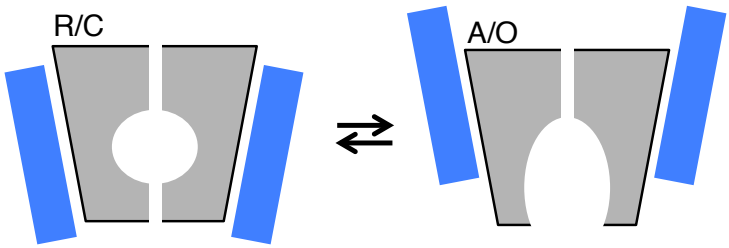

Figure 2.2.3.2. The two most populated conformational states of a voltage-gated ion channel with strong coupling between the pore domain and the voltage sensors: resting/closed (R/C) and activated/open (A/O).

However, the kinetic models considering only two states of the voltage sensor (activated and resting) are not able to reproduce the sigmoidal shape of the activation curves specific for *Shaker* [78–81] (see also Appendix **2.1**, Figure A2.1.2.1): one or several intermediate states are required. Later, several intermediate states of *Shaker* were indeed captured experimentally using sophisticated techniques such as charge reversal mutagenesis [82,83], Trp mutagenesis [69,84] and cadmium binding [85]. In Kv1.2, the existence of several intermediate conformations between resting and activated ones was demonstrated using brute force and steered molecular dynamics simulations [86,87]. Schwaiger and coworkers [88,89] have shown that at least one of these intermediate states (obtained by MD simulations) is relatively stable. In particular, they have estimated the free energy profile of the transition between the fully activated voltage sensor of the Kv1.2/Kv2.1 chimera and the following intermediate state and demonstrated that the latter indeed corresponds to a free energy well. For other voltage-gated ion channels, such as hERG, KCNQ1/KCNE1, the bacterial voltage-gated sodium channels NachBac and NavAB, the intermediate states of the voltage sensor were revealed as well [90–93].

A consensus appearing from the experimental and computational results might be summarized as follows [94]: in the VSD of voltage-gated ion channels, the intermediate states along with the activated and resting ones are defined by a specific net of salt bridges between the positive residues of S4 and its countercharges from S2, S3 and in some cases of S1. In particular, in

the Kv1.2 activated state, R6, K5, R4, R3 form salt bridges with E2, D, E1 and E0 respectively [66,67]. In the Kv1.2 resting state, the top residues of S4, namely R3, R2 and R1, are in interactions with E2, D and E1 respectively [86,87,95–98]. Accordingly, intermediate states of the voltage sensor correspond to one, two, *etc.* stepwise shift of the S4 positive residues to countercharges located one turn of a helix lower or upper during deactivation or activation processes respectively [86–89].

Our group [86], performing brute force and steered molecular dynamics simulations of the Kv1.2 channel, revealed five conformational states of the voltage sensor that were called α, β, γ, δ and ε (see Figure 2.2.3.3). In the α state (activated), the following salt bridges network is established: R6-E2, K5-D, R4-E1 and R3-E0. The two remaining residues, R1 and R2, were found to interact with the phospholipids of the upper bilayer leaflet. In the following states, the positive residues of S4 move downward altering their countercharges to those located one turn of a helix lower. Hence, in the ε state (resting), R6, K5, R4 and R3 interact with the phospholipids of the lower bilayer leaflet, and R1 and R2 form salt bridges with D and E2 respectively. The displacement of S4 during the entire transition from α to ε is estimated to be about 12 Å.

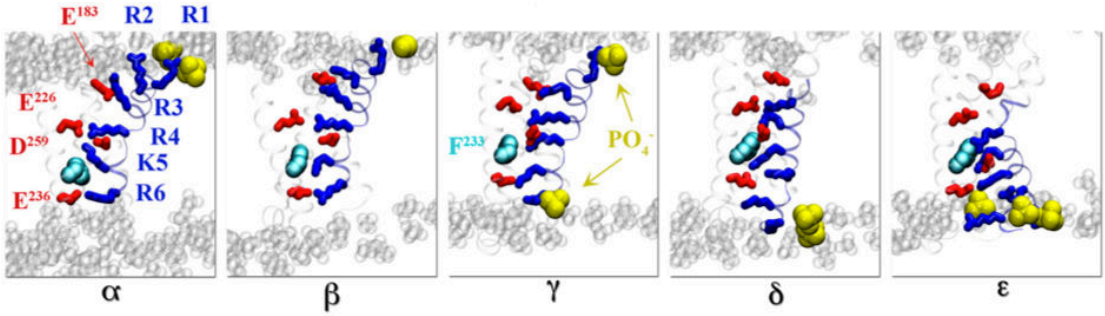

Figure 2.2.3.3. The conformational states of the Kv1.2 voltage sensor (α, β, γ, δ and ε). α and ε correspond to the activated and resting states respectively; β, γ and δ relate to the intermediate states. The positive residues of S4 (R1, R2, R3, R4, K5 and R6) and the negative residues of S1 (E183/E0), S2 (E226/E1 and E236/E2) and S3 (D259/D) are colored in blue and red respectively. The conserved phenylalanine (F233), which composes a hydrophobic barrier for the S4 positive residues, is in cyan. The phosphate groups of the phospholipids are shown in yellow. The figure is adapted from [86].

The electric force driving the Kv1.2 voltage sensor to alternate between its conformational states is set by the membrane potential. Due to the specific architecture of the voltage sensor, this force is focused in the region where highly conserved F233 resides. This residue, along with several other residues of S1, S2 and S3, composes the so-called hydrophobic plug [67,69–71].

Transferring of the S4 positive residues across the membrane gives rise to small currents (gating currents), initially predicted by Hodgkin and Huxley

(see **2.1.3**). The time integral of these gating currents at a particular membrane potential gives a gating charge (see also Appendix **2.1**) [99,100]. In the molecular model of Delemotte *et al.* [86], 11.2 elementary charges were transferred during the entire transition from α to ε, which is in a good agreement with the estimated experimentally gating charge of the *Shaker* channel (12-14 elementary charges) [79,80,101–103].

2.2.4. Working cycle of Kv1.2, a typical voltage-gated potassium channel: coupling to the pore domain

As it was previously mentioned, in the *Shaker* and *Shaker*-type channels, coupling between the VSD and the PD is rather strong: conformational rearrangements of the voltage sensor driven by changes in the membrane potential are transferred to the pore. Several experimental observations indicate that the pore opening is attributed to the last transition(s) of the voltage sensor activation. While following partial activation the gating current tails are fast, they become very slow and have a distinct rising phase after a depolarization large and long enough to fully activate the channel [79,99,104,105], indicating that the late transition along the activation path is very slowly reversible compared to the earlier ones. By introducing the ILT mutations into the S4 helix (the triple mutation V369I/I372L/S376T), the last transition of the voltage sensor can be isolated and detected experimentally. Using this strategy, Ledwell *et al.* [106,107] demonstrated that, in the *Shaker* ILT mutants, the pore opening is indeed coupled to this last transition of the voltage sensor. Del Camino with colleagues [108] captured the so-called activated/not-open state using an open state blocker, 4-aminopyridene. According to their findings, the pore undergoes some rearrangements during the resting/closed-activated/not-open transition; however, throughout this process the intracellular gate remains an effective barrier for potassium ions. Different properties of the early and late steps of the voltage sensor activation may stem from changing the level of cooperatively between the channel domains: the early steps may involve conformational rearrangements of the individual voltage sensors, whereas the late steps may be concerted, engaging simultaneous action of the four voltage sensors and the pore. Indeed, several independent experimental groups [76,109–112] demonstrated that the opening process of *Shaker* is concerted, while the transitions of the voltage sensors occur independently. Pathak *et al.* [76] further suggested that opening of the pore is accompanied by cooperative movement of S4 (in addition to the transmembrane rearrangement) that he called “gating” movement.

Some of these experimental findings along with several approximations are implemented in kinetic models of the *Shaker* and *Shaker*-type channels' gating. The latters differ by the number of independent (within a single voltage sensor) and cooperative (concerted motion of the four voltage sensors and the pore) states [69,113–118]. The development of kinetic models to describe the gating mechanism is of high importance as, on the one hand, a model provides a quantitative test, whether the proposed mechanism can simultaneously account for all the experimental observations; and, on the other hand, it may help to interpret possible alterations of the channel gating when structural modifications are introduced. One of the most recent kinetic models [69] proposes five kinetic states for the *Shaker* channel: one open (O) and four closed (C) (see Figure 2.2.4.1). Of particular notice, these kinetic states represent real conformational states of *Shaker* (see Figure 2.2.3.3): the four closed states (C1, C2, C3 and C4) differ by the salt bridges network within the voltage sensors and correspond to the resting and three intermediate conformational states, and the open state (O) relates to the activated/open conformation. The kinetic model of Tao *et al.* captures several important properties of the *Shaker* gating: 1) strong coupling between the voltage sensors and the pore; 2) opening of the pore occurs after conformational changes of the voltage sensors; 3) opening of the pore is a cooperative process; 4) five kinetic states (C1-C4 and O) differing by the voltage sensors' and the pore's conformations.

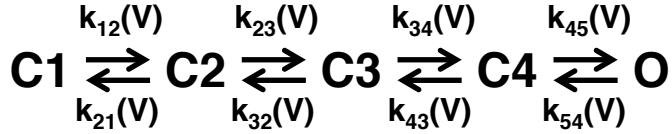

Figure 2.2.4.1. Kinetic model describing the *Shaker*'s gating [69]. The states from C1 to C4 correspond to different conformation of the voltage sensor (resting and several intermediate) and the closed pore. The O state relates to the activated/open channel. $\boldsymbol{k_{xy}(V)}$ is a kinetic constant, which depends on the applied voltage $\boldsymbol{V}$.

2.2.5. Molecular basis for coupling between the voltage sensor and the pore

Coupling is the effective communication between the voltage sensor and the pore that allows opening of the channel upon changing of the membrane potential [119]. This property is critical for voltage-gated ion channels' functioning: if coupling is disrupted, activation of the voltage sensor does not

lead to the pore opening, and the pore opening does not promote the activation of the voltage sensor.

In the *Shaker* and Kv1.2 channels, coupling is mostly mediated by interactions between the S4-S5 linker (an interfacial helix connecting the voltage sensor to the pore), and the terminus of S6 [120–125] (see Figure 2.2.2.1). The Kv1.2 crystal structure (the activated/open state) reveals that the S4-S5 linker crosses over the top of S6 and makes multiple amino acid contacts with it; in turn, the S6 terminus by curving parallel to the membrane plane constitutes a kind of a platform or "receptor" for S4-S5 [122]. The chimeragenesis experiments performed by Lu and colleagues [120,121] provided the first evidence advocating for the importance of the S4-S5/S6 interactions for coupling. In particular, they found that, in order to engineer voltage dependency into KcsA, they had to transfer to this channel the voltage sensor (from S1 to S4), the S4-S5 linker and the S6 terminus of *Shaker*. The required part of S6 corresponded to the region, which, in the Kv1.2 crystal structure, makes contact with the S4-S5 linker. Their experiments showed that the interface between S4-S5 and S6 is both necessary and sufficient to reconstruct a functioning voltage-gated ion channel, *i.e.* a channel where the VSD and the PD are coupled. Molecular dynamics (MD) simulations of Kv1.2 and the Kv1.2/Kv2.1 chimera predict that S4-S5 interacts with S6 during the entire gating process [86,87]. Coupling mediated by the S4-S5/S6 interactions has been additionally revealed in hERG, HCN, KCNQ1 and KAT1 channels [126–130].

In the Kv1.5 channel, by performing glycine, alanine and proline scanning of S4-S5 and S6, Labro *et al.* revealed two groups of residues that either physically transduce the mechanical energy or keep the correct interface intact [123]. The residues at the contact interface, namely N518, F519, F522 and Y523 (N480, F481, F484 and Y485 in *Shaker*; N412, F413, F416 and Y417 in Kv1.2) of S6 and I422 and T426 (I384 and T388 in *Shaker*; I316 and T320 in Kv1.2) of S4-S5 (see Figure 2.2.5.1), mediate the electromechanical coupling between the voltage sensor and the pore, while the other residues of S4-S5 and the S6 C-terminus serve stabilizing and structural roles, orienting the S4-S5 linker and the C-terminus of S6 correctly. Substitution of N518, F519, F522 and Y523 to glycine and alanine was not tolerated, resulting in non-functional channels. Among these residues, F519 is the most critical one, as even a bulky hydrophobic residue (leucine) at this position did not produce any measurable current. Labro *et al.* also concluded that, in Kv1.5, coupling between the voltage sensor and the pore is mostly mediated by the van-der-Waals type of interactions. In the *Shaker* channel, Haddad and colleagues [124] identified two residues of S4-S5 and S6 (I384 and F484

respectively), whose mutagenesis dramatically altered the strength of coupling. In the I384N and F484G mutants specifically, they observed a drastic separation between the Q/V[1] and I/V[2] curves (see Appendix **2.1**), indicating that the voltage sensor activation is no longer coupled to the pore opening. However, when I384 was substituted into Ala, in the resulting mutant, the separation between the Q/V and I/V curves was significantly reduced, indicating stronger coupling between the voltage sensor and the pore. Interestingly, I384 and F484 are highly conserved among the members of the Kv1 subfamily.

In addition to van-der-Waals interactions, electrostatic attractions and repulsions between residues of S4-S5 and of S6 also play an important role in coupling. In the experiments with the S4-S5Kv2.1inKv1.5 chimera (the S4-S5 linker of Kv1.5 was replaced with that of Kv2.1), Labro *et al.* showed that charge reversal mutagenesis of S6, namely, substitution of EDT (526-528 in Kv1.5) with QKR (423-425 in Kv2.1), was critical to restore channel functionality [123] (in *Shaker* and Kv1.2, these residues are E488T489D490 and E420T421E422 respectively). Performing MD simulations of the Kv1.2/Kv2.1 chimera, Nishizawa and colleagues observed a salt bridge between K380 of S4-S5 and E488 of S6 (*Shaker* numeration; in Kv1.2, these residues are K312 and E420). They suggested that E488 accounts for a major part of the S4-S5/S6 coordinated movement, *i.e.* coupling [131].

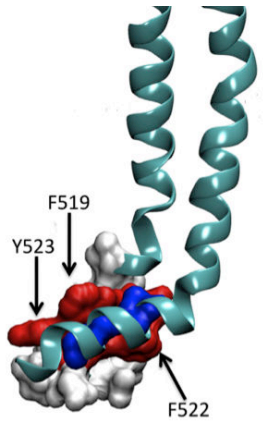

Figure 2.2.5.1. The interface between the S4-S5 linker and the S6 terminus of Kv1.5. The positions in S6 that tolerated an alanine substitution are shown in white; the residues that did not tolerate this substitution are shown in red. The S6 residues that did not tolerate a substitution form a crevice, in which residues of the S4-S5 linker fit. This crevice is largely created by the aromatic residues F519, F522 and Y523. The residues of the S4-S5 linker, residing in the S6 crevice, are shown in blue. The figure is adapted from [123].

[1] gating current vs. voltage
[2] ionic current vs. voltage

Apart from S4-S5 and S6, other TM helices and even cytoplasmic domains might participate in coupling between the voltage sensor and the pore. In the Kv1.2 crystal structure, a small interface was found at the extracellular side of the channel, formed by the interaction of the S1 segment of the voltage sensor with S5 of the pore [66,67,132]. It has been suggested that this interface plays a role in the effective translocation of the charged S4 helix upon membrane voltage changes [132]. In the *Shaker* channel, disulfide bond formation between pairs of engineered cysteines demonstrated the proximity between S4 of the voltage sensor and S5 of the pore [133,134], suggesting that the S4 and S5 interaction is involved in coupling as well. Applying similar method to the hERG channel, the cytoplasmic N-terminus was shown to be located nearby the S4-S5 linker, possibly participating in the network of interactions that mediate coupling between the voltage sensor and the pore [135–137].

Finally, the intrinsic topology of the S6 segment plays an important role in coupling. In the Kv1.2 crystal structure, the so-called PVP motif provides appropriate bending of S6, allowing this helix to interact with the S4-S5 linker [66,67,122]. In *Shaker*, substitution of P475 (the second Pro in the PVP region) by a hydrophilic residue results in a constitutively open channel with impaired coupling between the voltage sensor and the pore [138,139].

2.2.6. Particular features of Kv7.1: sequence similarities and dissimilarities with Kv1.2

While Kv1.2 is a good model for studying ionic transport, activation/deactivation, gating, *etc.*, several other members of the Kv family are also important therapeutic targets. One of them is Kv7.1 (the gene name is *KCNQ1*), a voltage-gated potassium channel, which is expressed in the heart. There, in association with the KCNE1 auxiliary subunit, Kv7.1 produces the I_{Ks} current that plays an important role in repolarization of the cardiac action potential [140] (see **2.2.1**). Additionally, Kv7.1 is expressed in the inner ear, the small intestine, the pancreas, the thyroid gland, the forebrain neuronal networks and brainstem nuclei, the lung and the ovaries [141]. In the inner ear, Kv7.1 conducts potassium current into the scala media to generate the potassium-rich endolymph solution, whereas in the small intestine tip cells, this channel regulates sodium-coupled glucose uptake.

Several mutations in genes encoding Kv7.1 and its auxiliary subunits (KCNEs) result in long QT syndrome (LQTS, see Figure 2.2.6.1) that predisposes affected individuals to cardiac sudden death. The most common forms of inherited LQTS are the autosomal Romano-Ward and the recessive Jervell and Lange-Nielsen syndromes. Unlike the Romano-Ward syndrome that affects only the heart, the less common Jervell and Lange-Nielsen syndrome also leads to hearing loss by disruption of endolymph generation, resulting in inner ear collapse [142]. Gain-of-function mutations (which confers new or enhanced activity to Kv7.1/KCNE1; opposite of loss-of-function mutations) have also been described to be associated with short QT syndrome (SQTS, see Figure 2.2.6.1) and atrial fibrillations [143]. These syndromes emphasize the critical influence of the Kv7.1/KCNE1 channels on the cardiac action potential. Additionally, Kv7.1 dysfunction can impact neurodevelopment and body size (dysfunction of the thyroid) and insulin secretion (dysfunction of pancreatic β-cells). For the review of generic disorders linked to the mutations of Kv7.1, see [142,144–147].

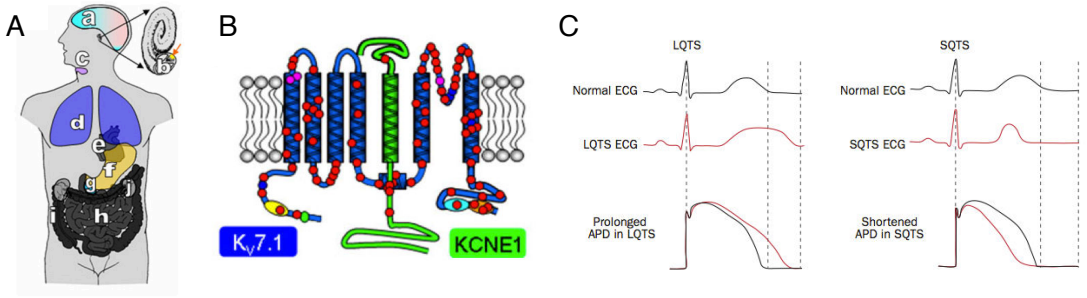

Figure 2.2.6.1. Therapeutic importance of Kv7.1. A. Kv7.1 and its auxiliary subunits are expressed in the brain (a), inner ear (b), thyroid gland (c), lung (d), heart (e), stomach (f), pancreas (g), small intestine (h), colon (i) and kidney (j). B. Mutations in Kv7.1 (blue) and KCNE1 (green) that cause loss- or gain-of-functioning (red circles denote LQTS and SQTS mutations). C. Schematic representation of a normal Electrocardiogram (ECG, black) and typical ECGs for patients with LQTS (left, red) and SQTS (right, red), illustrating QT lengthening and QT shortening respectively (top and middle panels). Tracing of normal ventricular action potential (black) and tracings that display epicardial action potential prolongation in LQTS (left, red) and action potential abbreviation in SQTS (right, red) (bottom panel). A and B are adapted from [142]; C is adapted from [148].

As Kv1.2, Kv7.1 is a homotetramer. The alignment between the Kv1.2 and Kv7.1 subunits (see Figure 2.2.6.2) indicates a higher similarity in the PD than in the VSD [149]: 32.4 % and 17.1 % respectively.

Despite the low similarity between their voltage sensors, some crucial residues of Kv1.2 are conserved in Kv7.1. In particular, in the Kv7.1 channel, S4 carries four positive residues: R1, R2, R4 and R6. The two remaining residues, R3 and K5 (found in Kv1.2), are substituted with Q and H respectively. Quite interestingly, in Kv7.1, the residue preceding R6 is negatively charged (D242), which is significantly different from Kv1.2. This

aspartate is highly conserved in the Kv7 subfamily and may play an important role in voltage dependency as its neutralization affects the activation curve [150]. The two glutamate residues of S2 (E1 and E2) and the aspartate residue of S3 (D), being countercharges to S4, are conserved in Kv7.1. The phenylalanine residue of S2, composing the hydrophobic plug, is present in both Kv1.2 and Kv7.1.

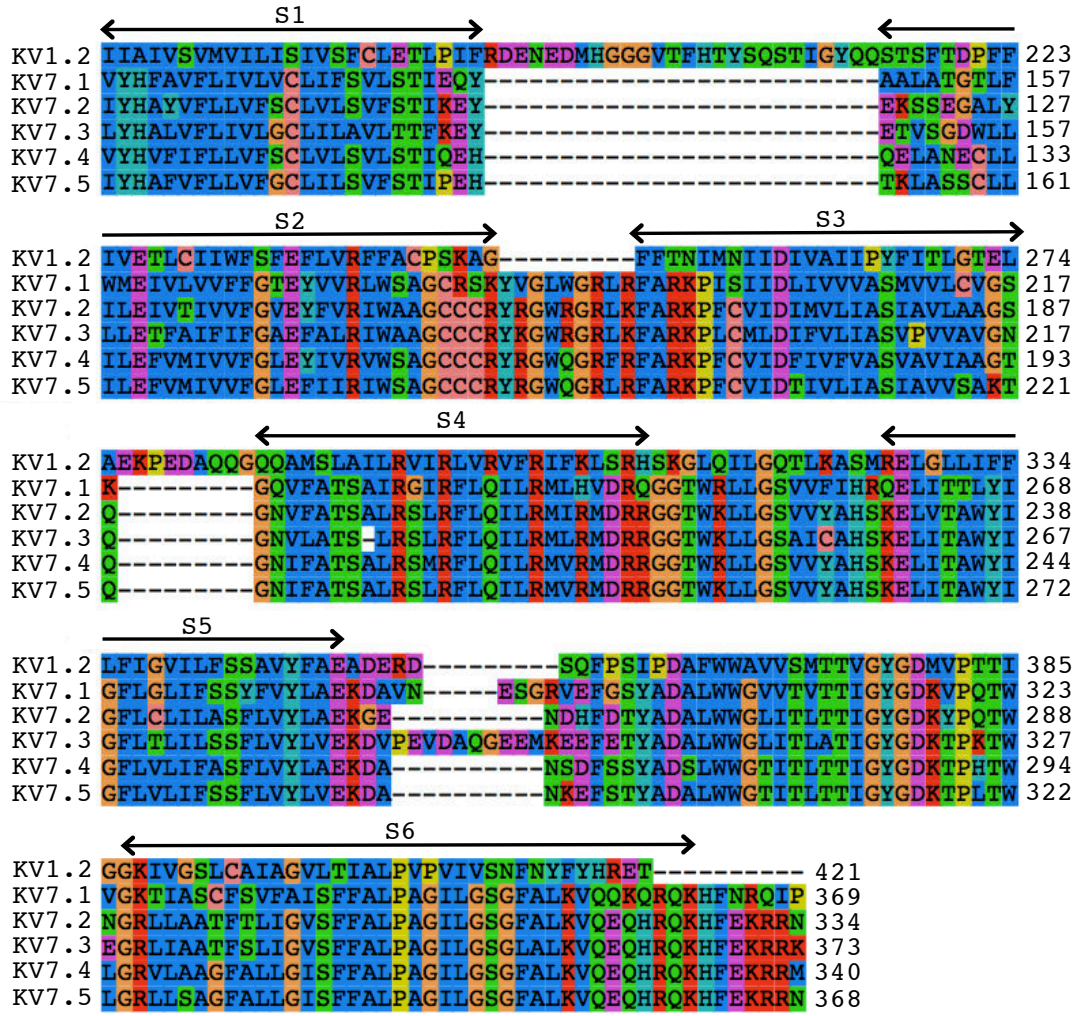

Figure 2.2.6.2. Multiple sequence alignment of the members of the Kv7 subfamily with Kv1.2. The secondary structure elements of Kv1.2 (from S1 to S6) are indicated by the arrows.

The loops, connecting the TM segments of the voltage sensor, are drastically different in Kv1.2 and Kv7.1. Hence, while in Kv1.2, the intracellular S2-S3 loop is rather short and slightly positively charged (K247), in Kv7.1, this loop is 9 residues longer and carries 6 positively charged residues (R181, K183, R190, R192, R195 and K196). Interestingly, the S2-S3 region is extremely well conserved among the members of the Kv7 subfamily. Moreover, several mutations of this region were shown to cause inherited cardiac diseases (see Figure 2.2.6.1B) [142,151–155], suggesting an important role of S2-S3 in functioning of the Kv7 channels. Recent NMR data indicate

that the S2-S3 loop adopts an α-helical conformation [156]. The extracellular S1-S2 loop is 26 residues shorter in Kv7.1 than that in Kv1.2.

The voltage sensor of Kv7.1 seems to function in a similar fashion as that of Kv1.2. Charge reversal mutagenesis of the S4 positive residues and E1 (E160) of S2 performed by Wu *et al.* indicate existence of at least three different states of the Kv7.1 voltage sensor, namely, fully activated, intermediate and resting [91]: in the fully activated and resting states of Kv7.1, similar to Kv1.2, the E1 residue of S2 is found in interactions with R4 and R1 respectively. In agreement with these experiments, for other members of the Kv7 subfamily (Kv7.2 and Kv7.4), Micelli and colleagues demonstrated that a decreased positive charge at the N-terminal end of S4 stabilizes the activated state of the voltage-sensor, while neutralization of a positive charge at the C-terminal end of S4 favors the resting conformation [157,158].

The pore domains of Kv7.1 and Kv1.2 share more similarity than their voltage sensors. The sequence of the selectivity filter is almost fully conserved in these channels: in Kv7.1 and Kv1.2, this sequence corresponds to TVGYG and TIGYG respectively. The hinge region is as well partially conserved being PVP in Kv1.2 and PVG in Kv7.1. The phenylalanine of S6 (F481 in Kv1.2 and F351 in Kv7.1) is present in both of these channels. Moreover, as in the case of Kv1.2, this residue seems to participate in coupling between the voltage sensor and the pore of Kv7.1. Indeed, mutagenesis of F351 along with two other hydrophobic residues of S6 (L353 and V355) drastically changes voltage dependency of Kv7.1 [159]. Several other residues involved in coupling in Kv1s are substituted in Kv7.1: whereas the mutagenesis of N518, F522 and Y523 into alanine or glycine was not tolerated in Kv1.5 [123] (see **2.2.5**), in Kv7.1, these residues are replaced with glycine (G350), lysine (K354) and valine (V355). Finally, in Kv7.1, the S6 helix has a unique sequence, SFF (338-340), which may participate in association with the KCNE1 auxiliary subunit [160].

2.2.7. Particular features of Kv7.1: coupling

Another important difference between Kv1.2 and Kv7.1 that we would like to emphasize is in the coupling between the voltage sensor and the pore. For Kv1.2 and Kv7.1, two different models of coupling were proposed: the mechanical lever and ligand/receptor model respectively [130,161] (see Figure 2.2.7.1).

In the mechanical lever model (see Figure 2.2.7.1A) proposed for the Kv1.2 and *Shaker* channels [130], the pore is strongly coupled to the voltage sensors: the S4-S5 linker establishes a strong interaction with the S6 terminus, which prevents the pore opening even if a single voltage sensor is not in the fully activated state [121]. When all the four voltage sensors become activated, the pore opens being pulled by the displaced S4-S5 linkers (levers). This scheme is implemented in the kinetic models describing the gating process of Kv1.2 and *Shaker* (see **2.2.4**). In these models, the latter is represented as a sequence of several relatively independent transitions within individual voltage sensors, terminated by the concerted conformational change leading to the pore opening.

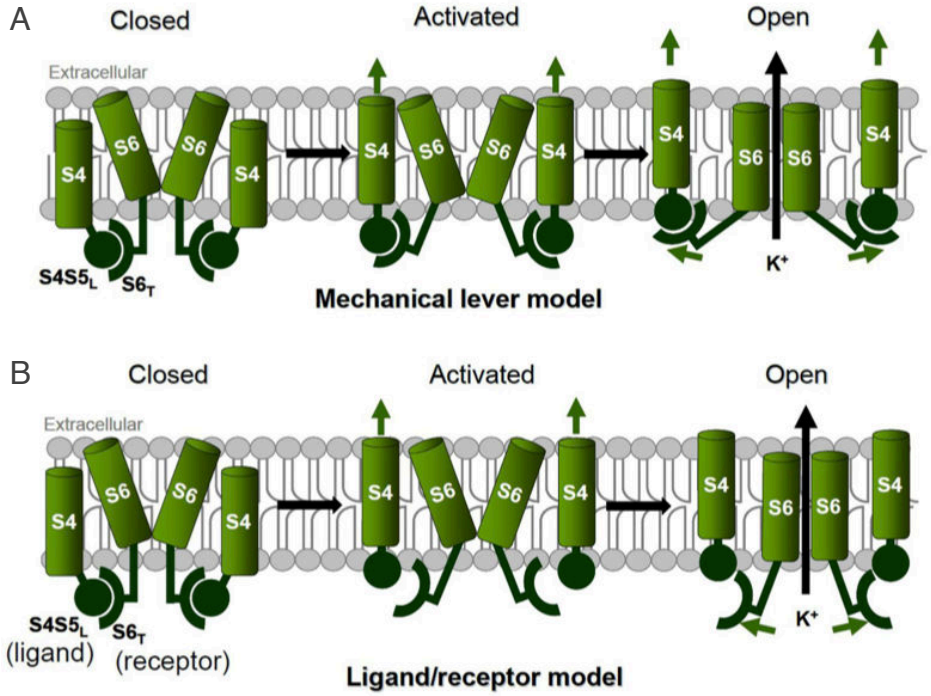

Figure 2.2.7.1. Two models of coupling between the voltage sensor and the pore. A. The mechanical lever model with a strong coupling between the voltage sensor and the pore, as suggested for Kv1.2 and *Shaker*. B. The ligand/receptor model with a loose coupling between the voltage sensor and the pore, as suggested for Kv7.1. The figure is adapted from [130].

In contrast to the Kv1.2 and *Shaker* channels, coupling between the voltage sensors and the pore of Kv7.1 is rather loose. Several experimental observations advocate for this:

- in Kv7.1, the F/V [3] and G/V [4] curves (see Appendix **2.1**), which respectively track the S4 displacement and ionic current, overlap [162], indicating that the voltage sensors and the pore change their

[3] fluorescence vs. voltage
[4] conductance vs. voltage

conformational state simultaneously; the latter also suggests that the pore opening may occur before all four voltage sensors are fully activated; for comparison, in *Shaker*, the Q/V[5] curve (see Appendix **2.1**), which as F/V tracks the S4 displacement, is separated from G/V by a shift [99,100];

- in Kv7.1, an instantaneous current is detected [163]; considering that Kv7.1 posses an intrinsically open pore (a significant number of point mutations give rise to the constitutively open channel [163]), a fraction of constitutive conductance is probably caused by inability of the voltage sensors to keep the pore fully closed;
- the Kv7.1 heteroteramers, in which two voltage sensors are constitutively activated due to the R231C mutation, have a significant probability of spontaneous opening even though the two other voltage sensors remain in their resting states [164];
- introducing mutations in individual subunits of the Kv7.1 tetramer, Meisel *et al.* [165] revealed a linear relationship between the shift in the voltage dependence of activation and the number of mutated subunits, suggesting that each subunit produces an incremental contribution to channel gating in contrast to the Kv1.2 and *Shaker* channels.

The ligand/receptor model (see Figure 2.2.7.1B) captures the loose coupling between the voltage sensors and the pore in Kv7.1 [130]: when the voltage sensors are resting, the S4-S5 linker binds to the S6 terminus as a ligand to its receptor, constraining the pore in a closed conformation; during the activation, S4 drags the S4-S5 linker away from S6, releasing the pore and leading therefore to its opening. This model is in agreement with the experimental data obtained by Choveau and colleagues [129]. In their work, Choveau *et al.* designed peptides sharing similar amino acid sequence with the S4-S5 linker (the ligand) and with the S6 terminus (the receptor) of Kv7.1. Co-expression of the S4-S5 peptides and the channel results in a reduction of the voltage-dependent potassium current; in contrast, the S6 peptides up-regulate the channel's activity, by competing with the endogenous S6 and decreasing the inhibitory effect of the S4-S5 linker binding to the endogenous S6. The kinetic models describing the gating process of Kv7.1 consider loose coupling between the voltage sensors and the pore; these models are allosteric and take into account the fact that the pore opening may occur before all four voltage sensors become activated [163,164,166,167].

[5] gating current vs. voltage

2.3. Regulation of ion channels' functioning by the cell membrane

The key function of lipid bilayers, being a barrier to unregulated solute movement, can be achieved by just one or a few lipid species. A cell membrane, however, is composed of any number of more than 200 different lipid species [168]. This variety is required for another important function, namely, regulation of proteins embedded into the cell membrane. This regulation may be mediated via specific chemical interactions between protein groups and individual lipid molecules as well as via non-specific effects, when the cell membrane behaves as an entity with collective physical properties (thickness, intrinsic monolayer curvature, compression and bending moduli). In this section, we will briefly discuss the non-specific and specific regulation of ion channels' functioning by the cell membrane and describe in more details the regulative effect of phosphatidylinositol-4,5-bisphosphate (PIP_2), a minor lipid of the inner bilayer leaflet. The two last subsections are devoted to the modulation of Kv1.2 and Kv7.1, the two main objects of our interest, by PIP_2.

2.3.1. Stabilization of poorly populated ion channels' states by the modified bilayer content

Before describing in details the non-specific and specific regulation of ion channels' function by the cell membrane, it is interesting to point to the reader ways in which such a mechanism has been taken advantage of. In general, lipids regulate ion channels embedded into the cell membrane by modifying the relative stabilities of their conformational states: application or depletion of some lipids may affect the free energy underlying the gating process and even shift the thermodynamic equilibrium from one metastable state to another. This interesting effect can be used experimentally for trapping

voltage-gated ion channels in specific conformations when resolving a high-resolution structure.

Among the challenges to obtain high-resolution structures of different states of voltage-gated ion channels are the technical difficulties associated with the simultaneous and vectorial application of an electric field to a population of molecules. These conditions have not been achieved experimentally in membrane-reconstituted systems. Therefore, structures of voltage-gated ion channels obtained so far correspond to conformational states stable at 0 mV; structures of other conformational states corresponding to the most populated ones at negative or positive membrane voltages remain unresolved. A plausible alternative to the application of electric fields is the modification of the surrounding lipid content that leads to the redistribution of the probabilities of voltage-gated ion channels' states. This idea was first implemented by Perozo and colleagues [169], when they succeeded to trap the voltage sensor of KvAP in its activated and resting states without application of electric fields but by reconstituting this channel in different lipid bilayers. Indeed, Perozo *et al.* demonstrated that the activated conformation of the KvAP voltage sensor is more stable than its resting one in a 1-palmitoyl-2-oleoyl-*sn*-glycero-3-phosphocholine/1-palmytoyl-2-oleoyl-glycero-3-phospho-1-glycerol (POPC/POPG) bilayer at a 3:1 ratio. The resting conformation, on the other hand, was mostly populated when KvAP was reconstituted in a positively charged 1,2-dioleoyl-3-trimethylammonium-propane (DOTAP) bilayer.

2.3.2. Non-specific regulation of ion channels' functioning by the cell membrane

Embedding ion channels into the cell membrane *per se* perturbs lipids packing and dynamics [170,171]. Moreover, conformational changes during the gating process may affect the protein/bilayer interface and, therefore, lead to further perturbation of the cell membrane (see Figure 2.3.2.1). This perturbation incurs an energetic cost that depends on the physical properties of the lipid bilayer, such as thickness, intrinsic curvature, compression and bending moduli [172–177]. The total energetic cost of an ion channel transition between two states A and B ($\Delta G_{tot}^{A\rightarrow B}$) may be decomposed into two free energy terms related to the protein conformational changes ($\Delta G_{prot}^{A\rightarrow B}$) and to the bilayer deformation ($\Delta G_{bilayer}^{A\rightarrow B}$):

$$\Delta G_{tot}^{A\to B} = \Delta G_{prot}^{A\to B} + \Delta G_{bilayer}^{A\to B}. \quad (2.3.2.1)$$

Several physical properties of cell membranes change upon mechanical stress. For instance, compressing or stretching (by applying positive or negative pressures respectively) affect the thickness of the membrane, the order parameter of the lipids and its elastic constants that reflect the ability to bend and to curve [178,179]. Similar modifications may be achieved by altering the bilayer content. Application of cholesterol affects several properties of the membrane (*e.g.*, the molecular order parameter, the lipid phase preference, the lateral pressure profile, the bilayer compression and bending moduli, the bilayer thickness and the intrinsic curvature [180–184]). Other well-known modulators are the polyunsaturated fatty acids (PUFAs). These lipids are somewhat conical in their shape, with the hydrocarbon chain occupying a larger packing place than the polar region. When applied to the membrane, they induce a negative curvature of the bilayer [185,186]. Moreover, PUFAs affect the packing of phospholipids and thus the fluidity of the bilayers [187]. Finally, other lipid metabolites and amphiphiles such as lipophilic drugs are also able to modify the physical properties of cell membranes [188].

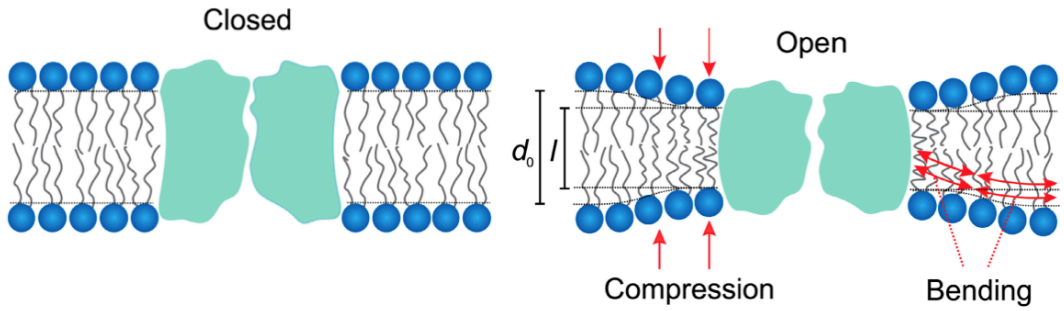

Figure 2.3.2.1. The so-called hydrophobic coupling between a bilayer-spanning membrane protein (ion channel) and its lipid bilayer host. A protein conformational change causes a local bilayer deformation (right). This deformation incurs an energetic cost that should be taken into account when estimating the free energy of an ion channel transition from the closed state (left) to the open one (right). The figure is adapted from [177].

Alteration of the physical properties of cell membranes may affect the opening probability of many ion channels. For some of them, such as the bacterial mechanosensitive channels MscL and MscS (see **2.1.1**), the mechanical stress is a primary stimulus, which triggers gating. Others, while being mainly regulated by membrane voltage or ligand binding, may still be affected by a mechanical stress [189]. In the *Shaker* channel, stretch (<40mmHg, within the usual range for studying mechanosensitive channels) facilitates the pore opening when the probability of opening due to membrane depolarization is low, but impairs further opening when the

probability of opening is already high [190]. Membrane stretch speeds up the rate of inactivation in voltage-gated sodium channels (α-subunit only) expressed in skeletal muscles. However, in the presence of a β-subunit, the membrane stretch fails to further modulate gating [191,192]. The opening of L- and N-type calcium channels is reversibly altered by events that affect membrane stretch, such as cell swelling [193] and membrane depletion of cholesterol [194].

Cholesterol modulates several ion channels [195,196]. For some voltage-gated potassium, sodium and calcium channels, cholesterol decreases the opening probability and the unitary conductance. Several transient receptor potential (TRP) channels (see **2.1.1**) are, on the other hand, inhibited by the removal of membrane cholesterol. There are some examples, when changing the level of membrane cholesterol affects the voltage dependency of the channel activation and inactivation (rev. [197]). PUFAs inhibit sodium current in cardiac, skeletal and smooth muscle cells, where in most cases they induce a left-shift of the steady-state inactivation [198,199]. They usually inhibit voltage-gated calcium current and modulate their time course of inactivation (rev. [200]). Most often, PUFAs inhibit potassium channels although there are some examples of enhanced potassium current [201–204]. In the case of cholesterol or PUFAs, additional effects induced by the direct interaction between these lipids and the ion channels may also take place [205–207].

2.3.3. Lipid content may contribute to the membrane potential

Finally, we would like to discuss another physical property of cell membranes that is especially important for voltage-gated ion channels and might be affected by the lipid content of a bilayer, namely the membrane potential. Several experiments indicate that changing polarity or charge of the lipid headgroups of the membrane affects the probability of voltage-gated ion channels to be in the open or closed states. Schmidt *et al.* reported that when KvAP is expressed in a bilayer composed of positively charged lipids (DOTAP) instead of zwitterionic or negatively-charged ones (1-palmitoyl-2-oleoyl-glycero-3-phospho-ethanolamine, POPE, and POPG), no channel activity is observed [208]. Similar results were obtained when KvAP was embedded into a bilayer of negatively charged (1,2-dioleocyl-glycero-3-succinate, DOGS) or polar (glucocerebrosides, GlucCer) lipids lacking the phosphate groups [208]. The modification of the lipid headgroups by

enzymes may affect the equilibrium state of a voltage-gated ion channel as well. Sphingomyelinase D targets sphingomyelin, a zwitterionic phospholipid present mainly in the outer bilayer leaflet [209]. This enzyme removes the choline group of sphingomyelin, yielding negatively charged ceramide-1-phosphate. Ramu *et al.* demonstrated that this modification of the outer bilayer leaflet favored the open state of the Kv channels [210,211]. Another enzyme, sphingomyelinase C, removes the entire headgroup of sphingomyelin, yielding ceramide, a polar lipid bearing no phosphate. The predominance of polar lipids in the outer bilayer leaflet favors the closed state of the Kv channels [211]. Other examples of altered channel conductance were reported [212,213].

In a recent work [214], we tested whether the membrane potential of three asymmetric bilayers, sphingomyelin/POPC, ceramide-1-phosphate/POPC and ceramide/POPC, differ. The results of MD simulations indicated that, for the neutrally charged bilayers, the transmembrane potential accounted for -60±50 mV. In the system with the ceramide-1-phosphate/POPC bilayer, the transmembrane potential was reduced to -130±50 mV. Hence, altering the charge of the lipids, composing the bilayer, may indeed affect the membrane potential and, therefore, potentially modifies the equilibrium state of voltage-gated ion channels embedded in this bilayer.

2.3.4. Specific regulation of ion channels' functioning by the cell membrane

Direct interaction between the lipids and ion channel's residues underlie the mechanism of specific regulation. In this case, several residues of the ion channel compose a binding site, where an interacting lipid binds with high affinity. Mutagenesis of these residues may affect the interactions between the ion channel and the lipid and, therefore, alter the regulative effect. Identification of such binding sites is a strong evidence for specific versus non-specific regulation of lipid content.

Besides modulating the physical properties of cell membranes, as previously discussed (see **2.3.2**), cholesterol and PUFAs may directly bind to ion channels. Xiao *et al.* identified a potential binding site for PUFAs, made up by N406 in DI-S6 of the cardiac voltage-gated sodium channel. When this residue is mutated, PUFA largely loses its inhibitory action on sodium current

[205]. In Kir2.1, Rosenhouse-Dantsker *et al.* revealed two specific regions that play a critical role in the sensitivity of this channel to cholesterol: mutations of residues composing these regions abrogated or significantly decreased the sensitivity of Kir2.1 to cholesterol [206]. In the Kv7.1 channel, W539 of a cytoplasmic region was proposed to interact with cholesterol [207].

In voltage-gated ion channels, the voltage sensors, and in particular the positive residues of S4 are potential binding sites for lipids composing a bilayer. Prior to the crystal structure determination, using site-directed spin labeling and electron paramagnetic resonance spectroscopy, Cuello *et al.*, showed that the S4 segment of the bacterial voltage-gated potassium channel KvAP is located at the bilayer/solution interface [215]. Similar results were obtained by MacKinnon and coworkers, who studied the mechanism of action of a voltage sensor toxin, VSTX1, from the Chilean Rose Tarantula [216]. Further, in the crystal structures of Kv1.2 [66] and the Kv1.2/Kv2.1 chimera [67], both resolved in an activated/open state, the top positive residues of S4 (R1 and R2) were indeed shown to be located at the level of a potential bilayer/solution interface. MD simulations of these channels embedded in a model phospholipid bilayer indicated that R1 and R2 come in interaction with lipid headgroups, establishing stable electrostatic interaction with their negatively charged phosphates [217–221]. In the models of the resting/closed state conformation, the resting state position of the S4 helix favors the interaction of its bottom positive residues (R4, K5 and R6) with headgroups of the inner membrane leaflet [95–97]. Modeling studies, uncovering the entire deactivation pathway, revealed that the top and bottom charges of S4 may interact respectively and simultaneously with the headgroups of the inner and outer membrane leaflets in given intermediate states [86,87] Further experiments demonstrated the important influence of lipid headgroups on the function of voltage-gated ion channels: reconstitution of the bacterial voltage-gated potassium channel KvAP in a bilayer that is composed of lipids lacking phosphate groups abolishes any ionic current [208]. As mentioned above (see **2.3.3**), the enzymatic modification of sphingomyelin headgroups [210,211] affects equilibrium between open and closed states of the Kv channels. Importantly, this effect was attributed to a specific part of the voltage sensor, indicating a direct interaction between the protein and the lipid headgroups [214,222].

In general, as illustrated in Figure 2.2.3.3, the phosphates of lipid headgroups provide binding sites for top and bottom positively charged residues of S4 when this helix is activated or resting respectively. This interaction between an ion channel and the surrounding lipids additionally stabilizes a specific conformation of the voltage sensor: activated or resting.

Modification of this interaction potentially shifts the thermodynamics equilibrium between different states of the ion channel as evidenced from experiments.

2.3.5. PIP_2 modulates functioning of many ion channels via direct interactions with their positive residues

Phosphatitylinositol-(4,5)-bisphosphate, $PI(4,5)P_2$, is the substrate for phospholipase C and constitutes up to 1 % of the phospholipids in the plasma membrane, where it is localized in the inner, cytoplasmic leaflet [223] (see Figure 2.3.5.1). $PI(4,5)P_2$ is one of the most important regulators of most studied ion channels [224,225]. Mutation of residues responsible for PIP_2 sensitivity may lead to severe genetic disorders (rev. [226,227]). Other phosphoinositides present in cell membranes, *e.g.* PI(4)P, $PI(3,4,5)P_3$ and $PI(3,4)P_2$, also regulate ion channels [228–231] (these phosphoinositides differ by the number and location of phosphate groups of the inositol ring). However, the variety of these ion channels is less broad than those regulated by $PI(4,5)P_2$, and, in addition, physiological concentration of PI(4)P, $PI(3,4,5)P_3$ and $PI(3,4)P_2$ is lower than that of $PI(4,5)P_2$'s concentration [232,233].

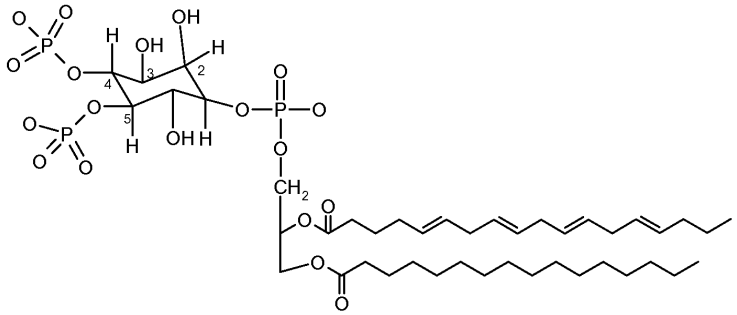

Figure 2.3.5.1. Structural formula of Phosphatitylinositol-(4,5)-bisphosphate (PIP_2).

$PI(4,5)P_2$ (further PIP_2) is a specific physiological regulator as evidenced from several factors. First, as previously mentioned, its concentration is higher compared to other phosphoinositides present in the cell. Second, since PIP_2 is found almost exclusively in the plasma membrane, the functional dependence on PIP_2 keeps ion channels inactive whenever they are not in the plasma membrane, *i.e.* during trafficking. And third, since plasma membrane PIP_2 can be transiently depleted by neurotransmitters activating phospholipase C, the activity of this group of ion channels can be regulated by the incoming signals.

Hilgmenann and Ball first reported the PIP_2 dependence of two cardiac ion transport proteins, the sodium-calcium exchanger and KATP channels, in excised patches [234]. Their basic observation was that the currents ran down strongly within a minute after excision of the patch but could be restored by application of Mg^{2+}/ATP to the cytoplasmic face of the membrane. The deduction was that rundown is caused by the dephosphorylation of PIP_2 in the inner leaflet of the membrane in the absence of normal cytoplasm, and that Mg^{2+}/ATP is a missing ingredient to fuel lipid kinases that continually restore PIP_2 concentrations by phosphorylating the inositol ring. After their discovery, a surprising number and variety of ion channels has been reported to be regulated by PIP_2. Among these channels, there are members of the Kir, Kv, hERG, HCN, CNG, Cav, TRP, K2P and ENaC subfamilies (rev. [224,225]) (see Figure 2.3.5.2). In general, for these channels, application of PIP_2 leads to gain-of-function effects, *e.g.* activation (Kir, Kv7, hERG, HCN, Cav, some TRP, K2P and ENaC), slowed inactivation or removal of inactivation (Kv, hERG). However, there are several exceptions: some TRP channels and CNG are inhibited by PIP_2.

The mechanism of Kir channels' regulation by PIP_2 is one of the best studied. For these channels, PIP_2 along with ions, polyamines, nucleotides and intracellular protein is the primary factor that induces activation. Prior to determination of a crystal structure, mutagenesis of Kir2.1 had revealed several key residues in the C-, N-termini and the region right after the second TM segment responsible for PIP_2 sensitivity [235,236]. These residues may compose one or several PIP_2 binding sites, indicating, therefore, a specific regulation of Kir2.1 by this lipid. In agreement with these findings, mutagenesis of homolog residues in other members of the Kir subfamily (Kir1.1, Kir6.2 and Kir5.1) reduces their apparent affinity for PIP_2 [237–239]. After MacKinnon and coworkers resolved the crystal structures of Kir2.1 alone and of its complex with a PIP_2 short-chain derivative, they demonstrated that previously identified regions come in proximity to each other and indeed form a PIP_2 binding site [240]. In the crystal structure of the complex, PIP_2 derivatives are located at the interface between the TM domain and the cytoplasmic domain, interacting with a cluster of positively charged and aromatic residues (RWR). Comparison between the Kir2.1 structures with and without PIP_2 derivatives allowed MacKinnon and coworkers to suggest the mechanism, underlying modulation of this channel by PIP_2 [240]. In particular, binding of PIP_2 induces conformational changes of a specific linker region and results in its contraction to a compact helical structure. This is accompanied by the translation of the entire cytoplasmic domain 6 Å closer to the membrane, which causes opening of the gate. Later, docking simulations and the electrophysiological experiments on specific single and double

mutants of Kir2.1 revealed a second PIP_2 binding site, which, however, is less specific to this lipid compared to the previously identified one [241].

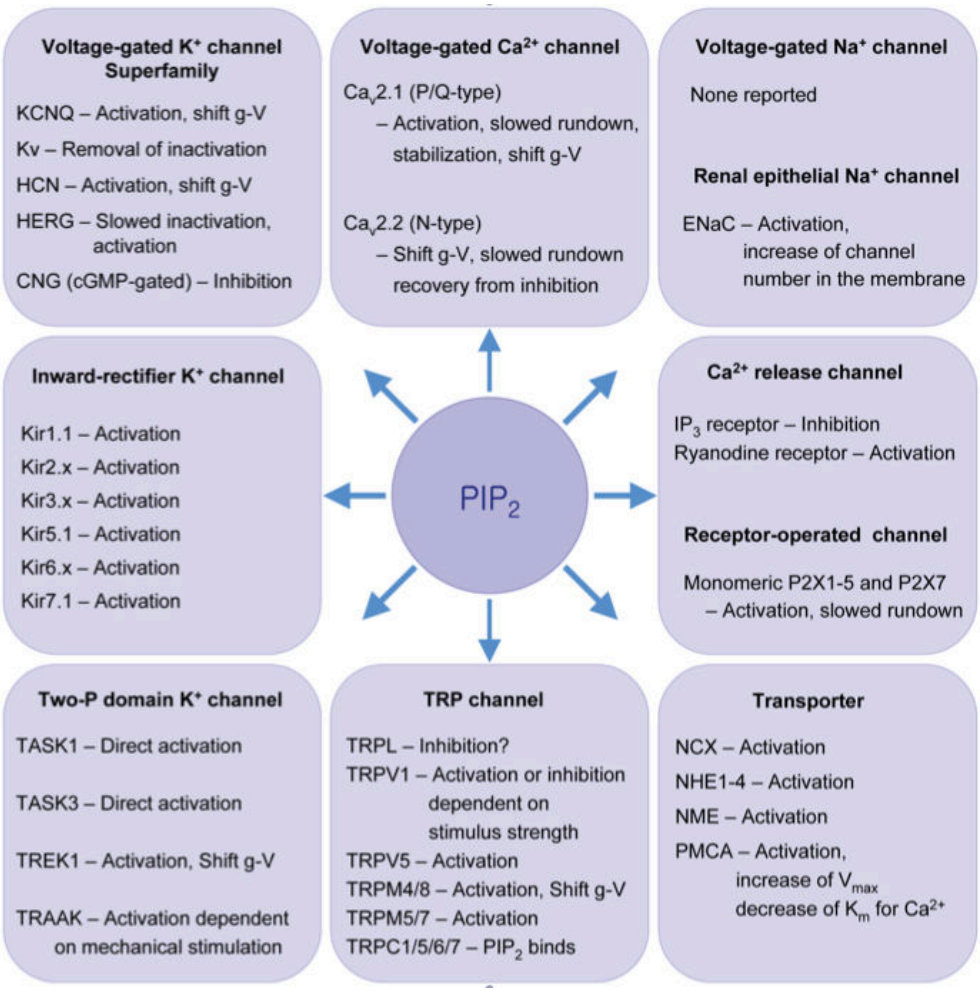

Figure 2.3.5.2. Ion channels and transporters sensitive to PIP_2. They include: Kir, inward rectifier potassium channels; Kv (including *KCNQ*), voltage-gated potassium channels; hERG, human *ether-a-go-go*-related gene potassium channels; HCN, hyperpolarization-activated channels; CNG, cyclic nucleotide-regulated channels; Cav, voltage-gated calcium channels; TRP, transient receptor potential; ENaC, epithelial sodium channel. The figure is adapted from [224].

The structure of another Kir family member (GIRK2) was also resolved by the MacKinnon group and demonstrates a more complicated mechanism of PIP_2-dependent gating compared to Kir2.1 [242]. This channel is modulated by both PIP_2 and G-proteins. In order to shed light on the gating mechanism of GIRK2, four structures were resolved: native without short PIP_2 derivatives, native with PIP_2 derivatives, R201A mutant, in which the G-protein activated gate is constantly open, without PIP_2 derivatives and R201A mutant with PIP_2 derivatives. Similar to Kir2.1, the crystal structures of the GIRK2 complexes with PIP_2 derivatives show that the latter lipids are coordinated by positively charged residues. Comparison among the four structures revealed that while the G-protein activates the G-loop gate, PIP_2 controls another channel gate located at the level of the inner helix [242]. In

particular, binding of PIP_2 initiates a rotation of the GIRK cytoplasmic domain, which propagates across the interface between the cytoplasmic domain/TM domain and results in an opening of the inner helix gate up to 11 Å.

Mutagenesis of some other ion channels such as Kv7.1, Kv7.2/Kv7.3, Kv1.2, SpIH (HCN), TRPM8, TRPM4 or deletion of short positively charged segments in TRPV1, hERG was shown to alter apparent PIP_2 sensitivity or the effect on functioning induced by PIP_2 [167,207,231,243–253], advocating for a specific regulation as in the case of the Kir subfamily. Finally, considering that the concentration of this lipid in the plasma membrane is very low, we expect that PIP_2 regulates the majority of ion channels via specific binding to their positive residues rather than via non-specific alteration of physical properties of the plasma membrane.

Which part of PIP_2, the highly negatively charged headgroup or the polyunsaturated hydrophobic tail, is responsible for the modulation of ion channels? Apparently, a minimum requirement is both a phosphate group and an acyl chain [228]. The negatively charged phosphate group establishes electrostatic interactions with positive residues of ion channels, while the acyl chain incorporates PIP_2 into the plasma membrane [228,254,255].

2.3.6. PIP_2 modulates functioning of the *Shaker* and Kv1.2 channels

Regulation of the *Shaker* and Kv1.2 channels' functioning by PIP_2 was recently reported by two experimental groups [250,256]. In contrast to the previously discussed Kir subfamily, both *Shaker* and Kv1.2 do not require PIP_2 for opening. However, this lipid induces an interesting dual effect on their activity. First of all, PIP_2 increases the maximal amplitude of ionic current (see Figure 2.3.6.1A): intracellular addition of PIP_2 enhances the current amplitude of *Shaker*, while patch excision of the membrane or addition of a PIP_2-scavenger polylysine to the inner side of the membrane leads to a current rundown [256]. Since, PIP_2 induces "a gain" of ionic current, this effect is accordingly called the gain-of-function. Similar results were obtained for the Kv1.2 channel [250]: degradation of PIP_2 by the voltage-dependent phosphatase CiVSP [257], inhibition of kinases responsible for PIP_2 synthesis or application of PIP_2-specific antibodies, all lead to accelerated decay of the ionic current amplitude. On the other hand, inhibition of phosphatates responsible for PIP_2 cleavage, decelerates the observed decay. Single channel

recordings indicated that the change in the ionic current amplitude can be attributed to different opening probabilities when PIP_2 is present or depleted from the patch, but not to a change in the unitary current size or the number of active ion channels [250].

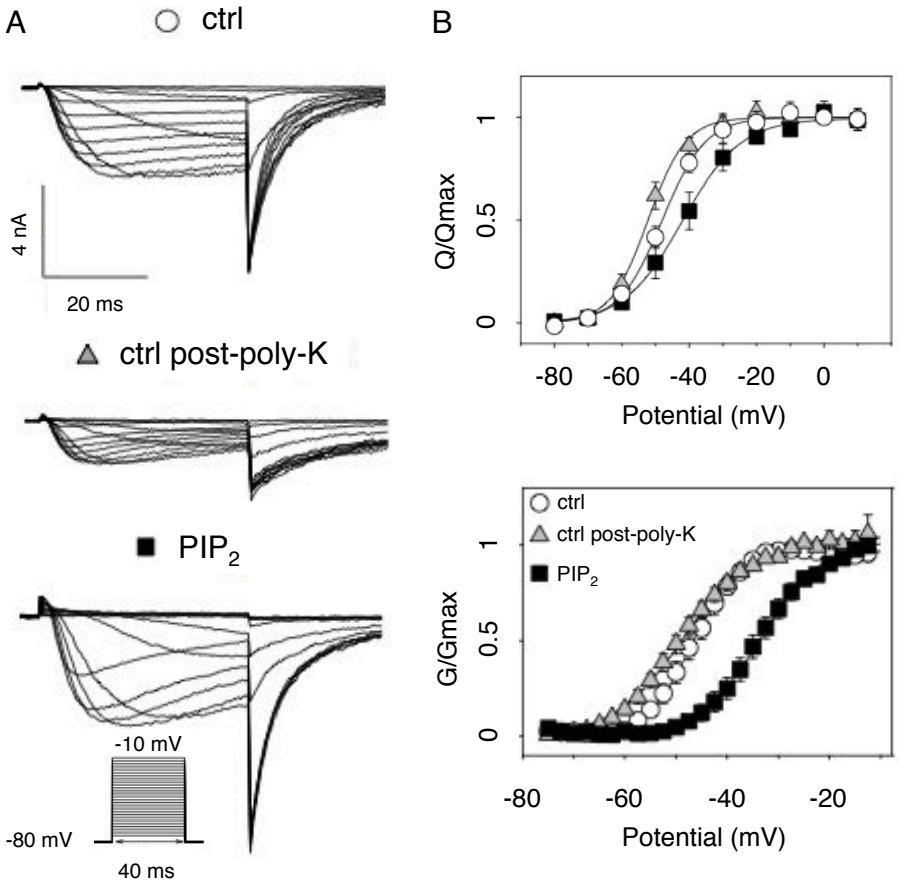

Figure 2.3.6.1. Dual effect of PIP_2 on the *Shaker* channel. A. Representative *Shaker* currents in response to the activation protocol (inset) after excision (top panel, "ctrl", empty circle), after application of polylysine (middle panel, "ctrl post-poly-K", gray triangle) and at steady-state, after PIP_2 application (bottom panel, "PIP_2", dark square). B. Mean relative gating current- (top) and conductance-voltage (bottom) (Q/Qmax and G/Gmax vs. V) relationships. The figure is adapted from [256].

The second effect induced by PIP_2 causes a loss-of-function of the *Shaker* and Kv1.2 channels: application of this lipid results in a rightward shift of the Q/V[1] and G/V[2] curves (see Appendix **2.1**), indicating a hindered motion of the voltage sensors [250,256]. This loss-of-function effect is indeed PIP_2-dependent as verified by the same set of experiments mentioned above (using polylysine, PIP_2-antibodies, CiVSP, *etc.*). The gain- and the loss-of-function were shown to have different kinetics characteristics and sensitivity to PIP_2 concentration in the plasma membrane [250,256], suggesting that they

[1] gating current vs. voltage
[2] conductance vs. voltage

are relatively independent. In particular, the loss-of-function effect has lower time course and higher sensitivity to PIP_2 compared to the gain-of-function one.

Additionally, PIP_2 alters the kinetics of activation and deactivation of the *Shaker* and Kv1.2 channels: in the presence of this lipid, the deactivation is accelerated, and the activation is decelerated [250,256].

2.3.7. PIP_2 modulates functioning of the Kv7 subfamily

The members of the Kv7 subfamily require PIP_2 for proper functioning [243,258,259]: *in vitro* depletion of this lipid from a patch of the plasma membrane drastically reduces ionic current. Furthermore, several mutations of the Kv7.1 channel associated with inherited cardiac diseases have been shown to affect PIP_2-dependent activation, indicating that this lipid is an important regulator of Kv7.1 *in vivo* [226,244,260,261].

What is the principal role of PIP_2 in the Kv7 channels' functioning? Two hypotheses have been put forward to address this question. First of all, PIP_2 may stabilize the pore of Kv7s in an open conformation [258] (Loussouarn *et al.*) through the mechanism similar to that previously revealed for the Kir channels [240,242] (see **2.3.5**). This is consistent with the fact that the pore domains of Kv7s and Kirs are homologous. The second hypothesis suggests that PIP_2 serves as an important element for coupling between the voltage sensor and the pore of Kv7s [167] (Zaydman *et al.*). Quite interestingly, modulation of other ion channels and even enzymes by PIP_2 can be as well interpreted in terms of this latter hypothesis, suggesting that the mechanism involved in this modulation is highly conserved [259]. For instance, the activation of the Kir2.1 channel by PIP_2 might be interpreted as enhancing of coupling between the TM domain and the cytoplasmic domain. Another example is the voltage-dependent phosphatase CiVSP, which is as well activated by PIP_2. The mechanism involved in this activation may consist of coupling of the voltage sensor displacement to the catalytic activity of the cytoplasmic domain [262].

The models proposed by Loussouarn *et al.* and Zaydman *et al.* are in agreement in the sense that PIP_2 does not directly affect the voltage sensor of the Kv7s channels. The latter was indeed verified experimentally [167], using the voltage-clamp fluorometry. In the voltage-clamp fluorometry, fluorescent

labeling of the S3-S4 linker generates measurable changes in fluorescence intensity (F) that are correlated with S4 movement during the voltage sensor activation; meanwhile, measurement of the whole-cell ionic current detects the pore opening. In other words, using this technique, one is able to track conformational changes of the voltage sensor and the pore simultaneously. The voltage-clamp fluorometry of the Kv7.1 wild type (WT) has demonstrated that depletion of PIP_2 dramatically reduces the ionic current amplitude, while leaving the F/V[3] curve (see Appendix **2.1**) unchanged, which indicates that PIP_2 does not affect the voltage sensor movement.

Here, we would like to discuss the set of experiments, verifying that PIP_2 is indeed required for coupling between the voltage sensor and the pore of Kv7.1 [167], because in the chapter summarizing our results, we will refer to these experiments. Mutagenesis of L353 to a charged residue, for instance lysine, locks the pore of Kv7.1 in an open conformation. If the latter is coupled to the voltage sensor then the activation of the voltage sensor will be perturbed by the lock open mutation. Hence, one is able to detect coupling between the voltage sensor and the pore by recording the F/V and G/V curves of the Kv7.1 WT and the L353K mutant and comparing them. Using this idea, Zaydman *et al.* demonstrated that application of PIP_2 to the L353K mutant shifts its F/V curve to more hyperpolarized voltages compared to the WT's one (see Figure 2.3.7.1), as if the pore opening promoted the activation of the voltage sensor. Depletion of PIP_2 with CiVSP, on the other hand, eliminates this shift, so the F/V curves of the L353K mutant and the WT become superimposable (see Figure 2.3.7.1). These findings clearly demonstrate that PIP_2 is required for the allosteric coupling between the activated state of the voltage sensor and the open state of the pore. Note, however, that they do not rule out the possibility of PIP_2 directly affecting the pore opening.

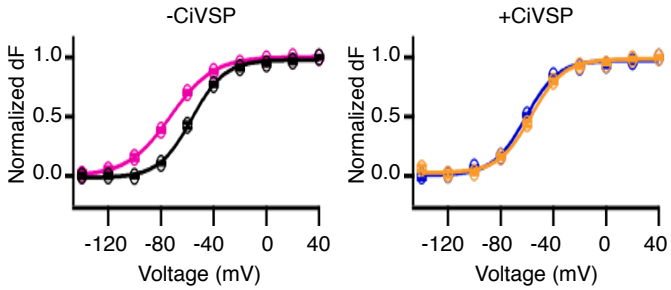

Figure 2.3.7.1. Voltage-clamp fluorometry experiments determining coupling between the VSD and the PD in Kv7.1. Normalized F/V curves of the WT (black), the WT+CiVSP (blue), L353K (magenta) and L353K+CiVSP (orange). The figure is adapted from [167].

[3] fluorescence vs. voltage

In order to gain an insight into the molecular level mechanism of the Kv7 channels' modulation by PIP_2, one must identify a putative binding site. In the Kv7 channels, several residues were shown to be responsible for PIP_2-sensitivity (rev. [259]). Some of these residues are located at the interface between the voltage sensor and the pore; others belong to the distal C-terminus (see Table 2.3.7.1). The group of residues located at the VSD/PD interface includes those of the S2-S3 loop [167,252], the S4-S5 linker [167,244,252,263] and the proximal S6 helix [167,243,249,251]. Some of these residues are highly conserved among the members of the Kv7 family (see Figure 2.2.6.2).

Table 2.3.7.1. Several residues of the Kv7 channels involved in PIP_2-dependent activation.

CHANNEL REGION	CHANNEL	RESIDUE	REFERENCE
S2-S3 loop	Kv7.1	R190 and R195	[167]
	Kv7.2	K162	[252]
S4-S5 linker	Kv7.1	H258 and R259	[167]
	Kv7.1/KCNE1	R243	[244]
	Kv7.2	K230	[252]
	Kv7.3	K222	[263]
proximal S6 helix	Kv7.1	K354, K358, R360 and K362	[249]
		K354, R360, H363 and R366	[167]
	Kv7.2	H328	[243]
		R325	[251]

Zaydman *et al.* [167] performed mutagenesis of all positively charged residues of the S2-S3 loop, the S4-S5 linker and the S6 proximal C-terminus exposed to the interface between the voltage sensor and the pore. Interestingly, they found three different effects: 1) a severe loss-of-function when the ionic current amplitude was drastically reduced compared to the WT (mutations of R190, R195, H258, R259, K354, R360, H363 and R366); 2) a moderate loss-of-function when the ionic current amplitude was slightly reduced (mutations of R192, R243, K358 and R362); and 3) a gain-of-function when the ionic current amplitude was increased (mutations of R181, K183, K196 and R249). While the loss-of-function, following the neutralization of positively charged residues, might be explained by an impairment of the PIP_2 binding site, the mechanism underlying the gain-of-function effect remains elusive.

In the recent study of Eckey *et al.* [253], the mutagenesis of positively charged residues of Kv7.1 exposed to the interface between the voltage sensor and the pore was performed as well. The comparison between the results

obtained by Zaydman *et al.* and Eckey *et al.* reveals discrepancies as to which residues are responsible for PIP_2 sensitivity and which are not. We suppose that the main reason of these discrepancies arises from the fact that Zaydman *et al.* and Eckey *et al.* considered different sources of PIP_2 during their experiments: while Zaydman *et al.* used endogenous PIP_2, whose level was controlled by CiVSP, Eckey *et al.* used exogenous short-chain derivatives of PIP_2. Hence, in the studies of Eckey *et al.*, the influence of endogenous PIP_2, which was not monitored, cannot be excluded. Note also, that Zaydman *et al.* and Eckey *et al.* performed their experiments on the Kv7.1 channel alone and on the Kv7.1/KCNE1 complex respectively, which may also be the reason of the discrepancies in their results.

Other residues of Kv7s responsible for PIP_2 sensitivity belong to the distal C-terminus. These include a positively charged cluster of the A-B helix linker [264], which is highly conserved among the Kv7.2-Kv7.4 channels. Interestingly, in Kv7.2, deletion of the A-B linker yields a functional PIP_2-dependent channel that is no more severely inhibited by PIP_2 depletion compared to the WT [265], suggesting that the A-B linker may not be the primary binding site for this lipid. In Kv7.1, Park *et al.* [244] identified two residues of the C helix (R539 and R555), whose mutagenesis decreases the apparent affinity of the Kv7.1/KCNE1 complex to PIP_2. Whether these residues along with those of S2-S3, S4-S5 and the proximal C-terminus compose a single PIP_2 binding site, affect this site allosterically or create a second PIP_2 binding site remains to be addressed.

REFERENCES

[1] A. Rubin, Biofizika, 3rd ed., MSU Press, Moscow, Russia, 2004.

[2] B. Hille, Ionic Channels of Excitable Membranes, 3rd ed., Sinauer Associates, Sunderland, MA, USA, 2001.

[3] J.-B. Kim, Channelopathies, Korean J. Pediatr., 57 (2014) 1–18.

[4] E.V. Zaklyazminskaya, H. Abriel, Prevalence of significant genetic variants in congenital long QT syndrome is largely underestimated, Pharmacol. Ion Channels Channelopathies, (2012) 72.

[5] H. Abriel, E.V. Zaklyazminskaya, Cardiac channelopathies: genetic and molecular mechanisms, Gene, 517 (2013) 1–11.

[6] S.M. Modell, D.J. Bradley, M.H. Lehmann, Genetic testing for long QT syndrome and the category of cardiac ion channelopathies, PLoS Curr., (2012) e4f9995f69e6c7.

[7] M. Piccolino, Luigi Galvani and animal electricity: two centuries after the foundation of electrophysiology, Trends Neurosci., 20 (1997) 443–448.

[8] F. Bezanilla, Ion channels: from conductance to structure, Neuron, 60 (2008) 456–468.

[9] S. Ochs, A History of Nerve Functions: From Animal Spirits to Molecular Mechanisms, Cambridge University Press, 2004.

[10] S.K. Bagal, A.D. Brown, P.J. Cox, K. Omoto, R.M. Owen, D.C. Pryde, B. Sidders, S.E. Skerratt, E.B. Stevens, R.I. Storer, N.A. Swain, Ion Channels as Therapeutic Targets: A Drug Discovery Perspective, J. Med. Chem., 56 (2013) 593–624.

[11] T.E. DeCoursey, Voltage-Gated Proton Channels: Molecular Biology, Physiology, and Pathophysiology of the HV Family, Physiol. Rev., 93 (2013) 599–652.

[12] W.A. Catterall, From ionic currents to molecular mechanisms: the structure and function of voltage-gated sodium channels, Neuron, 26 (2000) 13–25.

[13] H. Takeshima, S. Nishimura, T. Matsumoto, H. Ishida, K. Kangawa, N. Minamino, H. Matsuo, M. Ueda, M. Hanaoka, T. Hirose, Primary structure and expression from complementary DNA of skeletal muscle ryanodine receptor, Nature, 339 (1989) 439–445.

[14] A.J. Harmar, R.A. Hills, E.M. Rosser, M. Jones, O.P. Buneman, D.R. Dunbar, S.D. Greenhill, V.A. Hale, J.L. Sharman, T.I. Bonner, W.A. Catterall, A.P. Davenport, P. Delagrange, C.T. Dollery, S.M. Foord, G.A. Gutman, V. Laudet, R.R. Neubig, E.H. Ohlstein, R.W. Olsen, et al., IUPHAR-DB: the IUPHAR database of G protein-coupled receptors and ion channels, Nucleic Acids Res., 37 (2009) D680–D685.

[15] F.H. Yu, V. Yarov-Yarovoy, G.A. Gutman, W.A. Catterall, Overview of Molecular Relationships in the Voltage-Gated Ion Channel Superfamily, Pharmacol. Rev., 57 (2005) 387–395.

[16] F.H. Yu, W.A. Catterall, The VGL-chanome: a protein superfamily specialized for electrical signaling and ionic homeostasis, Sci. STKE, 2004 (2004) re15.

[17] B. Martinac, Mechanosensitive ion channels: molecules of mechanotransduction, J. Cell Sci., 117 (2004) 2449–2460.

[18] A.L. Hodgkin, A.F. Huxley, Currents carried by sodium and potassium ions through the membrane of the giant axon of Loligo, J. Physiol., 116 (1952) 449–472.

[19] A.L. Hodgkin, A.F. Huxley, The dual effect of membrane potential on sodium conductance in the giant axon of Loligo, J. Physiol., 116 (1952) 497–506.

[20] A.L. Hodgkin, A.F. Huxley, A quantitative description of membrane current and its application to conduction and excitation in nerve, J. Physiol., 117 (1952) 500–544.
[21] A.L. Hodgkin, A.F. Huxley, The components of membrane conductance in the giant axon of Loligo, J. Physiol., 116 (1952) 473–496.
[22] M.F. Schneider, W.K. Chandler, Voltage dependent charge movement of skeletal muscle: a possible step in excitation-contraction coupling, Nature, 242 (1973) 244–246.
[23] C.M. Armstrong, F. Bezanilla, Currents related to movement of the gating particles of the sodium channels, Nature, 242 (1973) 459–461.
[24] C.M. Armstrong, F. Bezanilla, Charge Movement Associated with the Opening and Closing of the Activation Gates of the Na Channels, J. Gen. Physiol., 63 (1974) 533–552.
[25] R.D. Keynes, E. Rojas, Kinetics and steady-state properties of the charged system controlling sodium conductance in the squid giant axon, J. Physiol., 239 (1974) 393–434.
[26] E. Rojas, M. Luxoro, Micro-injection of Trypsin into Axons of Squid, Nature, 199 (1963) 78–79.
[27] W.S. Agnew, S.R. Levinson, J.S. Brabson, M.A. Raftery, Purification of the tetrodotoxin-binding component associated with the voltage-sensitive sodium channel from Electrophorus electricus electroplax membranes, Proc. Natl. Acad. Sci. U. S. A., 75 (1978) 2606–2610.
[28] R.L. Rosenberg, S.A. Tomiko, W.S. Agnew, Single-channel properties of the reconstituted voltage-regulated Na channel isolated from the electroplax of Electrophorus electricus, Proc. Natl. Acad. Sci. U. S. A., 81 (1984) 5594–5598.
[29] A.M. Correa, F. Bezanilla, W.S. Agnew, Voltage activation of purified eel sodium channels reconstituted into artificial liposomes, Biochemistry (Mosc.), 29 (1990) 6230–6240.
[30] C.M. Armstrong, Interaction of tetraethylammonium ion derivatives with the potassium channels of giant axons, J. Gen. Physiol., 58 (1971) 413–437.
[31] B. Hille, Ionic selectivity, saturation, and block in sodium channels: a four-barrier model, J. Gen. Physiol., 66 (1975) 535–560.
[32] L.J. Mullins, The penetration of some cations into muscle, J. Gen. Physiol., 42 (1959) 817–829.
[33] O.P. Hamill, A. Marty, E. Neher, B. Sakmann, F.J. Sigworth, Improved patch-clamp techniques for high-resolution current recording from cells and cell-free membrane patches, Pflüg. Arch. Eur. J. Physiol., 391 (1981) 85–100.
[34] B. Sakmann, E. Neher, Single-channel recording, Plenum Press, 1983.
[35] Y. Zhao, S. Inayat, D.A. Dikin, J.H. Singer, R.S. Ruoff, J.B. Troy, Patch clamp technique: review of the current state of the art and potential contributions from nanoengineering, Proc. Inst. Mech. Eng., Part N: J. Nanoeng. Nanosyst., 222 (2008) 1–11.
[36] M. Noda, S. Shimizu, T. Tanabe, T. Takai, T. Kayano, T. Ikeda, H. Takahashi, H. Nakayama, Y. Kanaoka, N. Minamino, K. Kangawa, H. Matsuo, M.A. Raftery, T. Hirose, S. Inayama, H. Hayashida, T. Miyata, S. Numa, Primary structure of Electrophorus electricus sodium channel deduced from cDNA sequence, Nature, 312 (1984) 121–127.
[37] A. Kamb, J. Tseng-Crank, M.A. Tanouye, Multiple products of the Drosophila Shaker gene may contribute to potassium channel diversity, Neuron, 1 (1988) 421–430.
[38] M.J. Christie, R.A. North, P.B. Osborne, J. Douglass, J.P. Adelman, Heteropolymeric potassium channels expressed in Xenopus oocytes from cloned subunits, Neuron, 4 (1990) 405–411.
[39] E.Y. Isacoff, Y.N. Jan, L.Y. Jan, Evidence for the formation of heteromultimeric potassium channels in Xenopus oocytes, Nature, 345 (1990) 530–534.

[40] R. MacKinnon, Determination of the subunit stoichiometry of a voltage-activated potassium channel, Nature, 350 (1991) 232–235.
[41] W.A. Catterall, Structure and function of voltage-sensitive ion channels, Science, 242 (1988) 50–61.
[42] D.M. Papazian, L.C. Timpe, Y.N. Jan, L.Y. Jan, Alteration of voltage-dependence of Shaker potassium channel by mutations in the S4 sequence, Nature, 349 (1991) 305–310.
[43] W. Stühmer, F. Conti, H. Suzuki, X. Wang, M. Noda, N. Yahagi, H. Kubo, S. Numa, Structural parts involved in activation and inactivation of the sodium channel, Nature, 339 (1989) 597–603.
[44] H.P. Larsson, O.S. Baker, D.S. Dhillon, E.Y. Isacoff, Transmembrane movement of the Shaker K+ channel S4, Neuron, 16 (1996) 387–397.
[45] N. Yang, R. Horn, Evidence for voltage-dependent S4 movement in sodium channels, Neuron, 15 (1995) 213–218.
[46] Y. Liu, M. Holmgren, M.E. Jurman, G. Yellen, Gated access to the pore of a voltage-dependent K+ channel, Neuron, 19 (1997) 175–184.
[47] L. Heginbotham, Z. Lu, T. Abramson, R. MacKinnon, Mutations in the K+ channel signature sequence, Biophys. J., 66 (1994) 1061–1067.
[48] D.A. Doyle, J. Morais Cabral, R.A. Pfuetzner, A. Kuo, J.M. Gulbis, S.L. Cohen, B.T. Chait, R. MacKinnon, The structure of the potassium channel: molecular basis of K+ conduction and selectivity, Science, 280 (1998) 69–77.
[49] Y. Zhou, J.H. Morais-Cabral, A. Kaufman, R. MacKinnon, Chemistry of ion coordination and hydration revealed by a K+ channel-Fab complex at 2.0 Å resolution, Nature, 414 (2001) 43–48.
[50] R. MacKinnon, S.L. Cohen, A. Kuo, A. Lee, B.T. Chait, Structural conservation in prokaryotic and eukaryotic potassium channels, Science, 280 (1998) 106–109.
[51] T.W. Allen, S. Kuyucak, S.H. Chung, Molecular dynamics study of the KcsA potassium channel, Biophys. J., 77 (1999) 2502–2516.
[52] J. Aqvist, V. Luzhkov, Ion permeation mechanism of the potassium channel, Nature, 404 (2000) 881–884.
[53] T.W. Allen, S.H. Chung, Brownian dynamics study of an open-state KcsA potassium channel, Biochim. Biophys. Acta BBA - Biomembr., 1515 (2001) 83–91.
[54] M.S.P.S. Indira H Shrivastava, Molecular dynamics simulations and KcsA channel gating, Eur. Biophys. J. EBJ, 31 (2002) 207–16.
[55] B. Roux, S. Bernèche, W. Im, Ion Channels, Permeation, and Electrostatics: Insight into the Function of KcsA, Biochemistry (Mosc.), 39 (2000) 13295–13306.
[56] M.S. Sansom, I.H. Shrivastava, K.M. Ranatunga, G.R. Smith, Simulations of ion channels - watching ions and water move, Trends Biochem. Sci., 25 (2000) 368–374.
[57] S. Berneche, B. Roux, Molecular dynamics of the KcsA K(+) channel in a bilayer membrane, Biophys. J., 78 (2000) 2900–2917.
[58] P.C. Biggin, G.R. Smith, I. Shrivastava, S. Choe, M.S. Sansom, Potassium and sodium ions in a potassium channel studied by molecular dynamics simulations, Biochim. Biophys. Acta, 1510 (2001) 1–9.
[59] S.S. Azam, T.S. Hofer, B.R. Randolf, B.M. Rode, Hydration of Sodium(I) and Potassium(I) Revisited: A Comparative QM/MM and QMCF MD Simulation Study of Weakly Hydrated Ions, J. Phys. Chem. A, 113 (2009) 1827–1834.
[60] G.A. Gutman, K.G. Chandy, S. Grissmer, M. Lazdunski, D. McKinnon, L.A. Pardo, G.A. Robertson, B. Rudy, M.C. Sanguinetti, W. Stühmer, X. Wang, International Union of Pharmacology LIII: Nomenclature and molecular relationships of voltage-gated potassium channels, Pharmacol. Rev., 57 (2005) 473–508.
[61] K.S. Elmslie, Action Potential: Ionic Mechanisms, John Wiley & Sons, Ltd., 2001.

[62] B.P. Bean, The action potential in mammalian central neurons, Nat. Rev. Neurosci., 8 (2007) 451–465.
[63] H.C. Lai, L.Y. Jan, The distribution and targeting of neuronal voltage-gated ion channels, Nat. Rev. Neurosci., 7 (2006) 548–562.
[64] A.O. Grant, Cardiac Ion Channels, Circ. Arrhythm. Electrophysiol., 2 (2009) 185–194.
[65] U. Ravens, E. Cerbai, Role of potassium currents in cardiac arrhythmias, Europace, 10 (2008) 1133–1137.
[66] S.B. Long, E.B. Campbell, R. MacKinnon, Crystal structure of a mammalian voltage-dependent Shaker family K+ channel, Science, 309 (2005) 897–903.
[67] S.B. Long, X. Tao, E.B. Campbell, R. MacKinnon, Atomic structure of a voltage-dependent K+ channel in a lipid membrane-like environment, Nature, 450 (2007) 376–382.
[68] J.A. Freites, D.J. Tobias, S.H. White, A voltage-sensor water pore, Biophys. J., 91 (2006) L90–92.
[69] X. Tao, A. Lee, W. Limapichat, D.A. Dougherty, R. MacKinnon, A gating charge transfer center in voltage sensors, Science, 328 (2010) 67–73.
[70] J.J. Lacroix, F. Bezanilla, Control of a final gating charge transition by a hydrophobic residue in the S2 segment of a K+ channel voltage sensor, Proc. Natl. Acad. Sci. U. S. A., 108 (2011) 6444–6449.
[71] C.S. Schwaiger, S.I. Liin, F. Elinder, E. Lindahl, The conserved phenylalanine in the K+ channel voltage-sensor domain creates a barrier with unidirectional effects, Biophys. J., 104 (2013) 75–84.
[72] J. Payandeh, T. Scheuer, N. Zheng, W.A. Catterall, The crystal structure of a voltage-gated sodium channel, Nature, 475 (2011) 353–358.
[73] X. Zhang, W.L. Ren, P. DeCaen, C.Y. Yan, X. Tao, L. Tang, J.J. Wang, K. Hasegawa, T. Kumasaka, J.H. He, J.W. Wang, D.E. Clapham, N. Yan, Crystal structure of an orthologue of the NaChBac voltage-gated sodium channel, Nature, 486 (2012) 130–134.
[74] L.M. Mannuzzu, M.M. Moronne, E.Y. Isacoff, Direct physical measure of conformational rearrangement underlying potassium channel gating, Science, 271 (1996) 213–216.
[75] A. Cha, F. Bezanilla, Characterizing voltage-dependent conformational changes in the Shaker K+ channel with fluorescence, Neuron, 19 (1997) 1127–1140.
[76] M. Pathak, L. Kurtz, F. Tombola, E. Isacoff, The Cooperative Voltage Sensor Motion that Gates a Potassium Channel, J. Gen. Physiol., 125 (2005) 57–69.
[77] J. Zheng, W.N. Zagotta, Patch-Clamp Fluorometry Recording of Conformational Rearrangements of Ion Channels, Sci. Signal., 2003 (2003) pl7.
[78] T. Hoshi, W.N. Zagotta, R.W. Aldrich, Shaker potassium channel gating I: Transitions near the open state, J. Gen. Physiol., 103 (1994) 249–278.
[79] W.N. Zagotta, T. Hoshi, J. Dittman, R.W. Aldrich, Shaker potassium channel gating II: Transitions in the activation pathway, J. Gen. Physiol., 103 (1994) 279–319.
[80] N.E. Schoppa, F.J. Sigworth, Activation of Shaker potassium channels I: Characterization of voltage-dependent transitions, J. Gen. Physiol., 111 (1998) 271–294.
[81] N.E. Schoppa, F.J. Sigworth, Activation of Shaker potassium channels II: Kinetics of the V2 mutant channel, J. Gen. Physiol., 111 (1998) 295–311.
[82] D.M. Papazian, X.M. Shao, S.-A. Seoh, A.F. Mock, Y. Huang, D.H. Wainstock, Electrostatic interactions of S4 voltage sensor in shaker K+ channel, Neuron, 14 (1995) 1293–1301.
[83] S.K. Tiwari-Woodruff, M.A. Lin, C.T. Schulteis, D.M. Papazian, Voltage-Dependent Structural Interactions in the Shaker K+ Channel, J. Gen. Physiol., 115 (2000) 123–138.

[84] J.J. Lacroix, S.A. Pless, L. Maragliano, F.V. Campos, J.D. Galpin, C.A. Ahern, B. Roux, F. Bezanilla, Intermediate state trapping of a voltage sensor, J. Gen. Physiol., 140 (2012) 635–652.

[85] U. Henrion, J. Renhorn, S.I. Börjesson, E.M. Nelson, C.S. Schwaiger, P. Bjelkmar, B. Wallner, E. Lindahl, F. Elinder, Tracking a complete voltage-sensor cycle with metal-ion bridges, Proc. Natl. Acad. Sci., (2012).

[86] L. Delemotte, M. Tarek, M.L. Klein, C. Amaral, W. Treptow, Intermediate states of the Kv1.2 voltage sensor from atomistic molecular dynamics simulations, Proc. Natl. Acad. Sci. U. S. A., 108 (2011) 6109–6114.

[87] M.Ø. Jensen, V. Jogini, D.W. Borhani, A.E. Leffler, R.O. Dror, D.E. Shaw, Mechanism of voltage gating in potassium channels, Science, 336 (2012) 229–233.

[88] C.S. Schwaiger, P. Bjelkmar, B. Hess, E. Lindahl, 3_{10}-helix conformation facilitates the transition of a voltage sensor S4 segment toward the down state, Biophys. J., 100 (2011) 1446–1454.

[89] C.S. Schwaiger, S.I. Börjesson, B. Hess, B. Wallner, F. Elinder, E. Lindahl, The free energy barrier for arginine gating charge translation is altered by mutations in the voltage sensor domain, PloS One, 7 (2012) e45880.

[90] M. Zhang, J. Liu, M. Jiang, D.-M. Wu, K. Sonawane, H.R. Guy, G.-N. Tseng, Interactions between charged residues in the transmembrane segments of the voltage-sensing domain in the hERG channel, J. Membr. Biol., 207 (2005) 169–181.

[91] D. Wu, K. Delaloye, M.A. Zaydman, A. Nekouzadeh, Y. Rudy, J. Cui, State-dependent electrostatic interactions of S4 arginines with E1 in S2 during Kv7.1 activation, J. Gen. Physiol., 135 (2010) 595–606.

[92] P.G. DeCaen, V. Yarov-Yarovoy, E.M. Sharp, T. Scheuer, W.A. Catterall, Sequential formation of ion pairs during activation of a sodium channel voltage sensor, Proc. Natl. Acad. Sci. U. S. A., 106 (2009) 22498–22503.

[93] C. Amaral, V. Carnevale, M.L. Klein, W. Treptow, Exploring conformational states of the bacterial voltage-gated sodium channel NavAb via molecular dynamics simulations, Proc. Natl. Acad. Sci. U. S. A., 109 (2012) 21336–21341.

[94] W.A. Catterall, Ion Channel Voltage Sensors: Structure, Function, and Pathophysiology, Neuron, 67 (2010) 915–928.

[95] V. Yarov-Yarovoy, D. Baker, W.A. Catterall, Voltage sensor conformations in the open and closed states in ROSETTA structural models of K(+) channels, Proc. Natl. Acad. Sci. U. S. A., 103 (2006) 7292–7297.

[96] F. Khalili-Araghi, V. Jogini, V. Yarov-Yarovoy, E. Tajkhorshid, B. Roux, K. Schulten, Calculation of the gating charge for the Kv1.2 voltage-activated potassium channel, Biophys. J., 98 (2010) 2189–2198.

[97] E. Vargas, V. Yarov-Yarovoy, F. Khalili-Araghi, W.A. Catterall, M.L. Klein, M. Tarek, E. Lindahl, K. Schulten, E. Perozo, F. Bezanilla, B. Roux, An emerging consensus on voltage-dependent gating from computational modeling and molecular dynamics simulations, J. Gen. Physiol., 140 (2012) 587–594.

[98] M.M. Pathak, V. Yarov-Yarovoy, G. Agarwal, B. Roux, P. Barth, S. Kohout, F. Tombola, E.Y. Isacoff, Closing in on the resting state of the Shaker K(+) channel, Neuron, 56 (2007) 124–140.

[99] E. Stefani, L. Toro, E. Perozo, F. Bezanilla, Gating of Shaker K+ channels I: Ionic and gating currents, Biophys. J., 66 (1994) 996–1010.

[100] F. Bezanilla, The Voltage Sensor in Voltage-Dependent Ion Channels, Physiol. Rev., 80 (2000) 555–592.

[101] N.E. Schoppa, K. McCormack, M.A. Tanouye, F.J. Sigworth, The size of gating charge in wild-type and mutant Shaker potassium channels, Science, 255 (1992) 1712–1715.

[102] S.A. Seoh, D. Sigg, D.M. Papazian, F. Bezanilla, Voltage-sensing residues in the S2 and S4 segments of the Shaker K+ channel, Neuron, 16 (1996) 1159–1167.
[103] S.K. Aggarwal, R. Mackinnon, Contribution of the S4 segment to gating charge in the Shaker K+ channel, Neuron, 16 (1996) 1169–1177.
[104] F. Bezanilla, E. Perozo, D.M. Papazian, E. Stefani, Molecular basis of gating charge immobilization in Shaker potassium channels, Science, 254 (1991) 679–683.
[105] F. Bezanilla, E. Perozo, E. Stefani, Gating of Shaker K+ channels II: The components of gating currents and a model of channel activation, Biophys. J., 66 (1994) 1011–1021.
[106] J.L. Ledwell, R.W. Aldrich, Mutations in the S4 region isolate the final voltage-dependent cooperative step in potassium channel activation, J. Gen. Physiol., 113 (1999) 389–414.
[107] C.J. Smith-Maxwell, J.L. Ledwell, R.W. Aldrich, Uncharged S4 residues and cooperativity in voltage-dependent potassium channel activation, J. Gen. Physiol., 111 (1998) 421–439.
[108] D. del Camino, M. Kanevsky, G. Yellen, Status of the intracellular gate in the activated-not-open state of Shaker K+ channels, J. Gen. Physiol., 126 (2005) 419–428.
[109] L.M. Mannuzzu, E.Y. Isacoff, Independence and cooperativity in rearrangements of a potassium channel voltage sensor revealed by single subunit fluorescence, J. Gen. Physiol., 115 (2000) 257–268.
[110] N. Zandany, M. Ovadia, I. Orr, O. Yifrach, Direct analysis of cooperativity in multisubunit allosteric proteins, Proc. Natl. Acad. Sci. U. S. A., 105 (2008) 11697–11702.
[111] O. Yifrach, N. Zandany, T. Shem-Ad, Examining cooperative gating phenomena in voltage-dependent potassium channels: taking the energetic approach, Methods Enzymol., 466 (2009) 179–209.
[112] D.G. Gagnon, F. Bezanilla, The contribution of individual subunits to the coupling of the voltage sensor to pore opening in Shaker K channels: effect of ILT mutations in heterotetramers, J. Gen. Physiol., 136 (2010) 555–568.
[113] W.N. Zagotta, T. Hoshi, R.W. Aldrich, Shaker potassium channel gating III: Evaluation of kinetic models for activation, J. Gen. Physiol., 103 (1994) 321–362.
[114] N.E. Schoppa, F.J. Sigworth, Activation of Shaker potassium channels III: An activation gating model for wild-type and V2 mutant channels, J. Gen. Physiol., 111 (1998) 313–342.
[115] O.S. Baker, H.P. Larsson, L.M. Mannuzzu, E.Y. Isacoff, Three transmembrane conformations and sequence-dependent displacement of the S4 domain in shaker K+ channel gating, Neuron, 20 (1998) 1283–1294.
[116] A. Loboda, C.M. Armstrong, Resolving the gating charge movement associated with late transitions in K channel activation, Biophys. J., 81 (2001) 905–916.
[117] D. Sigg, F. Bezanilla, E. Stefani, Fast gating in the Shaker K+ channel and the energy landscape of activation, Proc. Natl. Acad. Sci. U. S. A., 100 (2003) 7611–7615.
[118] M. Kanevsky, R.W. Aldrich, Determinants of voltage-dependent gating and open-state stability in the S5 segment of Shaker potassium channels, J. Gen. Physiol., 114 (1999) 215–242.
[119] S. Chowdhury, B. Chanda, Thermodynamics of electromechanical coupling in voltage-gated ion channels, J. Gen. Physiol., 140 (2012) 613–623.
[120] Z. Lu, A.M. Klem, Y. Ramu, Ion conduction pore is conserved among potassium channels, Nature, 413 (2001) 809–813.
[121] Z. Lu, A.M. Klem, Y. Ramu, Coupling between voltage sensors and activation gate in voltage-gated K+ channels, J. Gen. Physiol., 120 (2002) 663–676.
[122] S.B. Long, E.B. Campbell, R. MacKinnon, Voltage Sensor of Kv1.2: Structural Basis of Electromechanical Coupling, Science, 309 (2005) 903–908.

[123] A.J. Labro, A.L. Raes, A. Grottesi, D.V. Hoorick, M.S.P. Sansom, D.J. Snyders, Kv Channel Gating Requires a Compatible S4-S5 Linker and Bottom Part of S6, Constrained by Non-interacting Residues, J. Gen. Physiol., 132 (2008) 667–680.

[124] G.A. Haddad, R. Blunck, Mode shift of the voltage sensors in Shaker K+ channels is caused by energetic coupling to the pore domain, J. Gen. Physiol., 137 (2011) 455–472.

[125] E.V. Schow, J.A. Freites, A. Nizkorodov, S.H. White, D.J. Tobias, Coupling between the voltage-sensing and pore domains in a voltage-gated potassium channel, Biochim. Biophys. Acta, 1818 (2012) 1726–1736.

[126] M. Tristani-Firouzi, J. Chen, M.C. Sanguinetti, Interactions between S4-S5 linker and S6 transmembrane domain modulate gating of HERG K+ channels, J. Biol. Chem., 277 (2002) 18994–19000.

[127] N. Decher, J. Chen, M.C. Sanguinetti, Voltage-dependent gating of hyperpolarization-activated, cyclic nucleotide-gated pacemaker channels: molecular coupling between the S4-S5 and C-linkers, J. Biol. Chem., 279 (2004) 13859–13865.

[128] T. Ferrer, J. Rupp, D.R. Piper, M. Tristani-Firouzi, The S4-S5 linker directly couples voltage sensor movement to the activation gate in the human ether-a-go-go-related gene (hERG) K+ channel, J. Biol. Chem., 281 (2006) 12858–12864.

[129] F.S. Choveau, N. Rodriguez, F.A. Ali, A.J. Labro, T. Rose, S. Dahimène, H. Boudin, C.L. Hénaff, D. Escande, D.J. Snyders, F. Charpentier, J. Mérot, I. Baró, G. Loussouarn, KCNQ1 Channels Voltage Dependence through a Voltage-dependent Binding of the S4-S5 Linker to the Pore Domain, J. Biol. Chem., 286 (2011) 707–716.

[130] F.S. Choveau, F. Abderemane-Ali, F.C. Coyan, Z. Es-Salah-Lamoureux, I. Baró, G. Loussouarn, Opposite Effects of the S4-S5 Linker and PIP(2) on Voltage-Gated Channel Function: KCNQ1/KCNE1 and Other Channels, Front. Pharmacol., 3 (2012) 125.

[131] M. Nishizawa, K. Nishizawa, Coupling of S4 helix translocation and S6 gating analyzed by molecular-dynamics simulations of mutated Kv channels, Biophys. J., 97 (2009) 90–100.

[132] S.-Y. Lee, A. Banerjee, R. MacKinnon, Two Separate Interfaces between the Voltage Sensor and Pore Are Required for the Function of Voltage-Dependent K+ Channels, PLoS Biol, 7 (2009) e1000047.

[133] A. Broomand, R. Mannikko, H.P. Larsson, F. Elinder, Molecular Movement of the Voltage Sensor in a K Channel, J. Gen. Physiol., 122 (2003) 741–748.

[134] C.S. Gandhi, E. Clark, E. Loots, A. Pralle, E.Y. Isacoff, The orientation and molecular movement of a k(+) channel voltage-sensing domain, Neuron, 40 (2003) 515–525.

[135] C. Alonso-Ron, P. de la Peña, P. Miranda, P. Domínguez, F. Barros, Thermodynamic and kinetic properties of amino-terminal and S4-S5 loop HERG channel mutants under steady-state conditions, Biophys. J., 94 (2008) 3893–3911.

[136] P. de la Peña, C. Alonso-Ron, A. Machín, J. Fernández-Trillo, L. Carretero, P. Domínguez, F. Barros, Demonstration of physical proximity between the N terminus and the S4-S5 linker of the human ether-a-go-go-related gene (hERG) potassium channel, J. Biol. Chem., 286 (2011) 19065–19075.

[137] F. Barros, P. Domínguez, P. de la Peña, Cytoplasmic Domains and Voltage-Dependent Potassium Channel Gating, Front. Pharmacol., 3 (2012).

[138] D.H. Hackos, T.-H. Chang, K.J. Swartz, Scanning the Intracellular S6 Activation Gate in the Shaker K+ Channel, J. Gen. Physiol., 119 (2002) 521–531.

[139] M. Sukhareva, D.H. Hackos, K.J. Swartz, Constitutive Activation of the Shaker Kv Channel, J. Gen. Physiol., 122 (2003) 541–556.

[140] J.D. Osteen, K.J. Sampson, R.S. Kass, The cardiac IKs channel, complex indeed, Proc. Natl. Acad. Sci. U. S. A., 107 (2010) 18751–18752.

[141] T. Jespersen, M. Grunnet, S.-P. Olesen, The KCNQ1 potassium channel: from gene to physiological function, Physiol. Bethesda Md, 20 (2005) 408–416.
[142] S. Maljevic, T.V. Wuttke, G. Seebohm, H. Lerche, Kv7 channelopathies, Pflüg. Arch. Eur. J. Physiol., 460 (2010) 277–288.
[143] G. Seebohm, Kv7.1 in atrial fibrillation, Heart Rhythm Off. J. Heart Rhythm Soc., 6 (2009) 1154–1155.
[144] T.J. Jentsch, Neuronal KCNQ potassium channels: physiology and role in disease, Nat. Rev. Neurosci., 1 (2000) 21–30.
[145] J. Robbins, KCNQ potassium channels: physiology, pathophysiology, and pharmacology, Pharmacol. Ther., 90 (2001) 1–19.
[146] S. Maljevic, T.V. Wuttke, H. Lerche, Nervous system Kv7 disorders: breakdown of a subthreshold brake, J. Physiol., 586 (2008) 1791–1801.
[147] D.A. Brown, Kv7 (KCNQ) potassium channels that are mutated in human diseases, J. Physiol., 586 (2008) 1781–1783.
[148] J.R. Giudicessi, M.J. Ackerman, Potassium-channel mutations and cardiac arrhythmias - diagnosis and therapy, Nat. Rev. Cardiol., 9 (2012) 319–332.
[149] J.A. Smith, C.G. Vanoye, A.L. George, J. Meiler, C.R. Sanders, Structural Models for the KCNQ1 Voltage-Gated Potassium Channel, Biochemistry (Mosc.), 46 (2007) 14141–14152.
[150] G. Panaghie, G.W. Abbott, The Role of S4 Charges in Voltage-dependent and Voltage-independent KCNQ1 Potassium Channel Complexes, J. Gen. Physiol., 129 (2007) 121–133.
[151] Q. Wang, M.E. Curran, I. Splawski, T.C. Burn, J.M. Millholland, T.J. VanRaay, J. Shen, K.W. Timothy, G.M. Vincent, T. de Jager, P.J. Schwartz, J.A. Toubin, A.J. Moss, D.L. Atkinson, G.M. Landes, T.D. Connors, M.T. Keating, Positional cloning of a novel potassium channel gene: KvLQT1 mutations cause cardiac arrhythmias, Nat. Genet., 12 (1996) 17–23.
[152] F.Y. Shalaby, P.C. Levesque, W.-P. Yang, W.A. Little, M.L. Conder, T. Jenkins-West, M.A. Blanar, Dominant-Negative KvLQT1 Mutations Underlie the LQT1 Form of Long QT Syndrome, Circulation, 96 (1997) 1733–1736.
[153] I. Splawski, J. Shen, K.W. Timothy, M.H. Lehmann, S. Priori, J.L. Robinson, A.J. Moss, P.J. Schwartz, J.A. Towbin, G.M. Vincent, M.T. Keating, Spectrum of mutations in long-QT syndrome genes KvLQT1, HERG, SCN5A, KCNE1, and KCNE2, Circulation, 102 (2000) 1178–1185.
[154] W. Liu, J. Yang, D. Hu, C. Kang, C. Li, S. Zhang, P. Li, Z. Chen, X. Qin, K. Ying, Y. Li, Y. Li, Z. Li, X. Cheng, L. Li, Y. Qi, S. Chen, Q. Wang, KCNQ1 and KCNH2 mutations associated with long QT syndrome in a Chinese population, Hum. Mutat., 20 (2002) 475–476.
[155] C. Napolitano, S.G. Priori, P.J. Schwartz, R. Bloise, E. Ronchetti, J. Nastoli, G. Bottelli, M. Cerrone, S. Leonardi, Genetic testing in the long QT syndrome: development and validation of an efficient approach to genotyping in clinical practice, JAMA J. Am. Med. Assoc., 294 (2005) 2975–2980.
[156] D. Peng, J.-H. Kim, B.M. Kroncke, C.L. Law, Y. Xia, K.D. Droege, W.D. Van Horn, C.G. Vanoye, C.R. Sanders, Purification and Structural Study of the Voltage-Sensor Domain of the Human KCNQ1 Potassium Ion Channel, Biochemistry (Mosc.), (2014).
[157] F. Miceli, M.V. Soldovieri, C.C. Hernandez, M.S. Shapiro, L. Annunziato, M. Taglialatela, Gating Consequences of Charge Neutralization of Arginine Residues in the S4 Segment of Kv7.2, an Epilepsy-Linked K+ Channel Subunit, Biophys. J., 95 (2008) 2254–2264.

[158] F. Miceli, E. Vargas, F. Bezanilla, M. Taglialatela, Gating Currents from Kv7 Channels Carrying Neuronal Hyperexcitability Mutations in the Voltage-Sensing Domain, Biophys. J., 102 (2012) 1372–1382.
[159] I.R. Boulet, A.J. Labro, A.L. Raes, D.J. Snyders, Role of the S6 C-terminus in KCNQ1 channel gating, J. Physiol., 585 (2007) 325–337.
[160] G. Panaghie, K.-K. Tai, G.W. Abbott, Interaction of KCNE subunits with the KCNQ1 K+ channel pore, J. Physiol., 570 (2006) 455–467.
[161] V. Vardanyan, O. Pongs, Coupling of voltage-sensors to the channel pore: a comparative view, Front. Pharmacol., 3 (2012) 145.
[162] J.D. Osteen, C. Gonzalez, K.J. Sampson, V. Iyer, S. Rebolledo, H.P. Larsson, R.S. Kass, KCNE1 alters the voltage sensor movements necessary to open the KCNQ1 channel gate, Proc. Natl. Acad. Sci. U. S. A., 107 (2010) 22710–22715.
[163] L.-J. Ma, I. Ohmert, V. Vardanyan, Allosteric Features of KCNQ1 Gating Revealed by Alanine Scanning Mutagenesis, Biophys. J., 100 (2011) 885–894.
[164] J.D. Osteen, R. Barro-Soria, S. Robey, K.J. Sampson, R.S. Kass, H.P. Larsson, Allosteric gating mechanism underlies the flexible gating of KCNQ1 potassium channels, Proc. Natl. Acad. Sci., 109 (2012) 7103–7108.
[165] E. Meisel, M. Dvir, Y. Haitin, M. Giladi, A. Peretz, B. Attali, KCNQ1 channels do not undergo concerted but sequential gating transitions both in the absence and presence of KCNE1, J. Biol. Chem., (2012) jbc.M112.364901.
[166] J. Silva, Y. Rudy, Subunit interaction determines IKs participation in cardiac repolarization and repolarization reserve, Circulation, 112 (2005) 1384–1391.
[167] M.A. Zaydman, J.R. Silva, K. Delaloye, Y. Li, H. Liang, H.P. Larsson, J. Shi, J. Cui, Kv7.1 ion channels require a lipid to couple voltage sensing to pore opening, Proc. Natl. Acad. Sci., 110 (2013) 13180-13185.
[168] J.J. Myher, A. Kuksis, S. Pind, Molecular species of glycerophospholipids and sphingomyelins of human erythrocytes: improved method of analysis, Lipids, 24 (1989) 396–407.
[169] Q. Li, S. Wanderling, P. Sompornpisut, E. Perozo, Structural basis of lipid-driven conformational transitions in the KvAP voltage-sensing domain, Nat. Struct. Mol. Biol., 21 (2014) 160–166.
[170] D. Marsh, Protein modulation of lipids, and vice-versa, in membranes, Biochim. Biophys. Acta BBA - Biomembr., 1778 (2008) 1545–1575.
[171] J.A. Lundbæk, S.A. Collingwood, H.I. Ingólfsson, R. Kapoor, O.S. Andersen, Lipid bilayer regulation of membrane protein function: gramicidin channels as molecular force probes, J. R. Soc. Interface, 7 (2010) 373–395.
[172] S. Marcelja, Lipid-mediated protein interaction in membranes, Biochim. Biophys. Acta, 455 (1976) 1–7.
[173] H.W. Huang, Deformation free energy of bilayer membrane and its effect on gramicidin channel lifetime, Biophys. J., 50 (1986) 1061–1070.
[174] D.R. Fattal, A. Ben-Shaul, A molecular model for lipid-protein interaction in membranes: the role of hydrophobic mismatch, Biophys. J., 65 (1993) 1795–1809.
[175] C. Nielsen, M. Goulian, O.S. Andersen, Energetics of inclusion-induced bilayer deformations, Biophys. J., 74 (1998) 1966–1983.
[176] C. Nielsen, O.S. Andersen, Inclusion-induced bilayer deformations: effects of monolayer equilibrium curvature, Biophys. J., 79 (2000) 2583–2604.
[177] O.S. Andersen, R.E. Koeppe 2nd, Bilayer thickness and membrane protein function: an energetic perspective, Annu. Rev. Biophys. Biomol. Struct., 36 (2007) 107–130.
[178] L.F. Braganza, D.L. Worcester, Structural changes in lipid bilayers and biological membranes caused by hydrostatic pressure, Biochemistry (Mosc.), 25 (1986) 7484–7488.

[179] A.S. Reddy, D.T. Warshaviak, M. Chachisvilis, Effect of membrane tension on the physical properties of DOPC lipid bilayer membrane, Biochim. Biophys. Acta BBA - Biomembr., 1818 (2012) 2271–2281.
[180] D. Marsh, Liquid-ordered phases induced by cholesterol: a compendium of binary phase diagrams, Biochim. Biophys. Acta, 1798 (2010) 688–699.
[181] M. Patra, Lateral-Pressure Profiles in Cholesterol-DPPC Bilayers, ArXivcond-Mat0504101, (2005).
[182] E. Evans, W. Rawicz, Entropy-driven tension and bending elasticity in condensed-fluid membranes, Phys. Rev. Lett., 64 (1990) 2094–2097.
[183] J. Gallová, D. Uhríková, N. Kučerka, S. Doktorovová, S.S. Funari, J. Teixeira, P. Balgavý, The effects of cholesterol and β-sitosterol on the structure of saturated diacyl-phosphatidylcholine bilayers, Eur. Biophys. J., 40 (2011) 153–163.
[184] Z. Chen, R.P. Rand, The influence of cholesterol on phospholipid membrane curvature and bending elasticity, Biophys. J., 73 (1997) 267–276.
[185] M.J. Bruno, R.E. Koeppe, O.S. Andersen, Docosahexaenoic acid alters bilayer elastic properties, Proc. Natl. Acad. Sci., 104 (2007) 9638–9643.
[186] N. Dan, Lipid tail chain asymmetry and the strength of membrane-induced interactions between membrane proteins, Biochim. Biophys. Acta BBA - Biomembr., 1768 (2007) 2393–2399.
[187] R.D. Klausner, A.M. Kleinfeld, R.L. Hoover, M.J. Karnovsky, Lipid domains in membranes: evidence derived from structural perturbations induced by free fatty acids and lifetime heterogeneity analysis, J. Biol. Chem., 255 (1980) 1286–1295.
[188] P. Seeman, The membrane actions of anesthetics and tranquilizers, Pharmacol. Rev., 24 (1972) 583–655.
[189] C.E. Morris, Voltage-Gated Channel Mechanosensitivity: Fact or Friction?, Front. Physiol., 2 (2011).
[190] C.X. Gu, P.F. Juranka, C.E. Morris, Stretch-activation and stretch-inactivation of Shaker-IR, a voltage-gated K+ channel, Biophys. J., 80 (2001) 2678–2693.
[191] I.V. Tabarean, P. Juranka, C.E. Morris, Membrane stretch affects gating modes of a skeletal muscle sodium channel, Biophys. J., 77 (1999) 758–774.
[192] A. Shcherbatko, F. Ono, G. Mandel, P. Brehm, Voltage-dependent sodium channel function is regulated through membrane mechanics, Biophys. J., 77 (1999) 1945–1959.
[193] P.D. Langton, Calcium channel currents recorded from isolated myocytes of rat basilar artery are stretch sensitive, J. Physiol., 471 (1993) 1–11.
[194] B. Calabrese, I.V. Tabarean, P. Juranka, C.E. Morris, Mechanosensitivity of N-type calcium channel currents, Biophys. J., 83 (2002) 2560–2574.
[195] A. Maguy, T.E. Hebert, S. Nattel, Involvement of lipid rafts and caveolae in cardiac ion channel function, Cardiovasc. Res., 69 (2006) 798–807.
[196] J.R. Martens, K. O'Connell, M. Tamkun, Targeting of ion channels to membrane microdomains: localization of Kv channels to lipid rafts, Trends Pharmacol. Sci., 25 (2004) 16–21.
[197] I. Levitan, Y. Fang, A. Rosenhouse-Dantsker, V. Romanenko, Cholesterol and ion channels, Subcell. Biochem., 51 (2010) 509–549.
[198] Y.-F. Xiao, D.C. Sigg, A. Leaf, The antiarrhythmic effect of n-3 polyunsaturated fatty acids: modulation of cardiac ion channels as a potential mechanism, J. Membr. Biol., 206 (2005) 141–154.
[199] S. Bendahhou, T.R. Cummins, W.S. Agnew, Mechanism of modulation of the voltage-gated skeletal and cardiac muscle sodium channels by fatty acids, Am. J. Physiol., 272 (1997) C592–600.

[200] L.M. Boland, M.M. Drzewiecki, Polyunsaturated fatty acid modulation of voltage-gated ion channels, Cell Biochem. Biophys., 52 (2008) 59–84.
[201] X. Sun, D. Zhou, P. Zhang, E.G. Moczydlowski, G.G. Haddad, Beta-subunit-dependent modulation of hSlo BK current by arachidonic acid, J. Neurophysiol., 97 (2007) 62–69.
[202] G.K. Doolan, R.G. Panchal, E.L. Fonnes, A.L. Clarke, D.A. Williams, S. Petrou, Fatty acid augmentation of the cardiac slowly activating delayed rectifier current (IKs) is conferred by hminK, FASEB J. Off. Publ. Fed. Am. Soc. Exp. Biol., 16 (2002) 1662–1664.
[203] H. Sade, K. Muraki, S. Ohya, N. Hatano, Y. Imaizumi, Activation of large-conductance, Ca2+-activated K+ channels by cannabinoids, Am. J. Physiol. Cell Physiol., 290 (2006) C77–86.
[204] A.L. Clarke, S. Petrou, J.V. Walsh Jr, J.J. Singer, Modulation of BK(Ca) channel activity by fatty acids: structural requirements and mechanism of action, Am. J. Physiol. Cell Physiol., 283 (2002) C1441–1453.
[205] Y.F. Xiao, Q. Ke, S.Y. Wang, K. Auktor, Y. Yang, G.K. Wang, J.P. Morgan, A. Leaf, Single point mutations affect fatty acid block of human myocardial sodium channel alpha subunit Na+ channels, Proc. Natl. Acad. Sci. U. S. A., 98 (2001) 3606–3611.
[206] A. Rosenhouse-Dantsker, S. Noskov, S. Durdagi, D.E. Logothetis, I. Levitan, Identification of novel cholesterol-binding regions in Kir2 channels, J. Biol. Chem., (2013) jbc.M113.496117.
[207] F.C. Coyan, F. Abderemane-Ali, M.Y. Amarouch, J. Piron, J. Mordel, C.S. Nicolas, M. Steenman, J. Mérot, C. Marionneau, A. Thomas, R. Brasseur, I. Baró, G. Loussouarn, A Long QT Mutation Substitutes Cholesterol for Phosphatidylinositol-4,5-Bisphosphate in KCNQ1 Channel Regulation, PLoS ONE, 9 (2014) e93255.
[208] D. Schmidt, Q.-X. Jiang, R. MacKinnon, Phospholipids and the origin of cationic gating charges in voltage sensors, Nature, 444 (2006) 775–779.
[209] Y. Barenholz, S. Gatt, Sphingomyelin: metabolism, chemical synthesis, physical and chemical properties, in: J.N. Hawthorne, G.B. Ansell (eds.), Phospholipids, Elsevier/North-Holland Biomedical Press, Amsterdam, 1982: pp. 129–177.
[210] Y. Ramu, Y. Xu, Z. Lu, Enzymatic activation of voltage-gated potassium channels, Nature, 442 (2006) 696–699.
[211] Y. Xu, Y. Ramu, Z. Lu, Removal of phospho-head groups of membrane lipids immobilizes voltage sensors of K+ channels, Nature, 451 (2008) 826–829.
[212] J.E. Bell, C. Miller, Effects of phospholipid surface charge on ion conduction in the K+ channel of sarcoplasmic reticulum, Biophys. J., 45 (1984) 279–287.
[213] E. Moczydlowski, O. Alvarez, C. Vergara, R. Latorre, Effect of phospholipid surface charge on the conductance and gating of a Ca2+-activated K+ channel in planar lipid bilayers, J. Membr. Biol., 83 (1985) 273–282.
[214] M.A. Kasimova, M. Tarek, A.K. Shaytan, K.V. Shaitan, L. Delemotte, Voltage-gated ion channel modulation by lipids: Insights from molecular dynamics simulations, Biochim. Biophys. Acta, 1838 (2014) 1322–1331.
[215] L.G. Cuello, D.M. Cortes, E. Perozo, Molecular architecture of the KvAP voltage-dependent K+ channel in a lipid bilayer, Science, 306 (2004) 491–495.
[216] S.-Y. Lee, R. MacKinnon, A membrane-access mechanism of ion channel inhibition by voltage sensor toxins from spider venom, Nature, 430 (2004) 232–235.
[217] J.A. Freites, D.J. Tobias, G. von Heijne, S.H. White, Interface connections of a transmembrane voltage sensor, Proc. Natl. Acad. Sci. U. S. A., 102 (2005) 15059–15064.
[218] W. Treptow, M. Tarek, Environment of the gating charges in the Kv1.2 Shaker potassium channel, Biophys. J., 90 (2006) L64–66.
[219] V. Jogini, B. Roux, Dynamics of the Kv1.2 voltage-gated K+ channel in a membrane environment, Biophys. J., 93 (2007) 3070–3082.

[220] Z.A. Sands, M.S.P. Sansom, How Does a Voltage Sensor Interact with a Lipid Bilayer? Simulations of a Potassium Channel Domain, Struct. England1993, 15 (2007) 235–244.

[221] P. Bjelkmar, P.S. Niemelä, I. Vattulainen, E. Lindahl, Conformational changes and slow dynamics through microsecond polarized atomistic molecular simulation of an integral Kv1.2 ion channel, PLoS Comput. Biol., 5 (2009) e1000289.

[222] D.J. Combs, H.-G. Shin, Y. Xu, Y. Ramu, Z. Lu, Tuning voltage-gated channel activity and cellular excitability with a sphingomyelinase, J. Gen. Physiol., 142 (2013) 367–380.

[223] L. Stephens, A. McGregor, P. Hawkins, Phosphoinositide-3-kinases: Regulation by cell surface receptors and function of 3-phosphorylated lipids, in: S. Cockcroft (ed.), Frontiers of Molecular Biology, Biology of Phosphoinositides, Oxford University Press, Oxford, UK, 2000: pp. 32–107.

[224] B.-C. Suh, B. Hille, PIP2 is a necessary cofactor for ion channel function: how and why?, Annu. Rev. Biophys., 37 (2008) 175–195.

[225] N. Gamper, M.S. Shapiro, Regulation of ion transport proteins by membrane phosphoinositides, Nat. Rev. Neurosci., 8 (2007) 921–934.

[226] D.E. Logothetis, V.I. Petrou, S.K. Adney, R. Mahajan, Channelopathies linked to plasma membrane phosphoinositides, Pflüg. Arch. Eur. J. Physiol., 460 (2010) 321–341.

[227] E.A. Woodcock, P.M. Kistler, Y.-K. Ju, Phosphoinositide signalling and cardiac arrhythmias, Cardiovasc. Res., 82 (2009) 286–295.

[228] V. Telezhkin, J.M. Reilly, A.M. Thomas, A. Tinker, D.A. Brown, Structural Requirements of Membrane Phospholipids for M-type Potassium Channel Activation and Binding, J. Biol. Chem., 287 (2012) 10001–10012.

[229] A.M. Thomas, S.G. Brown, J.L. Leaney, A. Tinker, Differential phosphoinositide binding to components of the G-protein-gated K+ channel, J. Membr. Biol., 211 (2006) 43–53.

[230] T. Rohacs, C.M.B. Lopes, T. Jin, P.P. Ramdya, Z. Molnár, D.E. Logothetis, Specificity of activation by phosphoinositides determines lipid regulation of Kir channels, Proc. Natl. Acad. Sci. U. S. A., 100 (2003) 745–750.

[231] T. Rohacs, C.M.B. Lopes, I. Michailidis, D.E. Logothetis, PI(4,5)P2 regulates the activation and desensitization of TRPM8 channels through the TRP domain, Nat. Neurosci., 8 (2005) 626–634.

[232] G.B. Willars, S.R. Nahorski, R.A. Challiss, Differential regulation of muscarinic acetylcholine receptor-sensitive polyphosphoinositide pools and consequences for signaling in human neuroblastoma cells, J. Biol. Chem., 273 (1998) 5037–5046.

[233] L.R. Stephens, K.T. Hughes, R.F. Irvine, Pathway of phosphatidylinositol-(3,4,5)-trisphosphate synthesis in activated neutrophils, Nature, 351 (1991) 33–39.

[234] D.W. Hilgemann, R. Ball, Regulation of cardiac Na+,Ca2+ exchange and KATP potassium channels by PIP2, Science, 273 (1996) 956–959.

[235] M. Soom, R. Schönherr, Y. Kubo, C. Kirsch, R. Klinger, S.H. Heinemann, Multiple PIP2 binding sites in Kir2.1 inwardly rectifying potassium channels, FEBS Lett., 490 (2001) 49–53.

[236] C.M.B. Lopes, H. Zhang, T. Rohacs, T. Jin, J. Yang, D.E. Logothetis, Alterations in conserved Kir channel-PIP2 interactions underlie channelopathies, Neuron, 34 (2002) 933–944.

[237] C.L. Huang, S. Feng, D.W. Hilgemann, Direct activation of inward rectifier potassium channels by PIP2 and its stabilization by Gbetagamma, Nature, 391 (1998) 803–806.

[238] T. Baukrowitz, U. Schulte, D. Oliver, S. Herlitze, T. Krauter, S.J. Tucker, J.P. Ruppersberg, B. Fakler, PIP2 and PIP as determinants for ATP inhibition of KATP channels, Science, 282 (1998) 1141–1144.

[239] Z. Yang, H. Xu, N. Cui, Z. Qu, S. Chanchevalap, W. Shen, C. Jiang, Biophysical and molecular mechanisms underlying the modulation of heteromeric Kir4.1-Kir5.1 channels by CO2 and pH, J. Gen. Physiol., 116 (2000) 33–45.

[240] S.B. Hansen, X. Tao, R. MacKinnon, Structural basis of PIP2 activation of the classical inward rectifier K+ channel Kir2.2, Nature, 477 (2011) 495–498.

[241] S.-J. Lee, S. Wang, W. Borschel, S. Heyman, J. Gyore, C.G. Nichols, Secondary anionic phospholipid binding site and gating mechanism in Kir2.1 inward rectifier channels, Nat. Commun., 4 (2013) 2786.

[242] M.R. Whorton, R. MacKinnon, Crystal Structure of the Mammalian GIRK2 K+ Channel and Gating Regulation by G-Proteins, PIP2, and Sodium, Cell, 147 (2011) 199–208.

[243] H. Zhang, L.C. Craciun, T. Mirshahi, T. Rohacs, C.M.B. Lopes, T. Jin, D.E. Logothetis, PIP(2) activates KCNQ channels, and its hydrolysis underlies receptor-mediated inhibition of M currents, Neuron, 37 (2003) 963–975.

[244] K.-H. Park, J. Piron, S. Dahimène, J. Mérot, I. Baró, D. Escande, G. Loussouarn, Impaired KCNQ1–KCNE1 and Phosphatidylinositol-4,5-Bisphosphate Interaction Underlies the Long QT Syndrome, Circ. Res., 96 (2005) 730–739.

[245] B. Nilius, F. Mahieu, J. Prenen, A. Janssens, G. Owsianik, R. Vennekens, T. Voets, The Ca2+-activated cation channel TRPM4 is regulated by phosphatidylinositol-4,5-biphosphate, EMBO J., 25 (2006) 467–478.

[246] S. Brauchi, G. Orta, C. Mascayano, M. Salazar, N. Raddatz, H. Urbina, E. Rosenmann, F. Gonzalez-Nilo, R. Latorre, Dissection of the components for PIP2 activation and thermosensation in TRP channels, Proc. Natl. Acad. Sci. U. S. A., 104 (2007) 10246–10251.

[247] J.-S. Bian, T.V. McDonald, Phosphatidylinositol-4,5-bisphosphate interactions with the HERG K(+) channel, Pflüg. Arch. Eur. J. Physiol., 455 (2007) 105–113.

[248] G.E. Flynn, W.N. Zagotta, Molecular mechanism underlying phosphatidylinositol-4,5-bisphosphate-induced inhibition of SpIH channels, J. Biol. Chem., 286 (2011) 15535–15542.

[249] A.M. Thomas, S.C. Harmer, T. Khambra, A. Tinker, Characterization of a binding site for anionic phospholipids on KCNQ1, J. Biol. Chem., 286 (2011) 2088–2100.

[250] A.A. Rodriguez-Menchaca, S.K. Adney, Q.-Y. Tang, X.-Y. Meng, A. Rosenhouse-Dantsker, M. Cui, D.E. Logothetis, PIP2 controls voltage-sensor movement and pore opening of Kv channels through the S4-S5 linker, Proc. Natl. Acad. Sci. U. S. A., 109 (2012) E2399–2408.

[251] V. Telezhkin, A.M. Thomas, S.C. Harmer, A. Tinker, D.A. Brown, A basic residue in the proximal C-terminus is necessary for efficient activation of the M-channel subunit Kv7.2 by PI(4,5)P2, Pflüg. Arch. Eur. J. Physiol., 465 (2013) 945–953.

[252] Q. Zhang, P. Zhou, Z. Chen, M. Li, H. Jiang, Z. Gao, H. Yang, Dynamic PIP2 interactions with voltage sensor elements contribute to KCNQ2 channel gating, Proc. Natl. Acad. Sci., 100 (2013) 20093-20098.

[253] K. Eckey, E. Wrobel, N. Strutz-Seebohm, L. Pott, N. Schmitt, G. Seebohm, Novel Kv7.1-phosphatidylinositol-4,5-bisphosphate (PIP2) interaction sites uncovered by charge neutralization scanning, J. Biol. Chem., 289 (2014) 22749-22758.

[254] T. Rohacs, J. Chen, G.D. Prestwich, D.E. Logothetis, Distinct Specificities of Inwardly Rectifying K+Channels for Phosphoinositides, J. Biol. Chem., 274 (1999) 36065–36072.

[255] Y. Li, M.A. Zaydman, D. Wu, J. Shi, M. Guan, B. Virgin-Downey, J. Cui, KCNE1 enhances phosphatidylinositol-4,5-bisphosphate (PIP2) sensitivity of IKs to modulate channel activity, Proc. Natl. Acad. Sci. U. S. A., 108 (2011) 9095–9100.

[256] F. Abderemane-Ali, Z. Es-Salah-Lamoureux, L. Delemotte, M.A. Kasimova, A.J. Labro, D.J. Snyders, D. Fedida, M. Tarek, I. Baró, G. Loussouarn, Dual effect of phosphatidyl-(4,5)-bisphosphate PIP2 on Shaker K+ channels, J. Biol. Chem., 287 (2012) 36158–36167.

[257] Y. Murata, H. Iwasaki, M. Sasaki, K. Inaba, Y. Okamura, Phosphoinositide phosphatase activity coupled to an intrinsic voltage sensor, Nature, 435 (2005) 1239–1243.

[258] G. Loussouarn, K.-H. Park, C. Bellocq, I. Baró, F. Charpentier, D. Escande, Phosphatidylinositol-4,5-bisphosphate, PIP2, controls KCNQ1/KCNE1 voltage-gated potassium channels: a functional homology between voltage-gated and inward rectifier K+ channels, EMBO J., 22 (2003) 5412–5421.

[259] M.A. Zaydman, J. Cui, PIP2 regulation of KCNQ channels: biophysical and molecular mechanisms for lipid modulation of voltage-dependent gating, Membr. Physiol. Membr. Biophys., 5 (2014) 195.

[260] T. Yang, S.-K. Chung, W. Zhang, J.G.L. Mullins, C.H. McCulley, J. Crawford, J. MacCormick, C.-A. Eddy, A.N. Shelling, J.K. French, P. Yang, J.R. Skinner, D.M. Roden, M.I. Rees, Biophysical properties of 9 KCNQ1 mutations associated with long-QT syndrome, Circ. Arrhythm. Electrophysiol., 2 (2009) 417–426.

[261] A. Matavel, E. Medei, C.M.B. Lopes, PKA and PKC partially rescue long QT type 1 phenotype by restoring channel-PIP2 interactions, Channels Austin Tex, 4 (2010) 3–11.

[262] S.C. Kohout, S.C. Bell, L. Liu, Q. Xu, D.L. Minor, E.Y. Isacoff, Electrochemical coupling in the voltage-dependent phosphatase Ci-VSP, Nat. Chem. Biol., 6 (2010) 369–375.

[263] P. Zhou, H. Yu, M. Gu, F. Nan, Z. Gao, M. Li, Phosphatidylinositol-4,5-bisphosphate alters pharmacological selectivity for epilepsy-causing KCNQ potassium channels, Proc. Natl. Acad. Sci. U. S. A., 110 (2013) 8726–8731.

[264] C.C. Hernandez, O. Zaika, M.S. Shapiro, A Carboxy-terminal Inter-Helix Linker As the Site of Phosphatidylinositol-4,5-Bisphosphate Action on Kv7 (M-type) K+ Channels, J. Gen. Physiol., 132 (2008) 361–381.

[265] P. Aivar, J. Fernández-Orth, C. Gomis-Perez, A. Alberdi, A. Alaimo, M.S. Rodríguez, T. Giraldez, P. Miranda, P. Areso, A. Villarroel, Surface Expression and Subunit Specific Control of Steady Protein Levels by the Kv7.2 Helix A-B Linker, PLoS ONE, 7 (2012) e47263.

APPENDIX

A2.1. Experimentally recorded curves: I/V, G/V, Q/V and F/V

In the appendix to Chapter **2**, we would like to briefly discuss some of the electrophysiological curves describing the gating process of a voltage-gated ion channel, namely, I/V (ionic current vs. voltage), G/V (conductance vs. voltage), Q/V (gating current vs. voltage) and F/V (fluorescence vs. voltage).

A2.1.1. The ionic current and the conductance

Current-voltage (I/V) relationships are perhaps the most effective way to summarize the behavior of voltage-gated ion channels. A number of important and useful parameters that can not be easily accessed from the raw data can be readily derived from these plots, including: reversal potential, ionic dependence/selectivity, voltage-dependence (rectification), activation threshold, slope and cord conductance, as well as overall quality of voltage/patch clamp.

The factors that determine current flow though an open channel are the membrane potential (V), the conductance of the open pore (g) and the probability of the pore opening (P_0) [1,2]:

$$I_i = g(V)P_0(V)(V - V_e). \quad (2.1.1.1)$$

Here, V_e is the reversal potential of the ionic current through the pore.

If the reversal potential is known, a conductance voltage (G/V) curve can be readily calculated by dividing current at each potential by the driving force ($V - V_e$). These curves are typically sigmoidal (see Figure A2.1.2.1).

A2.1.2. The gating current and the gating charge

A free charge moving in the electric field is translated into transient ionic current. In the case of a voltage-gated ion channel, translation of the S4 positively charged residues across the plasma membrane induces small current, called gating (see Figure A2.1.2.1) [1,3], as this current is responsible for the change in the channel's opening probability. This small current may be visible using signal averaging techniques after blocking the bulk of the ionic current and using a subtraction procedure to eliminate the linear capacity current.

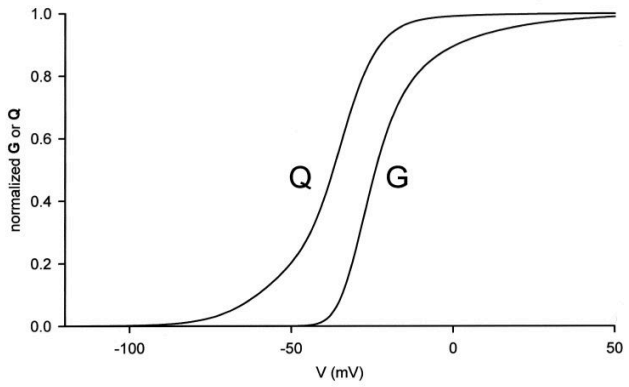

Figure A2.1.2.1. The voltage dependence of gating current (Q) and conductance (G) for a voltage-gated ion channel. The figure is adapted from [1,3].

The time integral of the gating current at a particular voltage V_1 is called the gating charge or $Q(V_1)$. The dependence of the gating current on the TM potential shows a sigmoid shape with asymptotes at extreme potentials (see Figure A2.1.2.1).

A2.1.3. Tracking the voltage sensor movement by measuring the fluorescence signal of the label

When recording the gating current of a voltage-gated ion channel, the bulk of ionic current must be blocked, thus preventing the simultaneous tracking of both the voltage sensor activation and the pore opening. The latter, however, is possible to achieve using more sophisticated voltage/patch clamp techniques combined with fluorescence recording. These techniques are accordingly called the voltage/patch clamp fluorometry [4-7].

In the voltage/patch clamp fluorometry of a voltage-gated ion channel, the voltage sensor domain (usually the extracellular S3-S4 loop) is labeled with a fluorophore. The label is attached to a site of interest performing cysteine mutagenesis and a chemical reaction with sulfhydryl-reactive fluorophores. Upon application of the electric field, S4 undergoes structural rearrangements, which may affect the vicinity of the labeled cysteine, *i.e.* fluorophore quantum yield, mobility, accessibility to quencher molecules, proximity to neighboring fluorophores and other factors. As a result, the fluorescence emission changes. In this way, the fluorophore serves as a localized, highly sensitive reporter of the voltage sensor activation. At the same time, current signals, which change as the result of channel opening, and ion flux serve as an indicator of channel functional states.

The dependence of the fluorescence intensity (F) on the applied voltage (the F/V curve) has a sigmoid shape with asymptotes at extreme potentials. For an example, see Figure 2.3.7.1, 4.3.4.2.

A2.2. Localization of voltage-gated potassium (Kv) channels

Table A2.2.1. Localization of the various members of the Kv family channels. In parentheses, the name of the gene is indicated. CNS denotes the central nervous system. For a complete description of each member of the Kv family including therapeutic importance see IUPHARM database: http://www.iuphar-db.org/DATABASE/FamilyMenuForward?familyId=81. The table is adapted from [8].

CHANNEL (GENE)	LOCALIZATION
Kv1.1 (*KCNA1*)	CNS (medulla, pons, cerebellum, midbrain, hippocampus and auditory nuclei), node of Ranvier and kidney
Kv1.2 (*KCNA2*)	CNS (pons, medulla, cerebellum, hippocampus, thalamus, cerebral cortex and spinal cord)
Kv1.3 (*KCNA3*)	T and B cells, macrophages, microglia, osteoclasts, platens, CNS (prominent in the olfactory bulb) and testis
Kv1.4 (*KCNA4*)	CNS (olfactory bulb, corpus striatum and hippocampus), heart, skeletal and smooth muscle and pancreatic islets
Kv1.5 (*KCNA5*)	Cardiac myocytes, CNS (hippocampus, cortex and pituitary), microglia, Schwann cells, macrophages and vascular smooth muscle
Kv1.6 (*KCNA6*)	Spinal cord, CNS, oligodendrocytes progenitor cells, astrocytes and pulmonary artery smooth muscle
Kv1.7 (*KCNA7*)	Heart, skeletal muscle, liver, lung, placenta and CNS
Kv1.8 (*KCNA10*)	Kidney, CNS, heart and skeletal muscle
Kv2.1 (*KCNB1*)	CNS (cerebral cortex, hippocampus, cerebellum), pancreatic β-cells, insulinomas and gastric cancer cells
Kv2.2 (*KCNB2*)	CNS (olfactory bulb, cortex, hippocampus and cerebellum) and pancreatic δ-cells
Kv3.1 (*KCNC2*)	CNS (fast spiking GABAergic interneurons), pancreatic islets, Renshaw cells (spinal interneurons), pancreatic β-cells
Kv3.3 (*KCNC3*)	CNS (brainstem, cerebellum, forebrain, Purkinje cells, motoneurons and auditory brainstem)
Kv3.4 (*KCNC4*)	CNS (brainstem and hippocampus granule cells) and skeletal muscle
Kv4.1 (*KCND1*)	CNS, heart, liver, kidney, thyroid gland and pancreas

CHANNEL (GENE)	LOCALIZATION
Kv4.2 (*KCND2*)	CNS (cerebellum, hippocampus, thalamus, forebrain and dorsal horn neurons) and rodent heart
Kv4.3 (*KCND3*)	CNS (cortex and cerebellum), atrial and ventricular myocytes, and smooth muscle
Kv7.1 (*KCNQ1*)	Heart, ear, skeletal muscle, liver, kidney, epithelia in kidney, lung and gastrointestinal tract
Kv7.2 (*KCNQ3*)	CNS (hippocampus, cortex, thalamus, cerebellum, brain stem), nodes of Ranvier and sympathetic and dorsal root ganglia
Kv7.4 (*KCNQ4*)	Outer hair cells and neurons of the auditory system and vascular smooth muscle
Kv7.5 (*KCNQ5*)	CNS (hippocampus, cortex and thalamus), skeletal muscle and vascular smooth muscle
Kv10.1 (*KCNH1* and *EAG1*)	CNS
Kv10.2 (*KCNH5* and *EAG2*)	CNS, muscle, heart, placenta, lung, liver, kidney and pancreas
Kv11.1 (*KCNH2*, *ERG1* and *HERG*)	Heart, CNS, endocrine cells and myocytes
Kv11.2 (*KCNH6*)	CNS and endocrine cells
Kv11.3 (*KCNH7*)	CNS
Kv12.1 (*KCNH8*)	CNS
Kv12.2 (*KCNH3*)	CNS
Kv12.3 (*KCNH4*)	CNS

REFERENCES

[1] F. Bezanilla, The Voltage Sensor in Voltage-Dependent Ion Channels, Physiol. Rev., 80 (2000) 555–592.

[2] W. Walz, A.A. Boulton, G.B. Baker, Patch-Clamp Analysis: Advanced Techniques, Springer Science & Business Media, 2002.

[3] E. Stefani, L. Toro, E. Perozo, F. Bezanilla, Gating of Shaker K+ channels: I Ionic and gating currents, Biophys. J., 66 (1994) 996–1010.

[4] L.M. Mannuzzu, M.M. Moronne, E.Y. Isacoff, Direct physical measure of conformational rearrangement underlying potassium channel gating, Science, 271 (1996) 213–216.

[5] A. Cha, F. Bezanilla, Characterizing voltage-dependent conformational changes in the Shaker K+ channel with fluorescence, Neuron, 19 (1997) 1127–1140.

[6] J. Zheng, W.N. Zagotta, Patch-Clamp Fluorometry Recording of Conformational Rearrangements of Ion Channels, Sci. Signal., 2003 (2003) pl7.

[7] M.M. Pathak, V. Yarov-Yarovoy, G. Agarwal, B. Roux, P. Barth, S. Kohout, F. Tombola, E.Y. Isacoff, Closing in on the resting state of the Shaker K(+) channel, Neuron, 56 (2007) 124–140.

[8] H. Wulff, N.A. Castle, L.A. Pardo, Voltage-gated potassium channels as therapeutic targets, Nat. Rev. Drug Discov., 8 (2009) 982-1001.

3 MÉTHODES

La modélisation moléculaire est un terme générique qui fait référence à des méthodes théoriques et techniques de calcul, qui sont appliquées pour modéliser et simuler le comportement des molécules, telles que la visualisation de deux et trois (2d et 3d) des structures tridimensionnelles, l'organisation des composés et leurs propriétés dans des bases de données, ou de simuler le comportement des molécules au niveau atomique. L'application de la modélisation moléculaire pour l'étude des protéines est une pratique courante de nos jours. D'une part, de même que la cristallographie aux rayons X, la résonance magnétique nucléaire (RMN)[1] et la microscopie électronique, les méthodes de modélisation moléculaire fournissent un aperçu des propriétés structurelles. D'autre part, certaines méthodes de modélisation moléculaire permettent d'accéder à la dynamique des protéines et ceci à des échelles de temps allant de la picoseconde à la microseconde.

Ce chapitre est consacré aux méthodes que nous avons utilisées pour étudier la modulation des canaux Kv1.2 et Kv7.1 par PIP_2, à savoir, la dynamique moléculaire (DM), la métadynamique et la modélisation par homologie.

En dynamique moléculaire (DM) (voir **3.1**), le système est représenté par un ensemble de particules (généralement des atomes) en interaction. En appliquant les lois de la mécanique classique, à partir de conditions initiales, on est en mesure de prédire l'évolution du système en fonction du temps (générer les coordonnées et les vitesses des atomes, *i.e.* obtenir une trajectoire). Les interactions entre les atomes sont décrites par plusieurs termes d'énergie (non liées : type van der Waals et électrostatiques et liés : énergies de valence et de déformation d'angles et de dièdres, *etc.*), spécialement conçus pour reproduire les propriétés structurales des biomolécules et paramétrés en conséquence. Basé sur les trajectoires de DM, on est en mesure d'avoir accès à des informations pertinentes liées aux propriétés structurales, dynamiques et thermodynamiques du système, pouvant être comparées à l'expériences.

[1] La RMN est aussi utilisée pour étudier la dynamique.

Le recours à la dynamique moléculaire standard en représentation tout atome pour explorer les régions critiques de l'espace des phases telles que celles associées à des hautes barrières d'énergie libre est inapproprié car le temps nécessaire pour observer des transitions pertinentes peut être remarquablement long. Pour pallier à cette limitation, plusieurs techniques permettant un échantillonnage adéquat ont été proposées. Une de ces techniques est la métadynamique (section **3.2**) : un potentiel de biais externe, fonction d'un ou plusieurs degré(s) de liberté choisi(s), est ajouté à l'Hamiltonien du système. Ce potentiel pousse le système loin des minima d'énergie libre locale permettant une meilleure exploration de l'espace de configurations. La distribution de Boltzmann peut être récupéré à partir des biais. La méthode de métadynamique *well-tempered* que nous avons utilisée est une technique avancée dans laquelle l'énergie du potentiel de biais est adaptée en fonction des regions déjà explorées. Par rapport à métadynamique classique, la convergence de l'énergie libre dans la méthode well-tempered est plus rapidement atteinte.

La modélisation moléculaire englobe également plusieurs méthodes permettant la prédiction de la structure tridimensionnelle de peptides et de protéines, parmi lesquelles la reconnaissance du repliement, et la modélisation par homologie. Cette dernière (voir **3.3**) est particulièrement utile pour la prédiction de la structure des protéines contenant plus de 100 acides aminés. La modélisation par homologie est basée sur le fait que les protéines apparentées en leur évolution ont en commun la même architecture tridimensionnelle. Par conséquent, la résolution de la structure d'un seul représentant d'une famille de protéines (modèle) permet de construire des modèles atomistiques d'autres membres de cette famille. Lorsque le pourcentage d'homologie avec la protéine modèle est élevé, on est capable de prédire une structure de la cible avec une résolution correspondant à celle de la cristallographie à basse résolution. A l'autre extrémité du spectre de précision, c'est-à-dans le cas d'une faible homologie, le modèle peut avoir jusqu'à 50% de la position de ses atomes prédits avec un RMSD de 3,5 Å (tandis que les autres résidus ont été modélisé avec des erreurs plus conséquentes). Même dans ces conditions, les modèles prédits ont un repliement plutôt correct et sont, par conséquent, susceptibles d'être utilisés pour prédire approximativement la fonction biochimique de la protéine.

3 METHODS

Molecular modeling is a collective term that refers to theoretical methods and computational techniques, which are applied to model and mimic the behavior of molecules, such as visualizing two and three dimensional (2d and 3d) structures, organizing compounds and their properties into databases, providing tools for analyzing molecular properties or simulating the behavior of molecules on the atomic level. Application of molecular modeling for investigation of proteins is a common practice nowadays. On the one hand, along with the X-ray crystallography, nuclear magnetic resonance (NMR)[1] and electron microscopy, some methods of molecular modeling provide an insight into the structural properties. On the other hand, some methods of molecular modeling are able to access dynamics of proteins in time scales ranging from picoseconds to microseconds.

This chapter is devoted to the methods, which we applied investigating modulation of the Kv1.2 and Kv7.1 channels by PIP_2, namely, molecular dynamics (MD), metadynamics and homology modeling.

In the molecular dynamics (MD) method (see **3.1**), the system is represented as a set of interacting particles, usually corresponding to atoms. By applying the laws of classic mechanics, starting from initial conditions one is able to predict the evolution of the system in time (the coordinates and velocities of atoms, *i.e.* so-called trajectories). The interactions between atoms are described by several energy terms (non bonded: electrostatic and van der Waals terms; and bonded: energy of bonds, valence and dihedral angles, *etc.*), specifically designed to reproduce the structural properties of biomolecules and parameterized accordingly. Based on the MD trajectories, one is able to get an access to experimentally relevant information related to structural, dynamical and thermodynamics properties of the system.

Resorting to standard all-atom molecular dynamics to explore critical regions of the phase space such as those associated with high free-energy barriers is inappropriate as the time needed to observe the relevant transitions can be remarkably long. In order to overcome this limitation, several

[1] NMR is as well used to study the dynamics of proteins

techniques allowing enhanced sampling have been suggested. One of these techniques is metadynamics (see **3.2**): an external history-dependent bias potential, being a function of the selected degree of freedom, is added to the Hamiltonian of the system. This potential pushes the system away from its local free energy minima allowing better exploration of the configuration space. The Boltzmann distribution is further recovered from the added bias potential. Well-tempered metadynamics is an advanced technique, in which the energy of the added bias potential decreases with the bias already deposited at this value of the selected degree of freedom. Compared to classic metadynamics, the convergence of the free energy in well-tempered metadynamics is faster to achieve.

Molecular modeling encompasses several methods for peptide and protein structure prediction: fold recognition, *ab initio* and homology modeling. This latter method (see **3.3**) is especially prominent for structure prediction of proteins containing more than 100 amino acids. Homology modeling relies on the fact that evolutionary related proteins usually share a three-dimensional architecture. Hence, resolving the structure of a single representative of a protein family (template) allows building atomistic models of other members of this family. When the percentage of homology with the template protein is high, one is able to obtain a structure matching those of low-resolution X-ray. At the other end of the accuracy spectrum, *i.e.* in the case of low homology, the model may have less than 50% atoms with an RMSD error of 3.5 Å (while the rest of the residues are modeled with larger errors). Even though, the latters have the correct fold and, therefore, might be used to predict approximate biochemical function of the protein.

3.1. Molecular Dynamics (MD) Simulations

In classical Molecular Dynamics (MD) simulations, a biological macromolecule is represented as a system of interacting particles, usually corresponding to individual atoms. The evolution of this system in time obeys the laws of classical mechanics, the Newton's equation of motion. The electronic degrees of freedom are neglected, which is valid assuming the Born-Oppenheimer approximation [1]. The latter states that electronic and nuclear motion in a molecule can be separated, and, therefore, the energy of this molecule can be represented in terms of nuclear coordinates only.

There are two principal limitations of the MD method one should be aware of:

- since this method neglects the electronic distribution of an atom, it is not able to tackle modeling of quantum effects, such as chemical reactions, charge transfer, *etc.*
- the results of simulations will be realistic only if the potential energy function mimics the forces experienced by the "real" atoms, or, in other words, if the considered force field describes well atomic interactions; fortunately, for simulations of proteins, the available force fields developed over the last 30 years have proved to be sufficiently accurate in terms of kinetic and thermodynamics properties when used at normal temperatures (around 300 K) and normal pressures (around 1 bar).

In addition to the aforesaid limitations of the MD method, we would like to emphasize another one, particularly related to the simulations of biologically relevant processes. These processes may occur at timescales from nanoseconds to seconds and may involve more than billions of atoms at a time. So far, using the MD methods, one was able to simulate micro- and milliseconds processes in the system of millions of atoms (see for instance [2,3]). Further extension of this threshold to second timescales will have to wait a decade or more.

3.1.1. The principle of MD

According to molecular mechanics, the motion of particles ($i = 1, \dots, N$) of a given system is described in terms of Newton's second law or the equation of motion [4]:

$$m_i \frac{d^2 \boldsymbol{r_i}}{dt^2} = \boldsymbol{F_i}, \tag{3.1.1.1}$$

where m_i and r_i are the mass and the coordinate of the i^{th} particle, and F_i is the force acting on it. A particle may correspond to an individual atom[1] (all-atom MD), a heavy atom with covalently bound hydrogens (united-atom MD) or to several heavy atoms (coarse-grained MD). Integration of the eq. (3.1.1.1) requires one to specify the initial positions and velocities of the particles and the instantaneous forces acting on them.

The interaction among atoms is specified by the potential $U(\boldsymbol{r_1}, \dots, \boldsymbol{r_N})$, which represents the potential energy of N interacting particles as a function of their positions $\boldsymbol{r_i}$. The latter is calculated based on empirical potentials, *force fields*, with a specific functional form, representing the physics and chemistry of the system of interest. Given the potential, the force acting upon the i^{th} particle is determined by the gradient with respect to the displacements of this particle:

$$\boldsymbol{F_i} = -\nabla_{\boldsymbol{r_i}} U(\boldsymbol{r_1}, \dots, \boldsymbol{r_N}) = -\left(\frac{\partial U}{\partial x_i}, \frac{\partial U}{\partial y_i}, \frac{\partial U}{\partial z_i}\right). \tag{3.1.1.2}$$

Due to the many-body nature of the problem, there is no analytical solution to the eq. (3.1.1.1) and, therefore, the equations of motion are discretized and solved numerically. The MD *trajectories*, describing the time evolution of the system in a phase space, are defined by both position $\boldsymbol{r_i}$ and velocity $\boldsymbol{v_i}$ vectors. Accordingly, the positions and velocities are propagated with a finite time interval using numerical integrators.

3.1.2. Ensembles of statistical thermodynamics

In experiments, one works with a thermodynamics state of the system, characterized by a given set of macroscopic parameters such as temperature T, pressure P and a number of particles N. In MD simulations, however, the system is described in terms of a microscopic state: if one considers atomic

[1] further, we will consider the all-atom MD simulations only

positions $\boldsymbol{r}$ and velocities $\boldsymbol{v}$ as the system's coordinates in a $6N$-dimensional configuration space, then each point in this space will correspond to a single microscopic state. A thermodynamics ensemble is a collection of points in a configuration space that have similar macroscopic properties or, in other words, correspond to a single thermodynamics state. Transformation between the MD data and the macroscopic properties, comparable with the experimental data, requires application of statistical mechanics laws.

In statistical mechanics, one can distinguish several types of ensembles that differ by a macroscopic parameter constrained [5]:

- Microcanonical ensemble (NVE): the number of atoms N, volume V and energy of the system E are constrained;
- Canonical ensemble (NVT): the number of atoms N, volume V and temperature T are constrained;
- Isobaric-isothermal ensemble (NPT): the number of atoms N, pressure P and temperature T are constrained;
- Grand canonical ensemble (μVT): the chemical potential μ, volume V and temperature T are constrained.

3.1.3. Ergodic hypothesis

Experiments are usually made on a macroscopic sample that contains an extremely large number of molecules sampling their configuration space. The result of an experiment, therefore, corresponds to an ensemble average estimated over a large number of observables considered simultaneously. In MD simulations, the systems considered are often much smaller in their size compared to experiments. It is possible, however, instead of calculating an ensemble average, to calculate a time average over a large number of the system's configurations, evolving sequentially in time. Hence, applying experiments or MD simulations, the system's properties may be estimated in the two different ways, namely, either through an ensemble average or through a time average. Regardless this difference, both methods provide the same results obeying the ergodic hypothesis, a fundamental axiom of statistical mechanics. This hypothesis states that the time average of a property A equals its ensemble average [5]:

$$\lim_{\tau\to\infty}\frac{1}{\tau}\int_{t=0}^{\tau} A\Big(\boldsymbol{v^N}(t),\boldsymbol{r^N}(t)\Big)dt = \iint d\boldsymbol{v^N}d\boldsymbol{r^N}A(\boldsymbol{v^N},\boldsymbol{r^N})\rho(\boldsymbol{v^N},\boldsymbol{r^N}) \qquad (3.1.3.1)$$

Here, τ is the time of MD simulations, and ρ is the probability density of an ensemble.

In order to satisfy the conditions of this axiom, MD simulations must be long enough, allowing the system to explore the configuration space. If this is the case, the generated trajectories can be further used to calculate experimentally relevant information, concerning structural, dynamical and thermodynamics properties. However, most of the time, the system remains stuck at one of the free energy minima due to the fact that crossing nearby barriers requires much higher energy than a thermal fluctuation. In this case, various methods, enhancing sampling of a configuration space, can be applied (see **3.2**).

3.1.4. Integration schemes

An integrator advances the trajectory over small time increments Δt. Here, we will briefly discuss popular integrator algorithms: Verlet, leap-frog and velocity Verlet [6–8]. In the basis of these algorithms, a discretization of the equations of motion is obtained by Taylor expansion:

$$\boldsymbol{r_i}(t+\Delta t) = \boldsymbol{r_i}(t) + \Delta t \boldsymbol{v_i}(t) + \frac{\Delta t^2}{2m_i}\boldsymbol{F_i}(t) + \frac{\Delta t^3}{3!}\dddot{\boldsymbol{r}}_{\boldsymbol{i}}(t) + \mathcal{O}(\Delta t^4), \quad (3.1.4.1)$$

$$\boldsymbol{v_i}(t+\Delta t) = \boldsymbol{v_i}(t) + \frac{\Delta t}{m_i}\boldsymbol{F_i}(t) + \frac{\Delta t^2}{2}\ddot{\boldsymbol{v}}_{\boldsymbol{i}}(t) + \frac{\Delta t^3}{3!}\dddot{\boldsymbol{v}}_{\boldsymbol{i}}(t) + \mathcal{O}(\Delta t^4). \quad (3.1.4.2)$$

In the Verlet algorithm [6], the atomic positions at $t + \Delta t$ is calculated based on the current positions and forces at t and the previous positions at $t - \Delta t$:

$$\boldsymbol{r_i}(t+\Delta t) = 2\boldsymbol{r_i}(t) - \boldsymbol{r_i}(t-\Delta t) + \frac{\Delta t^2}{m_i}\boldsymbol{F_i}(t) + \mathcal{O}(\Delta t^4). \quad (3.1.4.3)$$

The velocities are actually not needed to compute the trajectories, but they are useful for calculating observables (*e.g.* kinetic energy):

$$\boldsymbol{v_i}(t) = \frac{\boldsymbol{r_i}(t+\Delta t) - \boldsymbol{r_i}(t-\Delta t)}{2\Delta t} + \mathcal{O}(\Delta t^3). \quad (3.1.4.4)$$

Note that the updating of positions according to the eq. (3.1.4.3) gives rise to numerical imprecision because a small term of order Δt^4 is added, $\mathcal{O}(\Delta t^4)$.

In the leap-frog algorithm [7], the positions and velocities are obtained from readily available quantities:

$$\boldsymbol{v_i}\left(t+\frac{\Delta t}{2}\right)=\boldsymbol{v_i}\left(t-\frac{\Delta t}{2}\right)+\frac{\Delta t}{m_i}\boldsymbol{F_i}(t), \tag{3.1.4.5}$$

$$\boldsymbol{r_i}(t+\Delta t)=\boldsymbol{r_i}(t)+\Delta t\cdot\boldsymbol{v_i}(t+\frac{\Delta t}{2}). \tag{3.1.4.6}$$

The velocities are updated at half time steps and "leap" ahead the positions. The current velocities can be obtained from:

$$\boldsymbol{v_i}(t)=\frac{\boldsymbol{v_i}\left(t-\frac{\Delta t}{2}\right)+\boldsymbol{v_i}(\Delta t+\frac{\Delta t}{2})}{2}. \tag{3.1.4.7}$$

Numerical imprecision is minimized in the leap-frog algorithm.

In the Velocity Verlet algorithm, the positions, velocities and forces are given at the same time. The positions and velocities are updated according to:

$$\boldsymbol{r_i}(t+\Delta t)=\boldsymbol{r_i}(t)+\Delta t\cdot\boldsymbol{v_i}(t)+\frac{\Delta t^2}{m_i}\boldsymbol{F_i}(t)+\mathcal{O}(\Delta t^3), \tag{3.1.4.8}$$

$$\boldsymbol{v_i}(t+\Delta t)=\boldsymbol{v_i}(t)+\frac{\Delta t}{2m_i}(\boldsymbol{F_i}(t)+\boldsymbol{F_i}(t+\Delta t)+\mathcal{O}(\Delta t^3)). \tag{3.1.4.9}$$

The Velocity-Verlet scheme is algebraically equivalent to the original Verlet algorithm. The equations (3.1.4.3), (3.1.4.4) can be derived from the eq. (3.1.4.8), (3.1.4.9) by elimination of the velocities in the position update.

In order to ensure energy conservation, the step-size Δt has to be smaller than the period of the fastest oscillations present in the molecular system. The source of these fastest oscillations is bond vibrations. One may increase the step-size Δt at the expense of explicitly removing the bond vibrations via rigid length constraints. The latter is implemented in several algorithm of MD: SHAKE, RATTLE, LINCS, SETTLE (for water molecules only), *etc.* [9–12]. These algorithms may implement different strategies to constrain a bond length: choosing novel unconstrained coordinates (internal coordinates), introducing explicit constraint forces or minimizing constraint forces implicitly by the technique of Lagrange multipliers or projection methods.

In this work, the equations of motion were integrated using either the velocity Verlet algorithm if the simulations were performed with the NAMD software [13] (see **4.1**, **4.3**) or the leap-frog algorithm if the simulations were performed with the GROMACS software [14] (see **4.2**). In all the MD simulations, chemical bonds between hydrogen and heavy atoms were constrained to their equilibrium values. The integration time-step was chosen to be 2 fs.

3.1.5. Force fields

For all-atom MD simulations, one assumes that every atom experiences a force specified by a model *force field* accounting for the interaction of that atom with the rest of the system. Such force fields present a good compromise between accuracy and computational efficiency.

A common potential energy function, considered in most popular force fields, has at least four contributions [4]:

$$U_{total} = U_{bond} + U_{angle} + U_{dihedral} + U_{nb}. \quad (3.1.5.1)$$

The first three terms of the eq. (3.1.5.1) describe the stretching, bending and torsional bonded interactions respectively:

$$U_{bond} = \frac{k_l}{2}(l - l_0)^2, \quad (3.1.5.2)$$

$$U_{angle} = \frac{k_\theta}{2}(\theta - \theta_0)^2, \quad (3.1.5.3)$$

$$U_{dihedral} = \sum_n \frac{V_n}{2}(1 + (-1)^{n+1}\cos(n\varphi - \psi_n)). \quad (3.1.5.4)$$

Here, the *bond* term counts each covalent bond in the system, *angles* are the angles between each pair of covalent bonds sharing a single atom at the vertex, and the *dihedral* term describes atoms pairs separated by exactly three covalent bonds with the central bond subject to the torsion angle. An improper dihedral term governing the geometry of four planar covalently bonded atoms may be also included. In the eq. (3.1.5.2) and (3.1.5.3), l and θ are the valence bond and angle respectively, l_0 and θ_0 are their reference values, and k_l and k_θ are their harmonic force constants. In the eq. (3.1.5.4), φ, n, ψ_n and V_n are the torsion, multiplicity, phase angle and barrier height respectively. In some other, more sophisticated force fields different expressions of the *bond* term (cubic function in MM2, quartic function in MM3 and Merck's MMFF), *angle* term (quartic function in MM2) and *torsion* term (three terms in torsional expansion in MM2) may be considered. Additionally, some force fields include cross-terms, which reflect coupling between the internal coordinates. These terms are especially prominent for predicting the vibrational spectra. The examples of cross terms are stretch-stretch, stretch-bond, stretch-torsion, torsion-bend, *etc.* [4].

The final term of the eq. (3.1.5.1) describes the interaction between non-bonded atom pairs. This term is split into 1-body, 2-body, 3-body, *etc.* sub-terms:

$$U_{nb} = \sum_i U_{nb}(r_i) + \sum_i \sum_{j>i} U_{nb}(r_i, r_j) + \sum_i \sum_{j>i} \sum_{i<j<k} U_{nb}(r_i, r_j, r_k) + \ldots \quad (3.1.5.5)$$

Here, $U_{nb}(r_i)$ is an externally applied potential field set to zero for periodic simulation of condensed phases, and $U_{nb}(r_i, r_j)$, $U_{nb}(r_i, r_j, r_k)$, … are the 2-, 3-, … -body nonbonded potentials respectively. In general, a force field includes 2-body nonbonded potential and neglects higher order nonbonded potentials; this approximation is called pair-wise additive and is introduced in order to decrease the computational cost. Though some accurate force fields designed for small molecules may include the 3-body potential as well as higher order nonbonded potentials.

The nonbonded interactions between two atoms separated by more than two bonds (1,4 interactions and higher) are represented by Coulomb potential (electrostatic interactions), attractive dispersion modeling interactions between induced dipoles, short range repulsion modeling Pauli exclusion principle and induced polarization (van der Waals interactions). The latter, induced polarization, is neglected in most of the force fields due to its complex description and implementation.

In a common force field, the electrostatic interactions are calculated as a sum of interactions between pairs of point charges using the Coulomb's law:

$$U_{qq} = \sum_{i<j} \sum_j \frac{q_i q_j}{4\pi\varepsilon r_{ij}}, \quad (3.1.5.6)$$

where q_i is the i^{th} atomic charge, r_{ij} is the distance between the i^{th} and j^{th} point charges, and ε is the permittivity of the medium between these two charges. Alternatively, one may consider the central multipole expansion, which is based upon the electric moments or multipoles: the charge, dipole, quadrupole, octopole, *etc.* [4].

The van der Waals (vdW) interactions account for two types of forces: the dispersive and exchange/overlap forces. The dispersive force is due to instantaneous dipoles, which arise during the fluctuations in the electron clouds. An instantaneous dipole in a molecule can in turn induce a dipole in neighboring atoms, giving rise to an attractive effect. The exchange/overlap force can be understood in terms of the Pauli principle, which formally prohibits any two electrons in a system from having the same set of quantum numbers (the interaction is due to electrons with the same spin).

The van-der-Waals interactions are usually calculated using a simple empirical expression, *e.g.* the Lennard-Jones 12-6 function:

$$U_{vdW} = \sum_{i<j} \sum_j 4\varepsilon_{ij} \left[\left(\frac{\sigma_{ij}}{r_{ij}}\right)^{12} - \left(\frac{\sigma_{ij}}{r_{ij}}\right)^{6} \right], \quad (3.1.5.7)$$

where σ_{ij} and ε_{ij} are the collision diameter and the well depth respectively. Other functions, for instance Halgren or Buckingham potentials, may be considered in describing van der Waals interactions.

In general, a force field is defined by both, functional forms, the eq. (3.1.5.1)-(3.1.5.7), and their parameters, l_0, θ_0, k_l, k_θ, *etc.* The latters are derived experimentally and/or computationally. In particular, the reference values of valence bonds and angles may be obtained from microwave and X-ray spectroscopy, *ab initio* calculations; the force constants of valence bonds and angles – from infrared (IR) and Raman spectroscopy, *ab initio* calculations; the torsion parameters – from NMR, IR, Raman and microwave spectroscopy, *ab initio* calculations; the van der Waals parameters – from experimental densities and enthalpies of vaporization of solvents; partial atomic charges – from restricted electrostatic potential (RESP) procedure.

Finally, we would like to notice the important features of force fields. First, the force fields used in molecular modeling were primarily designed to reproduce structural properties but they can also be used to predict other properties, such as molecular spectra (note, however, that molecular mechanics force fields can rarely predict spectra with great accuracy). Second, force fields are *empirical*, which means that there is no correct form for a force field. And third, the functional form and parameters of force fields are assumed to be transferable, meaning that the same set of parameters can be used to model a series of related molecules or fragments of molecules, rather than having to define a new set of parameters for each individual molecule.

Popular force fields for MD simulations of biomolecular systems are AMBER [15], CHARMM [16], GROMOS [17] and OPLS-AA [18]. In this work, we considered CHARMM22 with CMAP correction and CHARMM36 force fields [19,20] in order to describe proteins and lipids respectively. These force fields are compatible with the MD softwares we used, NAMD [13] and GROMACS [14]. For phosphatidylinositol-4,5-bisphosphate (PIP_2) lipids (see **2.3.5**) compatible parameters developed by Lupyan *et al.* [21] were considered.

3.1.6. Periodic boundary conditions

Consider an isolated computational cell of 1000 atoms with dimensions 10x10x10. Among these 1000 atoms, 488 will be located at the cell surfaces and interact with vacuum; the number of atoms separated from vacuum by one atomic layer will be 296; *etc.* In fact, due to surface tension effects, only few atoms will correspond to a condensed phase, in which most of the biologically relevant processes occur. Modeling of such a process, therefore, requires addressing this problem, either by increasing the computational cell's size (which will require additional computational resources), or by applying some computational tricks.

One of these tricks is to use periodic boundary conditions (PBC). In PBC, the particles are enclosed in a simulation cell, which is replicated to infinity by periodic translations. A particle, leaving the cell on one side, (B, see Figure 3.1.6.1) is replaced by its copy entering the cell on the opposite site (B_{im}, see Figure 3.1.6.1). Each particle is a subject to the potential from all other particles in the system including images in the surrounding cells, thus entirely eliminating surface effects. Because every cell is an identical copy of all the others, all the image particles move together and need only be represented once inside the MD code.

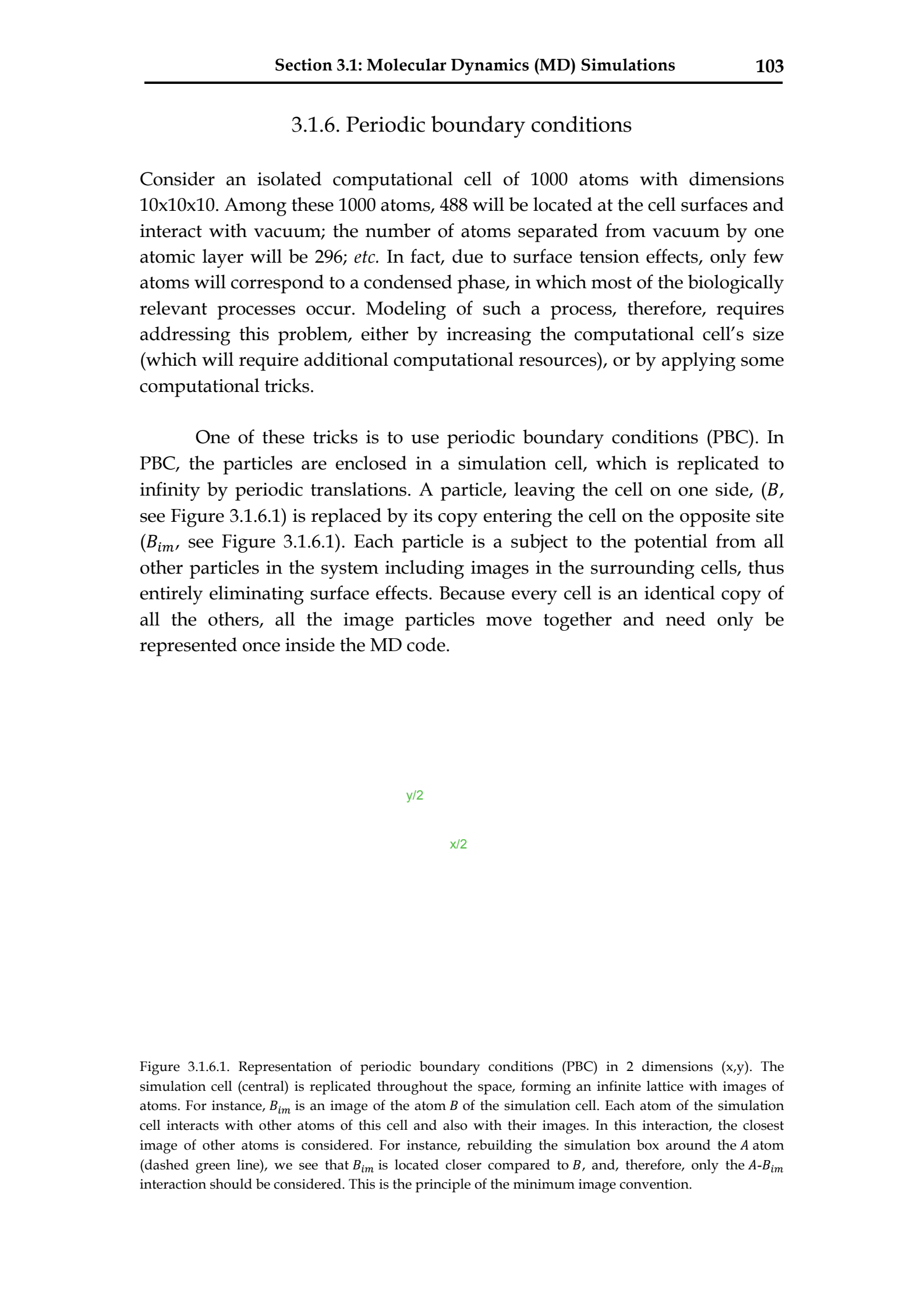

Figure 3.1.6.1. Representation of periodic boundary conditions (PBC) in 2 dimensions (x,y). The simulation cell (central) is replicated throughout the space, forming an infinite lattice with images of atoms. For instance, B_{im} is an image of the atom B of the simulation cell. Each atom of the simulation cell interacts with other atoms of this cell and also with their images. In this interaction, the closest image of other atoms is considered. For instance, rebuilding the simulation box around the A atom (dashed green line), we see that B_{im} is located closer compared to B, and, therefore, only the A-B_{im} interaction should be considered. This is the principle of the minimum image convention.

In practice, PBC is applied using the minimum image convention. In the minimum image convention, each atom interacts with just one image of every other atom in the system (the closest one). In Figure 3.1.6.1, the distance between A and B_{im} is shorter than that between A and B, and, therefore, only the A-B_{im} interaction but not the A-B one should be considered.

3.1.7. Calculation of non-bonded atomic interactions (Coulomb and vdW)

The most time-consuming part of MD simulations is the calculation of the non-bonded energy terms, *i.e.* Coulomb and van der Waals. While the number of bonded terms (bond, angle and torsional terms) is proportional to the number of atoms N, the number of non-bonded terms increases as the square of the number of atoms N^2. The most popular way to deal with the non-bonded interactions is to use a non-bonded cutoff. When a cutoff is employed, the interactions between all pairs of atoms that are further apart than the cutoff value are set to zero. Note that the use of a cutoff may not dramatically reduce the time taken to compute the number of non-bonded interactions. This is because one would have to compute $N(N-1)$ distances between N atoms. Collecting neighbor atoms in a list (first proposed by Verlet [6]), on the other hand, may significantly reduce the computational cost since, in this case, this list needs to be updated each 10 or 20 MD time steps only.

Application of a cutoff introduces a discontinuity in both the potential energy and the force near the cutoff value, which may create problems in MD simulations. There are several ways to tackle this discontinuity [4]. For instance, one may use a shifted potential, in which a constant term, equal to the value of the potential at the cutoff distance, is subtracted from the potential at all values. As the additional term is constant, it disappears when the potential is differentiated and so does not affect the force calculation in MD. An alternative way to eliminate discontinuities in the energy and force is to use a switching function. In this method, the potential energy function is multiplied by the switching function ranging from 1 at $r = 0$ to 0 at $r = r_c$, the cutoff distance. Application of the switching function smoothly brings the potential energy to 0 at the cutoff distance. Finally, one may gradually decrease the potential between two cutoff values: the potential takes its usual value until the lower cutoff distance; between the lower and upper cutoff

distances the potential is multiplied by the switching function, which ranges from 1 at the lower cutoff distance to 0 at the upper cutoff distance.

While long-range van der Waals interactions are often neglected, it is particularly important to properly model long-range Coulomb interactions decaying as $\frac{1}{r}$ because their range is usually greater than the half of the box length. One of the methods allowing to deal with the Coulomb long-range forces is the Ewald summation [22,23]. In this method, a particle interacts with all the other particles in the simulation box and also with all of their images. The charge-charge contribution to the potential energy due to all pairs of charges (located in the simulation box and also their images) can be written as:

$$U = \frac{1}{2}\sum_{|\boldsymbol{n}|=0}' \sum_{j=1}^{N}\sum_{i=1}^{N} \frac{q_i q_j}{4\pi\varepsilon_0 |\boldsymbol{r}_{ij}+\boldsymbol{n}|}. \quad (3.1.7.1)$$

Here, $\boldsymbol{n}$ is a translation vector of the unit cell: $\boldsymbol{n} = a\boldsymbol{l_x} + b\boldsymbol{l_y} + c\boldsymbol{l_z}$ with the unit cell vectors ($\boldsymbol{l_x}$, $\boldsymbol{l_y}$, $\boldsymbol{l_z}$) and the integers defining the simulation box a, b and c. The prime on the first summation indicates that the series do not include the interaction $i = j$ for $\boldsymbol{n} = 0$. The sum in the eq. (3.1.7.1) converges extremely slowly meaning that the calculation of long-range Coulomb interactions would require high computational demands. One may, however, apply a trick splitting the summation in the eq. (3.1.7.1) into two series, each of which converges more rapidly. A mathematical basis for this is the following equality:

$$\frac{1}{r} = \frac{f(r)}{r} + \frac{1-f(r)}{r}. \quad (3.1.7.2)$$

The aim is then to choose a functional form of $f(r)$, which will deal with a rapid variation of $1/r$ at small r and slow decay at large r.

In the Ewald method, each charge is surrounded by a Gaussian distribution $\rho_i(r)$ of equal magnitude but of an opposite sign:

$$\rho_i(r) = -\frac{q_i\alpha^3}{\pi^{3/2}} e^{-\alpha^2 r^2}, \quad (3.1.7.3)$$

where α is the parameters that defines the width of a Gaussian. The sum over point charges is now converted to a sum of interactions between charges plus their neutralizing Gaussian distributions. This dual sum, the "real" space summation, converges very rapidly. The rate of convergence depends on the width of a Gaussian α: the wider is the Gaussian, the faster is the convergence. A second charge distribution, which exactly cancels the first charge distribution, should be also added to the system. The summation of the second distribution is performed in the reciprocal space and converges more rapidly than the original point-charge sum. Note that in contrast to the real space summation, the summation in the reciprocal space converges more

rapidly with small α. Therefore, an appropriate width of a Gaussian should be chosen in order to provide proper balance between computational resources engaged in the real and reciprocal space summations.

Particle Mesh Ewald (PME) method [24] is a modification of a classic Ewald summation. In the PME method, the real and reciprocal sums are evaluated on a grid where charges are interpolated to the grid points. This allows much faster calculation of Coulomb energy term compared to the classic Ewald summation.

3.1.8. Thermostats

In the most straightforward MD simulations, a system is simulated in terms of a microcanonical ensemble (NVE), maintaining the number of particles, volume and energy constant. In experiments, however, instead of energy one usually monitors the temperature of the system T, and overall the system is described in terms of a canonical ensemble (NVT). In statistical mechanics, the temperature of the system T is defined via the average kinetic energy ($\overline{K}$) [5]:

$$k_B T = \frac{2\overline{K}}{s}, \tag{3.1.8.1}$$

$$\overline{K} = \frac{1}{t}\int_0^t K(t)dt, \tag{3.1.8.2}$$

where s is the number of the system's degrees of freedom. Hence, in MD simulations, in order to switch from microcanonical to canonical ensembles, the equations of motion have to be modified in such a way, which would allow maintaining of the average kinetic energy at a constant level. This can be accomplished implementing the so-called thermostat algorithms. Below, we will briefly discuss several popular thermostat algorithms implemented in MD codes: Berendsen, Langevin dynamics and Nosé-Hoover [25–27].

In the Berendsen thermostat [25], the system is coupled to an external heat bath that fixes the temperature at the desired value. The bath acts as a source of thermal energy, supplying or removing appropriate amount of heat from the system. The velocities are scaled at each step, such that the rate of change of the temperature is proportional to the difference in the temperature between the bath and the system:

$$\frac{dT(t)}{dt} = \frac{1}{\tau}(T_{bath} - T(t)), \tag{3.1.8.3}$$

where τ is a coupling parameter whose magnitude determines how tightly the bath and the system are coupled.

The Berendsen thermostat does not generate rigorous canonical averages and, therefore, is not recommended for productive MD runs. Two other thermostats that we are going to discuss, Langevin dynamics and Nosé-Hoover, are able to generate trajectories in a canonical ensemble.

In Langevin dynamics, the system is embedded into a Brownian medium, and its dynamics is described in terms of the following equations of motion:

$$m_i \frac{d\boldsymbol{v_i}}{dt} = -\frac{\partial U}{\partial \boldsymbol{r_i}} - \gamma_i \boldsymbol{v_i} + \boldsymbol{R_i}(t). \quad (3.1.8.4)$$

The friction coefficient γ_i represents viscous damping due to fictitious heat bath particles. The stochastic force $\boldsymbol{R_i}$ represents the effect of collisions with these particles, leading to diffusion. The damping and collisions are balanced in order to provide a constant temperature: the friction coefficient γ_i is related to the fluctuations of the random force $\boldsymbol{R_i}$ through the fluctuation-dissipation theorem [28]:

$$\langle \boldsymbol{R_i}(t) \rangle = 0, \quad (3.1.8.5)$$

$$\int \langle \boldsymbol{R_i}(0) \cdot \boldsymbol{R_i}(t) \rangle dt = 6 k_B T \gamma_i. \quad (3.1.8.6)$$

In the Nosé-Hoover thermostat [26,27], an additional degree of freedom s is introduced into the system's Hamiltonian. The equations of motion for this additional degree of freedom are integrated together with those for atomic coordinates and velocities. Here, s imposes an effect of an external heat reservoir. The following equations of motion are derived from the extended Hamiltonian:

$$\frac{d\boldsymbol{r_i}}{dt} = \boldsymbol{v_i}, \quad (3.1.8.7)$$

$$m_i \frac{d\boldsymbol{v_i}}{dt} = -\frac{\partial U}{\partial \boldsymbol{r_i}} - \zeta m_i \boldsymbol{v_i}, \quad (3.1.8.8)$$

$$\frac{\partial \ln(s)}{\partial t} = \zeta, \quad (3.1.8.9)$$

$$\frac{\partial \zeta}{dt} = \frac{1}{M_s} \left(\sum_{i=1}^{N} \frac{\boldsymbol{v_i^2}}{2} - g k_B T \right), \quad (3.1.8.10)$$

where, ζ is defined in terms of an additional degree of freedom s, M_s is a thermal inertia parameter, which regulates the rate of heat transfer between the system and the heat reservoir, and g is the number of the system's degrees of freedom considering s.

In this work, we used either Langevin dynamics if the simulations were performed with the NAMD software [13] (see **4.1**, **4.3**) or the Nosé-

Hoover thermostat if the simulations were performed with the GROMACS software [14] (see **4.2**).

3.1.9. Barostats

When modeling a condensed phase, it is important to monitor the system's pressure. In general, pressure is defined as an average force per slice area S, to which this force is applied:

$$p = -\frac{1}{S} \cdot \frac{1}{t} \int_0^t \boldsymbol{F}(t) dt. \quad (3.1.9.1)$$

Based on this definition and averaging pressure in all slices of the periodic system, one can obtain:

$$p = \frac{1}{3V} (2\langle K \rangle + \langle \sum_{i<j} (\boldsymbol{r_j} - \boldsymbol{r_i}) \boldsymbol{F_{ij}} \rangle), \quad (3.1.9.2)$$

where $\langle K \rangle$ is the average kinetic energy, and $\boldsymbol{F_{ij}}$ is the force of interaction between the i^{th} and j^{th} atoms.

Correcting pressure is achieved by rescaling the distance between interacting particles. This procedure is implemented in MD algorithms called barostats. In this subsection, we will briefly discuss some popular barostats: Berendsen, Andersen, Parinello-Rahman and Langevin piston [25,29–31].

Analogous to the Berendsen thermostat (see **3.1.8**), in the Berendsen barostat [25], the system is weakly coupled to an external bath using the principle of least local perturbation. An extra term is added to the equations of motion that provides a pressure change:

$$\left(\frac{dp}{dt}\right) = \frac{p_0 - p}{\tau_p}, \quad (3.1.9.3)$$

where p_0 is the pressure of the external bath, and τ_p is the time constant for coupling, according to which atomic coordinates are scaled. The resulting equations of motion read:

$$\frac{d\boldsymbol{r_i}}{dt} = \boldsymbol{v_i} - \frac{\beta(p_0 - p)}{3\tau_p} \boldsymbol{r_i}, \quad (3.1.9.4)$$

where β is the isothermal compressibility.

The Berendsen barostat does not yield MD trajectories in any known thermodynamics ensemble. Other barostats that we will discuss, Andersen, Parinello-Rahman and Langevin piston, are able to model the system's dynamics in terms of known thermodynamics ensembles.

In the Andersen barostat [29], the system's coordinates $\boldsymbol{r_i}$ are replaced by scaled coordinates ρ_i, and an extended Lagrangian of the system with a new variable Q is considered:

$$\rho_i = \frac{r_i}{V^{1/3}}, \tag{3.1.9.5}$$

$$L(\rho, \dot{\rho}, Q, \dot{Q}) = \frac{1}{2} Q^{2/3} \sum_{i=1}^{N} m_i \dot{\rho}_i^2 - \sum_{i<j=1}^{N} U(Q^{1/3} \rho_{ij}) + \frac{1}{2} M \dot{Q} - p_0 Q. \tag{3.1.9.6}$$

Then the equations of the motion with the Q variable may be defined as:

$$\frac{d\boldsymbol{r_i}}{dt} = \boldsymbol{v_i} + \frac{1}{3} \boldsymbol{r_i} \frac{d\ln(V)}{dt}, \tag{3.1.9.7}$$

$$m_i \frac{d\boldsymbol{v_i}}{dt} = -\frac{\partial U}{\partial \boldsymbol{r_i}} - \frac{1}{3} m_i \boldsymbol{v_i} \frac{d\ln(V)}{dt}, \tag{3.1.9.8}$$

$$\frac{M d^2 V}{dt^2} = -p_0 + \frac{\left(\frac{2}{3} \sum_{i=1}^{N} \frac{v_i^2}{2} - \frac{1}{3} \sum_{i<j=1}^{N} \frac{\partial U(r_{ij})}{\partial \boldsymbol{r_{ij}}} \cdot \boldsymbol{r_{ij}} \right)}{V} = p(t) - p_0. \tag{3.1.9.9}$$

If one interprets Q as the system's volume V, then the first two terms of the extended Lagrangian represent the Lagrangian of the unscaled system; the third and fourth terms are the kinetic and potential energies associated with Q. Here, p_0 and M are parameters that have to be chosen carefully. A physical interpretation of this algorithm is the following: assume that the system is simulated in a container and can be compressed by a piston. Therefore, Q is the coordinate of the piston (the system's volume V), $p_0 Q$ is the potential derived from acting on the piston with pressure p_0, and M is the mass of the piston. The Andersen barostat yields trajectories in an isobaric-isoenthalpic ensemble (NPH).

Parinello and Rahman [30] extended the algorithm proposed by Andersen, allowing the system to change its shape. Their barostat provides, therefore, anisotropic coupling that is critical for the systems with a lipid bilayer.

In the Langevin piston [31], the system is described in terms of Langevin dynamics (see **3.1.7**). The piston degree of freedom is represented as damping, resulting in:

$$\frac{d\boldsymbol{r_i}}{dt} = \boldsymbol{v_i} + \frac{1}{3V} \frac{dV}{dt} \boldsymbol{r_i}, \tag{3.1.9.10}$$

$$m_i \frac{d\boldsymbol{v_i}}{dt} = -\frac{\partial U}{\partial \boldsymbol{r_i}} - \frac{1}{3V} \frac{dV}{dt} m_i \boldsymbol{v_i}, \tag{3.1.9.11}$$

$$\frac{d^2 V}{dt^2} = \frac{1}{M} [p(t) - p_0] - \gamma \frac{dV}{dt} + R(t). \tag{3.1.9.12}$$

The coupling of the piston degree of freedom to a heat bath by means of the Langevin dynamics results in equations of motion, which formally produce trajectories in the isothermal-isobaric ensemble (NPT).

In this work, we used either Langevin piston if the simulations were performed with the NAMD software [13] (see **4.1**, **4.3**) or the Parinello-Rahman barostat if the simulations were performed with the GROMACS software [14] (see **4.2**).

3.2. Estimation of the free energy

Exploring the configuration space of the system such that its high free energy states are adequately sampled is central to the accurate determination of the free energy differences between the states of this system. This adequate exploration, however, may be difficult to achieve due to high free energy barriers separating regions of the configuration space and/or slow diffusion. In order to overcome high free energy barriers and/or slow diffusion, several techniques enhancing sampling of the configuration space have been suggested. Some of these techniques increase the probabilities of high free energy states by adding a bias to the equations of motion of the system, which changes its dynamics acting on the selected degrees of freedom (collective variables, CVs) [32–36].

In this work, in order to enhance sampling of the configuration space and estimate the free energy of the Kv1.2 activation/deactivation processes in POPC and POPC/PIP_2 (see **4.2**), we used metadynamics [32,33].

3.2.1. Free energy

The free energy is usually expressed as the Helmholtz function A or the Gibbs function G. One should consider the Helmholtz free energy for the system with constant number of particles, temperature and volume (canonical ensemble, constant NVT), whereas the Gibbs free energy should be considered for constant number of particles, temperature and pressure (isobaric-isothermal ensemble, constant NPT).

In the canonical ensemble, the Helmholtz free energy A of the system can be defined in terms of the canonical partition function $Q(N,V,T)$ [37]:

$$A = -\frac{1}{\beta}\ln\ Q(N,V,T), \qquad (3.2.1.1)$$

$$Q(N,V,T) = \frac{1}{h^{3N}N!}\int\int e^{-\beta\mathcal{H}(\boldsymbol{r},\boldsymbol{p})}d\boldsymbol{r}d\boldsymbol{p}, \quad (3.2.1.2)$$

where h is the Planck constant, $\beta = \frac{1}{k_B T}$, k_B is the Boltzmann constant, T is the temperature, and $\mathcal{H}(\boldsymbol{r},\boldsymbol{p})$ is the Hamiltonian describing the system with spatial coordinates $\boldsymbol{r}$ and momenta $\boldsymbol{p}$. In the eq. (3.2.1.2), the $N!$ term excludes the configurations, which differ only by particle transposition, and the $\frac{1}{h^{3N}}$ term is necessary to retrieve the correct correspondence with the high-temperature quantum-mechanical prediction. The canonical partition function Q, given by the eq. (3.2.1.2), may be viewed as a measure of the thermodynamic states accessible to the system in terms of spatial coordinates $\boldsymbol{r}$ and momenta $\boldsymbol{p}$.

The equation (3.2.1.1) connects thermodynamics and statistical mechanics in the canonical ensemble. From this equation it follows that calculating A is equivalent to estimating Q. Most often however, in both experiments and calculations, we are not interested in the free energy absolute value A but in the free energy differences ΔA between the states of the system:

$$\Delta A = \frac{1}{\beta}\ln\frac{Q_1}{Q_0}. \quad (3.2.1.3)$$

There are several approaches aimed at calculating ΔA [37]. One of them (which is also used in the metadynamics method) relies on estimating of the appropriate probability density function P. Consider the two states of the system, 0 and 1, which can be transformed through the continuous change of some parameter λ. This parameter is defined in such a way that λ_0 and λ_1 correspond to the system's states 0 and 1 respectively. Then the probability density function P can be expressed as:

$$P_X = P(\lambda_X) = \frac{\int e^{-\beta\mathcal{H}}\delta(\lambda-\lambda_X)d\boldsymbol{r}d\boldsymbol{p}}{\mathcal{N}} = \frac{Q_X}{\mathcal{N}}, \quad (3.2.1.4)$$

where δ is the Dirac delta function, $\mathcal{N}$ is the normalization constant, and X substitutes for 0 or 1. Combining the eq. (3.2.1.3) and (3.2.1.4) leads to:

$$\Delta A = -\frac{1}{\beta}\ln\frac{P_1}{P_0}. \quad (3.2.1.5)$$

The equation (3.2.1.5) provides a description for calculating ΔA: the probability distribution function $P(\lambda)$ for the range of λ comprised between λ_0 and λ_1 is obtained from computer simulations, usually as a histogram; then, the ratio $\frac{P_1}{P_0}$ is estimated.

3.2.2. Collective variables (CVs)

Before proceeding with the metadynamics method, we would like to briefly discuss the properties of collective variables. A collective variable (CV) is a function of the microscopic coordinates of the system. Depending on the nature of the process, one should choose a CV that would clearly reflect the transition of the system's initial to final states, considering all the relevant intermediates. CVs may be simple such as an interatomic distance, angle and dihedral or rather complex as path CVs [38]. Most importantly that they share two important properties [39]:

- they should include all the slow modes of the system: if any of the latter is not added to the CVs list then the free energy surface may not converge in a reasonable time;
- they should be limited in number: the use of many CVs implies that a high-dimensional space has to be explored.

Selecting an appropriate set of CVs is not straightforward and requires a good knowledge of the system of investigation. For the CV used in this work, see **4.2**.

3.2.3. The classic metadynamics

In the classic method of metadynamics (further metadynamics) [32,33], an external history-dependent bias potential, being a function of the selected CVs, is added to the Hamiltonian of the system. This potential pushes the system away from its local free energy minima allowing better exploration of the configuration space.

The metadynamics bias potential V at a given set of collective variables $S(R) = S_1(R), \dots, S_d(R)$, where R is the system microscopic coordinate, and time t can be written as:

$$V_G(S,t) = \int_0^t dt' \omega \, exp\left(-\sum_{i=1}^{d} \frac{(S_i(R) - S_i(R(t')))^2}{2\sigma_i^2}\right). \qquad (3.2.3.1)$$

Here, ω is an energy rate, and σ_i is the width of the Gaussian for the i^{th} CV. The energy rate is constant and is expressed in terms of a Gaussian height W and a deposition stride τ_G:

$$\omega = \frac{W}{\tau_G}. \qquad (3.2.3.2)$$

Knowing the added bias, the free energy of the system in the CVs space can be easily reconstructed as:

$$F(S) = -V_G(S, t \to \infty) + C, \quad (3.2.3.3)$$

where C is an irrelevant additive constant.

The error ε in a metadynamics run is a measure of how different the estimated and real free energy profiles are. This error was shown to be dependent on the system's size S_{range}, the width of the Gaussian σ, the energy rate ω and the intrinsic system diffusion coefficient in the CV space D [33]:

$$\varepsilon = C(d)\sqrt{\frac{S_{range}\sigma\omega}{D\beta}}, \quad (3.2.3.4)$$

where $C(d)$ is a constant depending on the dimensionality, namely, 0.5 for $d = 1$ and 0.3 for $d = 2$. The equation (3.2.3.4) is empirical. Similar dependence, however, was later derived theoretically [40].

The equation (3.2.3.4) requires knowing the diffusion coefficient in the CV space, whose calculation is often complicated due to the fact that the observed dynamics of the system is determined by a combination of both a systematic force coming from a free energy and the system's diffusion. So far, we did not estimate the diffusion coefficient in the CV space (this calculations are ongoing, see **5.1**), and therefore we had to use another method to estimate the error in the metadynamics run. In particular, we have estimated this error from fluctuation of the free energy profiles plotted along the metadynamics run. After extensive sampling of the configuration space (around 2.7 μs), these profiles started to oscillate around an average. We considered these corresponding oscillations as the error of the metadynamics run.

3.2.4. Well-tempered metadynamics

One of the major drawbacks of metadynamics is that the bias does not converge to the free energy but oscillates around it, raising a problem at which point the calculations should be terminated. A solution for this is provided by well-tempered metadynamics [41]. In well-tempered metadynamics, current Gaussian height decreases exponentially with the bias already deposited at this value of a set of CVs (S):

$$W(S, t) = \omega_{init}\tau_G e^{-\frac{V_G(S,t)}{k_B\Delta T}}. \quad (3.2.4.1)$$

Here, ω_{init} is the initial bias deposition rate and ΔT is an input parameter in temperature units. This formula is achieved by considering a different expression for a bias:

$$V = k_B \Delta T \ln\left(1 + \frac{\omega N(S,t)}{k_B \Delta T}\right), \quad (3.2.4.2)$$

where $N(S,t)$ is the histogram of the S variables collected during the simulations. Since $N(S,t)$ grows linearly with simulations time, the $W(S,t)$ tends to zero as $1/t$. This is fast enough for bias converging and, at the same time, slow enough not to depend on the system's initial conditions [41].

Well-tempered metadynamics is an efficient way to compute the free energy surface: first, by tuning ΔT one can increase barrier crossing and facilitate the exploration in the CVs space; and second, since a finite value of ΔT is used, the free energy region to be explored is limited to an energy range of the order $T + \Delta T$, avoiding an exploration of physically non-relevant regions [41].

In the well-tempered metadynamics method, a bias does not fully compensate the free energy surface but converges to:

$$V_G(S, t \to \infty) = -\frac{\Delta T}{T + \Delta T} F(S) + C. \quad (3.2.4.3)$$

Considering that the probability distribution $P(S,t)$ for the CVs space is:

$$P(S,t) \propto e^{\left(\frac{-F(S)-V(S,t)}{T}\right)}, \quad (3.2.4.4)$$

its reconstruction is straightforward [41]:

$$P(S) \propto e^{-\frac{F(S)}{k_B(T+\Delta T)}}. \quad (3.2.4.5)$$

3.2.5. Probability distribution for unbiased CVs

For unbiased degrees of freedom the probability distribution is distorted in a non-trivial way. One of the techniques tackling this problem, the Bonomi scheme [42], utilizes the following reweighting algorithm. If the system can be considered to be in instantaneous equilibrium under the action of the internal potential $U(R)$ and the bias $V(S(R),t)$, the biased probability at time t is:

$$P(R,t) = \frac{e^{-\beta(U(R)+V(S(R),t))}}{\int dR' e^{-\beta(U(R')+V(S(R'),t))}}. \quad (3.2.5.1)$$

This expression can be re-written in the following form, taking into account the Boltzmann distribution $P_0(R) = e^{-\beta U(R)/Z}$:

$$P(R,t) = e^{-\beta\left(V(S(R),t)+c(t)\right)} \cdot P_0(R), \quad (3.2.5.2)$$

$$c(t) = -\frac{1}{\beta}\log\left(\frac{\int e^{-\beta F(S)}dS}{\int e^{-\beta(F(S)+V(S,t))}dS}\right). \quad (3.2.5.3)$$

The evolution of the biased probability during the metadynamics simulations can be computed according to:

$$P(R,t+\Delta t) = e^{-\beta(\dot{V}(S(R),t)-<\dot{V}(S,t)>)\Delta t} \cdot P(R,t), \quad (3.2.5.4)$$

where the average in the exponent is calculated in the biased ensemble. Hence, knowing the biased probability at each step of the metadynamics simulations, one is able to recover the Boltzmann distribution from the eq. (3.2.5.2) and, therefore, to re-estimate the free energy as a function of a non-biased collective variable.

In practice, at each step the histogram $N(S,f)$ for the biased $S(R)$ and unbiased $f(R)$ degrees of freedom is estimated. Its evolution with time follows the eq. (3.2.5.4). The unbiased distribution of $f(R)$ is further calculated as:

$$P(f) = \frac{\sum_S(e^{+\beta V(S,t)}N_t(S,f))}{\sum_{S,f}(e^{+\beta V(S,t)}N_t(S,f))}. \quad (3.2.5.5)$$

In our work, since the sampling of the configuration space associated with the Kv1.2 voltage sensor's transitions was performed in terms of CV_{Ri}, we had to use the Bonomi scheme when re-estimating the corresponding free energies in terms of the gating charge (see **4.2.5**).

3.3. Homology modeling

Along with other computational methods as fold recognition and *ab initio*, homology modeling is a powerful tool for peptide and protein structure prediction. This method relies on the fact that proteins with evolutionary related sequences share a three-dimensional architecture [43]. Several successful examples, when a predicted structure was further approved experimentally [44–48], advocate in favor of homology modeling.

While experimental methods of structure determination as X-ray, NMR or electron microscopy are rather time and resource consuming, homology modeling might be a good additional approach enlarging the database of peptide and protein structures. Moreover, using homology modeling, one is able to characterize an entire family of proteins including thousands of members, if at least one structure of this family is resolved experimentally. What does this give in numbers? Currently, there are about 70 million protein sequences in Swiss-Prot[1] and TrEMBL[2], but the number of distinct protein families is estimated to be 13,000 [49]. Hence, in order to build the atomistic models of all the proteins of Swiss-Prot and TrEMBL, it is sufficient to resolve a structure of at least one representative per family, which reduces the experimental work around 5000 times.

A representative with the known structure is called a template. Identification of an appropriate template is one of a critical step in homology modeling. Several softwares were proposed in order to select a "good" template for a modeled protein (for instance, BLAST, PSI-PLAST [50], FASTA [51], *etc.*). These softwares allow identification of a template sharing maximum sequence similarity with a model. Once a template is selected, prediction of the structure of a modeled protein is feasible using homology modeling softwares (for instance, MODELLER [52], ROSETTA [53], *etc.*).

[1] http://web.expasy.org/docs/relnotes/relstat.html
[2] http://www.ebi.ac.uk/uniprot/TrEMBLstats

We should emphasize that the homology modeling is generally much less accurate than experimental methods. However, it can be helpful in proposing and testing hypothesis in molecular biology such as predictions of ligand binding sites, substrate specificities, function annotation, protein interaction pathways and drug design [54–60]. Homology modeling can also provide starting model for solving structures from X-ray, NMR and electron microscopy [61,62].

3.3.1. Identification of the homologues with known structures

The very first step of homology modeling is the identification of homologues with known structures by comparing the query sequence with all the sequences of structures from the PDB (protein data bank). This can be achieved with the dynamic programming method [63] and its derivatives [64,65]: these methods assign scores to insertions, deletions and replacements of amino acids and compute an alignment of two sequences that corresponds to the least costly set of such substitutions; the cost of such an alignment is usually a measure of similarity. One of the most popular softwares employing the programming method is BLAST [50]. BLAST searches protein sequence databases for optimal *local* alignments to the query. Briefly, this software breaks the query and database sequences into fragments and seeks matches between fragments. The matched fragments are then extended in either direction in an attempt to generate an alignment with a score exceeding a particular threshold. BLAST functions very well for alignment of sequences with high similarities. But when the sequence identity is below 30 %, BLAST is not reliable. A number of alternative strategies have been developed. These include template consensus sequences and profile analysis [66–69]. These approaches, based on either multiple sequence or structure alignments, are more sensitive because the consensus sequences are more representative of the sequence family and the profile reflects the conserved structural or functional preferences.

One of the most popular softwares implementing the position-specific profile search method is PSI-BLAST [50]. PSI-BLAST starts from performing a pairwise search of the database. Then the significant alignments are used by the software to construct a position-specific score matrix (PSSM). This matrix replaces the query sequence in the next round of database searching. The procedure may be iterated until no new significant alignments are found.

Once multiple homologues from the PDB have been identified, the next step is to select one or several templates that are most appropriate for building a model. In order to do so, one should consider sequence similarity between the query and the template as the primary criterion.

Usually the current alignment software seeks an alignment of global optimally with an empirical scoring function, which may misalign functionally important residues in the query and the templates. Therefore, one may have to improve the alignment by manual inspection. This is often required when the homology is well below 30 %. When correcting the alignment manually, one has to consider at least two important criteria: residues with important functions, either for protein activity of structural stability, should be aligned with residues of similar functions in the template, and insertions or deletions in the secondary structure should be pushed to the loop regions.

Within the slope of the slope of the present thesis, for instance, when building the homology structure of Kv7.1 (see **4.3**), we may consider two voltage-gated potassium channels with known structures (the activated/open state): Kv1.2 (PDB code 3LUT [70]) and the Kv1.2/Kv2.1 paddle chimera (PDB code 2R9R [71]). The percentage of homology between Kv1.2 and each of these channels is very similar. However, since for Kv1.2 we also have a model of the resting/closed state [72], we decided to be consistent and chose this channel as a template for Kv7.1. The alignment between Kv1.2 and Kv7.1 was performed with PSI-BLAST [50] and corrected manually according to [73]. For the final alignment, see Figure 2.2.6.2.

3.3.2. Accuracy of the homology modeling from similarity between a template and a model

Based on the sequence alignment between the template protein and the modeled one, the sequence of the latter can be divided in i) template-based regions where the template and the model are aligned, and ii) structurally variable regions (usually loops) where the template and the model diverge. The ratio of the template-based regions in the sequence defines the percentage of similarity between the template and the model. Depending on this percentage, the accuracy of the obtained model varies from low-resolution X-ray structures to structures with less than 50% atoms with an RMSD error of 3.5 Å (while the rest of the residues are modeled with larger errors).

From the previous studies experience, one is able to estimate the accuracy of the model from the percentage of its similarity with the template. Moreover, this estimation might also give an idea for which biological problems one can use this model. When the similarity is high (>40%), 90% of backbone atoms can be modeled within an RMSD error of 1 Å [60]. This accuracy is high enough to use this model for crystallographic structures refinement. When the sequence similarity is lower (about 30-40%), 80% of backbone atoms can be predicted to RMSD of 3.5 Å. The rest of residues are modeled with larger errors, especially in the insertion and deletion regions [74–77]. These models might be used for prediction of a binding site [78], the size of the ligand based on the volume of the binding site cleft [79] and also for construction of site-directed mutants with altered or destroyed binding capacity. If the similarity between sequences is very low (<30%), less than 50% of backbone atoms are predicted within an RMSD error of 3.5 Å. Even though, these models have the correct fold and, therefore, might be used to predict approximate biochemical function of the protein [52].

3.3.3. Building a model

In this subsection, we will briefly discuss how a homology model may be built using the MODELLER software [52] that we have considered in **4.3**. MODELLER relates to the class of homology modeling programs, which build a model by satisfaction of spatial restraints. These programs usually begin with generation of many distance and dihedral restraints on the structure of the target sequence using its alignment to the template as a guide. The form of these restraints was obtained from a statistical analysis of the relationships between similar protein structures: a database of 105 family alignments, including 416 proteins with known 3d structures, [80] was considered; by scanning this database, tables quantifying various correlations were obtained. These relationships are expressed in terms of conditional probability density functions (pdf's) and can be used directly as spatial restraints. Note that the form of spatial restraints was obtained from a database of protein structure alignments, *i.e.* empirically. If the percentage of homology between the model and the template is low, one should include additional restraints based on the available experimental data (NMR, cross-linking, fluorescence spectroscopy, image reconstitution in electron microscopy and site-directed mutagenesis).

Then, the spatial restraints and the CHARMM 22 force field terms [16] enforcing proper stereochemistry are combined into an objective function. The general form of this function is similar to the potential energy function of MD programs (see **3.1.5**). The final model is obtained by optimizing the objective function in Cartesian space. The optimization is carried out by the use of the variable target function method, employing methods of conjugate gradients and MD with simulated annealing [81,82].

For modeling of structurally variable regions, MODELLER [52] employs the *de novo* approach, which generates conformations using MD simulations, simulated annealing, exhaustive enumeration or heuristic sampling of a discrete set of (φ, ψ) angles, random tweak or analytical method. In contrast, other softwares (for instance, ROSETTA [53]) use the knowledge-based or combined approach, in which loops are modeled according to the information from the experimental database of protein structures. Application of the latter is limited due to relatively small number of known protein structures. For instance, we were not able to find known homologues for the S2-S3 loop conserved among the members of the Kv7 subfamily only (this was the criteria, why we have considered MODELLER in our work).

When building the Kv7.1 models, the pore domain and the major part of the voltage sensor domain were built close to the Kv1.2 templates. For the S2-S3 loop, which is conserved among the Kv7 family members but is drastically shortened in Kv1.2, additional restraints based on the available experimental data were applied: in particular, the conformation of this loops was imposed to be α-helical according to the recent NMR experiments [83].

3.3.4. Model assessment

MODELLER suggests several scoring functions allowing one to rank the final population of conformations. In our work, we have considered one of these functions, namely, Discrete Optimized Protein Energy (DOPE) [84]. DOPE is an atomic distance-distance statistical potential calculated from a sample of native protein structures. This scoring function is based entirely on the probability theory. Briefly, a statistical potential is defined as the negative logarithm of the joint pdf of the atomic Cartesian coordinates. The joint pdf is expressed as a product of pair pdfs. Next, the pair pdf is derived from a distance pdf, extracted from a single sample native structure and a reasonable

definition of the reference state. Finally, the pair pdfs are combined from a sample of many native structures of varying size to obtain the joint pdf.

After selecting several conformations corresponding to the best scoring function's values, one may verify these conformation using the PROCHECK program [85]. PROCHECK checks for proper protein stereochemistry: symmetry checks, geometry checks (*e.g.* chirality, bond lengths, bond angles and torsion angles) and structural packing quality.

For each Kv7.1 state, activated/open and resting/closed, we have prepared 50 homology models. Among them, five conformations were selected based on the best values of their DOPE scoring function. The latters were analyzed using the PROCHECK program. The final structures were selected based on the highest number of residues in the core regions of the Ramachandran plot and the lowest number of residues in the disallowed regions of the Ramachandran plot.

REFERENCES

[1] I. Mayer, Simple Theorems, Proofs, and Derivations in Quantum Chemistry, Springer, New York, NY, USA, 2003.

[2] D.S.D. Larsson, L. Liljas, D. van der Spoel, Virus Capsid Dissolution Studied by Microsecond Molecular Dynamics Simulations, PLoS Comput Biol, 8 (2012) e1002502.

[3] D.E. Shaw, R.O. Dror, J.K. Salmon, J.P. Grossman, K.M. Mackenzie, J.A. Bank, C. Young, M.M. Deneroff, B. Batson, K.J. Bowers, E. Chow, M.P. Eastwood, D.J. Ierardi, J.L. Klepeis, J.S. Kuskin, R.H. Larson, K. Lindorff-Larsen, P. Maragakis, M.A. Moraes, S. Piana, et al., Millisecond-scale Molecular Dynamics Simulations on Anton, in: Proceedings of the Conference on High Performance Computing Network, Storage and Analysis, ACM, New York, NY, USA, 2009: pp. 39:1–39:11.

[4] A. Leach, Molecular Modelling: Principles and Applications, 2nd ed., Prentice Hall, Harlow, England, 2001.

[5] D. Chandler, Introduction to Modern Statistical Mechanics, OUP USA, New York, NY, USA, 1987.

[6] L. Verlet, Computer "Experiments" on Classical Fluids. I. Thermodynamical Properties of Lennard-Jones Molecules, Phys. Rev., 159 (1967) 98–103.

[7] R. Hockney, Potential calculation and some applications, Methods in Computational Physics, Academic Press, New York, NY, USA, 1970.

[8] W.C. Swope, H.C. Andersen, P.H. Berens, K.R. Wilson, A computer simulation method for the calculation of equilibrium constants for the formation of physical clusters of molecules: Application to small water clusters, J. Chem. Phys., 76 (1982) 637–649.

[9] J.-P. Ryckaert, G. Ciccotti, H.J.C. Berendsen, Numerical integration of the cartesian equations of motion of a system with constraints: molecular dynamics of n-alkanes, J. Comput. Phys., 23 (1977) 327–341.

[10] H.C. Andersen, Rattle: A "velocity" version of the SHAKE algorithm for molecular dynamics calculations, J. Comput. Phys., 52 (1983) 24–34.

[11] B. Hess, H. Bekker, H.J.C. Berendsen, J.G.E.M. Fraaije, LINCS: A linear constraint solver for molecular simulations, J. Comput. Chem., 18 (1997) 1463–1472.

[12] S. Miyamoto, P.A. Kollman, SETTLE: An analytical version of the SHAKE and RATTLE algorithm for rigid water models, J. Comput. Chem., 13 (1992) 952–962.

[13] J.C. Phillips, R. Braun, W. Wang, J. Gumbart, E. Tajkhorshid, E. Villa, C. Chipot, R.D. Skeel, L. Kalé, K. Schulten, Scalable molecular dynamics with NAMD, J. Comput. Chem., 26 (2005) 1781–1802.

[14] B. Hess, C. Kutzner, D. van der Spoel, E. Lindahl, GROMACS 4: Algorithms for Highly Efficient, Load-Balanced, and Scalable Molecular Simulation, J. Chem. Theory Comput., 4 (2008) 435–447.

[15] W.D. Cornell, P. Cieplak, C.I. Bayly, I.R. Gould, K.M. Merz, D.M. Ferguson, D.C. Spellmeyer, T. Fox, J.W. Caldwell, P.A. Kollman, A Second Generation Force Field for the Simulation of Proteins, Nucleic Acids, and Organic Molecules, J. Am. Chem. Soc., 117 (1995) 5179–5197.

[16] A. D. MacKerell, D. Bashford, Bellott, R. L. Dunbrack, J.D. Evanseck, M.J. Field, S. Fischer, J. Gao, H. Guo, S. Ha, D. Joseph-McCarthy, L. Kuchnir, K. Kuczera, F.T.K. Lau, C. Mattos, S. Michnick, T. Ngo, D.T. Nguyen, B. Prodhom, W.E. Reiher, et al., All-Atom

Empirical Potential for Molecular Modeling and Dynamics Studies of Proteins, J. Phys. Chem. B, 102 (1998) 3586–3616.

[17] C. Oostenbrink, A. Villa, A.E. Mark, W.F. Van Gunsteren, A biomolecular force field based on the free enthalpy of hydration and solvation: The GROMOS force-field parameter sets 53A5 and 53A6, J. Comput. Chem., 25 (2004) 1656–1676.

[18] W.L. Jorgensen, D.S. Maxwell, J. Tirado-Rives, Development and Testing of the OPLS All-Atom Force Field on Conformational Energetics and Properties of Organic Liquids, J. Am. Chem. Soc., 118 (1996) 11225–11236.

[19] A.D. Mackerell Jr, M. Feig, C.L. Brooks 3rd, Extending the treatment of backbone energetics in protein force fields: limitations of gas-phase quantum mechanics in reproducing protein conformational distributions in molecular dynamics simulations, J. Comput. Chem., 25 (2004) 1400–1415.

[20] J.B. Klauda, R.M. Venable, J.A. Freites, J.W. O'Connor, D.J. Tobias, C. Mondragon-Ramirez, I. Vorobyov, A.D. MacKerell, R.W. Pastor, Update of the CHARMM all-atom additive force field for lipids: Validation on six lipid types, J. Phys. Chem. B, 114 (2010) 7830–7843.

[21] D. Lupyan, M. Mezei, D.E. Logothetis, R. Osman, A molecular dynamics investigation of lipid bilayer perturbation by PIP2, Biophys. J., 98 (2010) 240–247.

[22] P.P. Ewald, Die Berechnung optischer und elektrostatischer Gitterpotentiale, Ann. Phys., 369 (1921) 253–287.

[23] A.Y. Toukmaji, J.A. Board Jr., Ewald summation techniques in perspective: a survey, Comput. Phys. Commun., 95 (1996) 73–92.

[24] T. Darden, D. York, L. Pedersen, Particle mesh Ewald: An N·log(N) method for Ewald sums in large systems, J. Chem. Phys., 98 (1993) 10089–10092.

[25] H.J.C. Berendsen, J.P.M. Postma, W.F. van Gunsteren, A. DiNola, J.R. Haak, Molecular dynamics with coupling to an external bath, J. Chem. Phys., 81 (1984) 3684–3690.

[26] S. Nosé, A unified formulation of the constant temperature molecular dynamics methods, J. Chem. Phys., 81 (1984) 511–519.

[27] W.G. Hoover, Canonical dynamics: Equilibrium phase-space distributions, Phys. Rev. A, 31 (1985) 1695–1697.

[28] R. Kubo, Many-body theory: The First Tokyo Summer Institute of Theoretical Physics (lectures), Syokabo, Tokyo, Japan, 1966.

[29] H.C. Andersen, Molecular dynamics simulations at constant pressure and/or temperature, J. Chem. Phys., 72 (1980) 2384.

[30] M. Parrinello, A. Rahman, Polymorphic transitions in single crystals: A new molecular dynamics method, J. Appl. Phys., 52 (1981) 7182–7190.

[31] S.E. Feller, Y. Zhang, R.W. Pastor, B.R. Brooks, Constant pressure molecular dynamics simulation: The Langevin piston method, J. Chem. Phys., 103 (1995) 4613–4621.

[32] A. Laio, M. Parrinello, Escaping free-energy minima, Proc. Natl. Acad. Sci., 99 (2002) 12562–12566.

[33] A. Laio, A. Rodriguez-Fortea, F.L. Gervasio, M. Ceccarelli, M. Parrinello, Assessing the Accuracy of Metadynamics, J. Phys. Chem. B, 109 (2005) 6714–6721.

[34] E. Darve, A. Pohorille, Calculating free energies using average force, J. Chem. Phys., 115 (2001) 9169–9183.

[35] G.M. Torrie, J.P. Valleau, Nonphysical sampling distributions in Monte Carlo free-energy estimation: Umbrella sampling, J. Comput. Phys., 23 (1977) 187–199.

[36] S. Park, K. Schulten, Calculating potentials of mean force from steered molecular dynamics simulations, J. Chem. Phys., 120 (2004) 5946–5961.

[37] C. Chipot, A. Pohorille, Free Energy Calculations: Theory and Applications in Chemistry and Biology, Springer Science & Business Media, 2007.

[38] D. Branduardi, F.L. Gervasio, M. Parrinello, From A to B in free energy space, J. Chem. Phys., 126 (2007) 054103.

[39] A. Barducci, M. Bonomi, M. Parrinello, Metadynamics, Wiley Interdiscip. Rev. Comput. Mol. Sci., 1 (2011) 826–843.

[40] G. Bussi, A. Laio, M. Parrinello, Equilibrium Free Energies from Nonequilibrium Metadynamics, Phys. Rev. Lett., 96 (2006) 090601.

[41] A. Barducci, G. Bussi, M. Parrinello, Well-Tempered Metadynamics: A Smoothly Converging and Tunable Free-Energy Method, Phys. Rev. Lett., 100 (2008) 020603.

[42] M. Bonomi, A. Barducci, M. Parrinello, Reconstructing the equilibrium Boltzmann distribution from well-tempered metadynamics, J. Comput. Chem., 30 (2009) 1615–1621.

[43] Y. Xu, D. Xu, J. Liang, Computational Methods for Protein Structure Prediction and Modeling: Structure Prediction, 1st ed., Springer, 2010.

[44] W.J. Browne, A.C. North, D.C. Phillips, K. Brew, T.C. Vanaman, R.L. Hill, A possible three-dimensional structure of bovine alpha-lactalbumin based on that of hen's egg-white lysozyme, J. Mol. Biol., 42 (1969) 65–86.

[45] K.R. Acharya, D.I. Stuart, N.P. Walker, M. Lewis, D.C. Phillips, Refined structure of baboon alpha-lactalbumin at 1.7 Å resolution. Comparison with C-type lysozyme, J. Mol. Biol., 208 (1989) 99–127.

[46] C.A. Marhefka, B.M. Moore 2nd, T.C. Bishop, L. Kirkovsky, A. Mukherjee, J.T. Dalton, D.D. Miller, Homology modeling using multiple molecular dynamics simulations and docking studies of the human androgen receptor ligand binding domain bound to testosterone and nonsteroidal ligands, J. Med. Chem., 44 (2001) 1729–1740.

[47] D.-F. Wang, P. Helquist, N.L. Wiech, O. Wiest, Toward selective histone deacetylase inhibitor design: homology modeling, docking studies, and molecular dynamics simulations of human class I histone deacetylases, J. Med. Chem., 48 (2005) 6936–6947.

[48] L. Miguet, Z. Zhang, M. Barbier, M.G. Grigorov, Comparison of a homology model and the crystallographic structure of human 11beta-hydroxysteroid dehydrogenase type 1 (11betaHSD1) in a structure-based identification of inhibitors, J. Comput. Aided Mol. Des., 20 (2006) 67–81.

[49] M. Punta, P.C. Coggill, R.Y. Eberhardt, J. Mistry, J. Tate, C. Boursnell, N. Pang, K. Forslund, G. Ceric, J. Clements, A. Heger, L. Holm, E.L.L. Sonnhammer, S.R. Eddy, A. Bateman, R.D. Finn, The Pfam protein families database, Nucleic Acids Res., 40 (2012) D290–D301.

[50] S.F. Altschul, W. Gish, W. Miller, E.W. Myers, D.J. Lipman, Basic local alignment search tool, J. Mol. Biol., 215 (1990) 403–410.

[51] W.R. Pearson, D.J. Lipman, Improved tools for biological sequence comparison, Proc. Natl. Acad. Sci. U. S. A., 85 (1988) 2444–2448.

[52] N. Eswar, B. Webb, M.A. Marti-Renom, M.S. Madhusudhan, D. Eramian, M.-Y. Shen, U. Pieper, A. Sali, Comparative protein structure modeling using MODELLER, Curr. Protoc. Protein Sci., Chapter 2 (2007) Unit 2.9.

[53] C.A. Rohl, C.E.M. Strauss, D. Chivian, D. Baker, Modeling structurally variable regions in homologous proteins with ROSETTA, Proteins, 55 (2004) 656–677.

[54] Y. Zhou, M.E. Johnson, Comparative molecular modeling analysis of-5-amidinoindole and benzamidine binding to thrombin and trypsin: specific H-bond formation contributes to high 5-amidinoindole potency and selectivity for thrombin and factor Xa, J. Mol. Recognit. JMR, 12 (1999) 235–241.

[55] C.J. Françoijs, J.P. Klomp, R.M. Knegtel, Sequence annotation of nuclear receptor ligand-binding domains by automated homology modeling, Protein Eng., 13 (2000) 391–394.

[56] Q. Zhang, P. Zhou, Z. Chen, M. Li, H. Jiang, Z. Gao, H. Yang, Dynamic PIP2 interactions with voltage sensor elements contribute to KCNQ2 channel gating, Proc. Natl. Acad. Sci., 110 (2013) 20093-20098.

[57] J.W. Jung, J.H. An, K.B. Na, Y.S. Kim, W. Lee, The active site and substrates binding mode of malonyl-CoA synthetase determined by transferred nuclear Overhauser effect spectroscopy, site-directed mutagenesis, and comparative modeling studies, Protein Sci. Publ. Protein Soc., 9 (2000) 1294–1303.

[58] F. De Rienzo, F. Fanelli, M.C. Menziani, P.G. De Benedetti, Theoretical investigation of substrate specificity for cytochromes P450 IA2, P450 IID6 and P450 IIIA4, J. Comput. Aided Mol. Des., 14 (2000) 93–116.

[59] D.A. Nugiel, M.E. Voss, D.R. Brittelli, J.C. Calabrese, An approach to the design of novel cognitive enhancers using molecular modeling and X-ray crystallography, Drug Des. Discov., 12 (1995) 289–295.

[60] R. Sánchez, A. Šali, Comparative protein structure modeling as an optimization problem, J. Mol. Struct. THEOCHEM, 398–399 (1997) 489–496.

[61] A.S. Talukdar, D.L. Wilson, Modeling and optimization of rotational C-arm stereoscopic X-ray angiography, IEEE Trans. Med. Imaging, 18 (1999) 604–616.

[62] H. Ceulemans, R.B. Russell, Fast fitting of atomic structures to low-resolution electron density maps by surface overlap maximization, J. Mol. Biol., 338 (2004) 783–793.

[63] S.B. Needleman, C.D. Wunsch, A general method applicable to the search for similarities in the amino acid sequence of two proteins, J. Mol. Biol., 48 (1970) 443–453.

[64] T.F. Smith, M.S. Waterman, Identification of common molecular subsequences, J. Mol. Biol., 147 (1981) 195–197.

[65] O. Gotoh, An improved algorithm for matching biological sequences, J. Mol. Biol., 162 (1982) 705–708.

[66] W.R. Taylor, Identification of protein sequence homology by consensus template alignment, J. Mol. Biol., 188 (1986) 233–258.

[67] G.J. Barton, M.J. Sternberg, Flexible protein sequence patterns A sensitive method to detect weak structural similarities, J. Mol. Biol., 212 (1990) 389–402.

[68] M. Suyama, Y. Matsuo, K. Nishikawa, Comparison of protein structures using 3d profile alignment, J. Mol. Evol., 44 Suppl 1 (1997) S163–173.

[69] J.S. Lolkema, D.J. Slotboom, Estimation of structural similarity of membrane proteins by hydropathy profile alignment, Mol. Membr. Biol., 15 (1998) 33–42.

[70] S.B. Long, E.B. Campbell, R. MacKinnon, Crystal structure of a mammalian voltage-dependent Shaker family K+ channel, Science, 309 (2005) 897–903.

[71] S.B. Long, X. Tao, E.B. Campbell, R. MacKinnon, Atomic structure of a voltage-dependent K+ channel in a lipid membrane-like environment, Nature, 450 (2007) 376–382.

[72] L. Delemotte, M. Tarek, M.L. Klein, C. Amaral, W. Treptow, Intermediate states of the Kv1.2 voltage sensor from atomistic molecular dynamics simulations, Proc. Natl. Acad. Sci. U. S. A., 108 (2011) 6109–6114.

[73] J.A. Smith, C.G. Vanoye, A.L. George, J. Meiler, C.R. Sanders, Structural Models for the KCNQ1 Voltage-Gated Potassium Channel, Biochemistry (Mosc.), 46 (2007) 14141–14152.

[74] R.W. Harrison, D. Chatterjee, I.T. Weber, Analysis of six protein structures predicted by comparative modeling techniques, Proteins, 23 (1995) 463–471.

[75] S. Mosimann, R. Meleshko, M.N. James, A critical assessment of comparative molecular modeling of tertiary structures of proteins, Proteins, 23 (1995) 301–317.

[76] A.S. Yang, B. Honig, An integrated approach to the analysis and modeling of protein sequences and structures. I. Protein structural alignment and a quantitative measure for protein structural distance, J. Mol. Biol., 301 (2000) 665–678.

[77] J.M. Sauder, J.W. Arthur, R.L. Dunbrack Jr, Large-scale comparison of protein sequence alignment algorithms with structure alignments, Proteins, 40 (2000) 6–22.

[78] R. Matsumoto, A. Sali, N. Ghildyal, M. Karplus, R.L. Stevens, Packaging of proteases and proteoglycans in the granules of mast cells and other hematopoietic cells. A cluster of histidines on mouse mast cell protease 7 regulates its binding to heparin serglycin proteoglycans, J. Biol. Chem., 270 (1995) 19524–19531.

[79] L.Z. Xu, R. Sánchez, A. Sali, N. Heintz, Ligand Specificity of Brain Lipid-binding Protein, J. Biol. Chem., 271 (1996) 24711–24719.

[80] A. Sali, J.P. Overington, Derivation of rules for comparative protein modeling from a database of protein structure alignments, Protein Sci. Publ. Protein Soc., 3 (1994) 1582–1596.

[81] W. Braun, N. Go, Calculation of protein conformations by proton-proton distance constraints A new efficient algorithm, J. Mol. Biol., 186 (1985) 611–626.

[82] G.M. Clore, A.T. Brünger, M. Karplus, A.M. Gronenborn, Application of molecular dynamics with interproton distance restraints to three-dimensional protein structure determination. A model study of crambin, J. Mol. Biol., 191 (1986) 523–551.

[83] D. Peng, J.-H. Kim, B.M. Kroncke, C.L. Law, Y. Xia, K.D. Droege, W.D. Van Horn, C.G. Vanoye, C.R. Sanders, Purification and Structural Study of the Voltage-Sensor Domain of the Human KCNQ1 Potassium Ion Channel, Biochemistry (Mosc.), (2014).

[84] M. Shen, A. Sali, Statistical potential for assessment and prediction of protein structures, Protein Sci. Publ. Protein Soc., 15 (2006) 2507–2524.

[85] R.A. Laskowski, M.W. MacArthur, D.S. Moss, J.M. Thornton, PROCHECK: a program to check the stereochemical quality of protein structures, J. Appl. Crystallogr., 26 (1993) 283–291.

4 RÉSULTATS

Les interactions protéine-lipide jouent un rôle important dans le fonctionnement des canaux ioniques. Ces derniers comme toute autre protéine transmembranaires sont entourées par des lipides de la membrane plasmique qui imposent donc un environnement dans lequel les processus d'activation ont lieu. L'altération des propriétés physiques des membranes (telles que l'épaisseur de la bicouche hydrophobe, le paramètre d'ordre des lipides la composant, les constantes élastiques, *etc.*) peut affecter la dynamique des canaux ioniques conduisant à un effet observable sur leur fonctionnement. En outre, certains lipides peuvent former une interaction stable avec les résidus (acides aminés) des canaux ioniques. Cela change la stabilité relative de l'état lié par rapport à celui non lié et peut donc ainsi avoir un effet sur le fonctionnement.

Il existe plusieurs preuves plaidant en la faveur d'interactions spécifiques entre canaux ioniques et lipides de la membrane plasmique. Tout d'abord, pour certains canaux ioniques, la mutagénèse d'un seul résidu implique la réduction, voire l'abolition complète de leur fonctionnement induit par l'action de lipides, ce qui indique que ce résidu est impliqué dans la formation d'une liaison spécifique (par exemple, l'acide docosahexaénoique (DHA) [1], le cholestérol [2,3], *etc.*). Ensuite, des expériences en électrophysiologie, conjointement à des simulations de dynamique moléculaire, révèlent que ces résidus peuvent, s'ils sont exposés à l'interface bicouche/solution, interagir avec les têtes lipidiques [4–15], ce qui a pour effet d'altérer le processus d'ouverture des canaux ioniques.

Il existe également une troisième preuve de ces interactions spécifiques : plusieurs structures cristallographiques de canaux ioniques comprennent des fragments de molécules lipidiques inclues dans les structures protéiques [16–21]. Depuis que la cristallographie à rayons X est capable de détecter sélectivement des structures hautement ordonnées ayant une très faible mobilité, la présence de ces lipides authentifie l'existence d'interactions spécifiques entre ces derniers et les canaux ioniques [22]. Cependant, il est important de noter que ce n'est pas toujours le cas. En effet, de récentes simulations de dynamique moléculaire sur un canal à eau (aquaporin-0, AQP0 [23]) ont révélé que, bien qu'étant entouré d'une couche de

phospholipides (code PDB 2B6O [24]), ce canal n'a pas de site d'ancrage spécifique au phospholipide en question. De prime abord, si l'on se base sur des données d'énergie d'interaction, les résultats de ces simulations suggèrent l'existence de sept candidats potentiels parmi les résidus d'AQP0 qui pourraient former un site de liaison spécifique au phospholipide. Cependant, la mutagénèse *in silico* de ces résidus n'a pas modifié significativement la position des lipides, comparée à la structure originale d'AQP0, ce qui démontre l'absence de liaisons spécifiques protéine-lipide dans ce cas particulier.

Le phosphatidylinositol-4,5-bisphosphate (PIP_2) est un lipide mineur du feuillet interne de la membrane plasmique qui module le fonctionnement de plusieurs canaux ioniques [25]. La concentration de cette molécule fortement chargée négativement ne dépasse pas 1% de la teneur globale en lipide de la membrane [26]. On peut donc supposer que l'effet sur le fonctionnement induit par le PIP_2 résulte de l'interaction spécifique de ce lipide avec les canaux ioniques plutôt que due à un changement global des propriétés physiques de la membrane plasmique. Cette dernière hypothèse est confirmée directement pour les canaux de la famille Kir : dans les structures cristallines résolues récemment de Kir2.1 et GIRK2 plusieurs résidus chargés positivement forment un site de liaison pour un PIP_2 dérivé à chaîne courte [19,20]. Cette hypothèse est également avancée pour d'autres canaux : il a été montré que la mutagenèse des canaux Kv7.1, Kv7.2/Kv7.3, Kv1.2, SpIH (HCN), TRPM8, TRPM4 ou la suppression de courts segments chargés positivement dans la séquence des canaux TRPV1 et hERG altère l'affinité apparente du PIP_2 ou l'effet de celui-ci sur le fonctionnement de ces canaux [3,27–39].

Dans ce travail, nous nous concentrons sur la modulation des canaux Kv1.2 et Kv7.1 par PIP_2. Bien que ces deux canaux appartiennent à la même famille, leur réponse à l'application de PIP_2 est différente. Dans Kv7.1, PIP_2 est absolument nécessaire pour l'ouverture du canal : un appauvrissement en PIP_2 de la membrane plasmique réduit considérablement le courant ionique [40]. En outre, des expériences récentes mettent en évidence l'importance de PIP_2 pour le couplage entre le VSD et le pore dans Kv7.1. En l'absence de ce lipide, l'activation du domaine sensible à la tension ne donne pas lieu à l'ouverture du pore, et un pore ouvert ne favorise pas l'activation du VSD [37]. Kv1.2 est par contre capable de s'ouvrir sans PIP_2 et ne nécessite donc pas ce lipide pour maintenir le couplage VSD/pore. Cependant, PIP_2 semble induire un effet dual intéressant : d'une part, il augmente l'amplitude du courant ionique, et, d'autre part, il favorise l'apparition de courant de porte (*gating currents*) à des voltages plus hyperpolarisés, indiquant un

encombrement stérique du mouvement des VSD [35,41].

Bien qu'un effort considérable ait été consacré à la question de la modulation par PIP_2 des canaux Kv1.2 et Kv7.1, des questions importantes restent à explorer :

- Quels sont les sites de liaison des Kv1.2 et Kv7.1 et du PIP_2 ?
- Par quel mécanisme l'interaction du PIP_2, entraîne-t-elle d'une part un gain-de-fonction (augmentation du courant ionique) et d'autre part une perte-de-fonction (encombrement du mouvement du VSD) dans le Kv1.2 ?
- Comment PIP_2 contrôle ou facilite-t-il le couplage entre le VSD et le pore dans Kv7.1 ?
- Pourquoi, à l'inverse du Kv1.2, le Kv7.1 nécessite-t-il le PIP_2 pour le couplage entre le VSD et le pore ?
- Les sites de liaison du PIP_2 aux Kv1.2 et Kv7.1 sont-ils homologues ? Le mécanisme moléculaire de modulation du PIP_2 est-il similaire ou complètement différent ?

Dans ce travail, en utilisant des simulations de DM combinées avec des expériences en électrophysiologie, nous avons tenté de répondre à ces questions. Ce chapitre est divisé en trois sections. Dans la Section **4.1**, nous présentons nos résultats concernant la modulation de Kv1.2 par PIP_2. En particulier, nous identifions les sites de liaison putatifs de PIP_2 et démontrons que les interactions mises en jeu peuvent être responsables de l'effet dual observé expérimentalement. Dans la Section **4.2**, nous étendons notre investigation en utilisant la métadynamique : nous déterminons les modifications induites par PIP_2 sur les profils d'énergie libre qui décrivent les deux premières transitions du VSD le long du chemin d'activation. La dernière section, **4.3**, est consacrée au Kv7.1. Ici, nous identifions un site de liaison putatif de PIP_2 et proposons un mécanisme qui explique son rôle dans le couplage entre le VSD et le pore. Combinant nos investigations théoriques avec une approche expérimentale, nous montrons pourquoi le couplage indépendant du PIP_2 est affaibli dans Kv7.1. Lors de la discussion de la Section **4.3**, nous tentons de comprendre pourquoi les deux canaux homologues, Kv1.2 et Kv7.1, ainsi que d'autres membres de la famille Kv7 se comportent différemment en présence de PIP_2.

4 RESULTS

Protein-lipid interactions play an important role in the functioning of ion channels. The latters as other transmembrane proteins are surrounded by lipids of the plasma membrane, imposing, therefore, an environment in which the processes of gating take place. Alteration of its physical properties (such as the thickness of the hydrophobic bilayer, the order parameter of the composing lipids, the elastic constants, *etc.*) may affect the dynamics of ion channels leading to an observable effect on their functioning. In addition, some lipids may form a stable interaction with ion channels by high-affinity binding to their residues. This changes the relative stability of the bound state compared to the unbound one and, therefore, may as well cause an effect on functioning.

There are several evidences advocating for specific interactions between ion channels and lipids of the plasma membrane. First, for some ion channels, mutagenesis of their single residue reduces or completely abolishes the effect on functioning induced by lipids, indicating that this residue is involved in formation of a specific binding site (for instance, docosahexaenoic acid (DHA) [1], cholesterol [2,3], *etc.*). Second, electrophysiological experiments along with MD simulations report that residues exposed to the bilayer/solution interface may interact with lipid headgroups [4–15], altering the process of ion channels' gating.

There is also a third evidence: in several crystal structures of ion channels, pieces of lipid molecules were resolved along with the proteins [16–21]. Since the X-ray crystallography is able to detect only high-ordered regions with very low mobility, these lipids probably establish specific interactions with ion channels [22]. Note, however, that this is not always the case. Recent MD simulations of the lens-specific water channel aquaporin-0 (AQP0) [23] have revealed that while, in the crystal structure, this channel is surrounded by a shell of phospholipids (PDB code 2B6O [24]), it does not have a specific phospholipid binding site. At first, based on the interaction energy data, these simulations suggested seven candidate residues of AQP0, which may form a specific phospholipid binding site. However, *in silico* mutagenesis of these residues did not substantially modify the positions of the lipids compared to the WT of AQP0, which advocates against the

presence of specific protein-lipid interactions.

Phosphatidylinositol-4,5-bisphosphate (PIP_2) is a minor lipid of the inner plasma membrane leaflet, which is shown to modulate the functioning of several ion channels [25]. The concentration of this highly negatively charged lipid does not exceed 1 % of the overall membrane content [26]. One may, therefore, assume that an effect on functioning induced by PIP_2 is mediated by binding of this lipid to an ion channel rather than due to a global change of physical properties of the plasma membrane. The latter hypothesis was directly confirmed for Kir channels: in the recently resolved crystal structures of Kir2.1 and GIRK2 several positively charged residues were shown to form a binding site for a short chain PIP_2 derivative [19,20]. For other channels, this hypothesis holds as well: mutagenesis of Kv7.1, Kv7.2/Kv7.3, Kv1.2, SpIH (HCN), TRPM8, TRPM4 or deletion of short positively charged segments in TRPV1, hERG was shown to alter apparent PIP_2 sensitivity or the effect on functioning induced by PIP_2 [3,27–39].

In this work, we focus on the modulation of the Kv1.2 and Kv7.1 channels by PIP_2. While these two channels belong to the same family, their response to PIP_2 application is different. In Kv7.1, PIP_2 is absolutely required for opening: depletion of this lipid from the plasma membrane dramatically reduces ionic current [40]. Furthermore, recent experiments highlight the importance of PIP_2 for coupling in Kv7.1. In the absence of this lipid, the activation of the voltage sensor does not lead to the pore opening, and the open pore does not promote the activation of the voltage sensor [37]. Kv1.2, on the other hand, is able to open without PIP_2 and does not require this lipid for coupling. Application of PIP_2 to this channel results though in an interesting dual effect: on the one hand, amplitude of ionic current increases, and, on the other hand, gating current appears at more hyperpolarized voltages, indicating hindered motions of the voltage sensors [35,41].

While an extensive amount of work was devoted to the issue of Kv1.2 and especially of Kv7.1 modulation by PIP_2, important questions remain unexplored:

- Where is a putative PIP_2 binding site in Kv1.2 and in Kv7.1?
- In Kv1.2, by which mechanism does PIP_2 binding results, on the one hand, in a hindered motion of the voltage sensor and, on the other hand, in an increase of ionic current?
- How does PIP_2 mediate coupling in Kv7.1?
- Why is PIP_2 required for coupling between the voltage sensor and the pore in Kv7.1 but not in Kv1.2?

- Are the PIP_2 binding sites in Kv1.2 and Kv7.1 homologous and is the molecular mechanism of PIP_2 modulation similar or completely different?

Here, using MD simulations combined with electrophysiological experiments, we attempted to address these questions. Chapter **4** is divided in three sections. In Section **4.1**, we present our results concerning the Kv1.2 modulation by PIP_2. In particular, we identify putative binding sites of PIP_2 and demonstrate which interactions might be responsible for the aforesaid dual effect observed experimentally. In the following section, **4.2**, we extend our investigation using the metadynamics method: we determine the alterations of the free energy profiles, underlying the first two voltage sensor transitions along the activation path, induced by PIP_2. The last section, **4.3**, is devoted to Kv7.1. Here, we identify a putative binding site of PIP_2 and propose how this lipid may mediate coupling between the voltage sensor and the pore. Taking advantage of a combined modeling and experimental approach, we demonstrate why lipid-independent coupling in Kv7.1 is weakened. In the discussion of Section **4.3**, we attempt to rationalize why the two homologous channels, Kv1.2 and Kv7.1 and also other members of the Kv7 family, show different response to PIP_2 application.

4.1. Modulation of the Kv1.2 channel by PIP_2

In Chapter **2**, we have highlighted that a vast variety of ion channels are modulated by PIP_2 (see **2.3.5**). Recently, the experimental group of Gildas Loussouarn (INSERM, Thorax Institute, Nantes), with whom we are collaborating, has reported that the voltage-gated potassium channel *Shaker* is as well sensitive to this lipid [41]: PIP_2 depletion results in a dual effect on ionic and gating currents (see **2.3.6**). First, the amplitude of the ionic current becomes significantly reduced. The latter can be further recovered when applying exogenous PIP_2 (see Figure 2.3.6.1). Since, PIP_2 induces "a gain" of ionic current, this effect was accordingly called gain-of-function. Second, the application of PIP_2 or its depletion cause respectively right- and leftward shifts of the Q/V curve (gating current vs. membrane potential) (see Figure 2.3.6.1). This second effect was called loss-of-function, since PIP_2 delays the movement of the voltage sensor by acting either directly or allosterically. In addition to this influence on the equilibrium properties of the channel, PIP_2 was shown to affect the kinetics of the voltage sensor transitions as well: application of this lipid slowed the activation and accelerated the deactivation. Another experimental group [35] obtained similar results at the same time. The dual effect on the *Shaker* functioning caused by PIP_2 application seems rather contradictory. Indeed, this lipid stabilizes simultaneously two opposite states of the channel: the activated/open (an increase of ionic current) and the resting/closed (a delay of gating current). This apparent contradiction may be resolved by uncovering the molecular level mechanism that underlies PIP_2 modulation of *Shaker*.

In order to explore the mechanism of PIP_2 modulation, we aimed to identify the PIP_2 binding sites in both the activated/open and resting/closed states of a close homologue of the *Shaker* channel, Kv1.2. Using unconstrained MD simulations, we have identified three potential binding sites, in which a single PIP_2 molecule formed salt bridges with at least two Kv1.2 positive residues (see **4.1.2**). In one of these binding sites, the interaction between the protein and the lipid was shown to be state-dependent: PIP_2 either anchored the S6 terminus in the activated/open state of Kv1.2 or the bottom of S4 in its

resting/closed state. Based on the obtained results, we proposed a model of Kv1.2/*Shaker* modulation by PIP_2 that is able to rationalize the experimental data. This project was accomplished in collaboration with the experimental group of Gildas Loussouarn. The results were published in the Journal of Biological Chemistry [41], and the molecular modeling was extensively reported in Biophysica and Biochimica Acta, Biomembranes [15].

4.1.1. Methods: preparation of the systems for an MD run

The structure of the Kv1.2 activated/open state was resolved experimentally and is available at the protein data bank (PDB code 3LUT [42]); the model of the resting/closed state was previously obtained in our group by applying brute force and steered molecular dynamics (MD) simulations [12]. The models of the activated/open and resting/closed states considered here include the TM part and the T1 domain of Kv1.2.

Considering that the lateral diffusion within a lipid bilayer is rather slow [43] compared to time scales traditionally reached in MD simulations, we increased the probability of interaction between Kv1.2 and PIP_2 by surrounding the former with a ring of these lipids (excess of PIP_2). Note also that the stoichiometry the Kv1.2 channel : PIP_2 molecules is not known. The structure of the Kv1.2 activated/open and resting/closed states were initially embedded in a palmitoyl-oleyl-phosphatidylcholine (POPC) hydrated bilayer (368 and 376 molecules in the systems with the activated/open and resting/closed states); and further, POPC molecules surrounding the channel in the inner bilayer leaflet were replaced by PIP_2 (64 and 54 molecules in the systems with the activated/open and resting/closed states). Overall, the systems with the activated/open and resting/closed states contained 343,434 and 346,867 atoms respectively.

The systems with the two states were hydrated and solvated by KCl salt up to a physiological concentration of 150 mM. CHARMM22 with the CMAP correction and CHARMM36 force fields were used for the protein and POPC respectively [44,45]. To describe PIP_2, the compatible force field developed by Lupyan *et al.* was considered [46]. Water molecules were represented by the TIP3P model [47].

The MD simulations were performed using NAMD 2.8 [48]. The two systems were equilibrated for 100 ns. At the first step of the equilibration (2

ns), the atoms of Kv1.2 were fixed to ensure relaxation of the surrounding lipid molecules and the solution. For the following 8 ns MD run, only the backbone atoms of Kv1.2 were restrained with gradually releasing the force constants (from 1 kcal/mol/Å to 0), enabling reorganization of the side-chain groups. Finally, all restraints were released and the entire system was further equilibrated for 90 ns. The root mean square deviation (RMSD) of the channel structure from the initial one reached a plateau after ~ 35 ns.

The MD simulations were performed in the NPT ensemble: the Langevin dynamics was applied to keep the temperature (300 K) and the pressure (1 atm) fixed. The equations of motion were integrated using a multiple time-step algorithm. The time-step of the simulations was 2.0 fs. Short- and long-range forces were calculated every 1 and 2 time-steps respectively. Long-range electrostatic were calculated using Particle Mesh Ewald (PME). The cutoff distance of short-range electrostatic calculations was taken to be 11 Å. A switching function was used between 8 and 11 Å to smoothly bring the vdW forces and energies to 0 at 11 Å. During the calculations chemical bonds between hydrogen and heavy atoms were constrained to their equilibrium values. Periodic boundary conditions were applied. The simulations were performed on the SGI ALTIX ICE Machine JADE at the CINES supercomputer center (Montpellier, France).

A PIP_2 binding site was identified counting the number of salt bridges formed between positively charged residues of the channel and headgroups of the lipid. In particular, we measured the minimal distance between the Nitrogen atoms of arginine and lysine charged groups of the channel and the Oxygen atoms of the PIP_2 phosphates. The salt bridges were assumed formed if the calculated distance was 3.2 Å or less. The analysis was performed for the last 65 ns of each trajectory, *i.e.* when the RMSD of the Kv1.2 structure from the initial configuration reached a plateau (see above).

4.1.2. Results: in Kv1.2, there are three potential sites of PIP_2 binding

During the first steps of the equilibration process, the PIP_2 molecules relaxed around the channel, forming interactions with its positively charged residues. In order to characterize these interactions, we have calculated the average number of salt bridges formed between each PIP_2 molecule and all positive residues of Kv1.2 exposed to the lower bilayer leaflet/solution interface (see

4.1.1). The result of this analysis is reported in Figure 4.1.2.1. In the activated/open state of the channel (see Figure 4.1.2.1, top panels), 8 PIP_2 molecules out of 64 interacted with more than one positive residue of Kv1.2. Among these 8 PIP_2 molecules, we could distinguish three groups, in which PIP_2 was occupying different binding sites. In particular, (i) three PIP_2 lipids were located at the interface between the voltage sensor and the pore (see Figure 4.1.2.1, shown in red); (ii) four PIP_2 lipids were found in interaction with the S4-S5 linkers of adjacent subunits (see Figure 4.1.2.1, shown in blue); and (iii) one PIP_2 molecule was anchored to the S2-S3 loop (see Figure 4.1.2.1, shown in green). In the Kv1.2 resting/closed state, we also found PIP_2 occupying the aforesaid binding sites (see Figure 4.1.2.1, bottom panels): four PIP_2 lipids were bound between the voltage sensor and the pore, two PIP_2 lipids were interacting with S4-S5s of adjacent subunits, and two PIP_2 lipids were anchored to the S2-S3 loop. As in the activated/open state of the channel, these PIP_2 molecules formed salt bridges with more than one positive residue of Kv1.2 simultaneously. Further, we will discuss each of the identified binding sites in more details.

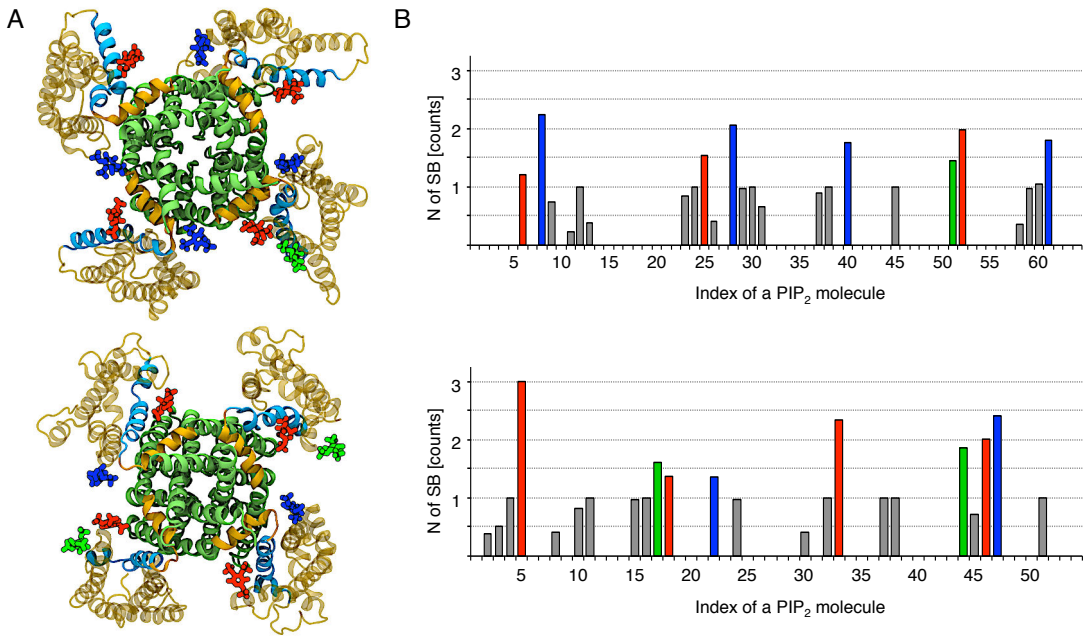

Figure 4.1.2.1. In Kv1.2, there are three potential sites of PIP_2 binding that are similar in the activated/open (top panels) and resting/closed (bottom panels) states. A. The snapshots of the MD trajectories representing different binding sites. PIP_2 headgroups occupying the same binding site are colored in red (i), blue (ii) and green (iii). The T1 domain of Kv1.2 and the lipid tails of PIP_2 are not shown for clarity. B. The number of salt bridges formed between each PIP_2 molecule and positive residues of Kv1.2. Color-code of the diagrams is consistent with (A).

The binding site located at the VSD/PD interface

While the spatial location of the PIP_2 molecule bound between the voltage sensor and the pore was similar in the activated/open and resting/closed states of Kv1.2 (see Figure 4.1.2.1A), the interacting residues were partially different (see Figure 4.1.2.2A, B). In the Kv1.2 activated/open state (see Figure 4.1.2.2A), PIP_2 was located in close proximity to the S6 terminus (R419) in three out of four subunits. The same PIP_2 molecule formed a salt bridge with the middle residue of the S4-S5 linker (K322). In addition, after ~ 80 ns of the MD run, in one of the subunits a positive residue of the T1/S1 linker (R147) came in close contact with the PIP_2 molecule. Altogether, in this subunit, the three residues K322, R419 and R147 formed a binding pocket for the PIP_2 molecule. In the Kv1.2 resting/closed state (see Figure 4.1.2.2B), the S6 helix is located further from the bilayer/solution interface and, therefore, is not accessible for PIP_2. As in the activated/open state of the channel, PIP_2 interacted with K322 of S4-S5. However, this lipid formed also salt bridges with the bottom positive residues of S4 (R303, K306 and R309). In particular, in all four subunits, a single PIP_2 molecule that was found in interaction with the middle residue of S4-S5 interacted also with S4. Hence, the molecular models showed that the proximity of the positive residues of the S4-S5 linker and of the bottom of S4 provide an excess of positive charges that forms a binding pocket for the highly negatively charged PIP_2 molecules.

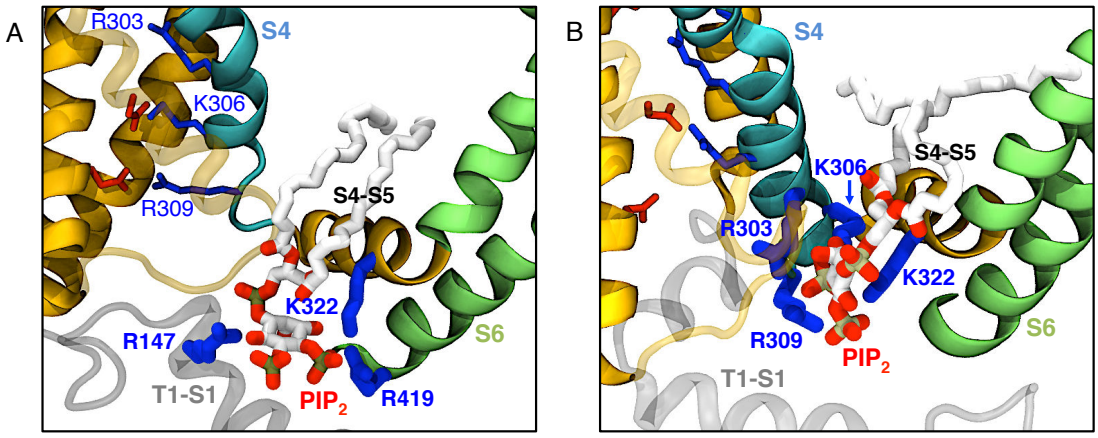

Figure 4.1.2.2. The PIP_2 binding site of Kv1.2 located at the interface between the voltage sensor and the pore. The voltage sensor apart of S4 is present in yellow. S4 is shown in light blue. The pore domain and the T1 domain are present in green and grey respectively. A. In the Kv1.2 activated/open state, PIP_2 attracts R419 of the S6 terminus and forms a salt bridge with K322 of the S4-S5 linker. Another residue of the T1-S1 linker participates in formation of this binding site. B. In the Kv1.2 resting/closed state, PIP_2 remains in interaction with K322 of the S4-S5 linker and forms salt bridges with the bottom positive residues of S4. The figure is adapted from [15].

We have further monitored more thoroughly the position of the PIP_2 molecules in the Kv1.2 activated/open and resting/closed states. In

particular, we have defined a vector ***L*** connecting the centers of mass (COMs) of the PIP_2 headgroup and the part of the channel that does not undergo large conformational changes during the activated/open to resting/closed transition (the top of S5 and S6, the pore helix and the selectivity filter) and estimated a projection of this vector on the axis perpendicular to the bilayer plane, L_z. According to the obtained results (see Figure 4.1.2.3A, B), in the Kv1.2 activated/open state, PIP_2 extends farther into the aqueous phase compared to its location in the Kv1.2 resting/closed state. The estimated difference in L_z is ~ 8±3 Å (see Figure 4.1.2.3B). This observation is consistent with the fact that in the Kv1.2 resting/closed or activated/open states, PIP_2 interacts with either S4 of the voltage sensor or with the S6 terminus respectively: while the bottom residues of S4 are located at the lower bilayer leaflet/solution interface, the positive residue of S6 is shifted further from this interface into the solution.

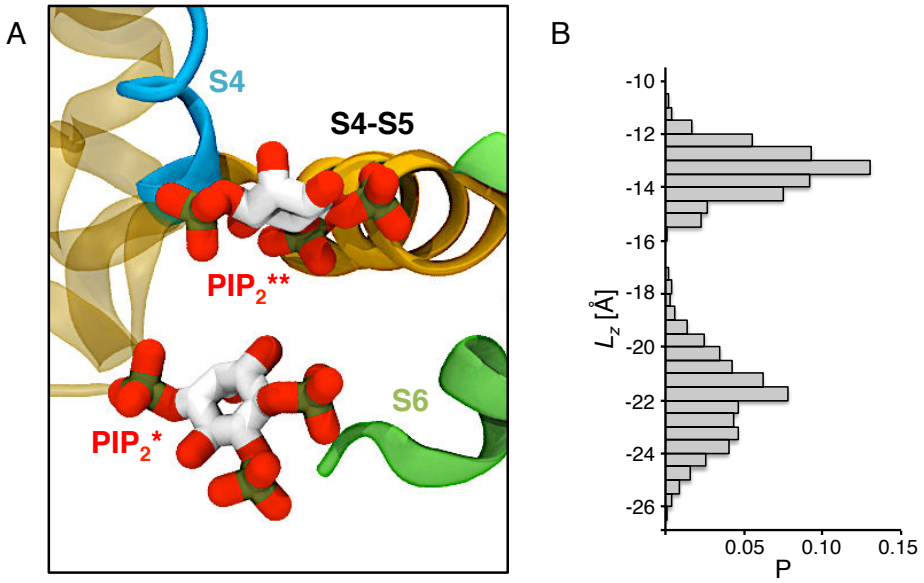

Figure 4.1.2.3. PIP_2 extents farther into the solution in the Kv1.2 activated/open state compared to the resting/closed one. A. The superimposed equilibrium positions of PIP_2 in the Kv1.2 activated/open (*) and resting/closed states (**). The channel in the activated/open state is shown for the reference. B. The probability distribution (P) of the vector ***L*** projection on the axis perpendicular to the bilayer plane ($\boldsymbol{L_z}$) in the activated/open (A/O) and resting/closed (R/C) states of Kv1.2. The vector ***L*** connects the COM of PIP_2 headgroup and the COM of the top of S5 and S6, the pore helix and the selectivity filter.

The binding site composed of the S4-S5 linkers of adjacent subunits

In the activated/open and resting/closed states of the channel, there were PIP_2 molecules forming salt bridges with K312 and R326 located each at one end of two nearby S4-S5s (see Figure 4.1.2.4A). Specifically, in the Kv1.2 activated/open state, four PIP_2 molecules were in interaction with K312 and R326 simultaneously. In the Kv1.2 resting/closed state, only two PIP_2

molecules were involved in this type of interaction. In each of the other potential binding sites, two different PIP_2 molecules interacted with the two external positive residues of S4-S5 preventing formation of the salt bridges network between subunits.

The binding site composed of the S2-S3 loop

In the Kv1.2 activated/open and resting/closed states, we found respectively one and two PIP_2 molecules anchored to the S2-S3 loop (K247). These PIP_2 molecules were also interacting with R417 of the T1-S1 linker (see Figure 4.1.2.4B). Interestingly, this binding site is in very close proximity to the one found at the VSD/PD interface (see Figure 4.1.2.1A). However, while the former is accessible for lipids of bulk bilayer, the latter is buried between the two domains of Kv1.2. In other words, the S2-S3 loop is located along a potential path, by which PIP_2 approaches the site at the VSD/PD interface, and, therefore, we hypothesize that interactions between S2-S3 and PIP_2 are rather intermittent.

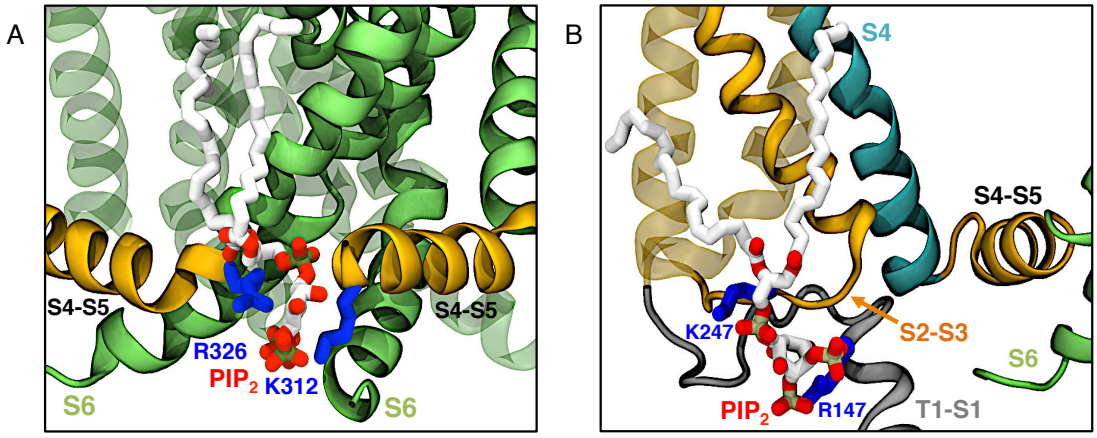

Figure 4.1.2.4. The PIP_2 binding site composed of the S4-S5 linkers of adjacent subunits (A) and of the S2-S3 loop (B). A. The activated/open state is shown. PIP_2 interacts with the external positive residues of the S4-S5 linkers of two nearby subunits. Here, the voltage sensors and the T1 domain are not shown for clarity. B. The resting/closed state is shown. PIP_2 forms salt bridges with the S2-S3 loop (K247) and the T1-S1 linker (R147).

4.1.3. Discussion: state-dependent interaction between Kv1.2 and PIP_2 rationalizes the dual effect observed experimentally

PIP_2 modulates the *Shaker* channel affecting its ionic and gating currents (see **4.1**). Since the concentration of PIP_2 in a plasma membrane is rather low (up

to 1 % of the overall lipid content [26]), we can assume that this modulation is mediated via direct binding of PIP_2 to the channel. Here, we have identified three potential sites of PIP_2 binding to the close homologue of *Shaker*, Kv1.2 (see Figure 4.1.2.1). In one of these sites located at the VSD/PD interface, the PIP_2 molecule interacts either with the S6 terminus or the bottom of S4 state-dependently. Hence, in the Kv1.2 activated/open state, PIP_2 anchors K322 of the S4-S5 linker and comes in close proximity to R419 of the S6 terminus (see Figure 4.1.2.2A, 4.1.3.1A). This interaction may stabilize the Kv1.2 pore in its open conformation either directly via the salt bridge between R419 and PIP_2 or indirectly via enhancing of coupling between the activated voltage sensor and the open pore. The hypothesis of the open pore stabilization by PIP_2 (direct or indirect) is consistent with the experimental data reporting the gain-of-function effect for *Shaker* [35,41]. Indeed, as demonstrated by Rodriguez-Menchaca *et al.* [35], the gain of ionic current is caused by a PIP_2-dependent increase of a single channel open probability, which is consistent with stabilization of the *Shaker* pore in its open conformation.

Rodriguez-Menchaca *et al.* neutralized both K322 and R419 and measured the ionic current of the resulting mutants after application of PIP_2-specific antibodies. In the case of K322Q, but not of R419Q, a fraction of ionic current not blocked by PIP_2-antibodies was affected compared to the WT, indicating that K322 is rather responsible for PIP_2 sensitivity than R419 [35]. In contrast, other experimental groups [27,34,37], when working with the Kv7 channels that are homologous to *Shaker*, observed a decrease of PIP_2 apparent affinity and of ionic current when S6 positive residues were neutralized. This data better supports our model, in which the interaction between PIP_2 and the S6 terminus is important for the gain-of-function effect. Interestingly to note, the docking simulations performed by Rodriguez-Menchaca *et al.* indicated as well that R419 along with K322 participate in the coordination of PIP_2 [35].

In the Kv1.2 resting/closed state, PIP_2 located between the voltage sensor and the pore also interacts with K322 of the S4-S5 linker. However, instead of anchoring S6 as in the Kv1.2 activated/open state, PIP_2 forms multiple salt bridges with the bottom positive residues of S4 (R303, K306 and R309) (see Figure 4.1.2.2B, 4.1.3.1B). This interaction stabilizes the voltage sensor in the resting state and may result in the loss-of-function effect observed experimentally [35,41]. Indeed, the right-shift of the Q/V curve is consistent with the relative stabilization of the resting voltage sensor compared to the activated one. In agreement with our model, neutralization of K322 was shown to affect the PIP_2-dependent shift of the Q/V curve [35]. Interaction of PIP_2 with the S4 positive residues is more difficult to verify since the latters are directly involved in a voltage sensing machinery.

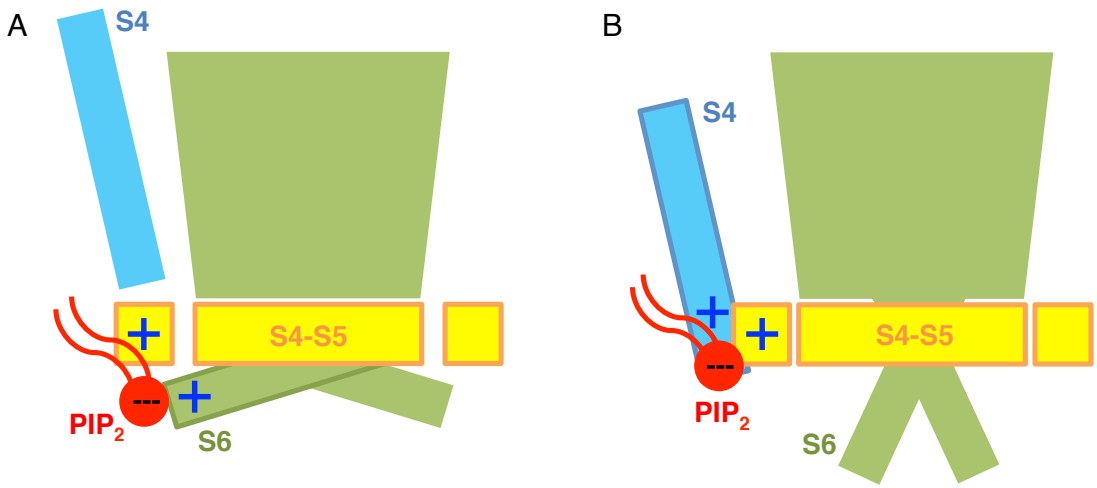

Figure 4.1.3.1. Schematic representation of the mechanism of the *Shaker* modulation by PIP_2. A. In the activated/open state of the channel, residues of the S6 terminus and of the S4-S5 linker coordinate the PIP_2 molecule. B. In the resting/closed state of the channel, residues of the S4 bottom and of the S4-S5 linker coordinate the PIP_2 molecule.

In the Kv1.2 activated/open state, PIP_2 located between the voltage sensor and the pore extents farther into the aqueous phase compared to the Kv1.2 resting/closed state (see Figure 4.1.2.3). We suppose that this latter effect may be facilitated by an external electric field. Depolarization of the membrane potential forces the S4 positive residues to move upwards, activating therefore the voltage sensor. Along with this process, negatively charged species including PIP_2 move downwards. For PIP_2 specifically, an external electric field may facilitate detachment from the S4 positive residues, located at the lower bilayer leaflet/solution interface, and movement toward S6, which resides farther in an aqueous phase.

In one of the binding sites, we observed the PIP_2 molecule forming a net of salt bridges between adjacent subunits (see Figure 4.1.2.4A). In particular, PIP_2 interacted with two residues located at the N- and C-terminuses of S4-S5s, K312 and R326. This interaction was more prominent in the activated/open state than in the resting/closed one, which allows us to hypothesize that linking of two nearby subunits may stabilize the pore in its open conformation. Interestingly, Rodriguez-Menchaca *et al.* after neutralization of one of these residues, R326, observed an effect on the fraction of ionic current not blocked by PIP_2-antibodies. Mutagenesis of the other residue, K312, did not cause significant changes compared to the WT [35].

In the crystal structure of the Kv1.2/Kv2.1 paddle chimera (pdb code 2R9R [21]), along with the channel atoms, some lipid fragments were resolved. One of these lipids is located at the interface between the voltage

sensor domain and the pore. Another one resides close to the S4-S5 linkers of adjacent subunits. Interestingly, binding sites of these lipids resembles the two PIP_2 binding sites identified here (see Figure 4.1.2.1). This raises new questions: whether these binding sites are unspecific to PIP_2 and may interact with different types of lipids. Does binding of other lipids induce some gain- or loss-of-function effects of ionic and gating currents? And if so, whether the molecular mechanism of modulation by other lipids is similar to the one proposed for PIP_2. Answering these questions will allow one to get a new perspective on regulation of voltage-gated potassium channels by the surrounding membrane content.

4.2. Alteration of the Kv1.2 activation and deactivation free energies induced by the presence of PIP_2

In the previous section, performing unconstrained MD simulations, we were able to identify the PIP_2 binding sites of Kv1.2. Based on the fact that some PIP_2 molecules interact with S4, when positive residues of the latter are exposed to the lower bilayer leaflet/solution interface, we proposed that this lipid stabilizes the resting state of the voltage sensor (see **4.1.3**). This hypothesis is consistent with the loss-of-function effect observed experimentally [35,41]: the rightward shift of the Q/V curve in the presence of PIP_2 indeed indicates different relative stability of the voltage sensor states, namely, either stabilization of the resting state or destabilization of the activated state. In this section, we will show how the free energy underlying the Kv1.2 voltage sensor transitions is affected by the presence of PIP_2 compared to the bare POPC bilayer.

Estimation of the free energy requires a good sampling of the system's configuration space. Quite often, the latter cannot be achieved using non-biased MD simulations, as the system tends to be trapped in a local minimum separated from other minima by high free energy barriers. In order to enhance sampling of the configuration space, several techniques introducing biases to the system's dynamics are proposed [49–53]. In this work, we used one of these techniques, namely, metadynamics [49,50] (see **3.3.3**, **3.3.4**). In the metadynamics method, an external history-dependent bias potential being a function of the selected reaction coordinates or collective variables (CVs) is added to the Hamiltonian of the system. This potential pushes the system away from its local free energy minima allowing better exploration of the conformational space. Knowing this history-dependent potential, one is able to reconstruct the corresponding free energy surface.

In order to estimate the free energy underlying the Kv1.2 voltage sensor transitions in the bare POPC bilayer and the bilayer with PIP_2 in its lower leaflet, we have devised the following strategy: i) split the full

activation/deactivation pathway in four transitions, namely ε-δ, δ-γ, γ-β and β-α (see Figure 2.2.3.3) and estimate the free energy for each transition separately; and ii) suggest a set of collective variables (further CVs) allowing an effective sampling of the system's conformational space.

A natural choice of a collective variable, which is able to describe the conformational rearrangements of the voltage sensor during its activation/deactivation, is the spatial translation of S4 across the bilayer. Indeed, upon application of an electric field, S4 moves upward or downward depending on the resulting membrane potential (see **2.2.3**). Schwaiger *et al.* [54,55] used this CV in order to sample the conformations of the Kv1.2/Kv2.1 chimera's voltage sensor, related to one of its transitions. In particular, they were interested in the early transition of the fully activated voltage sensor toward the resting state. Using steered MD [54] and umbrella sampling [55] along the vertical displacement of S4, Shwaiger *et al.* have estimated the energetics of this transition in the WT of the Kv1.2/Kv2.1 chimera and its several mutants. In our work, we have devised a more complex CV, which, in addition to the spatial translation of S4, includes another important degree of freedom associated with the voltage sensor's activation/deactivation, namely, the binding of the S4 positive residues to their countercharges (the negative residues of S1, S2 and S3 and the lipid headgroups) (see **4.2.2**). Using this CV, we have estimated the free energy surfaces of the ε-δ and δ-γ voltage sensor transitions in the bare POPC and POPC/PIP_2 bilayers (see **4.2.5**). Moreover, we have re-estimated the obtained free energy surfaces in terms of a gating charge, *i.e.* a CV that is usually tracked experimentally (see **4.2.3**, **4.2.5**). This has two major advantages: on the one hand, it allows the direct link to experiments to quantitatively check the results (the gating charge), and, on the other hand, it allows us to check the convergence of the results in a much more direct way (see **4.2.5**).

Overall our results show that in the presence of PIP_2, both the relative stability of the voltage sensor states (the δ-γ transition) and the free energy barriers separating them (the ε-δ and δ-γ transitions) are affected compared to the bare POPC bilayer. These findings, on the one hand, confirm the hypothesis about the stabilization of the Kv1.2 resting state by PIP_2 (see **4.1.3**) and, on the other hand, indicate different kinetics of the voltage sensor transitions in the absence and presence of this lipid, which is in agreement with the known experimental data [35,41]. This project was accomplished in collaboration with the computational group of Mike Klein at Temple University, Philadelphia in USA.

4.2.1. Methods: preparation of the systems for a metadynamics run

In this study, we have estimated the free energies for two transitions of the voltage sensor out of four: ε-δ and δ-γ. Among these three states considered, ε corresponds to the resting voltage sensor (R6, K5, R4 and R3 interact with the lower bilayer leaflet, R2 and R1 form salt bridges with E236 and D259 respectively); δ is the first intermediate state after the resting one along the activation path (R6, K5 and R4 interact with the lower bilayer leaflet, R3, R2 and R1 form salt bridges with E236, D259 and E226 respectively); and γ is the second intermediate state after the resting one along the activation path (R6 and K5 interact with the lower bilayer leaflet, R4, R3, R2 and R1 form salt bridges with E236, D259, E226 and E183 respectively) (see Figure 2.2.3.3, 4.2.1.1).

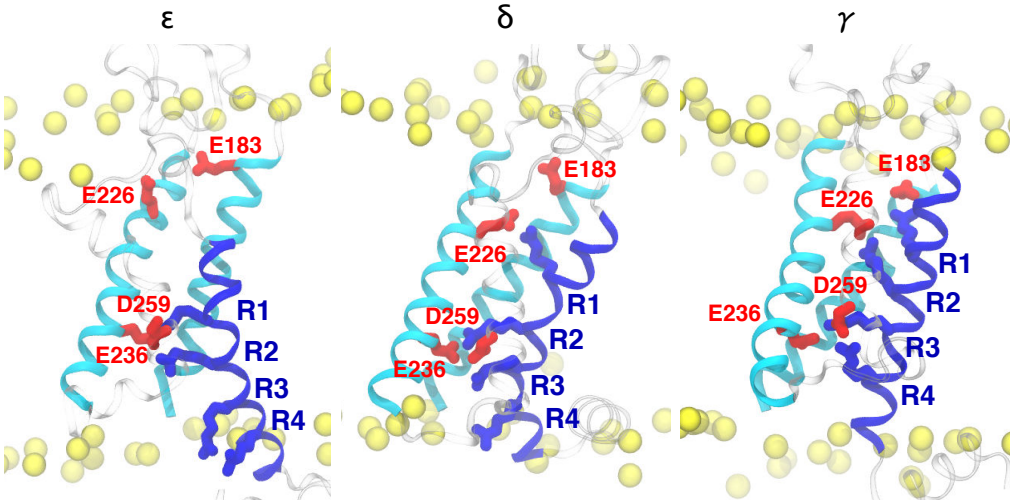

Figure 4.2.1.1. The three states of the voltage sensor that occur during the activation process starting from the fully resting (ε) state and following with two intermediate (δ and γ) states. In ε, R1 and R2 interact with D259 and E236. R3 and R4 are bound to the lipid headgroups of the bottom bilayer leaflet. In δ, R1 switches to E226. R2 and R3 interact with D259 and E236. R4 remains bound to the lipid headgroups. In γ, R1 and R2 interact with E183 and E226. R3 and R4 interact with D259 and E236. K5 and R6 in all three states are bound to the lipid headgroups of the lower bilayer leaflet. These residues are not shown for clarity. S4 is colored in blue; S1 and S2 are present in light-blue. Phosphorus atoms of the lipid headgroups are shown in yellow.

The structures of the three states were embedded in a bare POPC bilayer and in a POPC/PIP_2 bilayer with 10 PIP_2 molecules placed around the voltage sensor in the lower leaflet. We have chosen the systems with an excess of PIP_2 because, for some states of the voltage sensor considered in these simulations (δ and γ), the precise location of a PIP_2 binding site is not known. All six systems were solvated by a 150 mM NaCl solution. As in the previous chapter (see **4.1.1**), we used the same force fields to describe the protein, POPC and PIP_2 lipids: the CHARMM22 with the CMAP correction, CHARMM36 and the compatible force field developed by Lupyan *et al.* respectively [44–46].

The MD simulations were performed using GROMACS 4.6.5 [56]. We have chosen to use GROMACS because of the performance issue: using GROMACS and PLUMED [57] (the software for free energy calculations) we could produce ~ 20 ns of metadynamics simulations per day. For the equilibration, we have followed the protocol similar to the previously considered one (see **4.1.1**): consequent relaxation of the bilayer and the solution (2 ns), the side-chains of the protein (8 ns) and the entire system (90 ns). In each system, the RMSD of the structure from the initial one reached a plateau after ~25 ns of the MD run. The parameters of the MD simulations were taken similar to those considered in **4.1.1**, except the thermostat (instead of Langevin dynamics, this was Nosé-Hoover thermostat) and the barostat (instead of Langevin piston, this was Parinello-Rahman barostat).

4.2.2. Methods: devising the effective collective variable CV_{Ri}

The choice of a collective variable (see **3.3.2**) when estimating the free energy of a transition is not straightforward. It is required that this variable i) is able to distinguish well between the initial, final and all relevant intermediate states along the transition and ii) includes all the relevant slow degrees of freedom of the system. Here, we had to devise a collective variable that describes the transitions of the voltage sensor (ε-δ and δ-γ) and satisfies the aforesaid requirements.

When tracking the conformational rearrangements of the voltage sensor experimentally, one usually measures a gating charge transferred across the membrane (see **2.1.3**, Appendix to Chapter **2**, **2.1**). The gating charge indeed reflects the motion of S4, and its extreme values correspond directly to the initial and final conformations of the voltage sensor. However, its intermediate values may correspond to several rather different conformations of the voltage sensor, meaning that the gating charge is a degenerate collective variable. Hence, using it as a collective variable in the metadynamics simulations will probably result in inefficient sampling of the system's conformational space.

A good collective variable describing the transitions of the voltage sensor should include two principal events that occur during these transitions: i) binding/unbinding of the S4 positive residues to their countercharges, namely, the negative residues of S2, S3 and S1 and the lipid

headgroups of the upper and lower bilayer leaflets, and ii) spatial transition of the gating charges along the vector between two negative binding sites. Considering this, Delemotte *et al.* [58] devised a collective variable CV_{Ri} represented by the following mathematical expression:

$$CV_{Ri} = \kappa x + \left(B_{fin} - B_{init}\right). \quad (4.2.2.1)$$

Here, B_{init} and B_{fin} are the variables reporting the unbinding ($B = 0$) or binding ($B = 1$) of charge R_i to the initial and final binding sites respectively; x is the spatial translation of the charge along the vector joining the two binding sites; κ makes the eq. (4.2.2.1) dimensionally homogenous and can be used to fine-tune the relative weight of the two components. Note, that this form of a collective variable allows one to treat each gating charge transfer (R1, R2, R3, R4, K5 or R6) separately.

The number of possible binding sites for the S4 positive residues is reduced to four: i) phosphate groups of the top lipid bilayer, ii) top protein binding site comprising E226 and E183, iii) bottom protein binding site comprising E236 and D259 and iv) phosphate groups of the bottom lipid bilayer, POPC or PIP_2 (see Figure 4.2.2.1). The binding collective variables B_{init} and B_{fin} depend on the coordination number S between an S4 positive residue and a negative binding site via a sigmoid function (hence the quasi-binary on/off behavior):

$$B(S) = \frac{1}{1+a\cdot e^{-b(S-c)}}, \quad (4.2.2.2)$$

$$S\left(r_{ij}\right) = \sum_i \sum_j e^{-\frac{(r_{ij}-d_0)^2}{2r_0^2}}, \quad (4.2.2.3)$$

where i and j are the indices of the atoms belonging to the positively and negatively charged groups respectively, r_{ij} is the distance between them, d_0, r_0, a, b and c are parameters chosen to fit the equilibrium distribution of bound pairs.

For each of the ε-δ and δ-γ transitions of the voltage sensor, we have considered two CV_{Ri} collective variables (see Figure 4.2.2.1). One of them describes the charge transfer between the binding sites ii and iii (from E226 and E183 to E236 and D259). In the ε-δ and δ-γ transitions, this corresponds to the motion of R1 and R2 respectively. Another collective variable describes the charge transfer between the binding sites iii and iv (from E236 and D259 to the phosphate groups of the bottom lipid bilayer). In the ε-δ and δ-γ transitions, this corresponds to the motion of R3 and R4 respectively. Other positive residues of S4 were restrained at their negative binding sites (*i.e.* the corresponding CV_{Ri}s were restrained to their initial values).

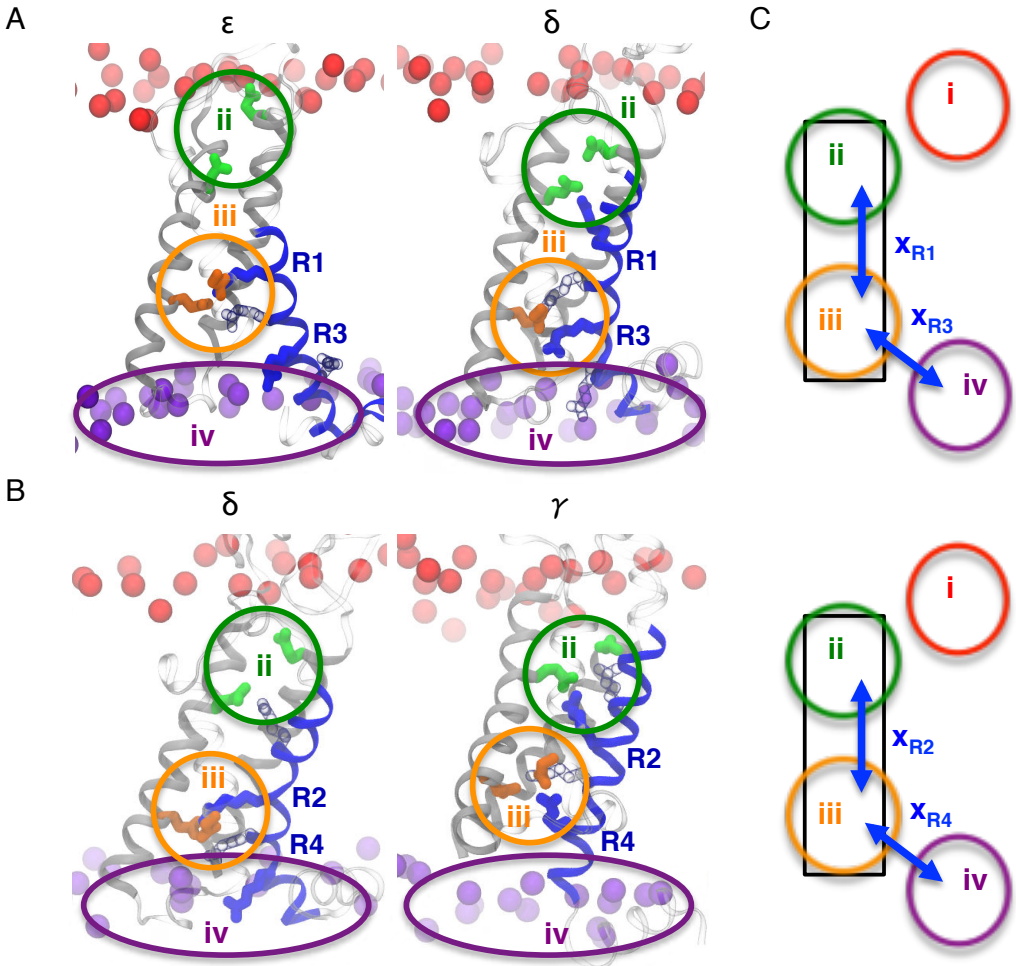

Figure 4.2.2.1. The ε-δ (A) and δ-γ (B) transitions of the voltage sensor in terms of $\boldsymbol{CV_{Ri}}$, a collective variable that reflects binding/unbinding of the S4 positive residues to their countercharges and spatial translation of S4 across the bilayer. A. During the ε-δ transition, R1 transfers between the binding sites ii (shown in green) and iii (shown in orange). Another residue, R3, transfers between the binding sites iii and iv (shown in violet). B. During the δ-γ transition, R1 and R3 remain bound to their countercharges at the binding sites ii and iii respectively. Meanwhile, R2 transfers between the binding sites ii and iii. Another residue, R4, transfers between the binding sites iii and iv. C. Schematic representation of the S4 positive charges' transfer between the negative binding sites during the ε-δ (top) and δ-γ (bottom) transitions of the voltage sensor. x_{R1}, x_{R2}, x_{R3}, x_{R4} stand for the vectors, along which a charge transfer occurs.

The parameters d_0, r_0, a, b and c considered during simulations are listed in Table 4.2.2.1 [58]. These parameters were estimated based on the short MD simulations (4 ns) of the γ state embedded into the bare POPC bilayer. In particular, the d_0 and r_0 parameters were obtained fitting the equilibrium distribution of bound pairs (R1-E183, R1-E226, R2-E183, R2-E226, R3-D259, R3-E236, R4-D259, R4-E236, K5-lipid phosphate group, R6-lipid phosphate group) to $e^{-\frac{(r_i-d_0)^2}{2r_0^2}}$, see the eq. (4.2.2.3). The remaining parameters a, b and c were chosen considering the properties of $B(S)$, see the eq. (4.2.2.2): this function should be 0 when $S(r_{ij}) = 0$ and 1 when the equilibrium

distribution of at least one bound pair is maximum ($e^{-\frac{(r_i-d_0)^2}{2r_0^2}}$ is maximum for at least one r_i); in between of its extreme values $B(S)$ should be similar to $e^{-\frac{(r_i-d_0)^2}{2r_0^2}}$. The parameter κ is empirical: 5.0 or 1.0 for the transfer between ii and iii or between iii and iv respectively [58].

Table 4.2.2.1. Parameters of the S4 positive residues binding to the sites (BS) i to iv.

	BS i and iv	BS ii and iii
d_0 [nm]	0.445	0.395
r_0 [nm]	0.041	0.018
a	0.51	0.46
b	6.95	7.78
c	0.32	0.82

4.2.3. Methods: re-estimation of the free energy in terms of the gating charge Q

Once the conformational space of the system well sampled, we were able to re-estimate the free energy profile in terms of an "experimental" collective variable, *i.e.* the gating charge, using the reweighting scheme proposed by Bonomi *et al.* [59] (see **3.3.5**). In this reweighting scheme, there are two principal steps. First, the evolution of the biased probability $P(R,t)$ during the metadynamics simulations is approximated as:

$$P(R,t+\Delta t) = e^{-\beta(\dot{V}(S(R),t)-<\dot{V}(S,t)>)\Delta t} \cdot P(R,t), \quad (4.2.3.1)$$

Here, $S(R)$ is the biased collective variable written as a function of the conformational state R of the system; $\dot{V}(S,t)$ is the derivative of the time-dependent bias potential. The average in the exponent is calculated in the biased ensemble. And second, the Boltzmann distribution $P_0(R)$ is recovered considering the following expressions:

$$P_0(R) = e^{+\beta\left(V(S(R),t)+c(t)\right)} \cdot P(R,t), \quad (4.2.3.2)$$

$$c(t) = -\frac{1}{\beta}\log\left(\frac{\int e^{-\beta F(S)}dS}{\int e^{-\beta(F(S)+V(S,t))}dS}\right), \quad (4.2.3.3)$$

where $F(S)$ is the free energy estimated in terms of the biased collective variable.

The gating charge Q is linked to the conformation of the voltage sensor λ through the following expression:

$$Q = \frac{\Delta G(\lambda_2,V)-\Delta G(\lambda_1,V)}{V}, \quad (4.2.3.4)$$

where $\Delta G(\lambda, V)$ is the reversible work component, which depends on the applied voltage V. The reversible work can be expressed in terms of the electrical distance $\delta^{\lambda}(r_i)$:

$$\Delta G(\lambda, V) = G(\lambda, V) - G(\lambda, 0) = \Delta V \cdot \sum_i q_i \cdot \delta^{\lambda}(r_i). \quad (4.2.3.5)$$

The latter reflects relation between the local electrostatic potential at a charge q_i, $\varphi^{\lambda}(r_i)$, and the applied voltage:

$$\delta^{\lambda}(r_i) = \frac{\partial}{\partial V}\varphi^{\lambda}(r_i). \quad (4.2.3.6)$$

In practice, the electrical distance is evaluated by performing MD simulations of the system under two different voltages. For each voltage, the local electrostatic potential $\varphi^{\lambda}(r_i)$ is estimated using the Poisson equation:

$$\varphi^{\lambda}(r_i) = \frac{1}{\varepsilon_0}\int_0^{r_i}\int_0^{r'} \rho(r)dr'dr, \quad (4.2.3.7)$$

where $\rho(r)$ is the local charge density. Knowing the local electrostatic potential, one is able to estimate the electrical distance as:

$$\delta^{\lambda}(r_i) = \left[\varphi^{\lambda}(r_i, \Delta V_2) - \varphi^{\lambda}(r_i, \Delta V_2)\right]/(\Delta V_2 - \Delta V_1). \quad (4.2.3.8)$$

Here, we approximated δ^{λ} by the best fit of the measured electrical distance in the γ state:

$$\delta(z) = \frac{1}{1+e^{-m(z-n)}}, \quad (4.2.3.9)$$

where z is the coordinate along the axis perpendicular to the bilayer, $m = 1.80654$ and $n = 0.0949$ [58]. Substituting the eq. (4.2.3.9) into the eq. (4.2.3.5) and then into the eq. (4.2.3.4), one can obtain the mathematical expression for the gating charge:

$$Q(z) = \frac{\Delta V}{V}\left(\sum_i \frac{q_i}{1+e^{-m(z_1-n)}} - \sum_i \frac{q_i}{1+e^{-m(z_2-n)}}\right). \quad (4.2.3.10)$$

This expression was considered in the reweighting scheme of Bonomi *et al.* (see above).

4.2.4. Methods: protocols and parameters of a metadynamics run

The equilibrated systems with the three conformations of the voltage sensor (see **4.2.1**) were taken as starting points for a well-tempered metadynamics run (see **3.3.4**). The metadynamics simulations were performed using PLUMED [57]. In order to speed up our calculations by orders of magnitude we used multiple simulations (walkers). The walkers simultaneously fill the

same free energy well. In this case, the history-dependent potential is given by the sum of the Gaussians laid by all walkers that otherwise do not interact [60]. In total, we have considered 42 walkers per metadynamics run (per transition of the voltage sensor). Among these 42 walkers, the systems with the two states (ε and δ or δ and γ) were spread equally.

We have considered the following parameters of well-tempered metadynamics for the CV_{Ri} collective variables. The Gaussians of 0.1 kJ/mol height was places every 1000 step. ΔT was set to 9000 K. The width of the Gaussian σ was 0.15 for CV_{R1} (the ε-δ transition) and CV_{R2} (the δ-γ transition) and 0.05 for CV_{R3} (the ε-δ transition) and CV_{R4} (the δ-γ transition).

For one walker, we have reached an optimal performance of ~ 20 ns per day (using 96 processors), meaning that for 42 walkers we could sample 840 ns per day (using 4032 processors). Further, we have estimated that in order to obtain a converged free energy surface, we should perform around 3 – 3.5 μs of metadynamics simulations (see **4.2.5**), which requires four days of calculations on the supercomputer. For this project, the simulations were performed on CURIE based in France at the TGCC and SUPERMUC based in Germany at the LRZ (PRACE allocation call #5).

4.2.5. Results: PIP_2 changes the relative stability of the voltage sensor states and also affects the free energy barriers separating them

The free energy surfaces obtained for the ε-δ or δ-γ transitions of the voltage sensor in the POPC and POPC/PIP_2 bilayers are reported in Figure 4.2.5.1. Here, $CV_{R1/R2}$ (R1 and R2 stand for the ε-δ and δ-γ transitions respectively) reflects a charge transfer between the top (from 0 to 2) and bottom (from 4 to 6) protein binding sites. Another collective variable, $CV_{R3/R4}$ (R3 and R4 stand for the ε-δ and δ-γ transitions respectively), is related to a charge transfer between the bottom protein binding site (from -0.75 to 0.25) and the lower bilayer leaflet (from 0.75 to 1.75) (see Figure 4.2.1.1, 4.2.2.1 for the ε, δ and γ conformations).

In both POPC and POPC/PIP_2, the ε and δ states correspond to free energy wells (see Figure 4.2.5.1, top panels for ε and all panels for δ), which indicates their relative stability. On the other hand, the γ state is present as a

free energy well in POPC (see Figure 4.2.5.1, bottom left) but not in POPC/PIP_2 (see Figure 4.2.5.1, bottom right). In the presence of PIP_2, the free energy of γ is rather high and is comparable to the free energy of the adjacent barrier separating it from δ.

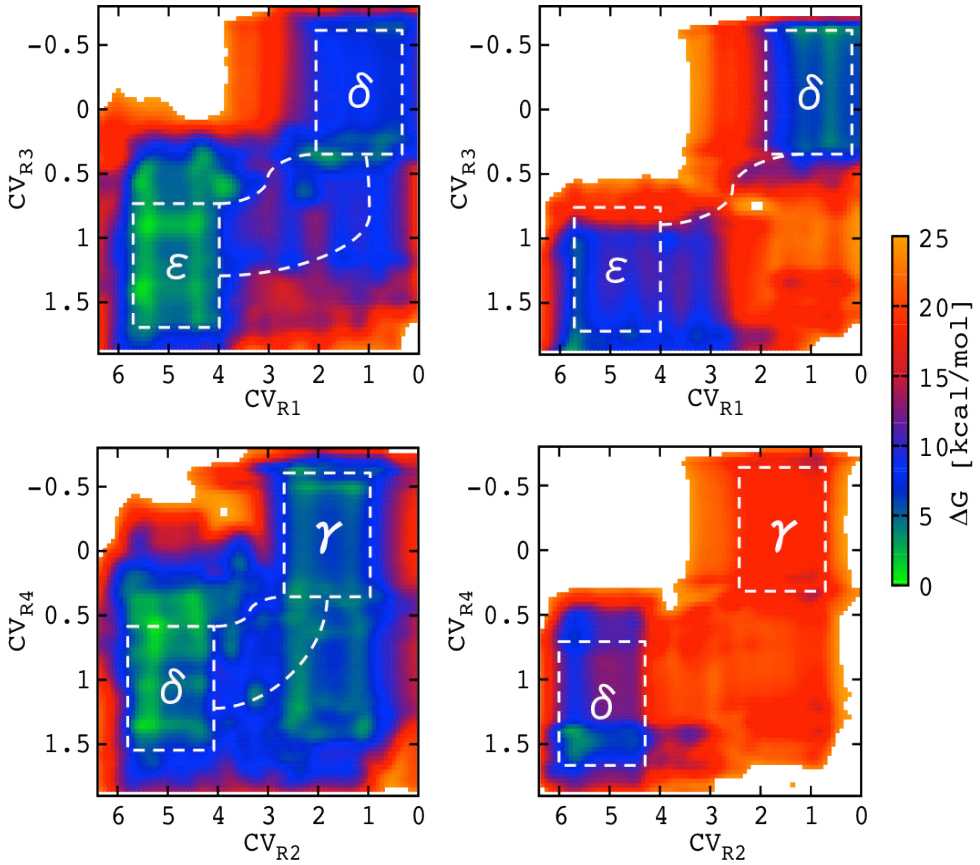

Figure 4.2.5.1. The free energy surfaces underlying the transitions of the voltage sensor: the ε-δ transition in the POPC bilayer (top left), the ε-δ transition in the POPC/PIP_2 bilayer (top right), the δ-γ transition in the POPC bilayer (bottom left), the δ-γ transition in the POPC/PIP_2 bilayer (bottom right). The hypothetical paths are shown as dashed lines, connecting the states (left panels and top right panel). The color-code bar denoting the free energy values is shown on the right.

For the transitions occurring in POPC, there is an additional free energy well at 0-2 of $CV_{R1/R2}$ and at 0.75-1.75 of $CV_{R3/R4}$ (see Figure 4.2.5.1, left panels). In the conformation related to this well, R3/R4 has already switched from the bottom protein binding site to the lower bilayer leaflet, while R1/R2 remains interacting with the top protein binding site. In the presence of PIP_2, however, the latter conformation of the voltage sensor is not stable relative to the defined states as ε or δ (see Figure 4.2.5.1, right panels). Another conformation with intact R3/R4 and transferred R1/R2, when both residues are bound at the bottom protein binding site, is not favorable neither in POPC nor in POPC/PIP_2 (see Figure 4.2.5.1, all panels).

Hence, one can assume that, in the POPC bilayer, the transitions between the states of the voltage sensor (ε-δ or δ-γ) most probably occur either

when both residues (R1/R2 and R3/R4) are transferred simultaneously, or when one residue (R3/R4) switches from the bottom protein binding site to the lower bilayer leaflet, and then consequently another residue (R1/R2) switches from the top protein binding site to the bottom one (see Figure 4.2.5.1, left panels). In the POPC/PIP_2 bilayer, the simultaneous transfer of R1 and R3 during the ε-δ transition is more favorable than the consequent switches of R3 and R1 (see Figure 4.2.5.1, top right panel); the transition from δ toward γ is of low probability due to relative instability of the latter.

Finally, we noticed that the free energy barriers separating ε and δ or δ and γ have different height in POPC and POPC/PIP_2. In particular, these barriers are several kcal/mol higher for the both transitions occurring in the presence of PIP_2 compared to those occurring in the bare POPC bilayer (see Figure 4.2.5.1, all panels).

Further, we re-estimated the free energy of the ε-δ and δ-γ transitions in terms of the gating charge, Q, using the reweighting scheme of Bonomi *et al.* [59] (see **4.2.3**). The result of this re-estimation is reported in Figure 4.2.5.2. Interestingly, the rough free energy surfaces calculated biasing CV_{R1}/CV_{R3} or CV_{R2}/CV_{R4} with many different local minima and saddle points, in the Q space, correspond to rather smooth free energy profiles with only two major minima separated by a unique free energy barrier. These minima correspond to thermodynamically stable states relative to experiments (patch clamp) and encompass large ensembles of structures with defined values of the gating charge, however, with rather heterogeneous patterns of salt bridges. Hereafter, we will call these states according to the starting configuration that they represent: E, Δ or Y for ε, δ or γ respectively.

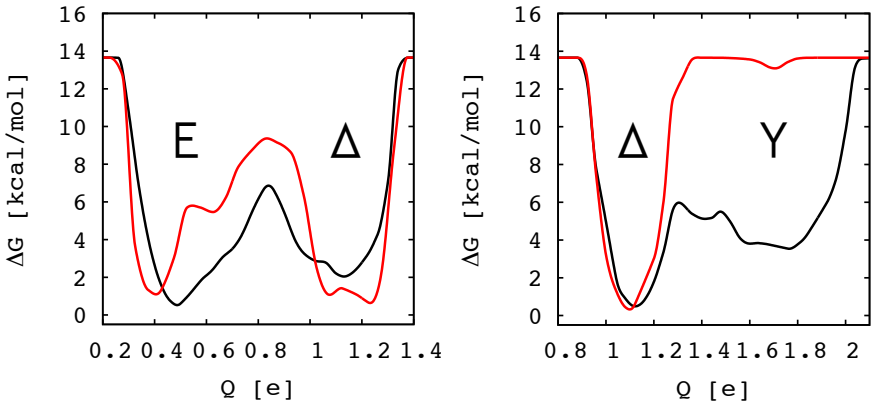

Figure 4.2.5.2. The free energy profiles re-estimated in the $\boldsymbol{Q}$ space. The POPC and POPC/PIP_2 systems correspond to the black and red curves respectively. E, Δ and Y relate to the large conformational ensembles encompassing the ε, δ and γ starting states respectively. The E-Δ and Δ-Y transitions are present on the left and right panels respectively.

The relative stability of the E, Δ and Y states as well as the free energy barriers separating them vary with the transition, E-Δ or Δ-Y, and with the type of a bilayer, in which the voltage sensor was embedded, POPC or POPC/PIP_2. In particular, while in POPC/PIP_2, the E and Δ states have similar free energy, in POPC, the E state is slightly more stable than the Δ one. Moreover, in the presence of PIP_2, both, the activation and deactivation barriers between these states are around 1.9 and 4.0 kcal/mol higher. The latters correspond to 8.3±0.7 and 8.8±0.7 kcal/mol for the transition occurring in the POPC/PIP_2 bilayer or to 6.4±0.7 and 4.8±0.7 kcal/mol for the transition occurring in the bare POPC bilayer (see Figure 4.2.5.2, left panel). Uncertainties (errors) of the free energy were evaluated from fluctuations of the free energy profiles plotted along the metadynamics run. The free energy differences between each of the two stable minima, E or Δ, and the barrier height separating them oscillate around an average after ~2.7 μs (POPC and POPC/PIP_2) (Figure 4.2.5.3, top panels). The corresponding fluctuations are of the order of 0.7 kcal/mol (POPC and POPC/PIP_2).

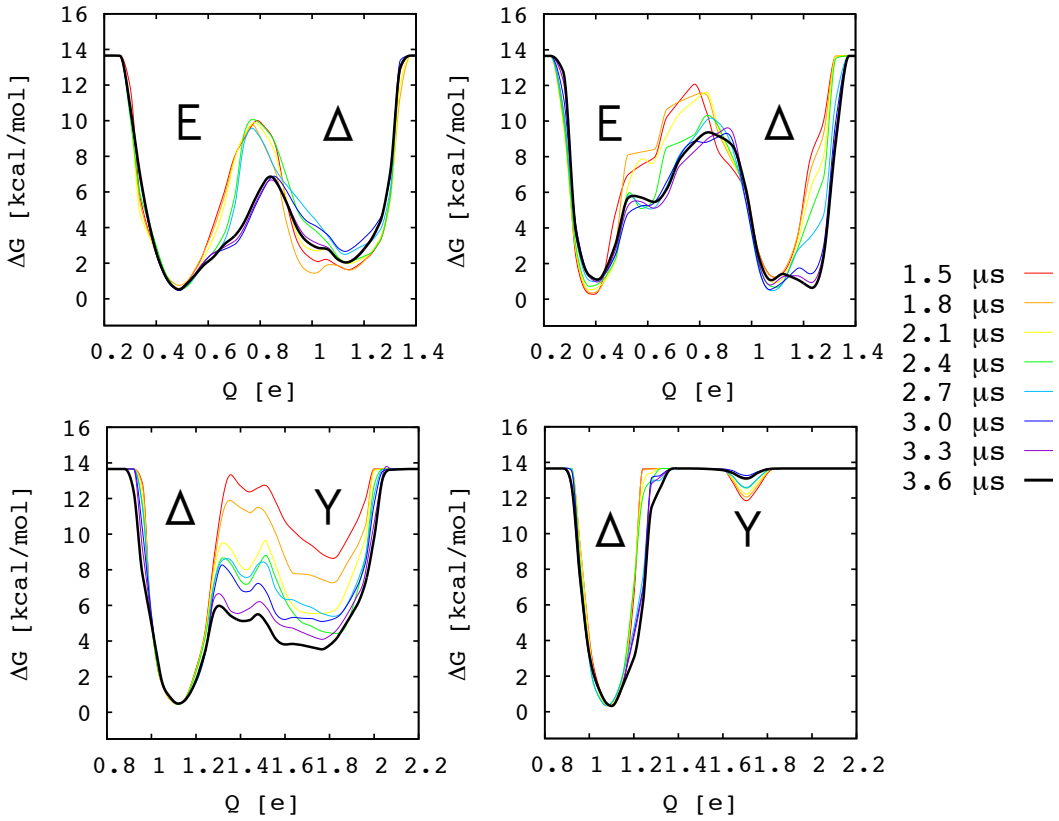

Figure 4.2.5.3. Estimation of an error for the four transitions of the voltage sensor: the E-Δ transition in POPC (top left), the E-Δ transition in POPC/PIP_2 (top right), the Δ-Y transition in POPC (bottom left) and the Δ-Y transition in POPC/PIP_2 (bottom right). The colored lines correspond to the free energy profiles estimated along the metadynamics runs (from 1.5 to 3.6 μs). The black lines relate to the final profiles. The present data demonstrates degree of convergence of the obtained free energy profiles.

For the other transition, Δ-Y, the Y state is less stable compared to the Δ one in both bilayers: the free differences between Δ and Y are 3.0±2.5 kcal/mol in POPC and 12.7±0.5 kcal/mol in POPC/PIP_2 (see Figure 4.2.5.2, right panel). However, while in the bare POPC bilayer, the Y state relates to a free energy well separated from Δ by 2.4±2.5 kcal/mol, in the presence of PIP_2, this well is hardly distinguished from the adjacent free energy barrier. Moreover, in POPC/PIP_2, the activation free energy barrier (from Δ toward Y) is higher compared to the one in POPC (13.3±0.5 and 5.4±2.5 kcal/mol respectively). Uncertainties (errors) were estimated following the same procedure as for the E-Δ transition (see Figure 4.2.5.3, bottom panels).

4.2.6. Results: characterization of the PIP_2 binding to the Kv1.2 voltage sensor

Visualizing the obtained metadynamics trajectories, we have noticed that there are two most probable configurations of the PIP_2 binding to the Kv1.2 voltage sensor. First, PIP_2 may access the S4 positive residue, transferring between the iii and iv binding sites, by diffusing toward S4 between the S3 helix and the S4-S5 linker (see Figure 4.2.6.1A). The same PIP_2 molecule forms a salt bridge with K322 of S4-S5. In this configuration, PIP_2 is located at the binding site between the voltage sensor and the pore, which we have previously identified for the entire TM domain of Kv1.2 (see **4.1**). And second, PIP_2 may access the S4 positive residue, transferring between the iii and iv binding sites, by diving under the voltage sensor between the S1 and S2 helices (see Figure 4.2.6.1B). Note that the latter configuration was observed for the isolated voltage sensor only; for the entire TM domain, the presence of other segments (mostly the T1-S1 linker) constrains the motion of the voltage sensor and reduces an access of PIP_2 from the side of the S1 and S2 helices.

Other S4 residues exposed to the lower bilayer leaflet/solution interface may also interact with a different PIP_2 molecule, which is located in close proximity to the N-terminal part of the S4-S5 linker. The same PIP_2 molecule forms a salt bridge with K312. This configuration partially resembles one of the PIP_2 binding sites of the entire TM domain: the binding site composed of the S4-S5 linkers of adjacent subunits (see **4.1**).

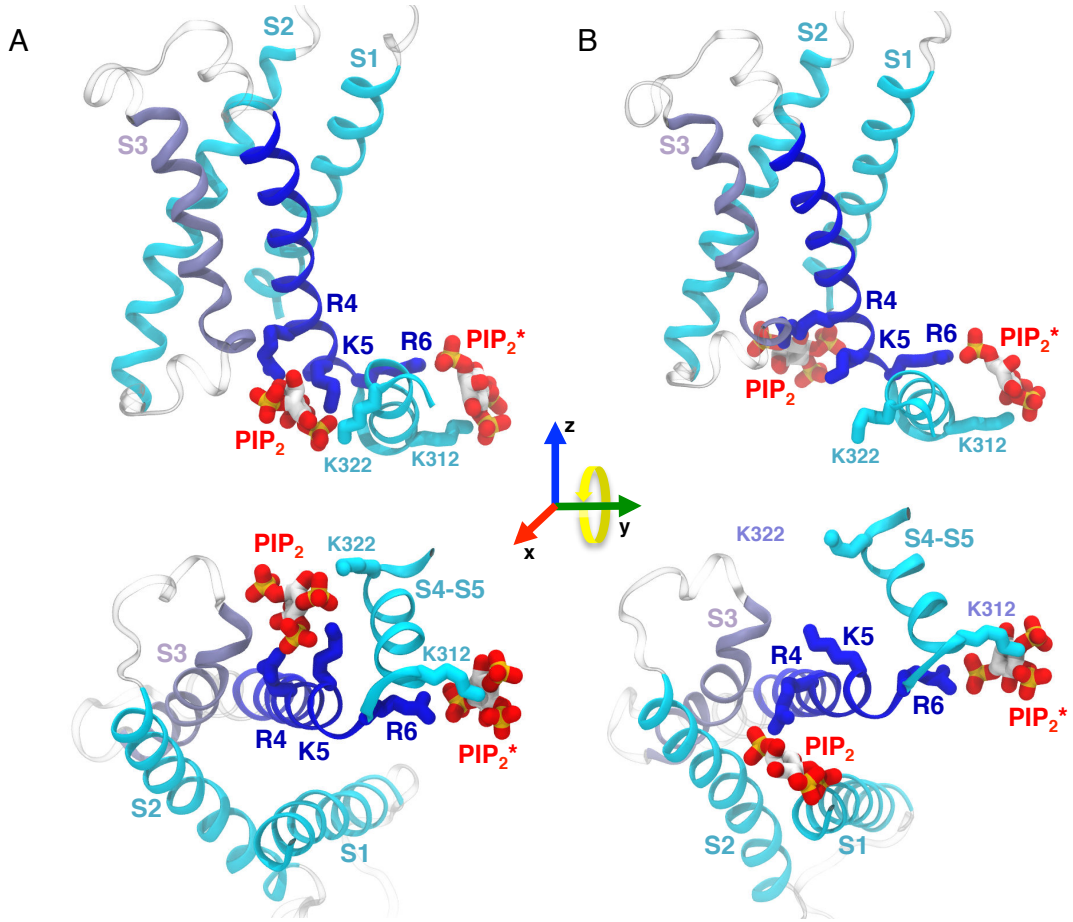

Figure 4.2.6.1. Binding of PIP_2 to the Kv1.2 voltage sensor. A. PIP_2 approaches S4 diffusing between S3 and S4-S5. B. PIP_2 approaches S4 by diving between S1 and S2. The terminal positive residue of S4, R6, interacts with another PIP_2 molecule (labeled with *). Upper and lower panels correspond to the side and bottom views respectively.

4.2.7. Discussion: the Q/V curve of *Shaker* is right-shifted in the presence of PIP_2 due to the drastic destabilization of the Y state

Here, we have estimated the free energy surfaces underlying the ε-δ and δ-γ transitions of the voltage sensor embedded in the two types of the bilayers, POPC and POPC/PIP_2. Using the reweighting scheme of Bonomi *et al.* [59] (see **4.2.3**, **3.3.5**), we further re-estimated the free energy in terms of the gating charge, a collective variable used for experimental measurements. We have found three large ensembles of structures, E, Δ and Y, corresponding to major minima on the free energy profiles and directly relating to the configurations detected in electrophysiological experiments (patch clamp).

The free energy barriers estimated here for the E-Δ or Δ-Y transitions occurring in the POPC or POPC/PIP_2 bilayers correspond to several

kcal/mol, which is consistent with the case when equilibrium properties and kinetics of the activation/deactivation processes are modulated by a membrane potential of the order of tens of mV. Indeed, according to Figure 4.2.7.1, representing the reshaping of the free energy profiles by an applied voltage of ±100 mV, for the E-Δ transition in POPC/PIP_2, the relative stability of the E and Δ states is inversed at negative and positive membrane potentials. E is more stable than Δ at -100 mV, and Δ is more stable than E at +100 mV (see Figure 4.2.7.1, top right panel). In POPC, while at +100 mV E is more stable than Δ, at -100 mV the two states have similar values of the free energy. Moreover, the height of the free energy barrier between E and Δ increases or decreases by ~ 0.8 kcal/mol at -100 mV and +100 mV respectively in the both bilayers. For the Δ-Y transition, the applied voltage also modulates the relative stability of the states and the height of the free energy barrier; however, the Δ state remains more stable than the Y one at both -100 mV and +100 mV.

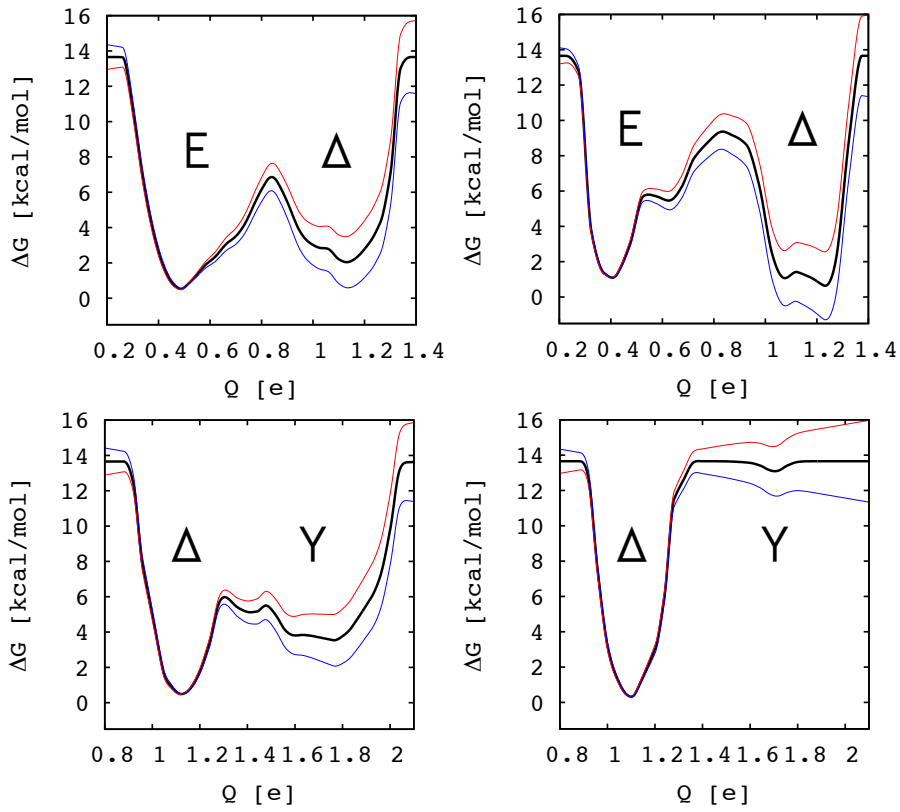

Figure 4.2.7.1. The reshaping of the free energy profiles by an applied voltage of +100 mV (red curve) and -100 mV (blue curve): the E-Δ transition in POPC (top left), the E-Δ transition in POPC/PIP_2 (top right), the Δ-Y transition in POPC (bottom left), the Δ-Y transition in POPC/PIP_2 (bottom right).

Using state of the art methodologies, we have demonstrated that the free energy profiles underlying the transitions of the voltage sensor in the presence of PIP_2 are different from those estimated in the bare POPC bilayer. Thus, for the Δ-Y transition, the activation barrier (in a direction from Δ

toward Y) is around 7.9 kcal/mol higher in POPC/PIP_2 than in POPC. On the other hand, the deactivation barrier (in a direction from Y toward Δ) almost vanishes when PIP_2 is present in the lower bilayer leaflet: it decreases from 2.4 in POPC to 0.6 kcal/mol in POPC/PIP_2. These findings, even though they correspond to one out of four transitions of the voltage sensor are consistent with the experimental data. Indeed, accelerated deactivation [35,41] and slowed activation [41] of *Shaker* induced by PIP_2 can be related to decrease of the deactivation barrier and increase of the activation barrier respectively. Furthermore, the experimental data demonstrates that PIP_2 affects the steady-state activation curve shifting it to more hyperpolarized membrane potentials [35,41]. We relate this loss-of-function effect to dramatic destabilization of the Y state observed in POPC/PIP_2 but not in bare POPC.

For the E-Δ transition, PIP_2 induces an increase of the free energy barrier separating E and Δ in the both directions, *i.e.* during the activation and deactivation. The relative stability of E and Δ remains similar to the one observed in the bare POPC bilayer. Hence, PIP_2 seems to affect only the kinetics of this transition slowing down both the activation and deactivation processes, while the thermodynamics equilibrium between states remains intact. This corresponds only partially to the experimental observations (slowed activation [41]).

So far we have shown that PIP_2 placed in the lower bilayer leaflet affects the kinetics and thermodynamics properties of the two transitions of the voltage sensor, E-Δ and Δ-Y. The two remaining transitions, Y-B and B-A, might be as well modulated by the presence of this lipid. The loss-of-function effect detected experimentally relates to several transitions of the voltage sensor. The exact number of these transitions is not known, however, the latters include the B-A transition since it leads to the channel opening. Moreover, the sigmoid shape of the steady-state activation curve indicates presence of one or several additional transitions, Y-B, possibly Δ-Y and E-Δ. Hence, in order to compare the known experimental data with the simulations, one should explore the free energy profiles underlying all four transitions of the voltage sensor and integrate the PIP_2 effects on each of these transitions. Estimation of the free energy profiles underlying the Y-B and B-A transitions is ongoing.

4.3. Modulation of the Kv7.1 channel by PIP_2

Kv7.1 is a voltage-gated potassium channel expressed in the heart, the intestines, the inner ear and other organs (see **2.2.6**). In the heart, it associates with the KCNE1 auxiliary subunit creating a complex that is responsible for the late phase repolarization of a cardiac membrane potential (see **2.2.1**). Dysfunction of Kv7.1 due to the various point mutations may cause one of the most severe and, importantly, rather common, cardiac disease: the Long QT Syndrome (LQTS). Individuals affected by LQTS have a high risk of sudden cardiac death [61–63] if appropriate treatment is not considered. Designing of pharmacological agents modulating the effects of Kv7.1 mutations requires thorough understanding of the structure-function relationship in the wild type channel and in its mutants. Hence, Kv7.1 attracts a high attention of the scientific community and represents an important object of investigation for both approaches, experimental and computational.

Kv7.1 as well as Kv1.2 is modulated by PIP_2. However, while Kv1.2 is still able to open when this lipid is depleted, in the case of Kv7.1, PIP_2 is absolutely required for opening [27,40,64]. Recent electrophysiological experiments [37] have revealed a mechanism of Kv7.1 modulation by PIP_2: this lipid acts as a coupling element, *i.e.* provides effective communication between the voltage sensor domain and the pore domain. The latters become completely uncoupled when PIP_2 is depleted: the voltage sensor activation does not lead to the pore opening, and the open pore does not promote the VSD activation.

Several residues of Kv7.1 located at the interface between the VSD and the PD were shown to be responsible for PIP_2-dependent coupling [37]. Indeed, selective mutagenesis of the S2-S3 loop, the S4-S5 linker and the S6 terminus, results in impaired coupling due to a decreased apparent affinity for PIP_2 and, therefore, in reduced ionic current (see Figure 4.3.1, blue bars). This effect was accordingly termed loss-of-function. Unexpectedly, mutations of nearby residues also located in the S2-S3 loop and the S4-S5 linker caused

an increase of ionic current, termed gain-of-function (see Figure 4.3.1, red bars).

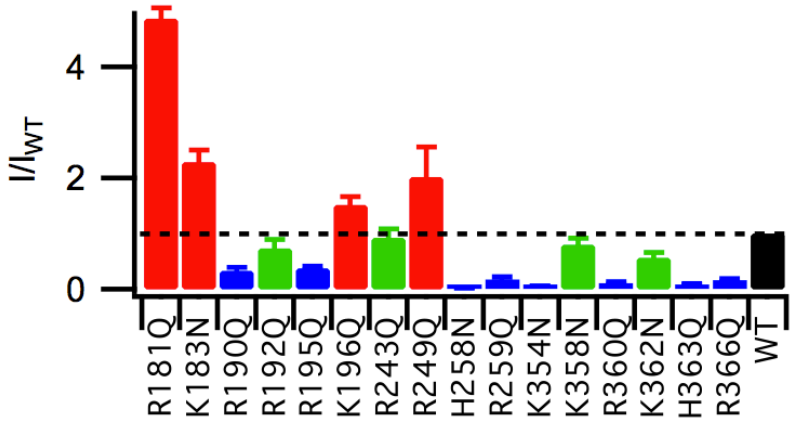

Figure 4.3.1. Mutagenesis of the loss- (blue) and gain- (red) of-function residues of Kv7.1 alters current amplitude compared to the WT (black). Here, bars represent normalized to the WT current amplitude. Mutations with a mild effect on current amplitude are shown in green. The figure is adapted from [37].

Kv7.1 and Kv1.2 belong to the same family of voltage-gated potassium channels and are rather homologous. However, in the latter, coupling does not require PIP_2 but is mediated through protein-protein interactions between the voltage sensor and the pore, in particular, between the S4-S5 linker and the S6 terminus [65–70] (see **2.2.5**). Why in Kv7.1 similar protein-protein interactions are not able to provide an effective communication between the voltage sensor and the pore remains unclear.

To date, the molecular model describing the protein-lipid (PIP_2-dependent) component of coupling in Kv7.1 and, moreover, its relation to the protein-protein one, is unexplored. The interactions between the loss- and gain-of-functions residues with PIP_2 are yet to be characterized. Whether the loss-of-function residues constitute a PIP_2 binding site or alternatively they affect protein-lipid interactions indirectly needs to be further examined. What is the gain-of-function mutagenesis effect that leads to observed increase of ionic current? We attempt here to answer these outstanding questions applying a combined theoretical and experimental approach.

In summary, we identified a PIP_2 binding site of Kv7.1 that involves residues playing a key role in PIP_2-dependent coupling. It appears that these residues are different in the activated/open and resting/closed states of the channel, revealing two modes of protein-lipid interactions: when the VSD is in the resting state, PIP_2 interacts with its S4 helix and is unable to anchor S6. When the pore is open, PIP_2 binds to S6 and moves away from the voltage

sensor releasing S4. Therefore, PIP_2 potentially favors the activated/open and resting/closed states of Kv7.1 over the activated/closed and resting/open ones, *i.e.* couples specific conformations of the voltage sensor to those of the pore. Further we estimated the nonbonded energy of interaction between S4-S5 and S6. Our findings indicate that this interaction is weakened by an electrostatic repulsion between some positive residues located in S4-S5 and S6. When this repulsion was eliminated experimentally by introducing a charge reversal mutation, our collaborators detected a lipid-independent component of coupling, which was not present in the WT Kv7.1. Finally, we discuss how the two components, lipid-protein and protein-protein, may interplay within Kv7.1 and why other channels modulated by PIP_2 (members of the Kv7 family and Kv1.2) have a different response to application of this lipid. This project was accomplished in collaboration with the experimental group of Jianmin Cui at the Washington University in Saint Louis, Saint Louis in USA. The electrophysiological experiments were designed and performed by his Ph.D. student Mark Zaydman.

4.3.1. Methods: preparation of the systems for an MD run

The molecular models of the Kv7.1 channel in its activated/open and resting/closed states were built using homology modeling. As templates, we considered respectively the Kv1.2 crystal structure [42] and the Kv1.2 model obtained from previous MD simulations [12]. The latter represents the Kv1.2 resting/closed state and is consistent with the models obtained by several other computational groups [13,71,72]. The percentage of the homology between Kv1.2 and Kv7.1 is 38% for the PD and 17% for the VSD (see Figure 2.2.6.2). The S2-S3 loop of Kv7.1 was modeled as an α-helix based on the recent NMR data [73].

50 different models of each state were prepared using MODELLER [74]. Among them 10 were chosen based on their best values of the scoring functions (DOPE). The quality of the models was analyzed using PROCHECK [75]. The structures with the highest number of residues in the core regions of the Ramachandran plot and the lowest number of residues in the disallowed regions were selected for the current study. They contained more than 95 % of residues in the favored regions and less than 5 % of residues in the disallowed regions.

For both states (activated/open and resting/closed), the channel was initially embedded in a palmitoyl-oleyl-phosphatidylcholine (POPC) hydrated bilayer. Two systems, with an excess of PIP_2 and with its low concentration, were considered when studying the activated/open state of Kv7.1. For the first system, the lipid molecules of the inner bilayer leaflet closest to the channel were replaced by PIP_2 (an excess of PIP_2). For the second system, only four PIP_2 molecules were placed at the intrasubunit binding site preserving the stoichiometry 1 lipid : 1 channel subunit (low concentration of PIP_2). For the resting/closed state of Kv7.1, we considered the system with a low concentration of PIP_2 only. All the systems were hydrated by a solution at 150 mM KCl salt concentration. CHARMM22 with the CMAP correction and CHARMM36 force fields were used for the protein and POPC respectively [44,45]. To describe PIP_2, the compatible force field developed by Lupyan *et al.* was considered [46]. Water molecules were represented by the TIP3P model [47].

The MD simulations were performed using NAMD 2.9 [48] applying similar parameters as previously described for the MD simulations of Kv1.2 (see **4.1.1**). The following protocol was used for the system with an excess of PIP_2 in order to identify a binding site in Kv7.1: first, the entire protein was constrained during 2 ns to ensure the relaxation of the surrounding lipids and the solution; in a second step, for 6 ns MD, only the backbone atoms were constrained with gradually decreasing force constants, enabling the reorganization of the side-chain groups; finally, all constrains were released and the system was further equilibrated during 100 ns. The RMSD from the initial structure of the channel calculated for the backbone atoms reached equilibrium values after a 50 ns run.

For the quantitative analysis of salt bridges in the WT systems a different protocol was applied. The protein backbone was constrained during longer time (100 ns) allowing PIP_2 to sample possible interactions with the channel's positive residues. Based on this trajectory, the time evolution of salt bridges formation was monitored. Several residues of Kv7.1 interacted with the lipid headgroups temporary, revealing different configurations of the system where corresponding salt bridges were either formed or broken. In total, for the activated/open and resting/closed states we have identified 9 and 8 most frequent configurations respectively. These were considered as starting points for the final equilibration step, including gradual release of the protein backbone and subsequent relaxation of the entire system during 100 ns for each of the starting configurations.

For the mutants' systems of the activated/open and resting/closed states (K183Q/E, R249Q/E and K358E), only one trajectory of 100 ns was considered. We have applied a similar protocol as described previously for the system with an excess of PIP_2.

The analyses were performed for the last 50 ns of equilibration for each system, *i.e.* when the RMSDs from the initial channel structure calculated for CA atoms reached a plateau (see above). To analyze the salt bridges formation between PIP_2 and Kv7.1, we measured the minimal distance between the nitrogen atoms of arginine and lysine charged groups and the oxygen atoms of the PIP_2 phosphates. The salt bridges were assumed formed if this distance was less than 3.2 Å. The probabilities of salt bridge formation were simultaneously estimated for four subunits of the channel as a ratio between the number of frames with a formed salt bridge to its total number. The error bars correspond to a standard deviation (SD) calculated between values obtained from several MD runs of the activated/open and resting/closed states of the WT Kv7.1.

The nonbonded energies of interactions between each residue of the S4-S5 linker and the S6 helix and vice versa were estimated using the per residue decomposition analysis. The nonbonded energy of interactions between the two entire regions, S4-S5 and S6, was calculated also. The following residues were taken into account for both analyses: 247 to 260 of S4-S5 and 323 to 358 of S6. In order to estimate an error, the last 50 ns of the trajectory were divided into 5 consecutive time windows. For each time window a mean value of nonbonded energy of the S4-S5/S6 interactions was calculated. The standard deviation between these values was considered as an error (SE). In total, for the activated/open and resting/closed states of the WT, 9 and 8 trajectories were taken into account respectively. Only one trajectory for each mutant (K183Q/E, R249Q/E and K358E) was analyzed. In the systems with R249E or K358E, frames with the formed R249E-K358 or R249-K358E salt bridges were not considered for the analysis.

The simulations were performed on CURIE based in France at the TGCC and SUPERMUC based in Germany at the LRZ (PRACE allocation call #5).

4.3.2. Results: PIP_2 interacts with the VSD and the PD of Kv7.1 in a state dependent manner

Using homology modeling [74] and the Kv1.2 structure [42] as a template, we built a model of the Kv7.1 channel in its activated/open state. First, we considered the system with an excess of PIP_2 (see **4.3.1**) and investigated the protein-lipid interactions in a well-equilibrated configuration using extensive MD simulations. Within 100 ns of an unconstrained MD run, the negatively charged lipids formed either short- or long-lived (several tens of ns) salt bridges with positive residues of Kv7.1. In order to identify a PIP_2 putative binding site, we estimated the average number of these salt bridges considering each lipid molecule individually (see Figure 4.3.2.1A). Among all lipids, four molecules interacted with several positive residues of Kv7.1 simultaneously, consistent with strong binding of PIP_2 to the channel. Moreover, these molecules formed salt bridges with a terminus of S6 that composes the Kv7.1 gate. Such an interaction, potentially stabilizing the positions of S6 in the open state of the channel, might hint to a reason why PIP_2 is required for Kv7.1 to properly function. The network of salt bridges between these four lipid molecules and Kv7.1 included also residues of the S2-S3 loop and the S4-S5 linker of the same subunit. Accordingly, this PIP_2 binding site was called "intrasubunit" (see Figure 4.3.2.1B, C). Supporting our findings, the regions composing this site were previously identified in several experimental works as important for PIP_2 modulation of the Kv7 family channels: S2-S3 [37,38], S4-S5 [28,37,38] and S6 [27,34,37,76]. A recent molecular modeling study of Kv7.1 in the activated/open state suggested as well S2-S3 and S4-S5 as potential interaction sites of PIP_2 [38]. Specifically, the authors found that PIP_2 interacts simultaneously with both of these regions, in agreement with our findings. However, Zhang *et al.* did not report the formation of salt bridges between PIP_2 and the S6 terminus, which our results suggest to be crucial for PIP_2-dependent coupling (see below).

As the overall PIP_2 lipid content of mammalian cells' membranes is ~ 1 % [26], we tested whether the network of salt bridges was similar at low PIP_2 concentration. Instead of relying on one trajectory, we performed 9 independent MD runs of 100 ns each of a system containing only four PIP_2 lipids, each initially placed at the intrasubunit binding site (see **4.3.1**). We then estimated the probabilities of salt bridges formation between specific positive residues of Kv7.1 and PIP_2. Of particular notice, all interactions previously identified in excess of PIP_2 were also observed at this low concentration, suggesting that these interactions are not affected by the presence of

additional PIP_2. Specifically, R190, R195 of the S2-S3 loop and R249 of the S4-S5 linker were found to form the most frequent interactions with PIP_2 (probability > 75 %) (see Figure 4.3.2.2A). Other residues bound to PIP_2 with lower probabilities (between 25 and 50 %). These include K183 and R192 of the S2-S3 loop and importantly K354 and K358 of the S6 terminus. Finally, the residues K196 and R259 were found to interact intermittently with the PIP_2 headgroups. Interestingly, a single PIP_2 molecule placed at the intrasubunit binding site formed salt bridges with both the loss- (R190, R192, R195 and K354) and the gain-of-function (K183 and R249) residues [37].

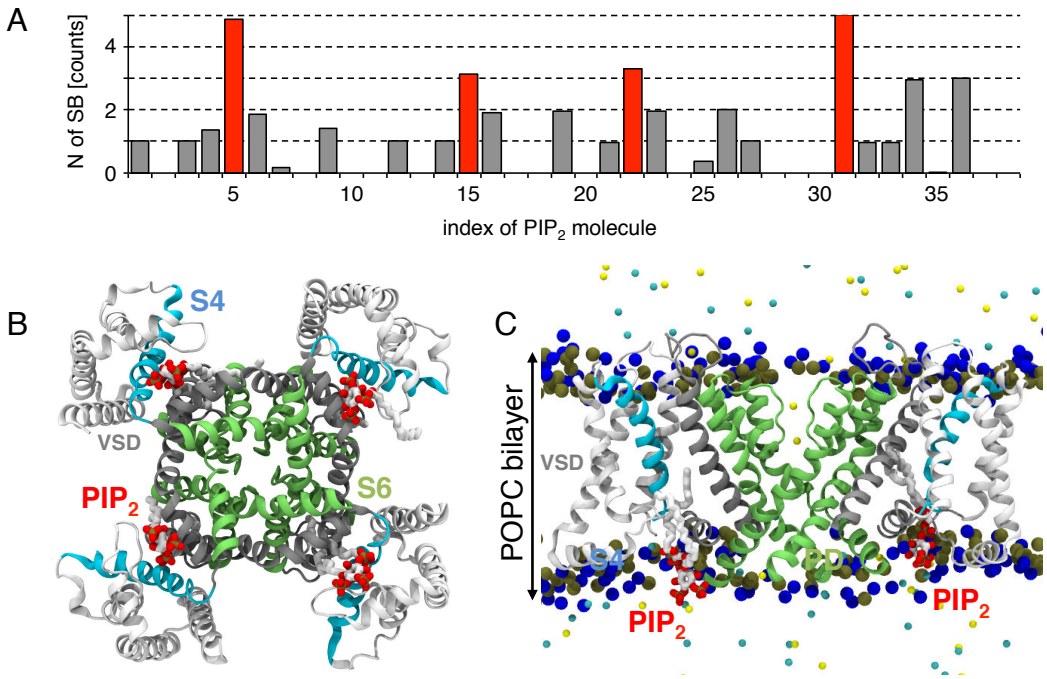

Figure 4.3.2.1. Identification of a PIP_2 putative binding site in Kv7.1. A. The average number of salt bridges formed between each PIP_2 molecule and positive residues of the channel exposed to the interface between the lower bilayer leaflet and the solution. Red bars correspond to PIP_2 molecules bound at the intrasubunit binding site. B, C. The PIP_2 intrasubunit binding site is located at the VSD/PD interface of Kv7.1. The channel in its activated/open state is present in ribbons. Color code: the VSD and the PD are shown in white and green respectively; S4 is highlighted in cyan. PIP_2 molecules are present as sticks with white hydrocarbon tails. Oxygen and phosphorus atoms of PIP_2 headgroups are colored in red and tan. The snapshots were taken after 50 ns of the equilibration. For clarity, only the phosphorus (tan) and nitrogen (blue) atoms of the POPC bilayer headgroups are shown. (B) and (C) correspond to the bottom and side views.

We also investigated the resting/closed channel state. A homology model of Kv7.1 in this state was built using the structure of the resting/closed state of Kv1.2 as a template [12,71] (see **4.3.1**). A system with four PIP_2 molecules initially placed at the intrasubunit binding sites was considered, and 8 MD runs for 100 ns each were performed for data analyses (see **4.3.1**). We found that the probabilities of salt bridges formation between PIP_2 and specific residues of Kv7.1 in this dataset were different from those in the

activated/open state. Most noticeably, PIP_2 molecules were not able to reach any of the S6 termini residues. In contrast, PIP_2 interacted with R237 and R243, the lower positive residues of S4 (see Figure 4.3.2.2A, B). This interaction, never observed in the activated/open state was rather frequent (probability between 50 and 75 %). Finally, PIP_2 interactions with R190, R249 and K183 remained as in the activated/open state but R195 was found to interact with PIP_2 with a lower probability (~ 50 %).

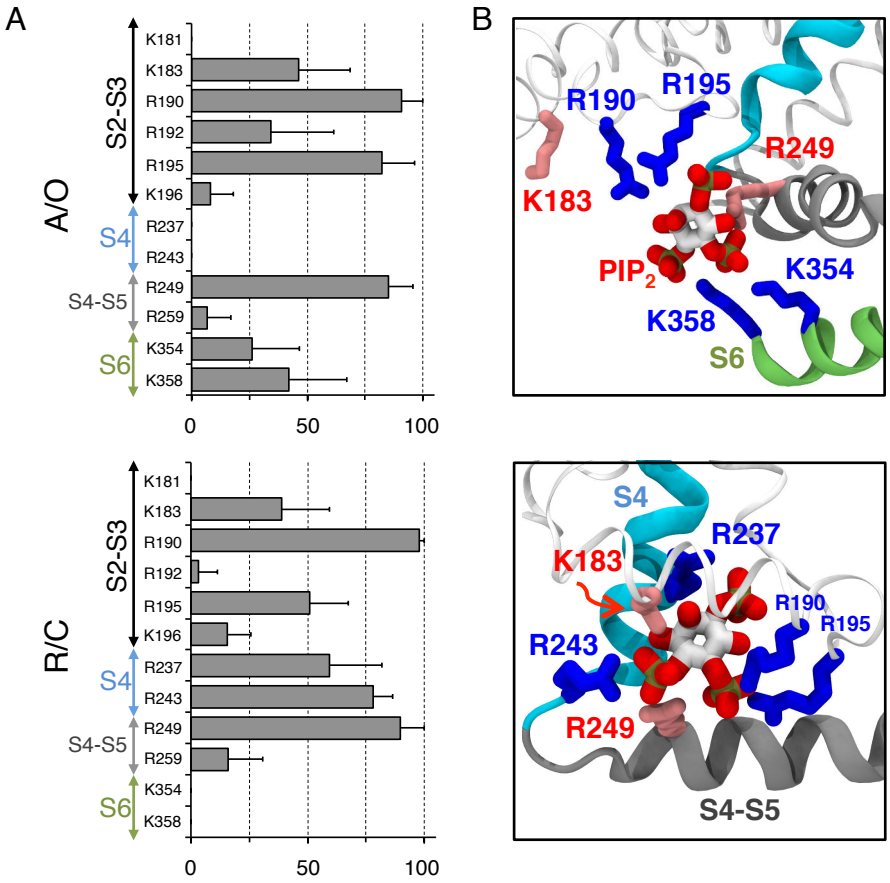

Figure 4.3.2.2. Coordination of PIP_2 by residues composing the intrasubunit binding site in the activated open (A/O, top panels) and resting/closed (R/C, bottom panels) states of Kv7.1. A. Probabilities of salt bridges formation between PIP_2 and positive residues of Kv7.1 among all subunits. Multiple MD runs are considered. The standards deviations (SDs) are represented as bars. B. Representative snapshots of the MD runs. Residues coordinating PIP_2: K183, R190 and R195 of the S2-S3 loop, R237 and R243 of S4, R249 of the S4-S5 linker, K354 and K358 of the S6 terminus. K183 and R249, the gain-of-function residues, are highlighted in red.

Interestingly, the most probable location of PIP_2 was slightly different in the two states of Kv7.1: the lipid was either shifted to S6 in the activated/open state or to the voltage sensor in the resting/closed state (see Figure 4.3.2.3). Hence, the model emerging from the extensive MD simulations predicts two modes of protein-lipid interactions each favored in a specific channel state. These modes, hereafter called activated/open and

resting/closed, differ by the residues involved in PIP_2 coordination, and by the location of this lipid with respect to the VSD or the PD.

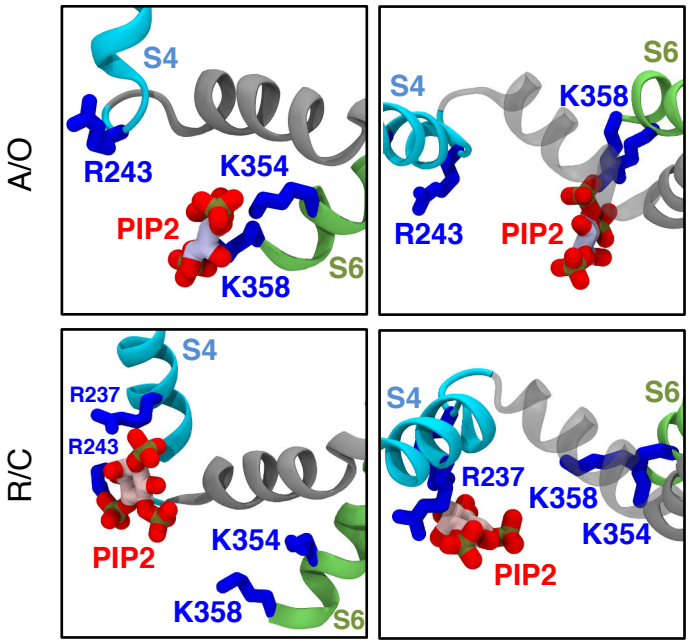

Figure 4.3.2.3. The equilibrium position of PIP_2 is different in the activated/open (A/O, top panels) and resting/closed (R/C, bottom panels) state of Kv7.1. Side (left panels) and top (right panels) views of the representative equilibrium position of PIP_2 at the intrasubunit binding site. Note that PIP_2 anchors the S6 terminus in the A/O state of Kv7.1. When the channel is R/C, the lipid is shifted toward the VSD to interact with the bottom of S4.

4.3.3. Results: mutations of K183 and R249, the gain-of-function residues, favor the activated/open mode of protein-lipid interactions

Mutagenesis of the Kv7.1 gain-of-function residues, namely K183 (S2-S3) and R249 (S4-S5), increases the ionic current [37] (see Figure 4.3.1). In order to determine a molecular-level rational for this effect, we performed additional MD simulations considering the K183Q/E and R249Q/E mutants in the two states of the channel. In the resting/closed state, three mutants (K183Q/E and R249Q) had a non-zero probability to form salt bridges between S6 and PIP_2, in contrast to the WT case, where S6 was not accessible to these lipids (see Figure 4.3.3.1A). In the activated/open state, the residues of the S6 helix of three mutants (K183Q/E and R249E) had higher probabilities to interact with PIP_2 compared to the WT (see Figure 4.3.3.1A). Hence, going from the WT to the K183Q/E mutants, these probabilities increased from 26 % to 60/45 % for K354, and from 42 % to 65/70 % for K358. Similarly, going from the WT to the R249E mutant, these probabilities increased from 26 % to 63 % for K354, and

from 42 % to 95 % for K358. Note here that for each mutant in the two states only one MD trajectory of 100 ns was considered. However, the effect of mutagenesis is unambiguous as the estimated probabilities changes upon a mutation are larger than the error bars obtained for the WT. The simulations indicated also that all the mutations induced a change in the equilibrium position of PIP_2 at the intrasubunit binding site. Indeed, in the WT resting/closed state, PIP_2 is close to the bottom positive residues of S4, while in all four mutants PIP_2 moved toward S6. Similarly, in the open/activated state of the mutants, the lipid was located closer to the S6 terminus and further away from the VSD compared to the WT (see Figure 4.3.3.1B).

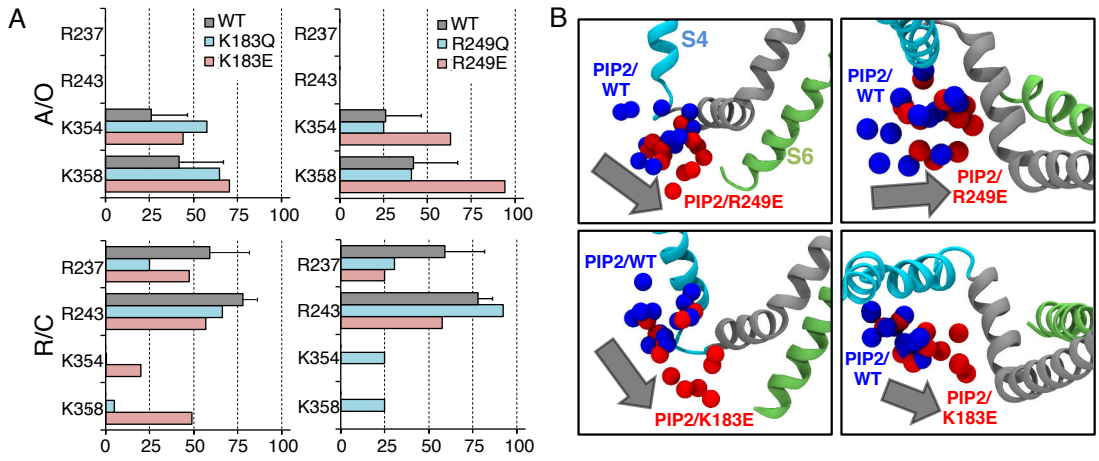

Figure 4.3.3.1. Mutations of the Kv7.1 gain-of-function residues, K183 and R249, shift the position of PIP_2 toward S6 in both the A/O (top panels) and R/C (bottom panels) states of the channel. A. Probabilities of salt bridges formation between PIP_2 and residues of Kv7.1. B. Shift of PIP_2 (grey arrow) between positions in the WT (blue spheres) and in the gain-of-function mutants (red spheres). Here, the systems with the most significant shifts are reported: R249E in the A/O state (left panel: side and top views) and K183E in the R/C state (right panel: side and top views).

In summary, neutralizing or charge reversing the gain-of-function residues, R249 or K183, induces (i) a redistribution of salt bridges between Kv7.1 and PIP_2; and (ii) a shift of this lipid toward S6, favoring the activated/open mode of protein-lipid interactions, which is consistent with the gain-of-function effect. This result provides an additional support to the molecular models used here.

4.3.4. Results: the S4-S5/S6 interactions are destabilized by repulsion between their positively charged residues

We analyzed the interactions between S4-S5 and S6 in the WT channel by

performing the per-residue decomposition analysis of the nonbonded energy (see **4.3.1**). The analysis revealed that, in the Kv7.1 activated/open and resting/closed states, unlike other residues, R249 of S4-S5 and K358 of S6 have a positive contribution, *i.e.* they destabilize the interaction between the S4-S5 linker and S6 (see Figure 4.3.4.1A). Therefore, we speculate that R249 and K358 weaken the protein-protein component of the VSD/PD coupling in the native channel.

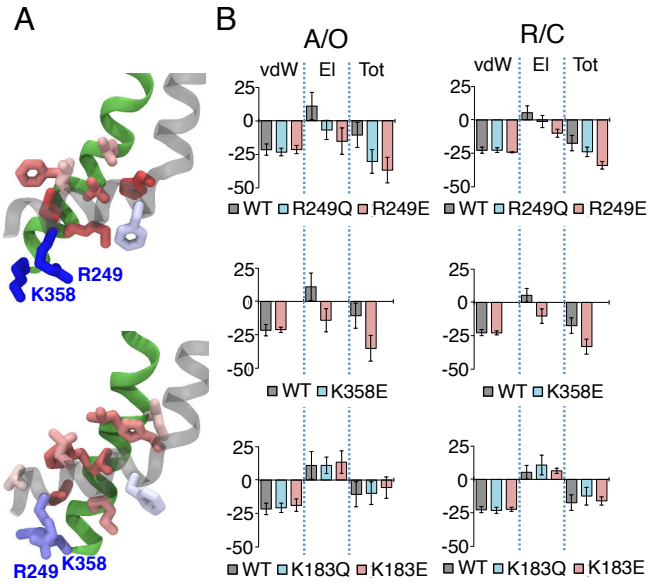

Figure 4.3.4.1. Several positive residues of S4-S5 and S6 modulate the strength of the S4-S5/S6 interactions. A. Per-residue decomposition analysis of the nonbonded energy of interaction between S4-S5 and S6 performed in the A/O (top) and R/C (bottom) states of the WT channel. The residues are colored corresponding to their contribution. R249 and K358 shown in blue provide a positive (repulsive) contribution. Several residues highlighted in red stabilize the interaction between these two regions. B. The nonbonded energies of the S4-S5/S6 interactions of R249Q/E (top panel), K358E (middle panel) and K183Q/E (bottom panel) compared to the WT's one reported for the A/O (left) and R/C (right) states of Kv7.1. Here vdW, El and Tot correspond to the van-der-Waals, electrostatic and total nonbonded energy respectively. The error bars (SE) are present.

We analyzed the nonbonded energy of the S4-S5/S6 interactions when K358 and R249 residues were mutated, considering the previously obtained trajectories for R249Q/E and a new MD run for K358E. Neutralization and charge reversal of R249 or charge reversal of K358 lowered this energy due to elimination of the electrostatic repulsion (see Figure 4.3.4.1B). Moreover, in both states of the channel, we observed a low probability of salt bridge formation between R249E and K358 (or R249 and K358E), which contributed additionally to the strengthening of the S4-S5/S6 interactions.

Since the molecular models suggest that the S4-S5/S6 interactions of the K358E mutant are strengthened, we suggested detecting its protein-protein component of coupling experimentally using the voltage-clamp

fluorometry method. In the previous studies of our collaborators [37], probing the Kv7.1 VSD/PD coupling they introduced the L353K mutation, which locked the channel's pore in an open state. L353 is located near the putative bundle crossing. Introduction of a positive or negative residue at this position results in a channel that remains open [77] as if the mutual electrostatic repulsion among the introduced charges destabilizes the closed state of the pore domain. When the two domains of the L353K mutant, the VSD and the PD are coupled, the pore being locked open facilitates the activation of the voltage sensor, which can be detected as a leftward shift of the F/V curve. After PIP_2 depletion this shift is completely eliminated, indicating a predominance of the protein-lipid component of coupling in the L353K mutant [37] (see **2.3.7**, Figure 2.3.7.1).

When similar experiments were performed for the K358E/L353K double mutant, depletion of PIP_2 reduced but did not eliminate the leftward shift of the F/V curve (see Figure 4.3.4.2A, comparing the solid/dashed red and solid green curves). Furthermore, in the absence of the lock open mutation, PIP_2 depletion resulted in a right shift of the K358E F/V curve, as if the closed pore hindered the voltage sensor activation (see Figure 4.3.4.2B, comparing the solid red and solid green curves). This right shift was not observed in similar experiments with the WT Kv7.1 [37] (see Figure 2.3.7.1). Furthermore, the F/V and G/V curves measured for the WT Kv7.1 are superimposable as if the multiple voltage sensor movements are not required to precede the gate opening [78], which is consistent with rather weak coupling between the voltage sensor and the pore. However, in the K358E mutant, the F/V and G/V curves were separated by a shift (see Figure 4.3.4.2B), which can be interpreted as a stronger interaction between the voltage sensor and the pore in the resting/closed state compared to the WT Kv7.1. Altogether, these experiments demonstrate the presence of a lipid-independent component of coupling in K358E, which we attribute given our modeling data to protein-protein interactions.

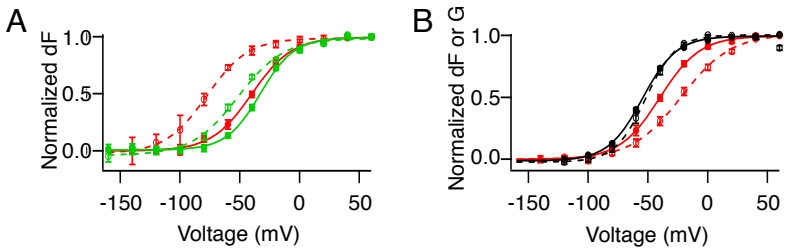

Figure 4.3.4.2. The protein-protein and protein-lipid components of coupling detected in K358E. A. Normalized F/V curves of K358E (red solid), K358E/L353K (red dashed), K358E+CiVSP (green solid) and K358E/L353K+CiVSP (green dashed). B. Normalized F/V (solid) and G/V (dashed) curves of K358E (red) and of the WT (black). Note that the latters are superimposed.

Motivated by our modeling results, our collaborators also tested the importance of electrostatic interactions between R249 and K358 for the Kv7.1 gating. In a double mutant cycle analysis [79], they found that both the R249E and K358E single mutations resulted in a delay of the current onset (see Figure 4.3.4.3A, top) and in a right shift of the G/V curves (see Figure 4.3.4.3A, bottom), consistent with a stronger interactions between the voltage sensor and the pore in the resting/closed state compared to the WT Kv7.1. The double mutation R249E/K358E caused a non-additive effect on the apparent free energy of the closed to open transition (see Figure 4.3.4.3A, bottom). These experiments indicate that residues 249 and 358 indeed interact in the WT Kv7.1. Neutralization of R249 or K358 produced intermediate effects compared to those of the charge reversal, supporting the importance of electrostatic interactions between these two residues (see Figure 4.3.4.3A).

The electrostatic repulsion between the S4-S5 linker and S6 is probably not limited to R249-K358 interactions. To test this hypothesis, our collaborators reversed the charges of nearby basic residues of S6. Similarly to R249E and K358E, they found that K354E, R360E, K362E, and R366E all caused a delay of the current onset (see Figure 4.3.4.3B, top) and a rightward shift of the G/V curve (see Figure 4.3.4.3B, bottom), confirming the existence of a functionally significant network of electrostatic interactions between S4-S5 and S6 residues. In summary, in the WT Kv7.1, R249 repels positively charged residues of S6, weakening the protein-protein component of coupling.

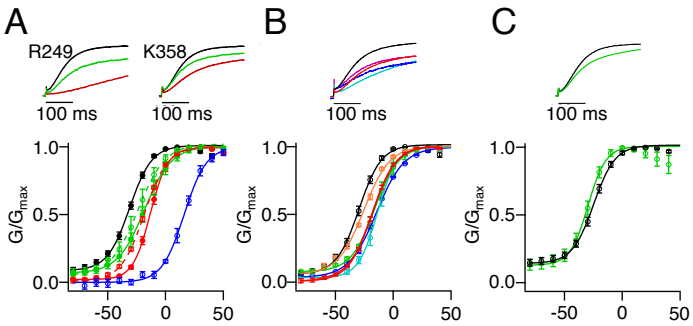

Figure 4.3.4.3. Mutagenesis of basic residues of the S4-S5 linker and the S6 terminus indicated the importance of electrostatic interactions between these two regions. A. Normalized currents of the WT (black), charge neutralizing (green – R249Q, K358N) and charge reversing (red – R249E, K358E) mutations (top panel). The G/V curves of the WT (black), R249Q (green solid), R249E (red solid, ΔΔG=0.56±0.14 kcal/mol), K358N (green dashed), K358E (red dashed, ΔΔG=0.68±0.07 kcal/mol) and R249E/K358E (blue solid, ΔΔG=2.60±0.13 kcal/mol) (bottom panel). B. Normalized currents (top panel) and the G/V curves of the WT (black), K354E (blue), K358E (red), R360E (cyan), K362E (magenta) and R366E (orange) (bottom panel). C. Normalized currents (top panel) and the G/V curves of the WT (black), K183N (green) (bottom panel).

For completeness, we checked whether the other gain-of-function residue, K183, affected the S4-S5/S6 interactions. The analysis of the nonbonded energy for the K183Q and K183E mutants did not reveal any significant changes compared to the WT (see Figure 4.3.4.1B), suggesting that K183 does not affect the protein-protein component of coupling. Experimentally, unlike the R249 and K358 mutations, K183N did not cause any delay in current onset (see Figure 4.3.4.3C, top) or right shift of the G/V curve (see Figure 4.3.4.3C, bottom), confirming the model prediction that this residue is not involved in the protein-protein component of coupling.

4.3.5. Discussion: PIP_2 is prominent for Kv7.1 due to weakened interactions between S4-S5 and S6

Coupling is an effective communication between the VSD and the PD of a channel that provides triggering conformational changes in the pore as a response of those in the voltage sensor. Recent experiments [37] have demonstrated that, in Kv7.1, coupling requires the presence of PIP_2. In this study, we took advantage of molecular modeling in order to uncover the details of PIP_2-dependent coupling. The MD simulations of Kv7.1 embedded in the bilayer containing PIP_2 revealed two modes of specific protein-lipid interactions. When the VSD is in the resting state, PIP_2 is located close to S4 interacting with its lower residues (see Figure 4.3.2.2). Being close to the VSD but far from the PD, this lipid is unable to reach S6 and to hold it close to the membrane/solution interface. As a result, the pore might relax to a conformation corresponding to the closed state, *i.e.* favors the resting/closed state of the channel. In contrast, when the pore is open, PIP_2 is shifted close to the PD and forms salt bridges with its S6 terminus (see Figure 4.3.2.2). Located further from S4, this lipid cannot interact with its positive residues, which potentially facilitates the activation of the voltage sensor, *i.e.* favors the activated/open state. Overall the present molecular model confirms that PIP_2 acts as a coupling element as was previously proposed [37]: PIP_2 potentially stabilizes the resting/closed and activated/open states of Kv7.1 over the resting/open and activated/closed ones.

Besides PIP_2-dependent coupling, in Kv7.1, there are protein-protein (S4-S5/S6) interactions that potentially mediate communication between the VSD and the PD. Here we demonstrated that these interactions are weakened by the electrostatic repulsion among positive residues of S4-S5 and S6.

A crosstalk between the protein-protein and protein-lipid components of coupling may be mediated by positive residues that are involved in the S4-S5/S6 interactions and, at the same time, participate in the PIP_2 intrasubunit binding site. In the K354E and R360E mutants, for example, the protein-lipid component of coupling is potentially impaired. We assume this based on the previous findings of our collaborators [37] where neutralization of these residues resulted in a severe loss of current attributed to disrupted interactions between Kv7.1 and PIP_2. On the other hand, introducing K354E or R360E mutations provides a negative charge on S6 and should strengthen the protein-protein component of coupling, similar to the case of K358E reported above (see Figure 4.3.4.1, 4.3.4.2). Thus, despite the impaired protein-lipid component of coupling the communication of the VSD with the PD might be still ensured through the strengthened protein-protein one. Indeed, for K354E and R360E, experiments showed only a mild decrease of current amplitude compared to the WT (see Figure 4.3.5.1), suggesting that the overall coupling between the VSD and the PD, in these mutants, is impaired only slightly.

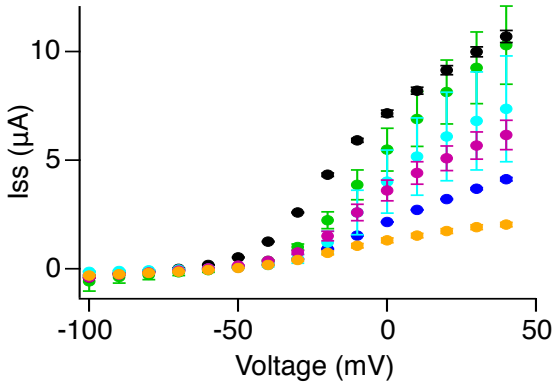

Figure 4.3.5.1. In K354E and R360E, there is only mild decrease of ionic current compared to the WT. The I/V curves of the WT (black), K354E (blue), K358E (green), R360E (cyan), K362E (magenta) and R366E (orange) mutants.

In the MD simulations we have considered the truncated Kv7.1 channel (residues 122 to 358), neglecting therefore its cytoplasmic domain. So far, two hypothetical PIP_2 binding sites located at this domain were proposed for members of the Kv7 family. The first one, the helix A-B linker suggested for Kv7.2-5 [80], is not relevant here since this helix linker is not conserved in Kv7.1. The second one, located at the distal C-terminus of Kv7.1, involves R539 and R555. R539W and R555C mutations (associated with long QT syndrome) were shown to decrease the channel's apparent affinity to PIP_2 [28]. Considering this effect, two hypotheses may be put forward: R539 and R555 residues either (i) form an independent PIP_2 binding site, or (ii) contribute directly/allosterically to the intrasubunit one found here. We found that the

R555C mutation eliminated the shift of the F/V curve caused by the lock open mutation, L353K (see Figure 4.3.5.2A), indicating that R555C disrupts the VSD/PD coupling. Since the depletion of PIP_2 from the intrasubunit binding site also disrupts the coupling in Kv7.1, we conclude that the distal C-terminus and the intrasubunit sites are not independent, and they affect each other either directly or allosterically. R539W had a less severe impact on the F/V curve (see Figure 4.3.5.2B). Recent experimental findings suggest that this residue may interact with other membrane elements besides PIP_2 [3].

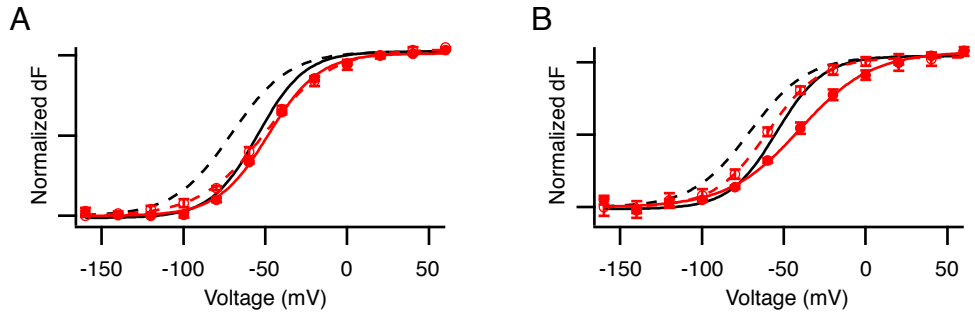

Figure 4.3.5.2. R555 and R539 residues compose the PIP_2 distal C-terminus site in Kv7.1. A. The F/V curves of the WT (black solid), L353K (black dashed), R555C (red solid) and R555C/L353K (red dashed). B. The F/V curves of the WT (black solid), L353K (black dashed), R539W (red solid) and R539W/L353K (red dashed).

In the previous work of our collaborators [37], they have indicated importance of R259 for sensitivity of Kv7.1 to PIP_2 lipids (see Figure 4.3.1). In the present simulations, however, this residue interacted rather rarely with PIP_2 placed at the intersubunit binding site. R259 is located at the C-terminus of the S4-S5 linker and, in our molecular model of Kv7.1, is separated from the intersubunit binding site by more than 15 Å distance and, additionally, by bulky hydrophobic F256. Interestingly, in the system with an excess of PIP_2, we observed that four lipid molecules, distinct from those bound at the intersubunit site, interacted with R259, which allows us to hypothesize the existence of a second binding site in Kv7.1. Recent experimental and computational results indicate as well that the TM part of Kv7.1 might comprise two PIP_2 binding sites [39].

The intrasubunit binding site shown here to play a crucial role in Kv7.1 is similar to the one previously found for the Kv1.2 channel [15,35,41]. In the Kv1.2 resting/closed state, PIP_2 interacts with the bottom of S4, in particular with the lower gating charges R303, K306 and R309. In its activated/open state, PIP_2 is shifted toward the gate anchoring R419 of S6. Hence, in Kv1.2 as well, PIP_2 appears to interact with the VSD/PD in a state dependent manner. Despite a similar overall architecture and, moreover, a state-dependent manner of protein-lipid interactions, the response of these channels to PIP_2 is

not identical. For both Kv1.2 and Kv7.1, application of this lipid leads to an increase of ionic current [27,35,40,41]. However, while in the case of Kv7.1, PIP_2 is absolutely required for opening, Kv1.2 is still able to open when this lipid is depleted. Considering the alignment between these two channels, we note that several S6 residues of Kv1.2 are not conserved in Kv7.1 (see Figure 4.3.5.3): (i) F416, involved in the S4-S5/S6 interactions [65,68,69,81], is substituted into K354; (ii) E420, which forms a salt bridge with the S4-S5 linker [82], strengthening the protein-protein component of coupling, is substituted into K358. It is interesting to note that, in Kv7.1, both K354 and K358, on the one hand, destabilize the S4-S5/S6 interactions (see Figure 4.3.4.1A) and, on the other hand, participate in PIP_2 coordination (see Figure 4.3.2.2). Furthermore, in Kv7.1, there is a long S2-S3 loop that provides two additional positive residues (R190 and R195) for PIP_2 coordination. In Kv1.2, S2-S3 is not conserved: it is shorter by nine residues, and R195 is substituted to a neutral residue (T252). These outlined differences could explain the relative predominance of the protein-lipid component of coupling over the protein-protein one in Kv7.1 compared to Kv1.2.

Figure 4.3.5.3. The alignment between Kv1.2 and the members of the Kv7 subfamily (from Kv7.1 to Kv7.4): the S4-S5 linker and the S6 helix are shown. The residues of Kv1.2 participating in coupling between the voltage sensor and the pore (K322, F416 and E420) are present in orange. In Kv7.1, F416 and E420 are substituted into K354 and K358 respectively (shown in blue). In other members of the Kv7 subfamily, while F416 is substituted into lysine (shown in blue), E420 is neutralized (glutamine). Additionally, the nearby residues (shown in red) are negatively charged.

As for Kv7.1, other members of the Kv7 family require PIP_2 to open [27]. However, several measured characteristics of their gating are different: (i) the F/V and G/V curves of Kv7.1 overlap [78], while the Q/V and G/V curves of Kv7.4 are separated by a shift [83]; (ii) following depolarization, in Kv7.1, a current onset occurs immediately, while there is delay of current, in Kv7.2/Kv7.3 (see Figure 4.3.5.4A, B); and (iii) an instantaneous current specific for Kv7.1 [84] is not observed for Kv7.2/Kv7.3 (see Figure 4.3.5.4C). Looking more carefully at the channels' sequences, we noticed that several residues of S6 composing the intrasubunit binding site or located in its proximity are substituted in Kv7.2-5 (see Figure 4.3.5.3). Thus, K358 is neutralized (Q), and two nearby residues, Q357 and N365, are substituted to a glutamate. When we reversed the charge of K358, in Kv7.1, we observed

similar gating features as Kv7.2-5 ones: (i) the F/V and G/V curves were separated (see Figure 4.3.4.2B); (ii) current onset was delayed (see Figure 4.3.4.3A, top); and (iii) the instantaneous current was reduced (see Figure 4.3.4.3A, bottom). Furthermore, other charge reversal mutations of S4-S5 and S6 also resulted in delayed onset and reduced instantaneous current (see Figure 4.3.4.3B). These results suggest that different gating among the Kv7 family members might be attributed to different strength of their S4-S5/S6 interactions.

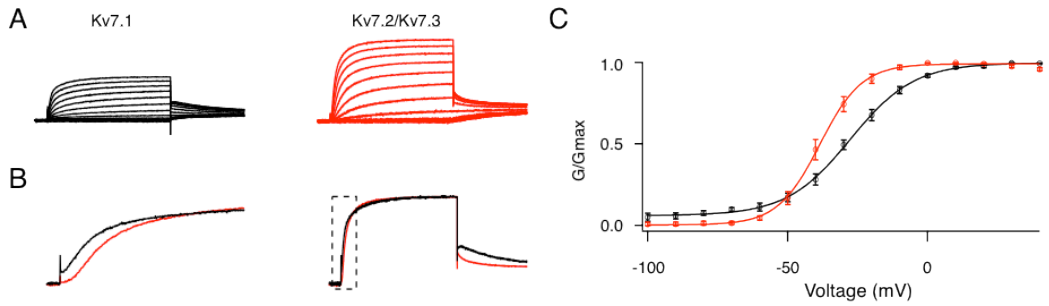

Figure 4.3.5.4. Comparing properties of the Kv7.1 (black) and Kv7.2/Kv7.3 (red) channels. A. Currents elicited by a family of depolarizing pulses. B. Time-courses of current onset; left shows expanded view of dashed boxed region. C. The G/V curves.

Alternatively, different gating properties of Kv7.2-5 compared to Kv7.1 might be due to the change of protein-lipid interactions, *i.e.* the presence of other PIP_2 binding site(s) in these channels. Indeed, a difference in protein-lipid interactions between Kv7.1 and Kv7.2 was recently highlighted by Zhang *et al.* [38]. Additionally, while in Kv7.2-5 the helix A-B linker is suggested to compose another PIP_2 binding site [80], in Kv7.1 this linker is not conserved.

In summary, combining MD simulations and based on our predictions electrophysiological experiments, we explored the two principal components of coupling in Kv7.1 mediated by protein-protein and protein-lipid interactions. Thought, in our simulations, a minimalist truncated model of Kv7.1 was considered, using this, we were able to rationalize previous experimental data [37] and to predict an interaction playing a key role in the protein-protein coupling that was further validated experimentally. Altogether, this brings confidence in the results obtained here: PIP_2-dependent coupling is especially prominent in this channel due to weak protein-protein interactions.

We note that while Kv7.1 is functional when it is expressed alone, most of the time, this channel forms complexes with the KCNE auxiliary subunits. For instance, in the heart, Kv7.1 is associated with KCNE1, and this complex

produces I_{KS} current, which plays a key role during late phase action potential repolarization. Hence, it is of particular importance to test whether the PIP_2-dependent mechanism of coupling and the interaction between S4-S5 and S6 are similar in Kv7.1 alone and in its complex with an auxiliary subunit. In order to address this question, further investigations are needed.

In other channels with similar overall architecture (Kv7.2-Kv7.5 and Kv1.2), a relative contribution from the two components of coupling potentially provides a spectrum of responses to voltage and PIP_2 application as gathered from a survey of their behavior. Whether the VSD/PD coupling is always mediated by the two components in voltage-gated channels requires further thorough investigation. Another important question, concerning the elements involved in the two components specifically, is whether other lipids besides PIP_2 contribute to the coupling between the VSD to the PD. We believe, in light of the present study, that a combined modeling and experimental approach would be the best tool to investigate these outstanding issues.

REFERENCES

[1] Y.F. Xiao, Q. Ke, S.Y. Wang, K. Auktor, Y. Yang, G.K. Wang, J.P. Morgan, A. Leaf, Single point mutations affect fatty acid block of human myocardial sodium channel alpha subunit Na+ channels, Proc. Natl. Acad. Sci. U. S. A., 98 (2001) 3606–3611.

[2] A. Rosenhouse-Dantsker, S. Noskov, S. Durdagi, D.E. Logothetis, I. Levitan, Identification of novel cholesterol-binding regions in Kir2 channels, J. Biol. Chem., (2013) jbc.M113.496117.

[3] F.C. Coyan, F. Abderemane-Ali, M.Y. Amarouch, J. Piron, J. Mordel, C.S. Nicolas, M. Steenman, J. Mérot, C. Marionneau, A. Thomas, R. Brasseur, I. Baró, G. Loussouarn, A Long QT Mutation Substitutes Cholesterol for Phosphatidylinositol-4,5-Bisphosphate in KCNQ1 Channel Regulation, PLoS ONE, 9 (2014) e93255.

[4] D. Schmidt, Q.-X. Jiang, R. MacKinnon, Phospholipids and the origin of cationic gating charges in voltage sensors, Nature, 444 (2006) 775–779.

[5] P. Bjelkmar, P.S. Niemelä, I. Vattulainen, E. Lindahl, Conformational changes and slow dynamics through microsecond polarized atomistic molecular simulation of an integral Kv1.2 ion channel, PLoS Comput. Biol., 5 (2009) e1000289.

[6] J.A. Freites, D.J. Tobias, G. von Heijne, S.H. White, Interface connections of a transmembrane voltage sensor, Proc. Natl. Acad. Sci. U. S. A., 102 (2005) 15059–15064.

[7] V. Jogini, B. Roux, Dynamics of the Kv1.2 voltage-gated K+ channel in a membrane environment, Biophys. J., 93 (2007) 3070–3082.

[8] Z.A. Sands, M.S.P. Sansom, How Does a Voltage Sensor Interact with a Lipid Bilayer? Simulations of a Potassium Channel Domain, Struct. England1993, 15 (2007) 235–244.

[9] W. Treptow, M. Tarek, Environment of the gating charges in the Kv1.2 Shaker potassium channel, Biophys. J., 90 (2006) L64–66.

[10] L. Monticelli, K.M. Robertson, J.L. MacCallum, D.P. Tieleman, Computer simulation of the KvAP voltage-gated potassium channel: steered molecular dynamics of the voltage sensor, FEBS Lett., 564 (2004) 325–332.

[11] F. Khalili-Araghi, V. Jogini, V. Yarov-Yarovoy, E. Tajkhorshid, B. Roux, K. Schulten, Calculation of the gating charge for the Kv1.2 voltage-activated potassium channel, Biophys. J., 98 (2010) 2189–2198.

[12] L. Delemotte, M. Tarek, M.L. Klein, C. Amaral, W. Treptow, Intermediate states of the Kv1.2 voltage sensor from atomistic molecular dynamics simulations, Proc. Natl. Acad. Sci. U. S. A., 108 (2011) 6109–6114.

[13] M.Ø. Jensen, V. Jogini, D.W. Borhani, A.E. Leffler, R.O. Dror, D.E. Shaw, Mechanism of voltage gating in potassium channels, Science, 336 (2012) 229–233.

[14] D.J. Combs, H.-G. Shin, Y. Xu, Y. Ramu, Z. Lu, Tuning voltage-gated channel activity and cellular excitability with a sphingomyelinase, J. Gen. Physiol., 142 (2013) 367–380.

[15] M.A. Kasimova, M. Tarek, A.K. Shaytan, K.V. Shaitan, L. Delemotte, Voltage-gated ion channel modulation by lipids: Insights from molecular dynamics simulations, Biochim. Biophys. Acta, 1838 (2014) 1322–1331.

[16] Y. Zhou, J.H. Morais-Cabral, A. Kaufman, R. MacKinnon, Chemistry of ion coordination and hydration revealed by a K+ channel-Fab complex at 2.0 Å resolution, Nature, 414 (2001) 43–48.

[17] X. Zhang, W.L. Ren, P. DeCaen, C.Y. Yan, X. Tao, L. Tang, J.J. Wang, K. Hasegawa, T. Kumasaka, J.H. He, J.W. Wang, D.E. Clapham, N. Yan, Crystal structure of an orthologue of the NaChBac voltage-gated sodium channel, Nature, 486 (2012) 130–134.

[18] J. Payandeh, T.M. Gamal El-Din, T. Scheuer, N. Zheng, W.A. Catterall, Crystal structure of a voltage-gated sodium channel in two potentially inactivated states, Nature, 486 (2012) 135–139.

[19] S.B. Hansen, X. Tao, R. MacKinnon, Structural basis of PIP2 activation of the classical inward rectifier K+ channel Kir2.2, Nature, 477 (2011) 495–498.

[20] M.R. Whorton, R. MacKinnon, Crystal Structure of the Mammalian GIRK2 K+ Channel and Gating Regulation by G Proteins, PIP2, and Sodium, Cell, 147 (2011) 199–208.

[21] S.B. Long, X. Tao, E.B. Campbell, R. MacKinnon, Atomic structure of a voltage-dependent K+ channel in a lipid membrane-like environment, Nature, 450 (2007) 376–382.

[22] H. Palsdottir, C. Hunte, Lipids in membrane protein structures, Biochim. Biophys. Acta, 1666 (2004) 2–18.

[23] C. Aponte-Santamaría, R. Briones, A.D. Schenk, T. Walz, B.L. de Groot, Molecular driving forces defining lipid positions around aquaporin-0, Proc. Natl. Acad. Sci. U. S. A., 109 (2012) 9887–9892.

[24] T. Gonen, Y. Cheng, P. Sliz, Y. Hiroaki, Y. Fujiyoshi, S.C. Harrison, T. Walz, Lipid-protein interactions in double-layered two-dimensional AQP0 crystals, Nature, 438 (2005) 633–638.

[25] B.-C. Suh, B. Hille, PIP2 is a necessary cofactor for ion channel function: how and why?, Annu. Rev. Biophys., 37 (2008) 175–195.

[26] L. Stephens, A. McGregor, P. Hawkins, Phosphoinositide-3-kinases: Regulation by cell surface receptors and function of 3-phosphorylated lipids, in: S. Cockcroft (ed.), Frontiers of Molecular Biology, Biology of Phosphoinositides, Oxford University Press, Oxford, UK, 2000: pp. 32–107.

[27] H. Zhang, L.C. Craciun, T. Mirshahi, T. Rohacs, C.M.B. Lopes, T. Jin, D.E. Logothetis, PIP(2) activates KCNQ channels, and its hydrolysis underlies receptor-mediated inhibition of M currents, Neuron, 37 (2003) 963–975.

[28] K.-H. Park, J. Piron, S. Dahimène, J. Mérot, I. Baró, D. Escande, G. Loussouarn, Impaired KCNQ1–KCNE1 and Phosphatidylinositol-4,5-Bisphosphate Interaction Underlies the Long QT Syndrome, Circ. Res., 96 (2005) 730–739.

[29] T. Rohacs, C.M.B. Lopes, I. Michailidis, D.E. Logothetis, PI(4,5)P2 regulates the activation and desensitization of TRPM8 channels through the TRP domain, Nat. Neurosci., 8 (2005) 626–634.

[30] B. Nilius, F. Mahieu, J. Prenen, A. Janssens, G. Owsianik, R. Vennekens, T. Voets, The Ca2+-activated cation channel TRPM4 is regulated by phosphatidylinositol-4,5-biphosphate, EMBO J., 25 (2006) 467–478.

[31] S. Brauchi, G. Orta, C. Mascayano, M. Salazar, N. Raddatz, H. Urbina, E. Rosenmann, F. Gonzalez-Nilo, R. Latorre, Dissection of the components for PIP2 activation and thermosensation in TRP channels, Proc. Natl. Acad. Sci. U. S. A., 104 (2007) 10246–10251.

[32] J.-S. Bian, T.V. McDonald, Phosphatidylinositol-4,5-bisphosphate interactions with the HERG K(+) channel, Pflüg. Arch. Eur. J. Physiol., 455 (2007) 105–113.

[33] G.E. Flynn, W.N. Zagotta, Molecular mechanism underlying phosphatidylinositol-4,5-bisphosphate-induced inhibition of SpIH channels, J. Biol. Chem., 286 (2011) 15535–15542.

[34] A.M. Thomas, S.C. Harmer, T. Khambra, A. Tinker, Characterization of a binding site for anionic phospholipids on KCNQ1, J. Biol. Chem., 286 (2011) 2088–2100.

[35] A.A. Rodriguez-Menchaca, S.K. Adney, Q.-Y. Tang, X.-Y. Meng, A. Rosenhouse-Dantsker, M. Cui, D.E. Logothetis, PIP2 controls voltage-sensor movement and pore opening of Kv channels through the S4-S5 linker, Proc. Natl. Acad. Sci. U. S. A., (2012).

[36] V. Telezhkin, A.M. Thomas, S.C. Harmer, A. Tinker, D.A. Brown, A basic residue in the proximal C-terminus is necessary for efficient activation of the M-channel subunit Kv7.2 by $PI(4,5)P_2$, Pflüg. Arch. Eur. J. Physiol., 465 (2013) 945–953.

[37] M.A. Zaydman, J.R. Silva, K. Delaloye, Y. Li, H. Liang, H.P. Larsson, J. Shi, J. Cui, Kv7.1 ion channels require a lipid to couple voltage sensing to pore opening, Proc. Natl. Acad. Sci., 110 (2013) 13180-13185.

[38] Q. Zhang, P. Zhou, Z. Chen, M. Li, H. Jiang, Z. Gao, H. Yang, Dynamic PIP2 interactions with voltage sensor elements contribute to KCNQ2 channel gating, Proc. Natl. Acad. Sci., 110 (2013) 20093-20098.

[39] K. Eckey, E. Wrobel, N. Strutz-Seebohm, L. Pott, N. Schmitt, G. Seebohm, Novel Kv7.1-phosphatidylinositol 4,5-bisphosphate (PIP2) interaction sites uncovered by charge neutralization scanning, J. Biol. Chem., 289 (2014) 22749-22758.

[40] G. Loussouarn, K.-H. Park, C. Bellocq, I. Baró, F. Charpentier, D. Escande, Phosphatidylinositol-4,5-bisphosphate, PIP2, controls KCNQ1/KCNE1 voltage-gated potassium channels: a functional homology between voltage-gated and inward rectifier K+ channels, EMBO J., 22 (2003) 5412–5421.

[41] F. Abderemane-Ali, Z. Es-Salah-Lamoureux, L. Delemotte, M.A. Kasimova, A.J. Labro, D.J. Snyders, D. Fedida, M. Tarek, I. Baró, G. Loussouarn, Dual effect of phosphatidyl (4,5)-bisphosphate PIP2 on Shaker K+ channels, J. Biol. Chem., 287 (2012) 36158–36167.

[42] S.B. Long, E.B. Campbell, R. Mackinnon, Crystal structure of a mammalian voltage-dependent Shaker family K+ channel, Science, 309 (2005) 897–903.

[43] P.F. Fahey, W.W. Webb, Lateral diffusion in phospholipid bilayer membranes and multilamellar liquid crystals, Biochemistry (Mosc.), 17 (1978) 3046–3053.

[44] A.D. Mackerell Jr, M. Feig, C.L. Brooks 3rd, Extending the treatment of backbone energetics in protein force fields: limitations of gas-phase quantum mechanics in reproducing protein conformational distributions in molecular dynamics simulations, J. Comput. Chem., 25 (2004) 1400–1415.

[45] J.B. Klauda, R.M. Venable, J.A. Freites, J.W. O'Connor, D.J. Tobias, C. Mondragon-Ramirez, I. Vorobyov, A.D. MacKerell, R.W. Pastor, Update of the CHARMM all-atom additive force field for lipids: Validation on six lipid types, J. Phys. Chem. B, 114 (2010) 7830–7843.

[46] D. Lupyan, M. Mezei, D.E. Logothetis, R. Osman, A molecular dynamics investigation of lipid bilayer perturbation by PIP2, Biophys. J., 98 (2010) 240–247.

[47] W.L. Jorgensen, J. Chandrasekhar, J.D. Madura, R.W. Impey, M.L. Klein, Comparison of simple potential functions for simulating liquid water, J. Chem. Phys., 79 (1983) 926.

[48] J.C. Phillips, R. Braun, W. Wang, J. Gumbart, E. Tajkhorshid, E. Villa, C. Chipot, R.D. Skeel, L. Kalé, K. Schulten, Scalable molecular dynamics with NAMD, J. Comput. Chem., 26 (2005) 1781–1802.

[49] A. Laio, M. Parrinello, Escaping free-energy minima, Proc. Natl. Acad. Sci., 99 (2002) 12562–12566.

[50] A. Laio, A. Rodriguez-Fortea, F.L. Gervasio, M. Ceccarelli, M. Parrinello, Assessing the Accuracy of Metadynamics, J. Phys. Chem. B, 109 (2005) 6714–6721.

[51] E. Darve, A. Pohorille, Calculating free energies using average force, J. Chem. Phys., 115 (2001) 9169–9183.

[52] G.M. Torrie, J.P. Valleau, Nonphysical sampling distributions in Monte Carlo free-energy estimation: Umbrella sampling, J. Comput. Phys., 23 (1977) 187–199.

[53] S. Park, K. Schulten, Calculating potentials of mean force from steered molecular dynamics simulations, J. Chem. Phys., 120 (2004) 5946–5961.

[54] C.S. Schwaiger, P. Bjelkmar, B. Hess, E. Lindahl, 3_{10}-helix conformation facilitates the transition of a voltage sensor S4 segment toward the down state, Biophys. J., 100 (2011) 1446–1454.

[55] C.S. Schwaiger, S.I. Börjesson, B. Hess, B. Wallner, F. Elinder, E. Lindahl, The free energy barrier for arginine gating charge translation is altered by mutations in the voltage sensor domain, PloS One, 7 (2012) e45880.

[56] B. Hess, C. Kutzner, D. van der Spoel, E. Lindahl, GROMACS 4: Algorithms for Highly Efficient, Load-Balanced, and Scalable Molecular Simulation, J. Chem. Theory Comput., 4 (2008) 435–447.

[57] G.A. Tribello, M. Bonomi, D. Branduardi, C. Camilloni, G. Bussi, PLUMED 2: New feathers for an old bird, Comput. Phys. Commun., 185 (2014) 604–613.

[58] L. Delemotte, M.A. Kasimova, M.L. Klein, M. Tarek, V. Carnavalle, Free energy landscape of ion-channel voltage-sensor-domain activation, submitted to Proc. Natl. Acad. Sci. U. S. A.

[59] M. Bonomi, A. Barducci, M. Parrinello, Reconstructing the equilibrium Boltzmann distribution from well-tempered metadynamics, J. Comput. Chem., 30 (2009) 1615–1621.

[60] P. Raiteri, A. Laio, F.L. Gervasio, C. Micheletti, M. Parrinello, Efficient Reconstruction of Complex Free Energy Landscapes by Multiple Walkers Metadynamics, J. Phys. Chem. B, 110 (2006) 3533–3539.

[61] E.V. Zaklyazminskaya, H. Abriel, Prevalence of significant genetic variants in congenital long QT syndrome is largely underestimated, Pharmacol. Ion Channels Channelopathies, (2012) 72.

[62] H. Abriel, E.V. Zaklyazminskaya, Cardiac channelopathies: genetic and molecular mechanisms, Gene, 517 (2013) 1–11.

[63] S.M. Modell, D.J. Bradley, M.H. Lehmann, Genetic testing for long QT syndrome and the category of cardiac ion channelopathies, PLoS Curr., (2012) e4f9995f69e6c7.

[64] M.A. Zaydman, J. Cui, PIP2 regulation of KCNQ channels: biophysical and molecular mechanisms for lipid modulation of voltage-dependent gating, Membr. Physiol. Membr. Biophys., 5 (2014) 195.

[65] S.B. Long, E.B. Campbell, R. MacKinnon, Voltage Sensor of Kv1.2: Structural Basis of Electromechanical Coupling, Science, 309 (2005) 903–908.

[66] Z. Lu, A.M. Klem, Y. Ramu, Ion conduction pore is conserved among potassium channels, Nature, 413 (2001) 809–813.

[67] Z. Lu, A.M. Klem, Y. Ramu, Coupling between voltage sensors and activation gate in voltage-gated K+ channels, J. Gen. Physiol., 120 (2002) 663–676.

[68] A.J. Labro, A.L. Raes, A. Grottesi, D.V. Hoorick, M.S.P. Sansom, D.J. Snyders, Kv Channel Gating Requires a Compatible S4-S5 Linker and Bottom Part of S6, Constrained by Non-interacting Residues, J. Gen. Physiol., 132 (2008) 667–680.

[69] G.A. Haddad, R. Blunck, Mode shift of the voltage sensors in Shaker K+ channels is caused by energetic coupling to the pore domain, J. Gen. Physiol., 137 (2011) 455–472.

[70] E.V. Schow, J.A. Freites, A. Nizkorodov, S.H. White, D.J. Tobias, Coupling between the voltage-sensing and pore domains in a voltage-gated potassium channel, Biochim. Biophys. Acta, 1818 (2012) 1726–1736.

[71] E. Vargas, V. Yarov-Yarovoy, F. Khalili-Araghi, W.A. Catterall, M.L. Klein, M. Tarek, E. Lindahl, K. Schulten, E. Perozo, F. Bezanilla, B. Roux, An emerging consensus on voltage-dependent gating from computational modeling and molecular dynamics simulations, J. Gen. Physiol., 140 (2012) 587–594.

[72] E.V. Schow, J.A. Freites, K. Gogna, S.H. White, D.J. Tobias, Down-state model of the voltage-sensing domain of a potassium channel, Biophys. J., 98 (2010) 2857–2866.

[73] D. Peng, J.-H. Kim, B.M. Kroncke, C.L. Law, Y. Xia, K.D. Droege, W.D. Van Horn, C.G. Vanoye, C.R. Sanders, Purification and Structural Study of the Voltage-Sensor Domain of the Human KCNQ1 Potassium Ion Channel, Biochemistry (Mosc.), (2014).

[74] N. Eswar, B. Webb, M.A. Marti-Renom, M.S. Madhusudhan, D. Eramian, M.-Y. Shen, U. Pieper, A. Sali, Comparative protein structure modeling using MODELLER, Curr. Protoc. Protein Sci., Chapter 2 (2007) Unit 2.9.

[75] R.A. Laskowski, M.W. MacArthur, D.S. Moss, J.M. Thornton, PROCHECK: a program to check the stereochemical quality of protein structures, J. Appl. Crystallogr., 26 (1993) 283–291.

[76] V. Telezhkin, J.M. Reilly, A.M. Thomas, A. Tinker, D.A. Brown, Structural Requirements of Membrane Phospholipids for M-type Potassium Channel Activation and Binding, J. Biol. Chem., 287 (2012) 10001–10012.

[77] I.R. Boulet, A.J. Labro, A.L. Raes, D.J. Snyders, Role of the S6 C-terminus in KCNQ1 channel gating, J. Physiol., 585 (2007) 325–337.

[78] J.D. Osteen, K.J. Sampson, R.S. Kass, The cardiac IKs channel, complex indeed, Proc. Natl. Acad. Sci. U. S. A., 107 (2010) 18751–18752.

[79] A. Horovitz, A.R. Fersht, Strategy for analysing the co-operativity of intramolecular interactions in peptides and proteins, J. Mol. Biol., 214 (1990) 613–617.

[80] C.C. Hernandez, O. Zaika, M.S. Shapiro, A Carboxy-terminal Inter-Helix Linker As the Site of Phosphatidylinositol-4,5-Bisphosphate Action on Kv7 (M-type) K+ Channels, J. Gen. Physiol., 132 (2008) 361–381.

[81] D.H. Hackos, T.-H. Chang, K.J. Swartz, Scanning the Intracellular S6 Activation Gate in the Shaker K+ Channel, J. Gen. Physiol., 119 (2002) 521–531.

[82] M. Nishizawa, K. Nishizawa, Coupling of S4 helix translocation and S6 gating analyzed by molecular-dynamics simulations of mutated Kv channels, Biophys. J., 97 (2009) 90–100.

[83] F. Miceli, M.R. Cilio, M. Taglialatela, F. Bezanilla, Gating currents from neuronal K(V)7.4 channels: general features and correlation with the ionic conductance, Channels Austin Tex, 3 (2009) 274–283.

[84] L.-J. Ma, I. Ohmert, V. Vardanyan, Allosteric Features of KCNQ1 Gating Revealed by Alanine Scanning Mutagenesis, Biophys. J., 100 (2011) 885–894.

5 PERSPECTIVES

Le but du présent travail a été de caractériser et de comprendre comment le PIP_2 module le fonctionnement de deux canaux potassiques sensibles à la tension : Kv1.2 et Kv7.1. Pour ces deux canaux, nous avons identifié un site d'interaction situé à proximité de l'interface entre le domaine sensible à la tension (VSD) et le pore (PD). Pour le canal de type *Shaker* (Kv1.2) nous avons également effectué une analyse quantitative de l'effet induit par le PIP_2 sur les deux premières transitions du VSD, de l'état activé vers l'état au repos. Nous avons plus particulièrement estimé les profiles d'énergie libre et déterminé la différence entre ces transitions lorsqu'elles ont lieu en présence ou non du PIP_2. Pour le Kv7.1, nous avons particulièrement caractérisé le rôle de PIP_2 dans le couplage entre le VSD et le pore. A l'inverse du Kv1.2, la composante protéine-protéine du couplage dans le Kv7.1 semble être affaiblie à cause de répulsions entre résidus positivement chargés portés par S4-S5 et S6. Ces régions contiennent les mêmes résidus qui coordinent le PIP_2 dans son site de liaison à l'interface VSD/PD. Nous proposons par conséquent qu'une molécule fortement chargée négativement comme PIP_2, dans se site, non seulement contribue à écranter la répulsion entre ces domaines, mais favorise également les états au repos/fermé et activé/ouvert du Kv7.1 par rapports aux états au repos/ouvert et activé/fermé, et donc couple des conformations spécifiques du VSD à celles du pore.

Ces résultats nous permettent maintenant d'envisager une poursuite de la recherche dans ce domaine (que nous avons débuté) vers trois axes différents :

- Tout d'abord l'accès aux cinétiques d'activation. Ici il s'agit de déterminer les constantes cinétiques des transitions (activation et dé-activation) du Kv1.2 dans les membranes avec et sans PIP_2. Considérant la théorie des etats de transition (*rate theory*), ces constantes cinétiques peuvent être déterminées à partir des profiles d'énergie libre qui décrivent le processus (pour chaque transition) et les coefficients de diffusion spécifiques dépendants de la position sur ces courbes. Jusqu'à présent nous disposons des profils d'énergie libre pour deux transitions ε-δ et δ-γ et avons déjà des résultats préliminaires concernant les deux autres, γ-β and β-α (utilisant les protocoles décrits dans la Section **4.2)**. En ce qui concerne les coefficients

de diffusion, nous avons implémenté des stratégies et protocoles pour utiliser l'approche des "Damped Harmonic Oscillators" proposée par Roux et Straub, et modifiée ultérieurement par Hummer.

- Identification du site de liaison du PIP_2 dans le complexe Kv7.1/KCNE1. Le canal Kv7.1 est en effet souvent associé à des sous unités périphériques. Dans le coeur, cette sous unité est le KCNE1. Tout comme le canal seul, le complexe Kv7.1/KCNE1 est également modulé par le PIP_2 : l'appauvrissement des membranes de ce lipide réduit d'une manière drastique le courant ionique. Cependant, selon de récents travaux expérimentaux, l'affinité du complexe Kv7.1/KCNE1 pour PIP_2 est significativement plus grande que celle du canal Kv7.1 seul, ce qui tend à indiquer que les interactions protéine-lipide dans ces complexes sont différentes. Pour la caractérisation des mécanismes d'action du PIP_2, il sera nécessaire de développer des modèles moléculaires du complexe Kv7.1/KCNE1 dans les états activé/ouvert et au repos/fermé avant de cherché les sites potentiels de liaison.

- Construction de modèles de la phosphatase dépendante du voltage CiVSP (incluant les domaines transmembranaires et le C-terminal cytoplasmique). Cette molécule est une enzyme dépendante du PIP_2 qui déphosphorylise les $PI(3,4,5)P_3$ et $PI(4,5)P_2$ lorsque la membrane plasmique est dépolarisée. L'enzyme est composée d'un domaine sensible à la tension (VSD) et d'un domaine phosphatase cytoplasmique. Ces deux domaines sont reliés par un "linker" de 18 acides aminés qui joue un rôle fondamental dans la fonction de la CiVSP. En particulier, cette région couple les changements conformationels du VSD a ceux de la phosphatase. Bien que les structures du VSD et de la phosphatase aient été résolues, la structure de la région intermédiaire reste inconnue, probablement a cause de sa flexibilité. Dans ce futur projet, fort de nos résultats et expertises acquises lors de l'étude du Kv7.1, nous prévoyons de déterminer le fonctionnement de la CiVSP aisi que sa modulation par le PIP_2.

5 PERSPECTIVES

In this work, we attempted to shed light on the modulation of the two voltage-gated potassium channels, Kv1.2 and Kv7.1, by PIP_2. We identified a PIP_2 binding site located at the interface between the voltage sensor and the pore and showed that this binding site is similar in Kv1.2 and Kv7.1. For Kv1.2, we performed quantitative analysis of the effect induced by PIP_2 on the first two transitions of the voltage sensor toward activation; in particular, we estimated the free energy difference between these transitions occurring in the bare POPC and POPC/PIP_2 bilayers. For Kv7.1, we explored the critical role of PIP_2 in coupling the voltage sensor motion to that of the pore. In contrast to Kv1.2, the protein-protein component of coupling in Kv7.1 was found to be weakened by the electrostatic repulsion between positively charged residues of S4-S5 and S6. The same positive residues were found to coordinate PIP_2 in its putative binding site at the VSD/PD interface. We propose that a highly negatively charged PIP_2 molecule located in this site, on the one hand, may screen the repulsion between the S4-S5 and S6 segments, and, on the other hand, may favor the resting/closed and activated/open states of the channel over the resting/open and activated/closed ones, *i.e.* couples specific conformations of the voltage sensor to those of the pore.

Inspired by our results, we started working in three directions, all dealing with the modulation of transmembrane proteins by PIP_2. Below, we would like to discuss the main purposes of these projects and to showcase some of the preliminary results.

5.1. Modulation of the kinetic constants of the Kv1.2 activation/deactivation processes by PIP_2

The aim of this work is to develop functional models uncovering the kinetics of the Kv1.2 activation/deactivation processes by applying classical MD simulations and sophisticated methods for the free energy estimation. To date, the kinetic parameters of an ion channel's gating are determined from fitting experimental curves and most often resort to *ad hoc* models such as the model of Hodgkin and Huxley. Experimental data on ion channel electrophysiological function have provided the basis for more detailed kinetic models of channel electrical function during gating. The most prominent class of models is the so-called discrete state Markov models (DSMMs), which rely on the assumption that the channel can reside in several well-defined states corresponding to local free energy minima. This implies the existence of several intermediate *kinetic* states that are linked by forward and backward kinetic constants (k_{ij}). So far, several strategies have been developed to uncover the voltage sensor's kinetics from experimental data using DSMMs [1–9]. Recently, Silva and coworkers [10] provided a framework linking molecular based models to the Kv7.1 activation macroscopic currents. However, the free energy calculations were performed in implicit solvent. Such a simplified model underestimates the gating charge associated with the channel activation but also neglects the lipid contribution that may play a crucial role in the voltage sensor's activation kinetics. Furthermore, the reaction coordinate used (translation and rotation of the S4 helix) was too simple to capture all the features of the conformational changes taking place. Here, we are going to use such DSMM but considering an explicit representations of the solvent and the membrane (all-atom MD simulations) in order to evaluate the kinetic rate constant of the Kv1.2 activation/deactivation processes occurring in the bare POPC and POPC/PIP_2 bilayers. The set of discrete states are obtained using an ensemble of carefully chosen collective variables (CV_{Ri}, see **4.2**) that encompasses all essential ingredients of the mechanism of the voltage sensor's activation (*i.e.*

salt bridge reorganization, interactions with lipids and S4 translation across the membrane) [11].

According to the rate theory, the kinetic rate constant of a process can be estimated knowing the underlying free energy surface and the position-dependent diffusion coefficient [12]. Molecular modeling provides methods for estimating both the multidimensional free energy surface (for instance, see **3.2**) and the diffusion coefficient [13–16]. So far, we have estimated the free energy of the two transitions of the Kv1.2 voltage sensor toward activation, ε-δ and δ-γ, in both POPC and POPC/PIP_2; the two remaining ones are γ-β and β-α. In contrast to the transitions present here (ε-δ and δ-γ), the latters (γ-β and β-α) occur in the 3d space: the collective variables to be biased correspond to the transfer either of the R2, R4 and R6 residues for the γ-β transition or of the R1, R3 and K5 residues for the β-α transition (see Figure 5.1.1). Note that convergence in the 3d space is much longer to achieve than in the 2d one, and, therefore, the free energy estimation for the γ-β and β-α transitions requires more computational resources than for the ε-δ and δ-γ ones. Using the same protocol as discussed in **4.2**, we have already started collecting data for the free energy surfaces of both the γ-β and β-α transitions in POPC and POPC/PIP_2.

The other ingredient, required for the estimation of the kinetic rate constant, is the state-dependent diffusion coefficient. Here, we are going to implement a strategy to estimate this coefficient for a number of points on the CV_{Ri} (collective variables') conformation space. We would like to note that estimation of a diffusion coefficient of a biological process is often complicated due to the fact that the observed dynamics of the system is determined by a combination of both a systematic force coming from a free energy and the system's diffusion. Therefore, one has to consider a trick, which will remove or at least significantly reduce contributions from a non-uniform free energy surface in the observed trajectories. For the latter, we chose the approach, which is based on the analysis of the Generalized Langevin Equation for a harmonic oscillator [14–16], see the eq. (3.1.8.4). Briefly, replacing $-\frac{\partial U}{\partial \boldsymbol{r_i}}$ with the harmonic oscillator force $-k\Delta z(t)$, where $\Delta z(t)$ is the displacement of the oscillator from its equilibrium position, and k is a Hooke's Law spring constant, and applying the formulas of statistical mechanics, one is able to express the local diffusion coefficient D as:

$$D = \frac{\langle \Delta z^2 \rangle}{\tau}. \qquad (5.1.1)$$

Here, τ is the correlation time of the reaction coordinate:

$$\tau = \frac{\int_0^\infty \langle \Delta z(t) \Delta z(0) \rangle dt}{\langle \Delta z^2 \rangle}. \quad (5.1.2)$$

These equations are exact for an *overdamped harmonic oscillator* only [16]. Therefore, at first, we will have to find a harmonic force constant that switches the dynamics of our system to an overdamped oscillator regime. The latter is a priority for our ongoing work.

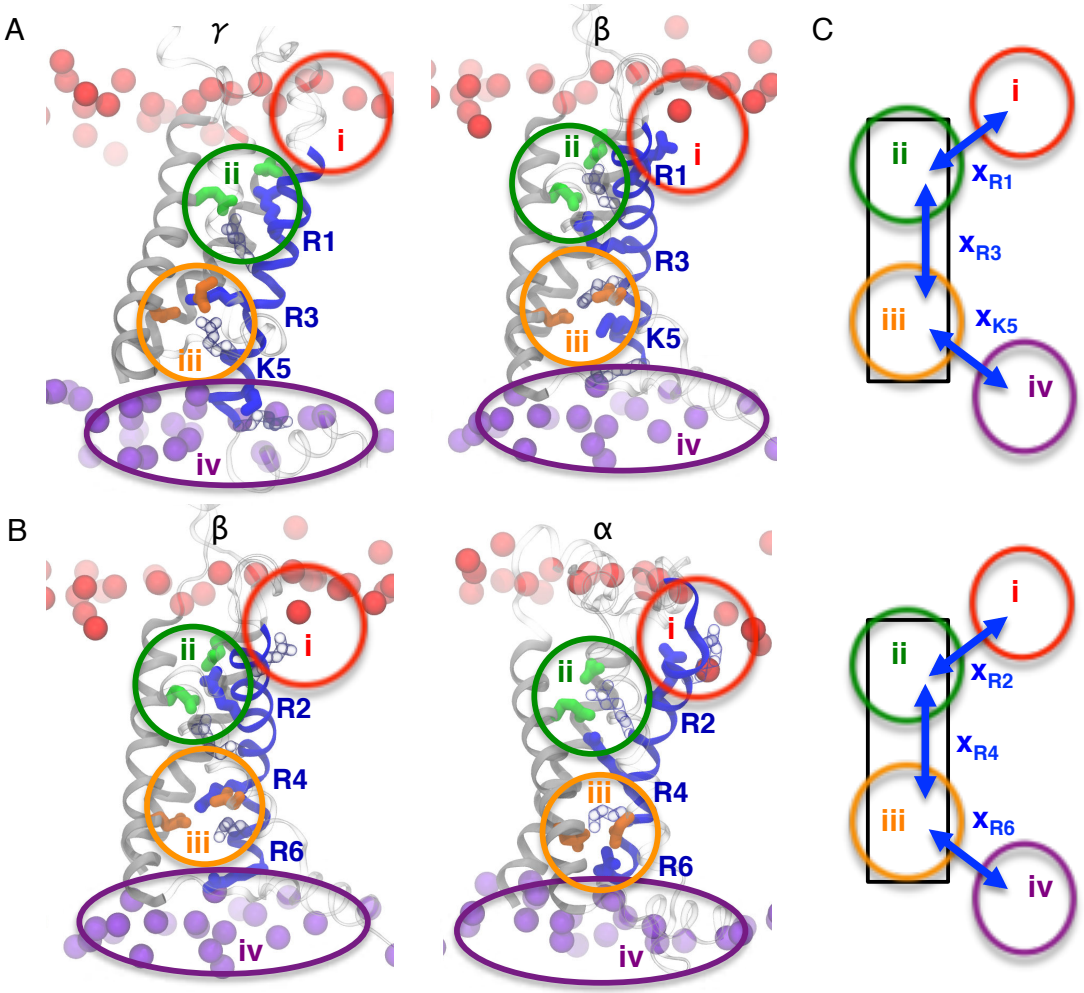

Figure 5.5.1. The γ-β (A) and β-α (B) transitions of the voltage sensor in terms of CV_{Ri}. (A) During the γ-β transition, R1 transfers between the binding sites i (shown in red) and ii (shown in green); R3 transfers between the binding sites ii and iii (shown in orange); K5 transfers between the binding sites iii and iv (shown in violet). (B) During the β-α transition, R1, R3 and K5 remain bound to their countercharges at the binding sites i, ii and iii respectively. Meanwhile, R2 transfers between the binding sites i and ii; R4 transfers between the binding sites ii and iii; R6 transfers between the binding sites iii and iv. (C) Schematic representation of the S4 positive charges' transfer between the negative binding sites during the γ-β (top) and β-α (bottom) transitions of the voltage sensor. x_{R1}, x_{R2}, x_{R3}, x_{R4}, x_{K5} and x_{R6} stand for the vectors, along which a charge transfer occurs.

5.2. Identification of a PIP_2 putative binding site of the Kv7.1/KCNE1 complex

The voltage-gated potassium channel Kv7.1 is usually found in association with one of its auxiliary subunits. In the heart, this auxiliary subunit is KCNE1, which induces several changes in the Kv7.1 channel's functioning: increase in single channel conductance, slow activation and positive shift in the voltage-dependence of activation and suppression of inactivation [17–20]. As Kv7.1, the Kv7.1/KCNE1 complex is regulated by PIP_2: depletion of this lipid dramatically reduces ionic current in both channels [21]. However, according to recent experimental data, the affinity of the Kv7.1/KCNE1 complex for PIP_2 is significantly higher compared to the Kv7.1 channel alone [22], which may indicate different protein-lipid interactions between these channels and PIP_2. In this project, we aim to develop a 3d model of the Kv7.1/KCNE1 complex in the activated/open and resting/closed states and to identify its PIP_2 putative binding site.

After extensive literature review, we have selected several experimental data, which may be used in building of the Kv7.1/KCNE1 model. This data includes the Cys-Cys cross-linking, NMR spectroscopy, helical perturbation analysis, *etc.* [22–38] (see Figure 5.2.1).

The available experimental data (apart of residues responsible for PIP_2 sensitivity) were introduced as restraints into an input file of MODELLER [39]. 600 different models of the KCNQ1/KCNE1 complex in the activated/open state were built. Among them 300 were selected based on the best value of the scoring function (DOPE). These 300 models were clustered by position and conformation of the KCNE1 TM part; inappropriate models were not considered for a further analysis. The resting 274 models were clustered by position and conformation of the entire KCNE1 subunit with different values of cutoff (ranging from 1.0 to 2.0 Å).

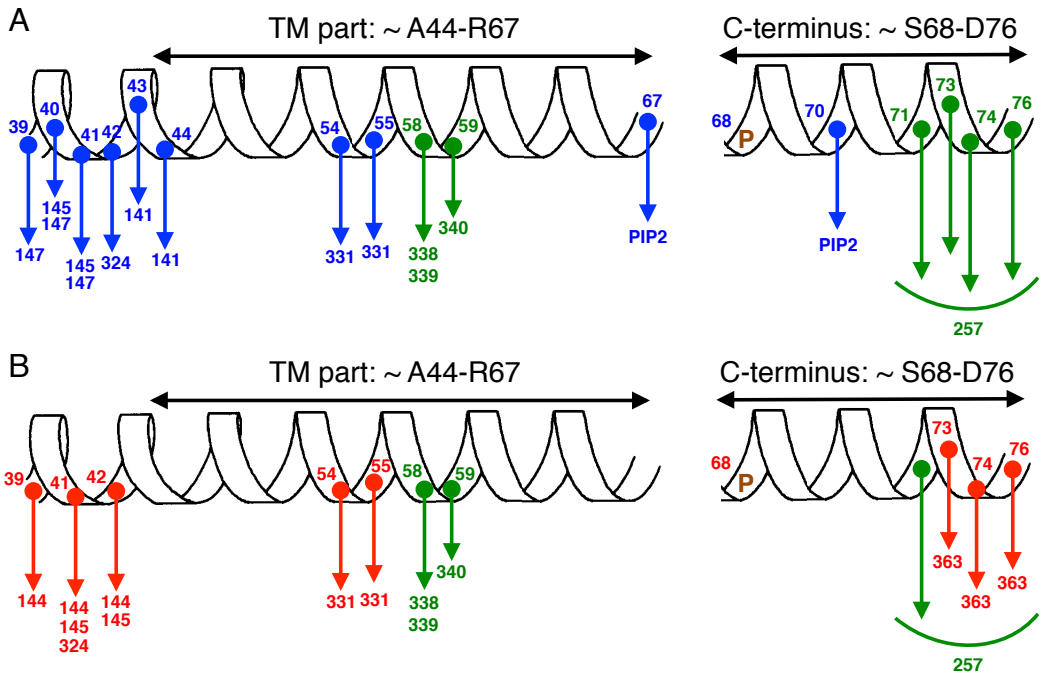

Figure 5.2.1. The available experimental data concerning the interactions between Kv7.1 and KCNE1: the activated/open (A) and resting/closed (B) states. The residues connected with an arrow (numbers only) are located in close proximity to each other; the upper and lower residues relate to KCNE1 and Kv7.1 respectively. The blue and red arrows correspond to the activated/open and resting/closed states. For the green pairs, the state, in which these residues interact, is not specified. In the activated/open state, two residues, R67 and K70, are shown to be responsible for PIP_2 sensitivity. **P** denotes possible phosphorylation of the S68 residue.

Our analysis has revealed two most populated clusters. Conformations corresponding to these clusters differ by the KCNE1 C-terminus: either K69 or R67 and K70 of this C-terminus face S6 in the conformation 1 and 2 respectively (see Figure 5.2.2). In order to make a choice between two of these conformations, we will identify their PIP_2 binding sites and compare our findings with the known experimental data [22].

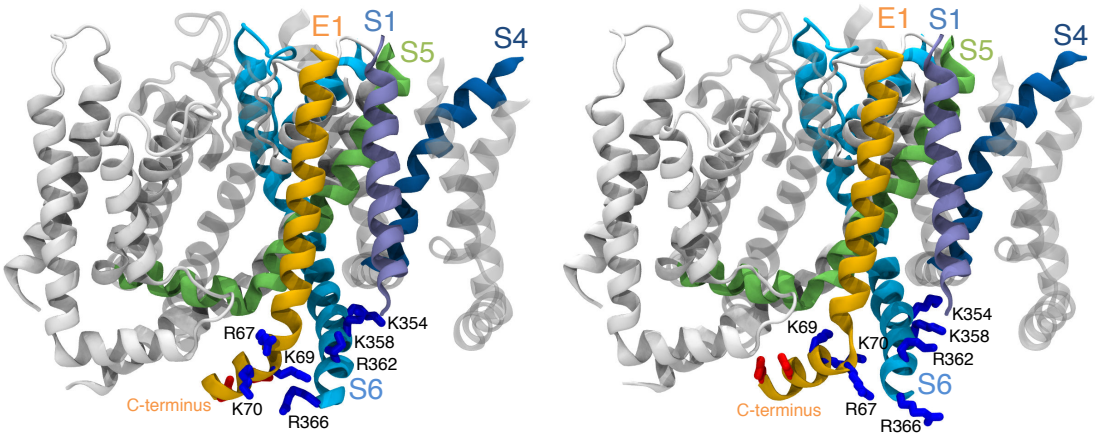

Figure 5.2.2. The Kv7.1/KCNE1 complex in the activated/open state: two conformations obtained after the clustering. In one of the conformations (left), the K69 residue of KCNE1 faces the C-terminus domain of Kv7.1. In the other conformation (right), the R67 and K70 residues of KCNE1 are turned toward the C-terminus of Kv7.1.

This next step of this project will be to build the Kv7.1/KCNE1 model in the resting/closed state and to identify its PIP_2 putative binding site (ongoing).

5.3. Building the model of the voltage-dependent phosphatase CiVSP (including the TM and C-terminal cytoplasmic domains)

The voltage-dependent phosphatase of *Ciona intestinalis* CiVSP is a PIP_2-dependent enzyme, which dephosphorylates $PI(3,4,5)P_3$ and $PI(4,5)P_2$ upon depolarization of the plasma membrane [40]. This enzyme is widely used in electrophysiological experiments to control the plasma membrane PIP_2 level. CiVSP consists of a voltage sensor domain (homologous to that of voltage-gated ion channels) and a cytoplasmic phosphatase domain. The two domains are connected through a short 18 amino acids linker region, which plays an important role in the CiVSP functioning. In particular, this region couples the conformational changes of the voltage sensor to those of the phosphatase [40]. While the high-resolution structures of the voltage sensor and the phosphatase were successfully resolved [41,42], the structure of the linker region due to its high flexibility remains elusive. In this project, we attempt to build the 3d model of this linker and, based on the latter, the entire model of CiVSP, in which the voltage sensor and the phosphatase are connected.

This project is at the stage of collecting experimental data, which is going to be used when building the model. For instance, the Cys-Cys linking experiments suggest that the linker region adapts the conformation of an α-helix [43]. The other experimental data obtained by the group of Villalba-Galea (not published) indicates that the isolated linker region of CiVSP selectively binds PIP_2. This may provide us a hint about the orientation of the linker toward the plasma membrane …

REFERENCES

[1] F. Bezanilla, E. Perozo, E. Stefani, Gating of Shaker K+ channels II: The components of gating currents and a model of channel activation, Biophys. J., 66 (1994) 1011–1021.

[2] W.N. Zagotta, T. Hoshi, R.W. Aldrich, Shaker potassium channel gating III: Evaluation of kinetic models for activation, J. Gen. Physiol., 103 (1994) 321–362.

[3] N.E. Schoppa, F.J. Sigworth, Activation of Shaker potassium channels III: An activation gating model for wild-type and V2 mutant channels, J. Gen. Physiol., 111 (1998) 313–342.

[4] L.S. Milescu, T. Yamanishi, K. Ptak, M.Z. Mogri, J.C. Smith, Real-time kinetic modeling of voltage-gated ion channels using dynamic clamp, Biophys. J., 95 (2008) 66–87.

[5] X. Tao, A. Lee, W. Limapichat, D.A. Dougherty, R. MacKinnon, A gating charge transfer center in voltage sensors, Science, 328 (2010) 67–73.

[6] A. Loboda, C.M. Armstrong, Resolving the gating charge movement associated with late transitions in K channel activation, Biophys. J., 81 (2001) 905–916.

[7] O.S. Baker, H.P. Larsson, L.M. Mannuzzu, E.Y. Isacoff, Three transmembrane conformations and sequence-dependent displacement of the S4 domain in shaker K+ channel gating, Neuron, 20 (1998) 1283–1294.

[8] M. Kanevsky, R.W. Aldrich, Determinants of voltage-dependent gating and open-state stability in the S5 segment of Shaker potassium channels, J. Gen. Physiol., 114 (1999) 215–242.

[9] J. Silva, Y. Rudy, Subunit interaction determines IKs participation in cardiac repolarization and repolarization reserve, Circulation, 112 (2005) 1384–1391.

[10] J.R. Silva, H. Pan, D. Wu, A. Nekouzadeh, K.F. Decker, J. Cui, N.A. Baker, D. Sept, Y. Rudy, A multiscale model linking ion-channel molecular dynamics and electrostatics to the cardiac action potential, Proc. Natl. Acad. Sci. U. S. A., 106 (2009) 11102–11106.

[11] M. Tarek, L. Delemotte, Omega Currents in Voltage-Gated Ion Channels: What Can We Learn from Uncovering the Voltage-Sensing Mechanism Using MD Simulations?, Acc. Chem. Res., (2013).

[12] H.A. Kramers, Brownian motion in a field of force and the diffusion model of chemical reactions, Physica, 7 (1940) 284–304.

[13] D.A. McQuarrie, Statistical Mechanics, 1st ed., University Science Books, 2000.

[14] T.B. Woolf, B. Roux, Conformational Flexibility of o-Phosphorylcholine and o-Phosphorylethanolamine: A Molecular Dynamics Study of Solvation Effects, J. Am. Chem. Soc., 116 (1994) 5916–5926.

[15] B.J. Berne, M. Borkovec, J.E. Straub, Classical and modern methods in reaction rate theory, J. Phys. Chem., 92 (1988) 3711–3725.

[16] G. Hummer, Position-dependent diffusion coefficients and free energies from Bayesian analysis of equilibrium and replica molecular dynamics simulations, New J. Phys., 7 (2005) 34.

[17] J. Barhanin, F. Lesage, E. Guillemare, M. Fink, M. Lazdunski, G. Romey, K(v)LQT1 and lsK (minK) proteins associate to form the I(Ks) cardiac potassium current, Nature, 384 (1996) 78–80.

[18] M.C. Sanguinetti, M.E. Curran, A. Zou, J. Shen, P.S. Spector, D.L. Atkinson, M.T. Keating, Coassembly of K(v)LQT1 and minK (IsK) proteins to form cardiac I(Ks) potassium channel, Nature, 384 (1996) 80–83.

[19] F. Sesti, S.A. Goldstein, Single-channel characteristics of wild-type IKs channels and channels formed with two minK mutants that cause long QT syndrome, J. Gen. Physiol., 112 (1998) 651–663.

[20] M. Tristani-Firouzi, M.C. Sanguinetti, Voltage-dependent inactivation of the human K+ channel KvLQT1 is eliminated by association with minimal K+ channel (minK) subunits, J. Physiol., 510 (Pt 1) (1998) 37–45.

[21] G. Loussouarn, K.-H. Park, C. Bellocq, I. Baró, F. Charpentier, D. Escande, Phosphatidylinositol-4,5-bisphosphate, PIP2, controls KCNQ1/KCNE1 voltage-gated potassium channels: a functional homology between voltage-gated and inward rectifier K+ channels, EMBO J., 22 (2003) 5412–5421.

[22] Y. Li, M.A. Zaydman, D. Wu, J. Shi, M. Guan, B. Virgin-Downey, J. Cui, KCNE1 enhances phosphatidylinositol-4,5-bisphosphate (PIP2) sensitivity of IKs to modulate channel activity, Proc. Natl. Acad. Sci. U. S. A., 108 (2011) 9095–9100.

[23] D.Y. Chung, P.J. Chan, J.R. Bankston, L. Yang, G. Liu, S.O. Marx, A. Karlin, R.S. Kass, Location of KCNE1 relative to KCNQ1 in the I(KS) potassium channel by disulfide cross-linking of substituted cysteines, Proc. Natl. Acad. Sci. U. S. A., 106 (2009) 743–748.

[24] X. Xu, M. Jiang, K.-L. Hsu, M. Zhang, G.-N. Tseng, KCNQ1 and KCNE1 in the IKs channel complex make state-dependent contacts in their extracellular domains, J. Gen. Physiol., 131 (2008) 589–603.

[25] A.R. Tapper, A.L. George, Location and orientation of minK within the I(Ks) potassium channel complex, J. Biol. Chem., 276 (2001) 38249–38254.

[26] Y.F. Melman, S.Y. Um, A. Krumerman, A. Kagan, T.V. McDonald, KCNE1 binds to the KCNQ1 pore to regulate potassium channel activity, Neuron, 42 (2004) 927–937.

[27] G. Panaghie, K.-K. Tai, G.W. Abbott, Interaction of KCNE subunits with the KCNQ1 K+ channel pore, J. Physiol., 570 (2006) 455–467.

[28] K. Nakajo, Y. Kubo, KCNE1 and KCNE3 stabilize and/or slow voltage sensing S4 segment of KCNQ1 channel, J. Gen. Physiol., 130 (2007) 269–281.

[29] P.J. Chan, J.D. Osteen, D. Xiong, M.S. Bohnen, D. Doshi, K.J. Sampson, S.O. Marx, A. Karlin, R.S. Kass, Characterization of KCNQ1 atrial fibrillation mutations reveals distinct dependence on KCNE1, J. Gen. Physiol., 139 (2012) 135–144.

[30] Y.H. Wang, M. Jiang, X.L. Xu, K.-L. Hsu, M. Zhang, G.-N. Tseng, Gating-related molecular motions in the extracellular domain of the IKs channel: implications for IKs channelopathy, J. Membr. Biol., 239 (2011) 137–156.

[31] A.R. Tapper, A.L. George, MinK subdomains that mediate modulation of and association with KvLQT1, J. Gen. Physiol., 116 (2000) 379–390.

[32] J.M. Rocheleau, S.D. Gage, W.R. Kobertz, Secondary structure of a KCNE cytoplasmic domain, J. Gen. Physiol., 128 (2006) 721–729.

[33] A. Lvov, S.D. Gage, V.M. Berrios, W.R. Kobertz, Identification of a protein-protein interaction between KCNE1 and the activation gate machinery of KCNQ1, J. Gen. Physiol., 135 (2010) 607–618.

[34] N. Strutz-Seebohm, M. Pusch, S. Wolf, R. Stoll, D. Tapken, K. Gerwert, B. Attali, G. Seebohm, Structural basis of slow activation gating in the cardiac IKs channel complex, Cell. Physiol. Biochem. Int. J. Exp. Cell. Physiol. Biochem. Pharmacol., 27 (2011) 443–452.

[35] C. Kang, C. Tian, F.D. Sönnichsen, J.A. Smith, J. Meiler, A.L. George, C.G. Vanoye, H.J. Kim, C.R. Sanders, Structure of KCNE1 and implications for how it modulates the KCNQ1 potassium channel, Biochemistry (Mosc.), 47 (2008) 7999–8006.

[36] W.D. Van Horn, C.G. Vanoye, C.R. Sanders, Working model for the structural basis for KCNE1 modulation of the KCNQ1 potassium channel, Curr. Opin. Struct. Biol., 21 (2011) 283–291.

[37] H. Chen, S.A.N. Goldstein, Serial perturbation of MinK in IKs implies an alpha-helical transmembrane span traversing the channel corpus, Biophys. J., 93 (2007) 2332–2340.

[38] C. Tian, C.G. Vanoye, C. Kang, R.C. Welch, H.J. Kim, A.L. George, C.R. Sanders, Preparation, functional characterization, and NMR studies of human KCNE1, a voltage-gated potassium channel accessory subunit associated with deafness and long QT syndrome, Biochemistry (Mosc.), 46 (2007) 11459–11472.

[39] N. Eswar, B. Webb, M.A. Marti-Renom, M.S. Madhusudhan, D. Eramian, M.-Y. Shen, U. Pieper, A. Sali, Comparative protein structure modeling using MODELLER, Curr. Protoc. Protein Sci., Chapter 2 (2007) Unit 2.9.

[40] Y. Murata, H. Iwasaki, M. Sasaki, K. Inaba, Y. Okamura, Phosphoinositide phosphatase activity coupled to an intrinsic voltage sensor, Nature, 435 (2005) 1239–1243.

[41] M. Matsuda, K. Takeshita, T. Kurokawa, S. Sakata, M. Suzuki, E. Yamashita, Y. Okamura, A. Nakagawa, Crystal structure of the cytoplasmic phosphatase and tensin homolog (PTEN)-like region of Ciona intestinalis voltage-sensing phosphatase provides insight into substrate specificity and redox regulation of the phosphoinositide phosphatase activity, J. Biol. Chem., 286 (2011) 23368–23377.

[42] L. Liu, S.C. Kohout, Q. Xu, S. Müller, C.R. Kimberlin, E.Y. Isacoff, D.L. Minor, A glutamate switch controls voltage-sensitive phosphatase function, Nat. Struct. Mol. Biol., 19 (2012) 633–641.

[43] K. Hobiger, T. Utesch, M.A. Mroginski, T. Friedrich, Coupling of Ci-VSP modules requires a combination of structure and electrostatics within the linker, Biophys. J., 102 (2012) 1313–1322.

6 CONCLUSION

Les canaux ioniques dépendant du voltage jouent un rôle central dans l'initiation et la propagation de l'influx nerveux, l'une des fonctions les plus importantes d'un organisme vivant, à savoir, l'excitabilité. Ces protéines sont en effet omniprésentes : elles se trouvent dans les systèmes nerveux central et périphérique, le cœur, les muscles, les intestins, l'oreille interne, les reins, *etc.* Le dysfonctionnement des canaux ioniques voltage-dépendants induit par des mutations sélectives dans leurs séquences peut causer des maladies héréditaires graves comme des convulsions bénignes familiales néonatales, une hyperexcitabilité du système nerveux périphérique (système nerveux), un syndrome de QT long et court, une arythmie cardiaque (le cœur), des myotonies et paralysies périodiques (muscles), la surdité (oreille interne), *etc.*

Du fait que les canaux ioniques voltage-dépendants sont impliqués dans un large éventail de processus physiologiques vitaux, leur fonctionnement est strictement réglementé par la cellule. PIP_2 représente un lipide mineur de la membrane plasmatique, qui module le fonctionnement de nombreux canaux ioniques, y compris ceux dépendant du voltage. Ce lipide interagit avec les résidus chargés positivement d'un canal ionique, comme directement démontré pour les canaux Kir [1,2] par cristalllographie, et indirectement pour plusieurs autres canaux ioniques [3–14]. Dans ce travail, nous avons exploré comment les deux canaux potassiques voltage-dépendants, Kv1.2 et Kv7.1, sont modulés par PIP_2. Alors que Kv1.2, grâce à la disponibilité de sa structure haute résolution, représente un bon modèle pour l'étude des processus fondamentaux tels que l'activation et le transport ionique, Kv7.1 est une cible thérapeutique importante. Ce dernier est exprimé dans le cœur et participe à la fin de la phase de repolarisation du potentiel d'action des cardiomyocytes.

Les principaux résultats issus de cette étude peuvent être résumés comme suit :

- Nous avons identifié trois sites potentiels de liaison de PIP_2 pour le Kv1.2. Un de ces sites se situe à l'interface entre le domaine sensible à la tension et le pore. Ici, en fonction de l'état du canal, on montre que le PIP_2 interagit avec différents résidus positifs. En particulier, lorsque le canal est dans l'état repos/fermé, le lipide chargé négativement forme

des ponts salins avec un résidu du milieu du domaine de liaison S4-S5 et des résidus du bas de l'hélice S4, ce qui pourrait stabiliser le VSD dans l'état de repos. Lorsque le canal est activé/ouvert, le PIP_2, tout en interagissant avec S4-S5, ancre l'extrémité de l'hélice S6. Cet ancrage stabilise éventuellement la conformation ouverte du pore. Nos résultats sont en bon accord avec les données expérimentales sur le *Shaker* et sont de surcroit en mesure de rationaliser ces données : en effet, un déplacement vers la droite de la courbe Q/V (courant de porte en fonction du voltage appliquée) en présence du PIP_2 peut être causée par la stabilisation du VSD au repos ; une augmentation du courant ionique est attribuée, elle, à une probabilité accrue de trouver le pore en conformation ouverte, ce qui est cohérent avec la stabilisation de l'état activé/ouvert par PIP_2. Nous avons trouvé un autre site de liaison de PIP_2, qui est situé à l'interface entre deux sous-unités adjacentes de Kv1.2. Dans ce site, PIP_2 forme un réseau de ponts salins entre deux domaines de liaison S4-S5, ce qui pourrait également stabiliser la conformation ouverte du pore. Cette dernière hypothèse est compatible avec des expériences de mutagenèse. Enfin, dans le troisième site de liaison, PIP_2 interagit avec la boucle S2-S3 et le segment de liaison T1-S1. La boucle S2-S3 est située le long d'un chemin, par lequel PIP_2 peut approcher l'interface VSD/PD. On émet l'hypothèse par conséquent que cette interaction entre S2-S3 et le PIP_2 est plutôt temporelle.

- Nous avons évalué les profils d'énergie libre qui caractérisent les deux premières transitions du VSD du Kv1.2 le long du chemin d'activation (E-Δ et Δ-Y) dans une bicouche lipidique POPC et dans une bicouche contenant plusieurs molécules de PIP_2 dans le feuillet inférieur. Pour ce faire, nous avons échantillonné l'espace conformationnel du système en fonction de variables collectives spécifiques qui reflètent les deux principaux éléments des transitions du VSD : i) la formation et rupture de ponts salins entre les résidus positifs de S4 et leurs contre-charges et ii) la translation spatiale de S4 à travers la membrane. Une fois l'espace conformationnel du système bien échantillonné, nous avons ré-estimé l'énergie libre en fonction d'une variable collective "expérimentale", à savoir, le courant de porte Q. Nos résultats indiquent que la stabilité relative des états du VSD diffère selon le milieu membranaire POPC vs. POPC/PIP_2. En particulier, alors que l'état Y est moins stable que l'état Δ quel que soit le type de bicouche, la différence d'énergie libre entre ces états est de l'ordre de 3.0 kcal/mol dans POPC et de 12.7 kcal/mol dans POPC/PIP_2. En outre, on a trouvé que la présence de PIP_2 modifie la hauteur des barrières qui séparent les états du VSD. L'effet est

particulièrement important pour la barrière d'activation Δ-Y (de Δ vers Y). Celle-ci augmente de 5.4 kcal/mol dans POPC à 13.3 kcal/mol dans POPC/PIP_2. Ces deux effets induits par la présence de PIP_2, bien que démontrés uniquement que pour deux transitions du VSD sur quatre, sont en accord avec les données expérimentales : la déstabilisation de l'etat Y peut expliquer le déplacement vers la droite de la courbe Q/V, et l'augmentation de la barrière d'activation Δ-Y est en accord avec le ralentissement de l'activation et l'accélération de la désactivation du VSD. On note cependant que les deux transitions restantes, Y-B and B-A peuvent être ainsi modulées par la présence de PIP_2. L'estimation de l'énergie libre qui leur correspond est en cours.

- Nous avons identifié le site de liaison de PIP_2 au Kv7.1 qui est impliqué dans le couplage. Dans ce site de liaison situé à l'interface VSD/PD, l'interaction entre PIP_2 et des résidus positifs de Kv7.1 est dépendant de l'état du canal. Lorsque le VSD est dans l'état de repos, PIP_2 interagit avec son hélice S4 et est incapable d'ancrer S6. Lorsque la porte (gate) est ouverte, PIP_2 se lie à S6 et s'éloigne du VSD libérant ainsi S4. Par conséquent, PIP_2 favorise potentiellement les états activé/ouvert et repos/fermé du VSD/pore par rapport aux états activé/fermé et repos/ouvert dans le Kv7.1, c'est à dire il couple des conformations spécifiques du VSD à ceux du pore. Par ailleurs, nous avons montré que dans Kv7.1, l'interaction entre les segments S4 et S5-S6 qui joue un rôle principal dans le couplage protéine-protéine de couplage est affaiblie par des répulsion électrostatiques entre certains de leurs résidus positifs. Lorsque cette répulsion a été éliminée expérimentalement par l'introduction d'une mutation de charge, une composante du couplage indépendante du lipide (c.à.d. en l'absence de lipide) qui n'était pas présente dans le Kv7.1 sauvage, a été détectée. Sur la base de nos résultats, nous concluons que, en raison des interactions faibles entre la S4-S5 et S6, le couplage dépendant de la présence du PIP_2 est particulièrement important dans Kv7.1.

- Enfin, nous avons comparé nos résultats correspondant au Kv1.2 et au Kv7.1. Les deux sites de liaison, pour lesquels l'interaction entre PIP_2 et les résidus positifs de ces canaux est dépendant de l'état du canal, sont homologues. Cependant, les résidus de coordination du PIP_2 au Kv1.2 et au Kv7.1 sont différents. En particulier, certains résidus de Kv7.1 qui participent à la formation du site de liaison de PIP_2 sont soit neutralisés ou mutés en résidus chargés négativement dans Kv1.2. Les derniers sont impliqués dans les interactions S4-S5/S6 et participent donc à la

composante protéine-protéine de couplage entre le VSD et le pore. Pour d'autres membres de la famille Kv7 (Kv7.2, Kv7.5), une partie des résidus homologues sont également mutés, impliquant que la composante protéine-protéine de couplage est plus importante dans ces canaux par rapport à Kv7.1. Nous proposons à la lumière de ces éléments que, dans tous ces canaux, une réponse différente à la présence du PIP_2 a comme origine une contribution relative différente des deux composantes de couplage : protéine-protéine et PIP_2-protéine.

En conclusion, dans ce travail, nous avons rationalisé les données expérimentales connues sur la modulation par PIP_2 de la fonction des canaux potassiques sensibles à la tension Kv1.2 et Kv7.1 et de déterminer les mécanismes moléculaires à son origine. Nous avons également estimé quantitativement comment la présence de PIP_2 dans la membrane modifie les profils d'énergie libre des deux premières transitions du domaine sensible à la tension (VSD) du Kv1.2. D'autres calculs son en cours pour évaluer les profils d'énergie libre des deux transitions restantes.

6 CONCLUSION

Voltage-gated ion channels play a central role in initiation and propagation of a nerve impulse, underlying therefore one of the most important properties of a living organism, namely, excitability. These proteins are indeed ubiquitous: they are found in central and peripheral nervous systems, heart, muscles, intestines, inner ear, kidneys, *etc.* Malfunctioning of voltage-gated ion channels induced by selective mutations in their sequences was shown to cause severe inherited diseases such as benign familial neonatal seizures, peripheral nerve hyperexcitability (nervous system), long and short QT syndromes, cardiac arrhythmia (heart), myotonias and periodic paralyses (muscles), deafness (inner ear), *etc.*

Due to the fact that voltage-gated ion channels are involved in a spectrum of vital physiological processes, their functioning is strictly regulated by the cell. PIP_2 represents a minor lipid of the plasma membrane, which modulates functioning of many ion channels including the voltage-gated ones. This lipid interacts with positively charged residues of an ion channel, which was directly demonstrated for the Kir channels [1,2] and indirectly for several other ion channels [3–14]. In the current work, we explored how the two voltage-gated potassium channels, Kv1.2 and Kv7.1, are modulated by PIP_2. While Kv1.2 represents a good model for investigating fundamental processes such as the ionic transport and the gating, Kv7.1 is an important therapeutic target. The latter is expressed in the heart and participates in the late repolarization phase of the cardiomyocyte's action potential.

The main results of our work may be summarized as follows:

- We have identified three potential PIP_2 binding sites in Kv1.2. One of these sites is located at the interface between the voltage sensor and the pore. Here, depending on the state of the channel, PIP_2 was shown to interact with different positive residues. In particular, when the channel is resting/closed, this negatively charged lipid forms salt bridges with the middle residue of the S4-S5 linker and the bottom of S4, potentially stabilizing the voltage sensor in the resting state. When the channel is activated/open, PIP_2 anchors the S6 terminus, while still interacting with S4-S5. The latter potentially stabilizes the open conformation of the

pore. Our findings are in a good agreement with the experimental data on *Shaker* and, moreover, are able to rationalize this data: indeed, a right-shift of the Q/V curve (gating current vs. applied voltage) may be caused by the stabilization of the resting voltage sensor; an increase of ionic current was further attributed to an increased single channel open probability, which is consistent with the stabilization of the activated/open state by PIP_2. We have found another PIP_2 binding site, which is located at the interface between two adjacent subunits of Kv1.2. In this site, PIP_2 forms a net of salt bridges between two nearby S4-S5 linkers, potentially stabilizing the open conformation of the pore. The latter hypothesis is consistent with known mutagenesis experiments. Finally, in the third binding site, PIP_2 interacts with the S2-S3 loop and the T1-S1 linker. The S2-S3 loop is located along a path, by which PIP_2 approaches the site at the VSD/PD interface, and, therefore, we posit that interaction between S2-S3 and PIP_2 is rather temporal.

- We have estimated the free energy profiles that characterize the first two transitions of the Kv1.2 voltage sensor along the activation path (E-Δ and Δ-Y) in the bare POPC bilayer and in the POPC bilayer with several PIP_2 molecules placed at the bottom leaflet. To do so, we have sampled the system's conformational space in terms of a newly devised collective variable, which reflects the two principal events of the Kv1.2 voltage sensor transitions: i) the binding/unbinding of the S4 positive residues to their countercharges and ii) the spatial translation of S4 across the bilayer. After the system's conformational space was well sampled, we re-estimated the free energy in terms of an "experimental" collective variable, namely, the gating charge. Our results indicate that the relative stability of the voltage sensor states is different in the POPC and POPC/PIP_2 bilayers. In particular, while the Y state is less stable than Δ (regardless the bilayer type), the free energy difference between these states corresponds to 3.0 and 12.7 kcal/mol in POPC and POPC/PIP_2 respectively. Moreover, PIP_2 was shown to affect the height of the barriers separating the voltage sensor states. The effect is especially prominent for the Δ-Y activation barrier (from Δ toward Y). The latter increases from 5.4 to 13.3 kcal/mol when going from the bare POPC bilayer to the POPC/PIP_2 one. The two effects induced by the presence of PIP_2, though being obtained only for two transitions of the voltage sensor out of four, are in agreement with the experimental data: the destabilization of the Y state may underlie the right-shift of the Q/V curve, and the increase of the Δ-Y activation barrier is consistent with slowed activation and accelerated deactivation of the voltage sensor.

Note, however, that the two remaining transitions, Y-B and B-A, may be as well modulated by the presence of PIP_2. The estimation of the free energy underlying the Y-B and B-A transitions is ongoing.

- We have identified the PIP_2 binding site in Kv7.1 that is involved in PIP_2-dependent coupling. In this binding site located at the VSD/PD interface, the interaction between PIP_2 and positive residues of Kv7.1 is state-dependent. When the VSD is in the resting state, PIP_2 interacts with its S4 helix and is unable to anchor S6. When the pore is open, PIP_2 binds to S6 and moves away from the VSD releasing S4. Therefore, PIP_2 potentially favors the activated/open and resting/closed states of Kv7.1 over the activated/closed and resting/open ones, *i.e.* couples specific conformations of the VSD to those of the pore. Further, we showed that, in Kv7.1, the interaction between S4-S5 and S6 mediating the protein-protein component of coupling is weakened by electrostatic repulsion between some of their positive residues. When this repulsion was eliminated experimentally by introducing a charge reversal mutation, a lipid-independent component of coupling, which was not present in the wild type Kv7.1, was detected. Based on our findings, we conclude that due to weak interactions between the S4-S5 and S6, the PIP_2-dependent coupling is especially prominent in Kv7.1.

- Finally, we compared our findings related to the Kv1.2 and Kv7.1 channels. The two binding sites, in which the interaction between PIP_2 and positive residues of these channels is state-dependent, are homologous. However, the residues coordinating PIP_2 in Kv1.2 and Kv7.1 are different. In particular, some residues of Kv7.1 participating in formation of the PIP_2 binding site are either neutralized or mutated in negative ones in Kv1.2. The latters are involved in the S4-S5/S6 interactions and mediate the protein-protein component of coupling between the voltage sensor and the pore. In other members of the Kv7 family (Kv7.2-Kv7.5), some of the homologous residues are as well mutated, and at the same time the protein-protein component of coupling is more prominent compared to Kv7.1. Therefore, we propose that, in all these channels, a different response to PIP_2 and also voltage application is potentially provided by a different relative contribution from the two components of coupling, the protein-protein and PIP_2-dependent ones.

In this work, we attempted to rationalize the known experimental data of the Kv1.2 and Kv7.1 modulation by PIP_2 and to provide a model of the

corresponding molecular mechanism. We also estimated quantitatively the alteration of the free energy profiles of the two first transitions of the Kv1.2 voltage sensor induced by the presence of PIP_2. In our ongoing work, we will continue calculating the free energy profiles for the two remaining transitions.

REFERENCES

[1] S.B. Hansen, X. Tao, R. MacKinnon, Structural basis of PIP2 activation of the classical inward rectifier K+ channel Kir2.2, Nature, 477 (2011) 495–498.

[2] M.R. Whorton, R. MacKinnon, Crystal Structure of the Mammalian GIRK2 K+ Channel and Gating Regulation by G Proteins, PIP2, and Sodium, Cell, 147 (2011) 199–208.

[3] H. Zhang, L.C. Craciun, T. Mirshahi, T. Rohacs, C.M.B. Lopes, T. Jin, D.E. Logothetis, PIP(2) activates KCNQ channels, and its hydrolysis underlies receptor-mediated inhibition of M currents, Neuron, 37 (2003) 963–975.

[4] K.-H. Park, J. Piron, S. Dahimène, J. Mérot, I. Baró, D. Escande, G. Loussouarn, Impaired KCNQ1–KCNE1 and Phosphatidylinositol-4,5-Bisphosphate Interaction Underlies the Long QT Syndrome, Circ. Res., 96 (2005) 730–739.

[5] S. Brauchi, G. Orta, C. Mascayano, M. Salazar, N. Raddatz, H. Urbina, E. Rosenmann, F. Gonzalez-Nilo, R. Latorre, Dissection of the components for PIP2 activation and thermosensation in TRP channels, Proc. Natl. Acad. Sci. U. S. A., 104 (2007) 10246–10251.

[6] J.-S. Bian, T.V. McDonald, Phosphatidylinositol-4,5-bisphosphate interactions with the HERG K(+) channel, Pflüg. Arch. Eur. J. Physiol., 455 (2007) 105–113.

[7] G.E. Flynn, W.N. Zagotta, Molecular mechanism underlying phosphatidylinositol-4,5-bisphosphate-induced inhibition of SpIH channels, J. Biol. Chem., 286 (2011) 15535–15542.

[8] A.M. Thomas, S.C. Harmer, T. Khambra, A. Tinker, Characterization of a binding site for anionic phospholipids on KCNQ1, J. Biol. Chem., 286 (2011) 2088–2100.

[9] A.A. Rodriguez-Menchaca, S.K. Adney, Q.-Y. Tang, X.-Y. Meng, A. Rosenhouse-Dantsker, M. Cui, D.E. Logothetis, PIP2 controls voltage-sensor movement and pore opening of Kv channels through the S4-S5 linker, Proc. Natl. Acad. Sci. U. S. A., 109 (2012) E2399–2408.

[10] V. Telezhkin, A.M. Thomas, S.C. Harmer, A. Tinker, D.A. Brown, A basic residue in the proximal C-terminus is necessary for efficient activation of the M-channel subunit Kv7.2 by PI(4,5)P_2, Pflüg. Arch. Eur. J. Physiol., 465 (2013) 945–953.

[11] M.A. Zaydman, J.R. Silva, K. Delaloye, Y. Li, H. Liang, H.P. Larsson, J. Shi, J. Cui, Kv7.1 ion channels require a lipid to couple voltage sensing to pore opening, Proc. Natl. Acad. Sci., 110 (2013) 13180-13185.

[12] Q. Zhang, P. Zhou, Z. Chen, M. Li, H. Jiang, Z. Gao, H. Yang, Dynamic PIP2 interactions with voltage sensor elements contribute to KCNQ2 channel gating, Proc. Natl. Acad. Sci., 110 (2013) 20093-20098.

[13] F.C. Coyan, F. Abderemane-Ali, M.Y. Amarouch, J. Piron, J. Mordel, C.S. Nicolas, M. Steenman, J. Mérot, C. Marionneau, A. Thomas, R. Brasseur, I. Baró, G. Loussouarn, A Long QT Mutation Substitutes Cholesterol for Phosphatidylinositol-4,5-Bisphosphate in KCNQ1 Channel Regulation, PLoS ONE, 9 (2014) e93255.

[14] K. Eckey, E. Wrobel, N. Strutz-Seebohm, L. Pott, N. Schmitt, G. Seebohm, Novel Kv7.1-phosphatidylinositol-4,5-bisphosphate (PIP2) interaction sites uncovered by charge neutralization scanning, J. Biol. Chem., 289 (2014) 22749-22758.

Les canaux potassiques (Kv) dépendants du voltage sont des protéines transmembranaires qui permettent le flux passif d'ions potassium à travers une membrane plasmique lorsque celle-ci est dépolarisée. Ils sont constitués de quatre domaines périphériques sensibles au voltage et un domaine central, un pore, qui délimite un chemin hydrophile pour le passage d'ions. Les domaines sensibles à la tension (VSD) et le pore sont couplés, ce qui signifie que l'activation des VSD déclenche l'ouverture du pore, et qu'un pore ouvert favorise l'activation des VSD.
Le phosphatidylinositol-4,5-bisphosphate (PIP_2) est un lipide mineur du feuillet interne de la membrane plasmique. Ce lipide fortement chargé négativement module le fonctionnement de plusieurs canaux ioniques, y compris les membres de la famille Kv. En particulier, l'application de ce lipide à Kv1.2 et Kv7.1, deux canaux homologues, augmente leur courant ionique. Cependant, alors que Kv1.2 est capable de s'ouvrir en l'absence de PIP_2, dans le cas de Kv7.1, ce lipide est absolument nécessaire pour l'ouverture du canal. En outre, dans Kv1.2, PIP_2 induit une perte de fonction, qui est manifesté par un mouvement retardé des VSD. Jusqu'à présent, les mécanismes sous-jacents à de telles modulations des canaux Kv par PIP_2 restent inconnus. Dans ce travail, nous tentons de faire la lumière sur ces mécanismes en utilisant des simulations de dynamique moléculaire (DM) combinées avec une approche expérimentale, entreprise par nos collaborateurs.
En utilisant des simulations de DM sans contrainte, nous avons identifié les sites potentiels de liaison du PIP_2 au Kv1.2. Dans l'un de ces sites, PIP_2 interagit avec le canal de sorte à former des ponts salins dépendants de l'état du canal, soit avec le VSD soit avec le pore. Sur la base de ces résultats, nous proposons un modèle pour rationaliser les données expérimentales connues. En outre, nous avons cherché à évaluer quantitativement la perte de fonction induite par la présence de PIP_2 au voisinage du VSD du Kv1.2. En particulier, nous avons calculé l'énergie libre des deux premières transitions le long de l'activation du VSD en présence et en l'absence de ce lipide. Nous avons constaté que PIP_2 affecte à la fois la stabilité relative des états du VSD et les barrières d'énergie libre qui les séparent. Enfin, nous avons étudié les interactions entre PIP_2 et un autre membre de la famille Kv, le canal Kv7.1 cardiaque. Dans le site de liaison de PIP_2 que nous avons identifié pour ce canal, l'interaction entre les résidus positifs de Kv7.1 et le lipide sont dépendants de l'état du VSD, comme dans le cas de Kv1.2. On montre que cette interaction est importante pour le couplage entre les VSD et le pore, couplage qui est par ailleurs affaibli à cause de la répulsion électrostatique entre quelques résidus positifs. Ces résultats et prédictions ont été vérifiés par les données expérimentales obtenues par nos collaborateurs.

Voltage-gated potassium (Kv) channels are transmembrane proteins that enable the passive flow of potassium ions across a plasma membrane when the latter is depolarized. They consist of four peripheral voltage sensor domains, responding to the applied voltage, and a central pore domain that encompasses a hydrophilic path for passing ions. The voltage sensors and the pore are coupled, meaning that the activation of the voltage sensors triggers the pore opening, and the open pore promotes the activation of the voltage sensors.
Phosphatidylinositol-4,5-bisphosphate (PIP_2) is a minor lipid of the inner plasma membrane leaflet. This highly negatively charged lipid was shown to modulate the functioning of several ion channels including members of the Kv family. In particular, application of this lipid to Kv1.2 and Kv7.1, two homologous channels, enhances their ionic current. However, while Kv1.2 is able to open without PIP_2, in the case of Kv7.1, this lipid is absolutely required for opening. Additionally, in Kv1.2, PIP_2 induces a loss of functioning, which is manifested by delayed motions of the voltage sensors. So far, the mechanism underlying the Kv channels modulation by PIP_2 remains unknown. In the present manuscript, we attempt to shed light on this mechanism using molecular dynamics (MD) simulations combined with experiments, which was undertaken by our collaborators.
Using unconstrained MD simulations, we have identified potential PIP_2 binding sites in Kv1.2. In one of these sites, PIP_2 interacts with the channel in a state-dependent manner forming salt bridges either with the voltage sensor or with the pore. Based on these findings, we propose a model rationalizing the known experimental data. Further, we aimed to estimate the loss of functioning effect induced by PIP_2 on the Kv1.2 voltage sensors. In particular, we have calculated the free energy of the first two transitions along the activation path in the presence and absence of this lipid. We found that PIP_2 affects both the relative stability of the voltage sensor states and the free energy barriers separating them. Finally, we studied the interactions between PIP_2 and another member of the Kv family, the cardiac channel Kv7.1. In the PIP_2 binding site that we have identified for this channel, the interaction between positive residues of Kv7.1 and the lipid was state-dependent, as in the case of Kv1.2. This state-dependent interaction, however, is prominent for coupling between the voltage sensors and the pore, which is otherwise weakened due to electrostatic repulsion of some positive residues. These findings are in a good agreement with the experimental data obtained by our collaborators.